NASA Contractor Report 3621

Interaction of Aerodynamic Noise With Laminar Boundary Layers in Supersonic Wind Tunnels

M. R. Schopper

CONTRACT NAS1-16572
APRIL 1984

NASA

NASA Contractor Report 3621

Interaction of Aerodynamic Noise With Laminar Boundary Layers in Supersonic Wind Tunnels

M. R. Schopper
Systems and Applied Sciences Corporation
Hampton, Virginia

Prepared for
Langley Research Center
under Contract NAS1-16572

National Aeronautics
and Space Administration

**Scientific and Technical
Information Office**

1984

SUMMARY

Motivated by the noise-boundary layer transition problem in supersonic tunnels, a study of the noise field and the noise-laminar boundary layer interaction was made. The noise field was modeled as a Mach wave radiation field consisting of discrete waves emanating from coherent turbulent entities moving downstream within the supersonic turbulent tunnel wall boundary layer. The individual disturbances are likened to miniature sonic booms and the laminar boundary layer is strafed by the waves as the sources move downstream. The mean, autocorrelation, and power spectral density of the field are expressed in terms of the wave shapes and their average arrival rate. The predicted rms amplitude distribution across the wind tunnel test section and the shape of the power spectral density curve agree with experimental data quite well. The emphasis in the analysis of the interaction of the wave field with the laminar boundary layer was on the weak shock behavior. The waves are refracted and focused by the boundary layer, and the two-dimensional linearized shock focusing equations, which are known, were rederived using the method of geometric acoustics for a nonuniform moving medium. The shock ray path differential equation was determined, and some typical ray trajectories through the boundary layer were computed. The waves are focused at what is termed the caustic layer. The caustic layer height within the laminar boundary layer was computed for a range of free-stream Mach numbers and source-to-free-stream convection velocity ratios. The heights were found to lie in the outer half of the boundary layer. A sonic boom theory scaling law which requires the value of the radius of curvature of the ray path at the caustic was used to estimate the amount of focusing at the caustic. Some example calculations showed that the focus factors of 2 to 6 occurred for incoming shock strengths of 1 to 0.01 percent of the free-stream pressure. Another element considered was the thickness of the very weak shocks associated with the radiation process. Shock thickness in the radiation pressure field could affect significant portions of the disturbance pressure signatures under certain conditions. The resulting smoothed shock fronts would tend to reduce the high-frequency content of the modeled noise spectrum and reduce the intensity of focusing because the focusing is a high-frequency phenomenon. An expression giving the ratio of the shock front thickness to laminar boundary layer thickness as a function of Mach number and Reynolds number shows that at a length Reynolds number of 10^6 this ratio may be close to one; for lower Reynolds numbers the ratio progressively increases. It is not clear whether the sound focusing effectively promotes early transition. Additional observations concerning the interaction are presented.

TABLE OF CONTENTS

	Page
SUMMARY	iii
1. INTRODUCTION	1
2. DESCRIPTION OF NOISE MODEL	4
Model and its Physical Basis	4
Features Compared With Published Findings	5
Optical evidence of wave field.-	5
Convection velocities.-	5
Amplitude distribution across test section.-	6
Free-stream spectra and other statistical properties.-	7
3. INTERACTION OF NOISE WITH LAMINAR BOUNDARY LAYER	15
Stationary Shock-Laminar Layer Interactions	15
Two-dimensional interactions.-	15
Reflected wave system.-	21
Three-dimensional interactions.-	21
Examples of Focusing of Weak Shocks	23
Noise-Laminar Layer Interaction	24
Thickness of weak shocks.-	25
General features.-	28
Height of caustic region.-	33
Estimate of focusing strengths.-	36
The search for experimental evidence of a caustic region.-.	40
Effect on Transition	43
Receptivity-Related Observations	46
Use of Pressure Transducers for Noise Measurements	48
4. CONCLUDING REMARKS	50
Appendix A - Noise Field Intensity Distribution Across Test Section	52
Appendix B - Estimates of the Boundary Layer Thickness and Displacement Thickness Along the Nozzle of the JPL 20-Inch Tunnel	55
Appendix C - Linearized Analysis of Weak Shock Wave-Supersonic Shear Layer Interaction	58
Appendix D - Geometric Acoustic Approach to the Weak Shock Wave Boundary Layer Interaction	73
Appendix E - Thickness of Shocks	84
Appendix F - Estimates of Radius of Curvature at the Caustic of Incoming Boundary Layer Noise Ray Paths	92

TABLE OF CONTENTS (Continued)

Page

Appendix G - Caustic Layer Height for Plate at an Angle of Attack . . . 101

5. REFERENCES 106

1. INTRODUCTION

The phenomenon of boundary layer transition is a process which is sensitive to the quality of the flow environment, and the flow environment in wind tunnels can be rather harsh, especially in supersonic tunnels. Thus the specter of free-stream disturbances has haunted the transition investigator more than any other tunnel user. This problem of the influence of the tunnel disturbance environment on transition provided the motivation for the present study. The interaction between acoustic disturbances and the laminar boundary layer in supersonic wind tunnels is examined. The study focuses on one aspect of the interaction which heretofore has not been discussed. The present report is a revised and extended version of a previous paper (ref. 1).

In well designed unheated supersonic wind tunnels it has been found that the greatest source of free-stream disturbance, especially at the higher Mach numbers, is the noise field generated by the turbulent boundary layers on the tunnel nozzle walls (refs. 2 to 5). It is this type of acoustic field which is considered in the present analysis. While the discussion is centered on the noise-laminar layer interactions occurring in wind tunnels, it is important to note that such interactions also occur on most flight vehicles. The boundary layer on the fuselage of flight vehicles is usually turbulent, and the radiated noise interacts with the laminar boundary layer near the leading edges of wings or fins. Thus the problem is not confined to the wind tunnel setting.

It is generally accepted that boundary layer transition on supersonic and hypersonic wind tunnel models is greatly affected by the noise radiated from the tunnel wall boundary layers (refs. 3, 6 to 9). Among the more prominent observations that have led to this acceptance are: (1) flight transition Reynolds numbers are generally higher than those from wind tunnels (ref. 10); (2) noise dominates the free-stream disturbances at the higher Mach numbers (refs. 2 to 5); (3) in many wind tunnels the transition Reynolds number, Re_t, has been found to vary inversely with free-stream fluctuating pressure levels; (refs. 3, 6, 7, 11 and 12); (4) transition results from many tunnels and flow conditions have been correlated using parameters that are assumed to be related to the noise field (refs. 6, 8, 13 to 16); (5) the space time cross-correlation curves of Kendall (refs. 17 and 18) showed that large disturbances in the model laminar boundary layer were related to the incoming noise field; and (6) some attempts at shielding models from the noise or exposing the model to laminar nozzle boundary layers have resulted in increased lengths of laminar flow (refs. 6, 18 and 19).

Not all evidence, however, conveniently fits the noise-transition hypothesis. The so-called unit Reynolds number effect (increase in Re_t with increase in unit Reynolds number) is often thought to be due to the tunnel noise, but the effect is not universally found in wind tunnels (refs. 20 to 24), while it is found in ballistic ranges where there is no boundary layer noise present (refs. 25 to 27). In higher Mach number heated tunnels, some researchers have concluded that the noise did not dominate the transition process (ref. 28). Not all data fit the transition correlation formulas (ref. 29 for example; and one can show that the JPL 20-inch data of ref. 30 also does not fit). Owen and Horstman (ref. 31) changed the free-stream noise level by changing the nozzle coolant gas from helium to air and no change in Re_t was observed on a slender cone at $M = 7.4$. Boundary layer transition remains an enigmatic phenomenon. Informative and interesting reviews of the sleuthing efforts over the past 20 years may be found in the

widely cited papers of Morkovin (refs. 32 to 37).

If the noise from the tunnel turbulent boundary layers indeed affects model transition results in supersonic tunnels, there must be an interaction mechanism (or mechanisms) present between the noise field and the laminar layer that would promote transition. On simple flat plate and cone models it is thought that the incoming noise field generates and perhaps feeds energy into Tollmien-Schlichting instability waves (TS waves) and that these waves then play an important part in transition. The process by which the noise field induces and affects TS waves, termed the receptivity process (refs. 33 and 36), is largely unknown. While the motivation for the present study was the noise-transition problem, the objective was to take a closer look at the noise-laminar layer interaction rather than a closer look at the noise-transition problem.

In the present study a very simple model of the noise radiation process is adopted. The radiated field is assumed to be composed of numerous discrete waveforms, each of which emanates from coherent turbulent entities that move downstream within the turbulent wall boundary layer at less than the free-stream velocity. The waveforms contain shocklets and are like miniature sonic booms which radiate from the moving fluid structures because of their supersonic speeds relative to the outer flow. Because the randomly spaced sources move downstream, their wave systems strafe the test-section models. The interaction between the noise field and the model laminar boundary layer is treated as being the refraction through the laminar layer of these weak waves as the field moves downstream. The analysis is restricted to the outer supersonic portion of the boundary layer, and only the shocklet portions of the incoming wavefronts are considered in the mathematical formulation.

A description of the wave radiation model is presented and its credibility is discussed by examining the physical basis of the model and comparing its features with those described in published turbulent boundary layer and tunnel noise measurement reports. One of the more interesting and important features of the noise model is that it allows some of the statistical properties of the field at a point in the test section to be expressed quite simply. The equations presented are well known in the fields of signal analysis and statistical communication theory.

Concerning the interaction analysis, the present results are obtained using two different approaches. In the first approach a linearized analysis that was first used by fluid dynamicists in the 1950's to analyze weak shock wave boundary layer interactions is used. In the second approach the results are derived using geometric acoustics and utilizing an energy density invariant for acoustic waves propagating in a nonuniform moving medium. This invariant was first derived by Blokhintsev (ref. 38) and has been used to describe sonic boom propagation (ref. 39) (the sonic boom is a weak shock wave system). The wavefronts are found to be focused in a region of the boundary layer. Borrowing wave-propagation terminology, this focal region is herein termed the "caustic region." Examples of wave behavior at a caustic are cited and estimates of the amount of focusing are presented. The caustic region height is estimated and is found to vary with tunnel Mach number, and the height is compared with the published heights of the experimentally determined region of maximum fluctuation level. While it is customary and most often quite appropriate to treat a shock as a discontinuity, for weak, acoustic-strength shocks the thickness can be appreciable. The thickness of weak shocks are analyzed and the focusing results are qualitatively reconsidered in view

of the finite thickness shock. Experimental evidence relating to the existence of the caustic region is reviewed. Some thoughts on the relevancy of the caustic region to transition are presented, and a few receptivity-related comments are offered. Finally, a short discussion concerning the efficacy of the microphone flat plate and the fluctuating pitot pressure methods of measuring the tunnel noise field is presented.

The most thorough analytical study to date of the interaction between the noise and the laminar boundary layer in supersonic wind tunnels is that of Mack (refs. 40 and 41). His calculations were for frequencies in the range where Kendall's free-stream measurements (ref. 18) showed significant energy content. One finds, however, that the wavelengths considered were long in comparison to the laminar boundary layer thickness (10 δ - 350 δ). Thus Mack's results can be considered to describe the interaction with the lower frequency components of the noise field, while the present results describe the interaction with the weak shock fronts, or, in the sense of Fourier decomposition, the very high-frequency components of the field (frequency $\to\infty$).

2. DESCRIPTION OF NOISE MODEL

To understand the nature of the interaction between the noise field and the laminar boundary layer one needs to know more about the structure and dynamics of the noise field. In spite of the great concern over the noise-transition problem in supersonic tunnels, the experimental effort that has gone into obtaining and correlating transition results far outweighs that which has been expended to understand the noise field. At least part of the reason for this situation is that definitive test section noise measurements are very difficult to make. In view of these uncertainties about the noise field and of the simple approach taken here to analyze the noise-laminar layer interaction, the noise field modeling is done in a very simple fashion.

Model and its Physical Basis

Inasmuch as the detailed noise measurements from which one can confidently extract a noise field model are not yet available, one must turn to the source of the noise, the turbulent boundary layer, to obtain further guidance. The literature on turbulent shear flow is immense and growing, and the prevailing views on the subject have been undergoing considerable change. In the mid-1950's the older view of turbulence as a mean flow plus random fluctuations began to give ground to a more mechanistic view. This was the result of increasing recognition that there appeared to be some order or coherent motion in turbulent flows. The trend in experimental research then shifted to the revelation and exploration of ordered or quasi-ordered motions, and within the last 10 years, with the help of sophisticated electronic techniques, computers, and optical methods, much information has been acquired about the structure of the turbulent boundary layer. Reviews of this research may be found in references 42 to 45. Some of the latest findings are contained in the coherent structure workshop report (ref. 46).

In spite of the recent concentrated research efforts, much remains unclear about the turbulence mechanisms and the coherent structures within the turbulent boundary layer (ref. 46). Nevertheless, there is now general agreement that within the boundary layer there are events or flow processes which appear to be quasi-cyclic over space and time, and that these structures dominate the behavior of turbulent flows. These boundary layer flow processes comprise the quasi-ordered structures which move downstream. A variety of flow processes have been discovered, and these have been described using such terminology as streaks (but no streakers in recent years), bursting, breakdowns, and ejections. The hope is that a coherent synthesis of the findings will be reached and that a relatively deterministic picture will emerge.

Most of the structurally oriented turbulence research has been conducted at low speeds and low Reynolds numbers, but it seems reasonable to assume that in the supersonic turbulent boundary layer the radiated noise will be closely tied to coherent structures of the same genus as those in low speed flows. Hence, the noise field is assumed to emanate from coherent structures or entities which are randomly spaced along the wall and moving downstream. The field is envisioned as resulting from interactions between momentum deficient fluid regions and the faster outer flow. Specifically it is modeled as being the result of interactions in which the faster flow is supersonic with respect to the low speed fluid entity, and thus the noise radiation is

in the form of weak shock wave systems. This type of radiation is called Mach wave radiation (ref. 47).

The noise radiation model is illustrated in figure 1. In the model the turbulent boundary layer is simply replaced by randomly spaced bodies next to the surface which travel downstream at less than the free-stream velocity. These "wall bodies" are slow enough so that the free-stream is supersonic with respect to them, and owing to their downstream movement any object in the test section would be strafed by the individual wave systems. The model may be viewed as a discrete version of Phillips' virtual, spacially random, moving wavy wall (ref. 47), and is akin to the displacement thickness acoustical model of Liepmann (ref. 48). As the free-stream Mach number, M_∞, increases more of the flow processes comprising the quasi-ordered flow structures acquire supersonic relative velocities and thus emit Mach wave radiation, and the streamwise accelerating fluid entities can radiate over a longer period of their lifetime. Again, for the present purposes, a simple model was deemed adequate.

Features Compared With Published Findings

In this section a check on the credibility of the model is made by a comparison of some of the model features with published findings. The comparisons are mainly qualitative. If the model were to be carried to the extreme, it could be quantified. By actually specifying the shapes of typical wall bodies and their speeds, one could use sonic boom theory (refs. 49 and 50) to determine the strengths and shapes of the radiated wave systems. With the additional specification of the average spacing between the bodies, the expressions which will be given later could then be used to estimate the values of various statistical properties of the field.

Optical evidence of wave field. - The noise field in the model is taken to be composed of the weak shock wave systems from the downstream moving wall bodies. There is ample evidence that the turbulent boundary layer does emit a Mach wave field from downstream moving sources, and perhaps the most appealing evidence comes from optical detection means. Such evidence is most prominently found in schlieren and shadowgraph photographs taken of supersonic ballistic range models having turbulent boundary layers (refs. 51 to 53). In ballistic ranges there are no turbulent boundary layers on the facility windows to mask weak disturbances in the test chamber, and photos reveal a structure of weak waves emanating from the model turbulent boundary layer. (It appears that a Mach wave radiation field from a Mach 6 wind tunnel model may be visible in fig. 14 of ref. 54.) The wave angles of the radiation pattern are greater than the local Mach angle and this indicates that the sources are moving downstream. Many supersonic jet noise reports also show photos of Mach wave radiation from turbulent shear layers (refs. 55 and 56). While it is difficult to infer from the ballistic range photographs that shocklets are present in the noise field emanating from the fully turbulent regions, shocklets from turbulent spots in the transition region are often readily identifiable (ref. 51). Microphone measurements of the noise field from supersonic jets reveal shocklet-type pressure traces (ref. 56).

Convection velocities. - The fact that the sources of the noise field are convected downstream is an important feature retained in the model. In addition to the optical evidence of downstream movement, free-stream measurements of

the convection velocities of the noise field have been reported. These have been made with hot-wire anemometers using either of two techniques. In the first method, two hot wires are used and space-time cross-correlation measurements are taken. In the second method, which is appropriate for the case in which the radiated noise clearly dominates the free-stream disturbance field, a single wire is used along with special assumptions about the field.

Convection velocity results from a number of investigations are shown in figure 2. Some comments are in order. The data came from five different tunnels. There is considerable scatter in the data and this reflects the difficulty in making these measurements. The data show a trend of increasing convection velocity with tunnel Mach number and this is consistent with the fact that with increasing M_∞ faster moving flow processes can radiate via Mach wave radiation. The relative Mach number between the free-stream and the convected field is greater than one. Values of the mean relative Mach number vary from 1.3 at $M_\infty = 2$ to 2.4 at $M_\infty = 8$ (at $M_\infty = 4.5$, the spread in the relative Mach number ranges from 1.3 to 2.6). The dual-wire convection velocity results shown are values obtained from dividing the separation distance between the wires by the time delay of the peak in the cross-correlation curve. This method of defining a convection velocity has frequently been used. By using the phase information in the Fourier transform of the cross-correlation curves, the convection velocity as a function of frequency may also be obtained. Kendall ($M_\infty = 4.5$) published such information for one separation distance (ref. 17), and found considerable dispersion (the results are also shown in fig. 15 of ref. 58). At the upper end of the spectrum the convection speed was nearly constant at 0.7 times the free-stream velocity u_∞, but at the lower end there was a rapid drop in speed. The convection speed of the lowest frequencies measured was found to be slightly less than 0.4 u_∞. In contrast to these results, Owen et al., (ref. 7), claim to have found no dispersion in two hypersonic tunnels, with the convection velocity remaining constant at 0.7 u_∞. No details are given. In an earlier report Owen and Horstman (ref. 31) presented hot-wire power spectra results from one of the tunnels, and the frequency range covered was about 10 Hz to 20 kHz. If this same frequency range was included in the later cross-correlation work (ref. 7), it should have been sufficient to reveal any dispersion. The apparent lack of dispersion at hypersonic speeds raises the possibility that at the higher Mach numbers dispersion may not be significant. The dispersion problem will be discussed further in a later section.

The large dispersion found by Kendall at $M_\infty = 4.5$ must be considered significant. It renders questionable the technique of defining a convection velocity from broad-band correlation curves using the quotient of the separation distance and the correlation peak time delay. Dispersion indicates that flow structures are traveling at different speeds, and when large dispersion is found it usually becomes important to know what kinds of sources are traveling at what speeds. The problem is difficult to unravel. In a later section it will be shown that one's intuition in relating frequency to size and speeds of eddies may not be a suitable guide. When the problem is better understood a distribution of sizes, shapes, spacings, and convection speeds could be given to the wall bodies in the present model.

Amplitude distribution across test section. - The wave systems emanating from the wall bodies may be likened to miniature sonic booms. It is interesting to note that sonic boom work has been conducted in supersonic wind tunnels throughout the last 20 years using miniature models whose lengths, 1/2 to 10 cm,

(refs. 59 and 60), would probably be typical of the length of the wall bodies in many tunnels. Results from sonic boom studies are used here to determine the uniformity of the wall body radiated noise fields. Measurements of the intensity of the noise field across a test section have been reported (refs. 2, 3, 61), and in these cases the rms level of the field has been found to be uniform except in the immediate vicinity of the wall boundary layer. A possible exception has been reported in reference 62 where noise and flow nonuniformities were found to focus along the centerline in a small Mach 5 axisymmetric nozzle. However, these nonuniformities were traced to disturbances originating from nozzle-wall machining errors.

A probe inside a test section receives signal contributions from sources located around the test section. When the probe is in the center of the test section it receives nearly equal direct contributions from all sources around the section (or equal contributions if the test section is circular). As the probe is moved off the centerline it receives stronger signal contributions from the closer wall regions and weaker ones from the opposite wall regions. Given a location inside the test section, the problem is to evaluate the total contribution from all regions around the test section. Sonic boom theory provides laws which describe how a weak shock signal decays with increasing distance from the source, and these laws can therefore be used to evaluate signal contributions from the various wall regions. Consequently, the uniformity of the total signal can be evaluated by comparing the signal sums for various points within the test section. This was done for both a circular-and square-shaped test section and the values were found to be quite uniform throughout most of the test section. The details of this exercise are presented in Appendix A. It is thus concluded that the wall body model gives a uniform rms noise field across most of the test section in agreement with the experimental observations.

Free-stream spectra and other statistical properties. - The wall body model is well suited to the task of describing some of the statistical properties of the radiated noise field. With assumptions imposing additional order on the model, the resulting statistical expressions turn out to be rather simple. Specifically, the analysis requires that there be some regularity to the shapes of the waveforms, and hence to the bodies. The feature of the random spacing of the bodies is retained. The simplest model in this case would be one in which all of the bodies have identical shapes. Because of its simplicity, this model will be adopted initially, but it will be seen later that the results can be generalized to a much more complicated wave field.

Given a field of randomly spaced identical waveforms, the problem is to determine various statistical quantities such as the mean, variance, and power spectral density (psd) of the fluctuations as sensed by a transducer at the center of a test section. As one might expect, the shape of the waveforms is quite important. It is thus necessary to keep in mind the fact that for a given wall body and its radiated wave pattern, the particular waveform sensed by a probe would depend on the flow quantity or quantities to which the probe is sensitive (e.g., static pressure, mass flux, etc.). For the weak disturbances considered here, the geometrical shape of the detected wave signature would be similar for many of the commonly measured flow quantities. Thus it would not be necessary to tag a wall body with a different geometrical wave shape for each flow quantity considered.

For weak disturbances the transducer system output signal can be considered as the electrical analog of the linear superposition of the individual flow

input pulse signals. For the analysis, the transducer system is first replaced by a special linear system. It is well known that the response or output of a linear system to any type of signal can be expressed, via the superposition principle, in terms of the system's impulse response function, h(t). The impulse response function is a function of time, t, which represents the output of the system when subjected to unit impulse input signal. The solution to the problem of the output of a linear system subjected to the random arrivals of unit impulses has been known for many years. This fact is taken advantage of by employing the tricks of (1) specializing h(t) of the linear system to be identical to the pulse shapes of the incoming fluid pulses, and (2) replacing the incoming fluid signal consisting of randomly spaced pulses by similarly randomly spaced unit impulses. In this situation the output of the linear system is a signal which is analogous to the output of the real transducer system. This approach to the problem is depicted in figure 3. The solution to the problem merely requires the adoption of existing formulas. Different waveforms can be modeled by simply changing h(t).

Some of the needed results (mean and variance of output signal) are embodied in what is sometimes called Campbell's theorem (based on Campbell's 1909 results - ref. 63). Perhaps the most frequently discussed problem of the response of a linear system to random impulsive inputs has been the shot noise problem. This problem was analyzed in the classic paper by Rice (ref. 64). Other analyses may be found in a number of books; the present analysis was taken from Lee's book (ref. 65). The particular random process describing the arrival times of the pulses assumed in the analysis is the so-called Poisson process. The derivation of the Poisson probability distribution and the assumptions involved may be found in a number of sources (ref. 66). The Poisson process has been found to adequately describe many random processes in which one counts the number of times an event occurs during some given time interval (e.g., emission of electrons from a substance, telephone calls received, traffic accidents); it will be assumed to be appropriate here. For waves with identical pulse forms f(t), and having an average arrival rate of α, the results are

$$\text{Mean:} \quad \mu = \alpha \int_{-\infty}^{\infty} f(t)\, dt$$

$$\text{Autocorrelation:} \quad R(\tau) = \mu^2 + \alpha \int_{-\infty}^{\infty} f(t) f(t+\tau)\, dt$$

$$\text{Power spectral density:} \quad S(\omega) = \mu^2\, \delta(\omega) + \frac{\alpha}{2\pi} \left| F(\omega) \right|^2$$

$$\text{where} \quad F(\omega) = \int_{-\infty}^{\infty} f(t)\, e^{-i\omega t}\, dt \,, \qquad (1)$$

$\delta(\omega)$ is the Dirac delta function, $i = \sqrt{-1}$, and ω is the angular frequency. The mean-square value of the signal is the value of the autocorrelation function at zero time delay, i.e., R(0). The variance of the signal is $R(0) - \mu^2$. (There is some arbitrariness in where the 2π factor is placed in the power spectral density function; $S(\omega)$ as given here is consistent with the result that the mean-square value of the signal equals $\int_{-\infty}^{\infty} S(\omega) d\omega$, which by symmetry is $2 \int_{0}^{\infty} S(\omega) d\omega$.)

The statistical properties of the signal are seen to depend in a simple manner on the shape of the pulses and their average arrival rate. It is important to note that the shape of the power spectral density curve is given by the Fourier transform of the pulse shape and does not depend on the average arrival rate. The arrival rate is only an amplitude factor. In this connection one might recall the sound of audience applause; as more people begin to clap one senses an increase in the noise intensity but no shift in the spectrum.

As stated earlier, the basic model is flexible enough to allow for a more complex field. Consider the case in which the pulses all have similar shapes but differ in amplitudes. If the pulse amplitude A is a random variable with finite variance, and if $f(t)$ now represents the basic pulse shape, the new results are identical to the proceeding ones, with the following exceptions: α is replaced by $\alpha\bar{A}$ in the expression for the mean, and by αA^2 in the expressions for the autocorrelation and psd, where the bar denotes the average value (ref. 67). The model can be further generalized to allow for a variety of pulse shapes to exist in the field. If n different wave shapes are considered to be present in the field, then n linear systems are to be assumed, with each having as input a train of Poisson distributed unit impulses. The average arrival rate for each type of pulse must be specified. The total signal is the sum of the outputs from each of the systems. The analysis is greatly simplified if all of the input pulse trains are considered to be statistically independent of each other (the cross-correlation functions are not zero, however, because each signal has a nonzero mean). The results may be written as

$$\text{Mean:} \quad \mu = \sum_i^n \mu_i = \sum_i^n \alpha_i \int_{-\infty}^{\infty} f_i(t)\, dt$$

$$\text{Autocorrelation:} \quad R(\tau) = \mu^2 + \sum_i^n \alpha_i \int_{-\infty}^{\infty} f_i(t) f_i(t+\tau)\, dt$$

$$\text{Power spectral density:} \quad S(\omega) = \mu^2\, \delta(\omega) + \frac{1}{2\pi} \sum_i^n \alpha_i \left| F_i(\omega) \right|^2$$

As the final generalization one can again consider that for each wave shape there is a distribution of amplitudes. In this case the α_i are replaced by $\alpha_i \overline{A_i}$ in the expression for the mean, and by $\alpha_i \overline{A_i^2}$ in the remaining two expressions.

The remaining portion of this section will be devoted to a crude testing of the statistical features of the model. As noted earlier, the shape of the power spectral density curve depends only upon the shape of the waveform and not upon its amplitude or average arrival rate. Thus the shape of the psd curve is the easiest model feature which can be tested by comparisons with published data. A one-waveform family will be used here and the comparison data will be that of Kendall (refs. 18, 68).* Kendall published spectral data obtained over a wide range of Mach numbers from the JPL 20-inch tunnel. The spectra amplitudes were plotted using an arbitrary scale and hence only the shapes of the curves are available. The "test" of the model is merely that of seeing if one can find a pulse shape, $f(t)$, which suits the data and which is physically plausible in some sense. An infinite number of pulse shapes can give the same psd; unfortunately, there is no pulse-shape data available for guidance here. Concerning further testing of the model it may

*Spectrum data for M = 4.5, Re/cm = 7.2×10^4 was obtained from private communication to I. E. Beckwith from J. M. Kendall, Feb. 1976.

be noted that in most experiments a high-pass filter is used, and thus the value of the mean of the signal is not available for comparison purposes. In these cases one may use f(t)'s based on what is expected in the free-stream, and the preceding equations may still be used providing the μ's are ignored. The mean-square value of the signal reported should correspond closely to the signal variance (depending on how much of the low-frequency portion of the spectrum was removed), and thus to the models' R(0) with the μ ignored.

Before presenting the test results, it is instructive to consider some general spectral properties of simple pulse shapes. Some of the remarks presented are based on findings from rather limited experimentation with different wave shapes. As may be seen from equation (1), F(0) is just the integral of f(t). Thus the shape of the spectral curve at the low frequencies is largely determined by the area under the f(t) curve. This is clearly illustrated in figure 4, where the psd curves for two pulse shapes are shown. The so-called N wave pulse has equal positive and negative area lobes, and its psd is approaching zero as $\omega \to 0$. In striking contrast, the triangular pulse, which has only one lobe, has a psd which is approaching its maximum at $\omega = 0$. The figure also illustrates other characteristics of simple pulse shapes. The N wave psd has its maximum at ω/ω_o near 0.7, where ω_o is 2π times the reciprocal of the time duration of the pulse. This is true of many shapes which have the symmetry property of the N wave and which have leading and trailing shocklets; such shapes have a maximum psd in the region of $\omega/\omega_o = 0.65 - 0.75$. If smoother signatures are considered by eliminating the leading and trailing shocks, the ω/ω_o value of the psd maximum approaches 1.0. If lopsided pulses which have nonzero integrals of f(t) are considered, the greater the lopsidedness the greater the value of S(0), and as the value of S(0) approaches and exceeds the existing maximum, the frequency of the maximum will approach zero. Concerning the dips in the psd of the N wave, these represent zeros of $F(\omega)$. Such zeros occur under certain conditions of symmetry or certain conditions where the crossover point in the signature divides the T interval rationally. While there are any number of wave shapes which have cyclical zeros in the psd, these should be considered as special cases. Generally there will be oscillations in the psd, and these become less as the wave shapes become more lopsided. This behavior is illustrated by the triangular wave in the figure. As the final observation, one may note that the high frequency drop-off rate for each of the signatures shown in the figure appears to be equal. This is not a coincidence and is due to the fact that both signatures have discontinuities. The smoother the pulse shape, the faster the psd decays with increasing ω. In general, if the k^{th} derivative is discontinuous, $F(\omega)$ behaves as $1/\omega^{k+1}$ at infinity (ref. 69) and hence $S(\omega)$ behaves as $1/\omega^{2k+2}$. This is nicely illustrated in figure 5, where the psd for triangular pulses are shown for conditions of zero and finite rise times. With a zero rise time the function itself is discontinuous, whereas for the cases of finite rise time as shown in the figure, the first derivative is discontinuous. The decay rate for the two finite rise time waves are seen to become equal at the high frequencies, and the decay rate for these waves is faster than for the zero rise time, or shock type, signature. Ideally one could examine measured spectra and determine whether shocklets were present in the wave signatures by merely looking at the spectra decay rate, but in practice the very high frequencies are often questionable because of transducer resonances, instrument roll-off, and decrease in signal to noise ratio.

The model test procedure will now be discussed. The procedure was to first select a basic wave shape with time duration $T = T_o$. Because one can expect a distribution of T's to be present due to variations in convection velocities and size of noise sources, eight families of wave shapes were used. They all

had the same shape and differed only in the value of T. The greatest average arrival rate was assumed to occur for $T = T_o$, and the rate dropped to zero for $0.3\ T_o \geq T \geq 1.7\ T_o$. The assumed distribution of relative average arrival rates vs. T resembled a discretized sine curve (positive portion only, with a maximum at T_o and zero outside of the $0.3\ T_o$ to $1.7\ T_o$ range). The selection of this distribution was rather arbitrary; no experimentation with different distributions has been attempted yet. A noise model in which the basic wave shapes are similar and only the time durations differ is a very convenient model. With this model the values of psd vs. ω/ω_o need be generated only once for the basic shape. Each point of the final psd representing the combined family case is obtained by a weighted average of the point on the basic psd curve with points over a limited range to each side of it. The procedure essentially amounts to a smoothing of the original psd curve. Once a basic wave shape was selected and the above smoothing procedure applied, the resulting curve of psd vs. ω/ω_o was compared with the data of Kendall. In figure 1 of reference 18 Kendall presented hot-wire spectral data obtained at a number of different tunnel Mach numbers. The data were presented in the form of a linear plot of power density on an arbitrary scale vs. nondimensional frequency. To make the present comparisons the data had to be read from the figure (a small one and accurate readings were difficult to obtain) and the nondimensional frequencies were converted to raw values. The data points for each Mach number were then overlaid on a log-log plot of the calculated model psd curve. The data plot was then shifted about to see if a match was possible. Shifting the plot vertically is permissible because absolute amplitudes have not been specified in either the data or the calculated results. Shifting the plot horizontally is equivalent to changing the ω_o of the data. Once a basic wave shape had been found which gave a good psd curve match with the data, the value of ω_o could be determined (the value of ω at the $\omega/\omega_o = 1$ abscissa value). Knowing ω_o the value of the physical length of the "typical" wave shape λ was determined from $\lambda = 2\pi\ u_s/\omega_o$, where u_s is the average convection velocity of the noise sources obtained from the data of figure 2 and estimated values of u_∞. There would be little lengthening of the individual wave signatures from the sources inasmuch as the distance from the walls would not be large in comparison with λ. Thus λ would correspond closely to the size of the typical wall body source, and the "test" of the model was in seeing if the λ was reasonable in comparison with the thickness of the wall boundary layer δ at the acoustic origin of the signals reaching the centerline probe. The values of δ had to be estimated, and the procedure for doing so, and the results, are given in Appendix B.

From testing of simple candidate pulse shapes it became clear that symmetrical shapes, such as the N wave, were not suitable. This is because their low frequency drop off rate is too great. Lopsided candidates, that is, those with nonzero $\int f(t)dt$ were found appropriate. One of the first suitable candidates found was the extended cosine-shaped pulse shown in figure 6. This figure compares Kendall's data (refs. 18, 68, see footnote p. 9) with the calculated spectrum using this particular pulse shape. It can be seen that the result matched the data fairly well with a signature wave length equal to $0.6\ \delta$ to $1.1\ \delta$. These values were deemed acceptable. While the pulse shape shown may seem rather unrealistic, until more information is available concerning typical pulse shapes and speeds, it can suffice. (Other successful shapes were found; some rather similar to the typical jet noise signature educed by Laufer, Schlinker, and Kaplan (ref. 56). This shape is rather triangular, and it is interesting to note that signatures from rockets with large exhaust plumes can exhibit triangular shapes - ref. 70).

Laufer (ref. 57) obtained earlier hot-wire data in the free-stream of the JPL 20-inch tunnel. Power spectra for free-stream Mach numbers at 2.0 and

4.5 were presented on a log-log plot. The Mach 2 high-frequency drop off rate has a slope of -2, and this is consistent with the idea of a noise field with shocklets present in the wave signatures. The Mach 4.5 drop-off rate, however, is greater than the Mach 2 rate. At the highest frequencies measured, approximately 115 kHz for $M_\infty = 4.5$ and 80 kHz for $M_\infty = 2$, the nondimensional Strouhal frequency, $\omega\delta/u_\infty$, at Mach 4.5 is presently estimated to be about 20% higher than the Mach 2 value. Thus one might expect that the upper frequencies for the Mach 4.5 case should be closer to showing asymptotic behavior. Some of the high Mach number data of Kendall also appears to show a drop-off rate which is greater than the low Mach number data. But even the computed power-spectrum curve shows some oscillation about the -2 slope and has not reached its asymptotic behavior, so the departure of data from a slope of -2 may not be significant. Laufer's data were obtained at a higher unit Reynolds number than Kendall's. A comparison of the spectra obtained by aligning the peaks in Laufer's data with the peaks in figure 6 shows that Kendall's data have an earlier high-frequency roll off. One effect which would contribute to such behavior is that of the finite thickness of the shock fronts.

The wall body model has thus been found to rather successfully model the shape of the psd data from Kendall (fig. 6). Whether the simple pulse shape found here would also work for other supersonic tunnels remains to be seen. If it does the procedure would be regarded as an engineering tool for estimating psd shapes in tunnels. There is some reason to believe, however, that the psd shape will not be a universal one. This would be due to the effects of finite shock thicknesses. Later in the report the subject of shock thickness will be discussed. The weaker the shock the thicker it is, and for the very weak shocks associated with the radiated noise, the shock thicknesses can be appreciable. For small to moderate size tunnels operating at low unit Reynolds numbers, the thickness of the shock fronts may form a sizable portion of the individual noise disturbance signal signatures. If this is indeed the case, then the spectrum from such tunnels, plotted on the ω/ω_0 basis, should show earlier high-frequency drop-off than for larger tunnels, with large unit Reynolds numbers. And for a given tunnel, the shock thickness effect would be to cause earlier roll off at the lower unit Reynolds numbers. The low unit Reynolds number data of Kendall shown in figure 6(a) do seem to show slightly less high-frequency energy than the high Reynolds number data. It is estimated later that for a wave strength of $\Delta p/p = 0.002$, a small but rather arbitrary value, the ratio of shock front thickness to signal signature length would be about 0.11 for the low Reynolds number case, and 0.063 for the high Reynolds number test. If these conditions are at all realistic, then it is plausible that different high-frequency behavior should be noticeable. The shock thickness effect would not appear to be the cause of the aforementioned Mach 2 and 4.5 different high-frequency behavior observed by Laufer. It may, however, account for some of the high-frequency differences between Laufer's and Kendall's data. At $M = 4.5$, the ratio of the shock thickness to the signal signature wavelength of Laufer's data is estimated to be about 0.02. This value is smaller than the above estimate for Kendall's data because of Laufer's higher unit Reynolds number. The shock thickness is also inversely proportional to the stream unit Reynolds number. For the Mach 2 case the thickness ratio is 0.04, and this is to be compared to the value of 0.16 for Kendall's $M = 2.4$ case. Because of the higher unit Reynolds numbers, the acoustic shocks under Laufer's test conditions are more abrupt than those in Kendall's tests, and based on this factor the spectra in Kendall's test would be expected to show an earlier high frequency drop-off. The Mach 4 data of Donaldson and Wallace (ref. 5) cover a unit Reynolds number range which encompasses that of Kendall's and show very little effect of unit Reynolds number

on the rate and location of the power spectrum high-frequency roll off. The decay rate is greater than Kendall's data show. No doubt many factors affect the high-frequency portion of the measured spectra. Instrumentation system response is probably one of the more important ones. A discussion of shock thicknesses will be presented later.

As more is learned about the noise field, a more complex model may be needed and the simple model can be generalized as shown here. The equations given here would appear to provide a rational basis for a correlation of noise data from numerous supersonic tunnels. The mean-square value of the signal (actually the variance) varies directly with the average arrival rate of the sound pulses and this rate would in turn depend on the convection velocities of the sources, and hence upon M_∞, and on the number of sources present. The latter would depend upon how many sources were spaced around the tunnel and hence upon the ratio of the tunnel perimeter at the acoustic origin of the signals reaching a probe to some boundary layer thickness parameter (and thus on the length Reynolds number, Re_x and M_∞). The number of sources would also depend upon the longitudinal spacing of the sources, and thus again on Re_x and M_∞ as well as the pressure gradient and heat transfer in the vicinity of the acoustic origins. The shape and amplitude of a typical pulse's f(t) would depend on the distance of the transducer from the wall (nondimensionalized by λ and thus again possibly by some boundary layer thickness); the shapes would also probably vary with M_∞ and Re_x. It is not surprising, therefore, that M_∞, Re_x, and test section perimeter show up in the empirical noise correlation work (refs. 71 to 73).

The author has had some success in estimating the shape of psd curves using the following simple procedure which is based on figure 6. First, the value of $f_o = \omega_o/2\pi$ is estimated and the following factors are then used: psd peaks at $f_{pk} = 0.2\ f_o$; psd is down from the peak by a factor of ½ at $f_{1/2} = 0.6\ f_o$, down from the peak by a factor of 1/10 at $f_{1/10} = 1.5\ f_o$, and similarly, $f_{1/20} = 2\ f_o$, and $f_{1/100} = 4\ f_o$. f_o is given by u_s/λ and this is approximated by $u_s/k\ \delta_{wall}$. The procedure for estimating f_o is thus: (1) compute u_s by multiplying u_∞ by a u_s/u_∞ value selected from figure 2; (2) select k from the k-M_∞ information given in figure 6(b); (3) determine δ at the tunnel wall acoustic origin by computing δ^* using the procedure given in Appendix B (a procedure which can be reduced to evaluating a single mathematical expression) and multiplying by the conversion rates δ/δ^* (a formula for this ratio is also provided); and (4) evaluating $f_o = u_s/k\delta$.

If a detailed plot of the power spectrum is desired, the following expressions may be used. Letting $z = \omega/\omega_o$, the mean-square value σ of the filtered signal band-passed from ω_1 to ω_2 can be represented by

$$\sigma_{z_1-z_2} = A\ \omega_o \int_{z_1}^{z_2} g(z)dz$$

where g is the function describing the psd data of Kendall and A is the amplitude proportionality constant. An approximate representation of the function g is given by

$$g(z) = \begin{cases} -5.56|0.15-z|^{1.02} & 0.03 \leq z \leq 0.7 \\ 0.9687/z^2 & z > 0.7 \end{cases}$$

Substituting and integrating gives

$$\sigma_{z_1-z_2} = A\,\omega_o\,[-2.752\,(0.15-z_1)^{2.02} - 5z_1 - 0.9687/z_2 + 4.061]$$

Letting $z_1 = 0.03$ yields

$$\sigma_{.03-z_2} = A\,\omega_o\,(3.8729 - 0.9687/z_2)$$

and if $z_2 \to \infty$

$$\sigma_{.03-\infty} = 3.8729\,A\,\omega_o$$

If g were to be assumed valid as $z \to 0$ (data is lacking for very low frequencies), then letting ε represent a frequency just slightly greater than zero, the mean-square signal level from ε to ∞ would be

$$\sigma_{\varepsilon-\infty} = 4.00\,A\,\omega_o$$

The integration is not extended to $z=0$ because in this case the value of μ^2 would have to be added to $\sigma_{\varepsilon-\infty}$, and there is no data available for μ.

Some time was spent trying to correlate the noise levels from various tunnels using some of the ideas contained in the present report. The success was mixed. It is likely that in the near future most noise prediction schemes will have mixed success because there appears to be some inconsistencies in the noise data. The most interesting of these involves three tunnels of the flexible-plate-type nozzle design. The three are, in order of increasing size, the AEDC-VKF tunnel D (30 cm × 30 cm, M = 1.5-5.0), the JPL 20-inch tunnel (51 cm × 48 cm, M = 1.6-5.6), and the AEDC-VKF tunnel A (102 cm × 102 cm, M = 1.5-6.0). In the AEDC facilities Donaldson and Wallace (ref. 5) have made Mach 4 hot-wire measurements in tunnel A (note of caution--this data is misplotted in Pate's widely cited reports, ref. 8) and Wallace has made similar measurements in tunnel D (presented by Pate in reference 9 along with the Donaldson and Wallace data). Laufer's JPL measurements (ref. 57) also include Mach 4 data. Over the same unit Reynolds number range the data from the JPL tunnel showed the highest noise level. Conventional wisdom states that for equal Mach number and unit Reynolds number the sound intensity should decrease as the tunnel size increases. The JPL data would be expected to fall between the two AEDC tunnel noise levels. The unusual pattern indicates that there may be something wrong with the data, or something unusual in one of the tunnels, or that the noise predicting concepts need reevaluation.

3. INTERACTION OF NOISE WITH LAMINAR BOUNDARY LAYER

The noise field has herein been considered to consist of wave systems emanating from discrete downstream moving sources. Each individual wave system is further considered to include one or more weak shock waves or shocklets. The interaction between the noise field and the laminar boundary layer is therefore taken to consist of a series of weak shock wave boundary layer interactions. The shocklet-laminar boundary layer interaction is a feature which has not been discussed in the noise-transition literature, and it is the study of this interaction which will be emphasized in the remainder of this report.

The two-dimensional interaction case will be highlighted in the following discussion. Such interactions are not necessarily considered to be the most important or the most prevalent, but they are the easiest to analyze. Strictly speaking, inasmuch as the noise sources are not two-dimensional sources and the radiated shocklet systems are conical, there are no true two-dimensional interaction regions. The simplest interaction case to consider is that of a flat plate. The intersection of a cone with a plane is a hyperbola. But since the relative Mach numbers between the free-stream and the noise sources are often low, the shocklet cone angles are large and the intersecting hyperbolas would have little curvature. The waves can thus be considered as locally planar and the apex region of each interaction as essentially two-dimensional. For sources which do not pass directly above the plate there would, of course, be no two-dimensional region. However, for interactions with bodies of revolution, in contrast to the flat plate case, each impinging shocklet system will produce a two-dimensional interaction region.

The most familiar condition for the shock wave boundary layer interaction is that in which the shock generator is stationary above a flat plate. By way of introduction, it is this stationary shock source case which is considered first. Later, when the noise laminar layer interaction is discussed, the shock system will be allowed to move downstream.

Stationary Shock-Laminar Layer Interactions

The problem of the interaction of stationary weak shock waves with boundary layers has not been considered a practical problem to investigate experimentally (the practical concern was with stronger shocks), but it has been examined theoretically. Much of this work was done around 1950 (refs. 74 to 76) and was usually restricted to the supersonic portion of the boundary layer. The work was abandoned because it was considered too simplified to describe observed shock wave interaction features for the cases of interest. The work is quite appropriate for the present purpose because the waves being considered are indeed weak and there is particular interest in how their strength varies in the outer region of the boundary layer. An allied field of research for this problem is sonic boom propagation. The sonic boom is an example of a weak shock propagating through a nonuniform medium, and a technique widely used in this research, namely geometric acoustics, was also applied to the present problem.

Two-dimensional interactions. - The problem considered first is that of the refraction through the boundary layer of a weak plane shock from a stationary source. The boundary layer in the interaction zone can be considered as a medium in which the fluid properties vary only in the vertical direction. In

wave propagation problems, a medium in which properties vary in only one direction, whether continuously or discontinuously, is often called a "stratified" or "layered" medium. The present problem is therefore the refraction of a weak plane shock through a horizontally stratified medium. The stratified medium presents a much simpler problem than the general nonuniform medium case, but the stratified problem is still difficult and one must often be satisfied with approximate solutions.

One solution technique that is used to solve the stratified problem is to approximate the continuously varying medium properties using a layered model. Here it is assumed that the medium properties in each layer are constant and that discontinuities exist in the properties at the layer boundaries. The propagation problem is then solved by examining the series of reflections and transmissions that occur as the wave reaches each of the interfaces between the layers. One can let the thickness of the layers approach zero, and in the limit obtain a differential equation describing some aspect of the problem. This was the approach used in the early studies of the weak shock boundary layer interaction.

In another solution technique the layered approximation is not used and from the outset the properties of the medium are allowed to vary continuously. But in this case, restrictions are imposed on the nature of the wave and property variations. The geometric acoustic method exemplifies this approach. In this technique, like geometric optics, waves are considered to propagate along ray paths, and ray tubes are used in the analysis.

The analysis for the layered approach to the problem will be discussed first and is based largely on Barry's method of solution (ref. 74). The details of the derivation are presented in Appendix C (which also contains analysis and discussion of the reflected wave field). In the analysis the supersonic shear layer is considered to be composed of a number of inviscid fluid layers which are separated by slip planes. Within each layer the fluid properties are assumed to be uniform. At each slip plane the incident wave splits into a reflected and a transmitted wave. The situation is depicted in figure 7. The change in Mach number across the weak waves is neglected. The heart of the analysis lies in the weak-wave assumption and the requirement that the static pressure and the flow deflection angle remain constant across a slip plane. Linearized theory is used and thus, provided the flow is not transonic, the pressure change across a wave is given by

$$\frac{\Delta p}{p} = \pm \frac{\gamma M^2}{\sqrt{M^2 - 1}} |\theta| \tag{2}$$

where γ is the ratio of specific heats, θ is the flow deflection angle caused by the wave, and the plus or minus sign is used when the wave is compressive or expansive, respectively. The flow deflection angle for the refracted wave is then obtained as

$$\frac{\theta}{\theta_\infty} = \frac{M_\infty}{M} \left(\frac{M^2 - 1}{M_\infty^2 - 1} \right)^{1/4} \tag{3}$$

where the subscript ∞ refers to the conditions just outside the boundary layer. Substituting for θ from equation (2) gives

$$\frac{\Delta p}{\Delta p_\infty} = \frac{M}{M_\infty}\left(\frac{M_\infty^2 - 1}{M^2 - 1}\right)^{1/4} \tag{4}$$

since the pressure is constant across the boundary layer. This equation is the principal result of the shocklet-boundary layer interaction analysis. The equation describes the wave strength as it propagates through the outer supersonic region of the boundary layer. The equation shows that the wave strength increases without bound as the Mach number approaches one. For a number of reasons this predicted behavior is not valid. Equation (2), upon which the result is based, is not valid near Mach one. As the wave strength increases the small disturbance assumption is violated and the three-wave model itself breaks down when the incident wave becomes so strong that the downstream flow is subsonic and thus no reflected wave is possible. While the infinity result is meaningless, the equation does show that focusing can be expected near the sonic line. The behavior of equations (3) and (4) are sketched in figure 8.

The wave strength can also be expressed in terms of the longitudinal velocity fluctuation using linearized theory. The result is

$$\frac{\Delta u}{\Delta u_\infty} = \frac{a}{a_\infty}\left(\frac{M_\infty^2 - 1}{M^2 - 1}\right)^{1/4} \tag{5}$$

where a is the sound speed.

It is easily shown from equation (4) that Δp reaches a minimum at $M = \sqrt{2}$. Thus if $M_\infty > \sqrt{2}$, the wave strength will initially decrease as the wave enters the boundary layer. The minimum at $M = \sqrt{2}$ can be associated with the fact that the nature of the reflected wave field changes from expansion to compression as M becomes less than the $\sqrt{2}$. Relations describing the reflected wave field are also derived and discussed in Appendix C. When $M_\infty > \sqrt{2}$, the value of the Mach number at which the wave recovers its initial strength is given by

$$M_{\Delta p=\Delta p_\infty} = \frac{M_\infty}{\sqrt{M_\infty^2 - 1}}$$

As shown in Appendix C, using oblique shock theory this result can be generalized to

$$M^2_{\Delta p=\Delta p_\infty} = \frac{M_\infty^2\left(\gamma + \frac{\gamma+1}{2}P_\infty\right) - P_\infty(P_\infty + 2)}{\gamma M_\infty^2 - \left(\gamma + \frac{\gamma+1}{2}P_\infty\right)}$$

where $P_\infty = \Delta p/p_\infty$. These equations are plotted in figure 9, and they show that as M_∞ becomes large the value of $M_{\Delta p=\Delta p_\infty}$ comes close to one. Thus the wave can be focused above its initial value only over a range of local boundary layer Mach numbers which are close to one. This becomes especially so when the initial wave strength is weak. Thus for weak waves, the vertical space in the boundary layer in which amplification can occur becomes very small as the stream Mach number becomes large (and it does not have to get very large). Also indicated in the figure are the conditions where the flow downstream of the shock at the pressure recovery point is subsonic.

Equations (3) or (4) have been derived by a number of researchers (refs. 74 to 79) using different methods. Henderson (ref. 80) has also treated the shock wave-boundary layer problem as a refraction process using the

layered profile and polar diagrams of pressure ratio versus deflection angle. Again, only the supersonic portion of the boundary layer was investigated, but a much more detailed discussion of the possible shock systems existing near the sonic line was included. The refraction process was concluded to be regular down to the "triple" point where the flow behind the incident wave is subsonic. Below this point the refraction becomes irregular and a Mach stem was always found to be present. The Mach stem continues to penetrate the layer with increasing pressure rise across it until it bifurcates into a lambda foot. The lambda foot is a complicated shock system containing multiple bifurcations and the process continues down to the sonic line with vanishing strength. Henderson found that weaker waves penetrate the layer further before becoming irregular. The leading leg of the lambda foot must originate from disturbances propagating upstream through the subsonic portion of the boundary layer, and the pressure along the sonic line would have to be obtained from subsonic theory. In a later article Henderson (ref. 81) mentions the fact that in interactions both free precursor and post-cursor waves may be produced in the subsonic flow below the sonic line. These free precursor and post-cursor waves would propagate, respectively, upstream and downstream of the interaction region. It will be noted in a later section that shock refraction experiments do reveal features rather similar to those described by Henderson. In this connection, numerical studies (refs. 82 and 83) of the sonic boom near the sonic line also show triple-point shock behavior as well as distortion of the sonic line upstream of the triple-point location.

The geometric acoustic approach will now be discussed briefly. This is a new approach for the boundary layer interaction problem and the details are given in Appendix D. In geometric acoustics the signal is considered to propagate along rays. The concept of rays is probably a familiar one from studies of elementary optics. Classically the method of geometric optics represents a specialized solution to the wave equation. This solution is for the limiting case of the wavelength of the disturbance approaching zero (ref. 84) (or the frequency approaching infinity). These restrictions are often stated in the manner that geometric optics is appropriate for the case in which the change in the properties of the medium over a wavelength are a small fraction of themselves. The similarities between light and sound propagation have long been recognized, and the criteria for the use of geometric methods are similar for both optic and acoustic propagation. Geometric methods are also appropriate for the propagation of discontinuous weak waves (ref. 85). Keller (ref. 86) has shown that weak shocks could be analyzed by the methods of geometric optics and stated that the theory of weak shocks could be called geometric acoustics. Friedlander (ref. 87) also developed the theory of geometric acoustics out of the need to describe the propagation of sound pulses, and, in fact, describes his book as an essay on the pulse solution of the wave equation. Thus geometric acoustics is eminently suited to the shocklet-boundary layer interaction problem.

Ray tubes and energy considerations are most often used in the determination of wave amplitudes. The ray tube is essentially a bundle of adjacent rays, and is a differential area quantity similar to the stream tube of fluid dynamics. For a plane wave the total energy density is $(\Delta p)^2/\rho a^2$, where ρ and a are the local mean values of the fluid density and sound speed, respectively (ref. 84), and for a nonmoving medium the wave normal direction is in the ray direction. For a stationary atmosphere the energy flow rate is invariant along a ray tube, and this quantity is equal to the energy density $(\Delta p)^2/\rho a^2$ times the volume flow rate aA_n, where A_n is the normal cross

sectional area of the ray tube. The invariant quantity is thus $(\Delta p)^2 A_n/\rho a$. The wave strength therefore depends on the fluid density, sound speed, and ray tube area, and these quantities would vary in a nonuniform medium. For a moving nonuniform medium, such as the horizontally stratified boundary layer, the situation is more complicated. In this case the wave normals and the ray directions no longer coincide and the use of a single velocity will no longer suffice. Blokhinstev (ref. 38) showed that the phase velocity of the wave, which is the velocity of the wave in the direction normal to its wave front, is the sum of the local sound speed and the component of the medium velocity in the direction of the wave front normal. That is

$$c_n = a + \vec{n} \cdot \vec{u}$$

where $\vec{n}$ is the unit vector normal to the wave front. He further showed that the velocity of the energy flow (often referred to as the group velocity), or the ray velocity, is the vector sum of the local sound speed and the medium velocity. That is,

$$\vec{c} = a\,\vec{n} + \vec{u}$$

The relationship between c_n and $\vec{c}$ is illustrated in figure 10. Blokhinstev found that the energy density was $(\Delta p)^2 c_n/\rho a^3$ and the volume flow rate $\vec{c} \cdot \vec{A}$. The invariant energy flow rate was, accordingly,

$$\frac{(\Delta p)^2}{\rho\, a^3}\, c_n\, (\vec{c} \cdot \vec{A}) = \text{constant} \qquad (6)$$

This result has since been derived in a number of other studies (see Appendix D for additional refs). Hayes (ref. 39) used equation (6) to study sonic boom propagation in a nonuniform atmosphere, and the present author found this work most helpful. Hayes refers to the expression in equation (6) as the Blokhinstev invariant. To apply the method to a propagation problem one other fact is needed to obtain the ray paths. For the case of a horizontally stratified medium, Rayleigh (ref. 88) gave a refraction law of the type of Snell's law as

$$a \sec \phi + u = \text{constant}$$

where, as in figure 10, ϕ is the angle of inclination of the wave front normal to the horizontal.

The shocklet-boundary layer solution is obtained by first attaching the coordinate system to the free-stream. In this case the free-stream becomes a uniform nonmoving medium, and the shock source becomes an object moving supersonically through the still atmosphere. The situation is depicted in figure 11. The problem is then very much like the sonic boom problem. The initial ray and wave normal angle conditions are identical, and ϕ is simply related to the Mach angle corresponding to the relative Mach number of the source. The boundary layer becomes a very nonuniform moving medium into which the wave propagates. From equation (6) the desired pressure rise ratio is

$$\frac{\Delta p}{\Delta p_\infty} = \left(\frac{\rho\, a^3}{\rho_\infty\, a_\infty^3} \; \frac{c_{n_\infty}}{c_n} \; \frac{c_\infty\, A_\infty}{c\, A} \right)^{1/2}$$

where the fact was used that $\vec{c}$ and $\vec{A}$ are collinear. The first fraction under the radical may be reduced to a/a_∞ by using the ideal gas law, assuming the static pressure is constant, and using the fact that $a^2 = \gamma RT$. Using the Snell's law, the second fraction can be written as $\cos \phi_\infty / \cos \phi$. Snell's law can be shown to yield the expected result that the wave is always inclined at the local Mach angle. Thus the previous ratio can be reduced to a ratio of Mach numbers. c is related to a, u, and ϕ through the law of cosines, and c_∞/c involves only the Mach number and $\cos \phi$. Using the fact that the horizontal separation distance between two rays remains at its initial value, the ratio A_∞/A may be expressed in terms of the slopes of the ray path. In Appendix D the differential equation of the ray path is derived, and this provides the ray slope information needed to evaluate A_∞/A. When the final results are converted back to the usual tunnel-fixed coordinate system, equation (4) is obtained. The rays are horizontal at the relative sonic line and the ray tube area vanishes. This fact provides the geometric acoustic explanation for why the computed pressure rise across the shock goes to infinity at the sonic line. The sonic line forms an envelope of all the locations where the ray tube areas vanish, and such an envelope is called a caustic. The problem of the pressure rise at a caustic is still a subject of research. According to geometric acoustics, signals do not propagate below the caustic or sonic line, but in reality disturbances do extend into the "shadow" zone. Such effects are considered in diffraction theories.

As just mentioned, geometric acoustics predicts that the shocklet is totally reflected at the caustic and the theory says nothing about what happens below the caustic. The same was true in the layered model approach; the analysis was applicable only above the sonic line. That the shocklet may be considered to be essentially reflected from the sonic line is substantiated by experiment. Surface pressure measurements in shock wave-boundary layer interaction experiments show rather smooth variations along the surface. In sonic boom experiments, pressure traces below the caustic do not show shock-like signatures. But it is known that in wind-tunnel experiments the pressure at the surface downstream of a weak interaction does reach the value that would be expected with no boundary layer present. This cannot be explained by ray theory, but a reasonable explanation can be offered while remaining in the acoustics-refraction milieu. This will now be done by contrasting the sonic boom and wind tunnel experiments.

There is an important difference between the sonic boom case and the usual flat plate shock wave-boundary layer experiment in which the shock is generated by some wedge-shaped body. The pressure wave from a supersonic aircraft typically has the shape of an N wave, and the wavelength of the disturbance is about the length of the aircraft. Most of the energy in the energy spectrum of an N wave is contained in wavelengths which are the order of the length of the N wave or less. These lengths are small in comparison with the large distances over which significant changes in the properties of the atmosphere occur. Thus geometric acoustics is not only applicable to the shocks in the pressure signature but it is appropriate for describing the bulk of the signature itself. One would therefore expect that most of the energy in the boom would be reflected at the caustic. The caustic, in a sense, acts like a low-pass filter, and in this case there is little energy to pass. The low-pass nature of the caustic is well known. Both theory and experiment show that below the caustic there is rapid attenuation in frequency and amplitude of the signal (refs. 89 to 91).

In typical shock wave-boundary layer interaction experiments, the wedge

generates a shock signature which is essentially a step function. The energy in the step function varies as $1/\omega^2$, and thus the bulk of the energy is in the low-frequency realm. The wavelengths containing most of the energy are therefore very long in comparison to the thickness of the boundary layer (the nonuniform medium). This is just the opposite of the sonic boom case. Even though the sonic line filters the shock and its attendant high frequencies, the bulk of the signal in the step function would be passed, with the very longest wavelengths being affected very little. It may be noted that in studies of the interaction of sonic booms with very small scale atmospheric inhomogeneities, the low frequencies are thought to pass relatively unchanged (e.g., ref. 92). Thus, from a refraction viewpoint, the surface pressure distribution would be expected to show a smooth variation, with the pressure level reaching that expected for the no boundary layer case. An allied and interesting but difficult experiment to conduct would be that of finding the effect of the shock body length on the surface pressure distribution beneath a laminar boundary layer. In this connection, an interesting basic problem to think about is that a compression shock, according to the usual fluid mechanics viewpoint, reflects from a free shear layer as an expansion system, yet geometric acoustics says that a shock should come from the sonic line. Thus, in contrast to the classical fluid mechanics view, does a shock exist in the wave reflected from a free shear layer?

Reflected wave system. - In the layered Mach number approach to the interaction problem, a reflected wave field was seen to exist along the entire shock front inside the layer. In the outer region of the boundary layer this reflected field is weak, but it can have a cummulative affect. Some sample calculations are presented in Appendix C (based on Marble, ref. 75) which show how the outer edge streamline is turned by the reflected field. In this interaction model the reflected shock observed in experiments is considered to be the result of the coalescence of the reflected compressive wave field originating near the sonic line. According to the model, the strength of the reflected wave is infinite inasmuch as the incident shock strength increases without bound.

In the geometric acoustic approach the partially reflected wave field in the outer boundary layer region is not an evident feature of the analysis. In fact, for a nonmoving medium the energy is conserved in the geometric acoustics approximation and no partial reflection of energy along the way is predicted (see ref. 84, p. 313, and ref. 93, p. 89). In the moving medium case there is an exchange of energy between the flow and the waves (see ref. 94, p. 325). The incident wave is reflected at the caustic and becomes singular in nature. The theory says that upon reflection there is a componentwise phase shift of $\pi/2$ (ref. 95). For shock shapes this shift is consistent with a singular reflected wave.

In Lighthill's interaction study, ref. 77, an incoming wave with a discontinuous increase in pressure or pressure gradient was found to reflect as a positive logarithmic infinity of these quantities. The logarithmic singularity in the reflected wave of a shock passing through a caustic has also been found in the linear sonic boom study of Fung & Seebass (see Appendix of ref. 90). As Lighthill mentions, it is perhaps realistic to expect that a shock step would be reflected from the sonic line as a pressure ridge (a rapid compression followed by a rapid expansion).

Three-dimensional interactions. - It is quite likely that the three-dimensional interaction will be the most prevalent form of the noise-laminar layer

interaction. On a flat plate, for example, all sidewall sources will produce three-dimensional interactions. Even for sources passing directly overhead, the radiated shocklet systems will consist of oblique or swept waves except in the apex region of the interaction. Obviously, the three-dimensional interactions are more complicated than the two-dimensional ones, and for this same obvious reason the present author does not have much to say about them.

For the case of a sonic boom propagating through a stationary atmosphere with a linear vertical sound speed gradient, Barger (ref. 96) has shown that the ray tube area can go to zero only on the ground track directly below the aircraft. If winds in the direction of the ground track are present, which is analogous to the two-dimensional boundary layer case (view the situation with the coordinate system attached to the free-stream), it would appear that the conclusion of Barger would still hold. Thus it can be inferred that in the shocklet-boundary layer interaction, caustic conditions can exist only directly below the shocklet source. It is not clear just how rapidly the maximum local focusing diminishes away from the "ground" track, but the focusing variation would no doubt depend on the Mach number and the distance of the shock source from the boundary layer.

In the sonic boom case there apparently has been some concern over the focusing conditions at the cutoffs away from the ground track (lateral cutoffs - see refs. in 97; the term cutoff refers to the termination of the shock system). Ray-tracing computer programs using geometric acoustic methods predict that infinite-like shock focusing can occur (ref. 97). Measurements of sonic booms near lateral cutoff conditions have shown caustic-like pressure signatures but the intensities were found to be very low (ref. 97). Ray-tracing computer programs (ref. 39) could be applied to the boundary layer case to study the lateral cutoff conditions, but it is likely that such programs, which usually use four rays to define a parallelogram-type ray tube, would compute a zero minimum area as the lower two rays pass through their turning points and head back out into the free-stream.

In oblique interactions the rays experience cross flow as they enter the boundary layer, and they thus tend to turn in the streamwise direction as they traverse through the boundary layer. One might initially think that the wave front normals would also tend to line up with the flow, but no such turning occurs. In a stratified medium, such as the flat plate case, the heading or azimuth of the wave normal in the planview remains constant along a ray (ref. 98). This means that, in the planview, the basic hyperbolic shape of the shock-boundary layer intersection does not change very much as the shock penetrates the layer.

As a final observation it is noted that the rays in the oblique interactions enter the boundary layer less steeply than do those in the two-dimensional interaction case (those along the ground track). It might be expected that these shallow rays do not penetrate the boundary layer as much, and this is indeed true. In the flat plate case the rays become horizontal, or parallel to the plate, when the flow Mach number component in the direction of the rays initial azimuth (in the planview) is unity. Thus the greater the obliquity of the ray in the planview, the greater is the flow Mach number and y/δ at which the maximum penetration is reached (δ is boundary layer thickness). Since the greatest local focusing probably occurs at these turning points, the height of this focusing increases with increasing distance from the apex region of the shock-plate intersection hyperbola.

Examples of Focusing of Weak Shocks

Most of the study within the last 15 years of the phenomenon of weak shock wave propagation has been done in connection with the sonic boom. Shock focusing investigations have been conducted both in the laboratory and in the field. In the laboratory, shock focusing has generally been studied by reflecting shocks from concave mirrors or by letting the shock refract through a nonuniform medium. The laboratory has the advantage of a well controlled environment, and shock shapes can be studied by optical means. Shocks from shock tubes, electrical sparks (they produce N waves), and supersonic projectiles have been used. There are problems associated with undesirable but important diffraction effects originating at the edges of mirrors, and there are pressure measurement resolution problems owing to the small scale of the shocks from the spark sources and projectiles. In the field studies the medium is the atmosphere and the shock wave source is usually a supersonic aircraft. In level flight, focusing and caustics can occur due to the sound speed gradient in the atmosphere; caustics can also be generated by aircraft turns and accelerations. Because of the greater length and time scales involved, detailed pressure signatures can be obtained. Of course no shadowgraph or Schlieren data are taken. The distinct disadvantage lies in the uncertainty of many of the important experimental parameters. It is also difficult to have enough pressure transducers at the right locations. A few results from some laboratory and field investigations will be presented here. The literature on laboratory and field investigations of sonic boom and underwater shock focusing is rather extensive.

In a short survey article dealing with the sonic boom, Carlson (ref. 99) briefly mentioned a laboratory experiment of shock focusing by Barger. In this experiment shock focusing by thermal gradients was produced by firing a supersonic ($M_\infty = 1.1$) projectile through a heated chamber. No pressure data is given, but three Schlieren photographs are presented for the cases of strong, moderate, and no thermal gradients perpendicular to the flight path. For the strong gradient case, where the speed of sound near the center of the chamber equaled the projectile speed, the shock fronts (bow and tail shocks) are seen to become normal to the flight path and to lose their identity. It is interesting to note that no reflected waves appear to be visible.

A somewhat similar experiment is briefly described in reference 100. The vertical sound speed gradient was produced by the mixing of air and CO_2. One schlieren photograph is shown along with a sketch illustrating its features. The leading shock was found to penetrate into the theoretical zone of silence, and no reflected shock is shown. The trailing shock exhibited a Y-shaped configuration near the caustic. The triple point was found to be the zone of maximum intensity. The authors state that the triple point is lower for the rear shock then for the front one; this statement is puzzling in view of the absence of a Y-shaped triple-point behavior in the front shock. A focus factor, defined as the ratio of the maximum Δp to that for the case of a homogeneous medium, of 1.7 was measured.

The most thorough of the ballistic range experiments has been that of Sanai, Toong, and Pierce (ref. 101). An air-CO_2 mixture produced the sound speed gradient. The Y-shaped triple-point configuration was found to exist, with the cusp portion extending to near the sonic cutoff region. A sketch of the situation is shown in figure 12. For very weak shocks the triple point was nearly coincident with the cutoff altitude, and as the input shock strengths were increased the triple point moved away from the cutoff height. The

greatest focusing occurred near the triple point where a focus factor of 1.7 was found.

The two most thorough field investigations of sonic boom focusing have been conducted by the French working group on sonic booms (ref. 100) and by a group headed by NASA Langley (refs. 90 and 97). Mostly ground level microphones were used by the French group (in one phase nearly 50 microphones were placed over a distance of about 5000 meters). For steady supersonic flight the rays at a caustic resulting from atmospheric refraction are nearly horizontal and hence this type of focusing is difficult to investigate with ground level instrumentation. This group thus concentrated on focusing resulting from aircraft maneuvers and low- and high-altitude linear accelerations. A maximum focus factor of 5 was measured for the acceleration and steady turn conditions and a factor of 9 was recorded for a turn-entry condition. The NASA group instrumented a 450-meter tower with microphones every 30 meters. For the steady flight case where the caustic occurred near mid-tower, both incident and reflected waves were detected by the microphones near the top of the tower. Near the caustic the signatures changed from the characteristic N wave shape to a U shaped configuration. Below the caustic the signature degenerated rapidly from the U shape into a signature containing no pronounced peaks (an auditory rumble was experienced rather than a boom; in an Appendix to ref. 97 Fung and Seebass presented computational estimates of the acoustic pressures below the caustic, and good agreement with the data was obtained near the caustic). A characteristic of the pressure signature near the cutoff condition was that pressure pulses (precursor waves) were frequently evident propagating ahead of the well-defined shock waves in the signature. A representative caustic focus factor for the steady flight conditions was considered to be 1.8. Except in the immediate vicinity of the caustic, geometric acoustics was found to be adequate for describing the shock shapes.

It is apparent from these experiments that the refraction process of a weak shock wave in a medium in which a sonic cutoff is present bears a rather strong resemblance to the process that was described earlier in the discussion of the weak shock-laminar boundary layer interaction. The triple-point configuration of Henderson's analysis (ref. 80) was found in the refraction experiments. The lambda foot bifuraction feature would be very difficult to detect in these experiments, but perhaps the precursor waves in the sonic boom field experiments are a manifestation of this process (Friedman & Chou (ref. 102) show how waves can get ahead of the shock near the cutoff; Myers and Friedman (ref. 103) also show that precursors can be expected). The shift of the N wave shape to the double-peaked U wave shape near the caustic shows shock shape behavior that is qualitatively in agreement with one of Lighthill's results of his boundary layer interaction analysis (ref. 77). Thus the present hypothesis that the laminar boundary layer focuses weak incoming shocks in the noise field appears to be reasonable.

Noise-Laminar Layer Interaction

The main point of the preceding discussions on shock behavior is that theoretical and experimental evidence leads one to believe that shocklets in the radiated tunnel noise field are focused within the laminar (and turbulent) boundary layers on wind tunnel test models. The emphasis in the paper will now shift to an exploration of this phenomenon.

In proceeding from a discussion of the stationary shock-boundary layer

interaction to that of the noise-laminar layer interaction, essentially three new features have to be considered: (1) the sources of the noise field travel downstream; (2) the streamwise length of the individual pressure signature is finite; (3) the boundary layer is subjected to continuous strafing due to random arrival of the waves. The first item must be considered to determine at what height within the boundary layer focusing will occur. The second item removes the problem from the infinite duration step shock realm. The last item is important because the mean fluctuation levels increase as more disturbances arrive.

Thickness of weak shocks. - A factor which has been considered, but not adequately discussed, is the thickness of the acoustic shocks. Actually, this element of the problem was overlooked until the investigation was nearly completed. This oversight occurred because of the habit of thinking that shocks are very thin. They indeed may be considered thin for most applications, but the present application is an unusual one. Here very weak shocks are considered as they propagate through the tunnel free-stream and inside thin laminar boundary layers. As will be seen shortly, the thickness of a weak shock is inversely proportional to the shock strength and the stream unit Reynolds number, and hence the shock thicknesses presently considered are greater than the shock thicknesses one normally considers. It is therefore conceivable that the thickness of the acoustic strength shock could be comparable to the thickness of the laminar boundary layer through which it is propagating in the acoustic-laminar layer interaction. Indeed, as was indicated earlier in connection with the modeling of the free-stream disturbance spectra, under low Reynolds number conditions the shock thickness may possibly exceed 10% of the source tunnel wall turbulent boundary layer thickness. Under such conditions, as discussed earlier, it is quite likely that measured spectra could show an early high-frequency roll off because of the smoother signal signatures associated with thicker shock fronts. This may well be one of the physical manifestations of finite thickness shock fronts, but an important issue to resolve in regard to the present work is to what extent does the discontinuous shock front approximation affect the appropriateness of the present analysis. The answer would appear as follows. (1) While the shocklet-boundary layer interaction should now be envisioned with finite thickness shock fronts, the refraction analysis is still valid because it is good for the high-frequency Fourier components of the signal regardless of the individual disturbance signature shapes, but the amount of focusing predicted assuming abrupt shock fronts should be considered an upper bound because shock fronts with finite thicknesses have less high-frequency energy to be focused. (2) The model of the pulse shapes used in the analysis of free-stream disturbance statistical properties should be altered to include finite thickness shock fronts. Before pursuing this any further, the matter of the shock thickness should be resolved. Appendix E contains the details of the derivation of the expressions for the thickness of a shock.

Inasmuch as the fluid properties vary smoothly through a shock, the definition of a shock thickness, like that of the boundary layer thickness, involves an arbitrary definition of the "edge" of the nonuniform region. The boundary layer edge is defined as the location where the velocity reaches some fraction f of the free-stream velocity, and likewise the shock thickness is defined as the distance over which the velocity change is a fraction f of the free-stream velocity. Letting Δ be the shock thickness based on f, it is shown in Appendix E (based on an analysis by Taylor and Maccoll, ref. 104) that for weak shocks the shock thickness Reynolds number may be represented by

$$Re_{\Delta} = \frac{8\gamma}{3} \frac{M_s^2}{M_s^2 - 1} \ln \frac{1+f}{1-f} \tag{7}$$

where M_s is the shock Mach number. This result is appropriate for oblique shocks if the shock Mach number normal to the wave is used. For air, $\gamma = 1.4$, and the shock Mach number and strength are related by (ref. 105, eq. 93)

$$M_s = \sqrt{\frac{6P}{7} + 1}$$

where $P=\Delta p/p$, and hence the shock thickness Reynolds number may also be expressed as

$$Re_{\Delta} = \frac{8\gamma}{3} \frac{6P + 7}{6P} \ln \frac{1+f}{1-f} \tag{8}$$

For very weak shocks $P << 1$ and the fraction $(6P + 7)/6P$ may be replaced by $7/6P$ and the shock thickness in air may be closely approximated by

$$\Delta = \left(\frac{4.356}{P} \ln \frac{1+f}{1-f}\right)/\text{unit Re} \tag{9}$$

This equation is the basis for the earlier statements that for weak shocks the thickness is inversely proportional to the shock strength and the unit Reynolds number.

The issue of the appropriateness of the refraction formulas will now be confronted. The refraction formulas are appropriate for high frequency signals or high frequency components of signals. To qualitatively assess the amount by which a theory based on the zero-thickness shock front might over predict the extent of focusing, one can comparatively examine the high frequency content of the zero- and finite-thickness shock front signals. As discussed earlier in the report, the zero-thickness shock signal has a spectrum with the slowest high frequency roll off. Shocks with finite thicknesses will have greater roll off and hence will have relatively less high-frequency energy which can be focused. The more abrupt the shock front the higher the frequency at which the ultimate roll off will begin. This is just a complicated way of stating the obvious fact that the more abrupt the wave front the more the signal will behave as a zero-thickness shock signal. A measure of the abruptness would be the ratio of the shock thickness to the signature wavelength, and in accordance with the idea that the signature wavelength is proportional to the radiating wall boundary layer thickness, the ratio may be represented by Δ/δ_{tw} where δ_{tw} is the thickness of the boundary layer on the tunnel wall. The smaller this ratio, the more the signal behaves as a zero-thickness shocked signature and the more appropriate the focusing predictions will be.

To get an idea of the magnitude of this ratio, eq. (9) was used with $P = 0.002$. δ_{tw} typically varies from about 1 cm for small tunnels to 10 cm for large tunnels. The unit Reynolds number range also varies considerably. A quick examination of refs. 106 and 7 to determine unit Reynolds number ranges for tunnels at NASA Langley and AEDC, respectively, shows that for tunnels in the Mach number range of 2 to 5 the Reynolds number per centimeter values typically fall in the 1.5×10^4 to 4×10^5 range. Thus for small tunnels ($\delta_{wall} = 1$ cm), Δ/δ_{tw} would vary from 0.9 to 0.03 and for large tunnels ($\delta_{wall} = 10$ cm) the ratio would vary from 0.09 to 0.003. The conclusion from this exercise is that for small and moderate tunnels operating at low unit Reynolds numbers the finite thickness of the shock front may occupy a significant portion of the individual disturbance signal signatures. In such cases

the focusing formulas may appreciably overestimate the maximum amount of focusing by the laminar boundary layer. Obviously, further study is needed to determine the quantitative effects of shock thickness on focusing.

Earlier in the report shock thickness estimates were presented in connection with spectra measurements of Kendall (ref. 18) and Laufer (ref. 57). The particulars for these estimates will now be provided. Concerning Kendall's $M = 4.5$ results in figure 6(a), the two unit Reynolds number conditions were 3.9×10^4 and 7.2×10^4 per centimeter. For the $M = 2.4$ case in figure 6(b), the unit Reynolds number was 3.9×10^4/cm. As given in Appendix B, the respective wall boundary layer thickness estimates are 4.01, 3.66, and 3.03 centimeters. The ratio of shock thickness to signature wavelength was computed from $\Delta/k\delta_{tw}$ using eq. (9) with $k = 0.78$ for $M = 4.5$ and 0.67 for $M = 2.4$ (from fig. 6). P was rather arbitrarily taken as 0.002 (P no doubt changes with M). The resulting ratios for the three conditions were, respectively, 0.11, 0.063, and 0.16. Laufer's spectra were given for $Re_{\theta_{wall}} = 30000$ for $M = 2$ and $M = 4.5$. Interpolation in tables of JPL tunnel boundary layer thickness and flow condition data of Dayman (ref. 107) provided the following unit Reynolds number and boundary layer thickness estimates corresponding to $Re_\theta \approx 30000$: $M = 2$, $Re/cm = 1.43 \times 10^5$, $\delta^* = 0.68$ cm (interpolating in Table 1 of Dayman), and using $\delta/\delta^* = 4.221$ from Shapiro's textbook (ref. 108), $\delta = 2.88$ cm; $M = 4.5$, $Re/cm = 1.32 \times 10^5$, $\delta^* = 2.50$ cm (using $M = 4.54$ results in Table B-1), $\delta/\delta^* = 2.186$, $\delta = 5.46$ cm. The values of k for $M = 2$ and 4.5 were taken, respectively, as 0.85 and 0.78. With $P = 0.002$, the resulting value of $\Delta/k\delta_{tw}$ were 0.037 for $M = 2$ and 0.024 for $M = 4.5$. These values are smaller than those for Kendall's conditions due to the larger unit Reynolds numbers in Laufer's tests.

There is one other ratio of interest, and this is the ratio of the shocklet thickness to the flat plate laminar boundary layer thickness, Δ/δ. The adiabatic laminar boundary layer thickness is given by

$$\delta = \frac{\sigma x}{\sqrt{Re_x}} \tag{10}$$

where σ depends on the free-stream Mach number and the value of $f = (u/u_\infty)_{y=\delta}$. Using equations (7), (8) and (10), the desired ratio is simply

$$\frac{\Delta}{\delta} = \frac{D/\sigma}{\sqrt{Re_x}} \tag{11}$$

where, in terms of either shock Mach number or shock strength,

$$D = \begin{cases} \dfrac{8\gamma}{3} \dfrac{M_s^2}{M_s^2 - 1} \ln \dfrac{1+f}{1-f} \\ \dfrac{8\gamma}{3} \dfrac{6P + 7}{6P} \ln \dfrac{1+f}{1-f} \end{cases} \tag{12}$$

For $f = 0.995$, a common value used for boundary layers, Mack (ref. 109) has determined σ for a number of free-stream Mach numbers for air, and a least-squares fit to his findings gives

$$\sigma = -0.02\, M_\infty^3 + 0.57\, M_\infty^2 - 0.31\, M_\infty + 6.12$$

Using equations (11) and (12) it is now a simple matter to determine the thickness ratio for a given free-stream Mach number and shock strength. Some representative results for $f = 0.995$ are displayed in figure 13. In the case of tunnel noise it is not clear just what values of M_s or P are appropriate, but the smaller values in the figure may be suitable. If so, then for laminar boundary layers, where Re_x would typically be less than, say, 3×10^6, it is likely that the acoustic shock thicknesses are of the order of the laminar boundary layer thickness in the noise-laminar layer interaction.

General features. - This section is devoted to a description of some of the general features of the interaction between an individual noise-field pressure disturbance and the laminar boundary layer. Additional details of some of the features will be presented in a later section. The emphasis is on the two-dimensional interaction. In the first part of the discussion the interaction is viewed as an inviscid wave refraction problem in which a boundary layer response is precluded and the boundary layer does not add to the fluctuation levels. This point of view is appropriate for the very high frequency components of the noise field because in this case the wavelengths are so small that they cannot shake the relatively immense boundary layer. A conjectural description of the low frequency behavior of the pressure wave will also be offered based primarily on known results from the stationary shock interaction case. This is done so that when the full problem is considered a better appreciation can be had of the boundary layer contribution to the fluctuations. Mack (refs. 40 and 41) has calculated the forced response of the laminar boundary layer to an acoustic field, and he has shown that at the lower frequencies large fluctuations can be induced in the layer. This section will close with a brief review of his results.

As a preliminary matter, the continuous arrival of the noise disturbances simply means that the average level of the fluctuations at a point in the flow increases in proportion to the average arrival rate of the disturbances (see the previous section DESCRIPTION OF NOISE MODEL). The disturbances are considered to arrive randomly in time, so there is no excitation of the boundary layer because of periodic arrivals.

In the shock refraction problem it is the relative Mach number between the wave and the flow that is important. The relative Mach number is, in fact, the proper one to use in the wave strength equation (4). For a stationary shock the relative Mach number and the flow Mach number are of course the same, but if the shock moves downstream, the relative Mach number is decreased. As a consequence of this, in a boundary layer interaction with a downstream moving shock the height of the caustic layer is raised. This is concretely illustrated in Figure 14, where a Mach number profile for a Mach 4 laminar boundary layer is shown along with a relative Mach number profile for the case of a shock moving downstream with a speed of $0.7\ u_\infty$. The Mach number profile was obtained using the boundary layer program of Price and Harris, (ref. 110) and the relative Mach number is found in this case by $M_r = M - 0.7\ M_\infty \sqrt{T_\infty/T}$. The figure shows that the height of the caustic layer increased from $0.38\ \delta$ to $0.92\ \delta$ as the shock speed changed from 0 to $0.7\ u_\infty$. The variation of the caustic height with convection speed of the shocklets in the noise field is a significant feature of the noise-laminar layer interaction. The heights of the caustic layers associated with the noise field will be discussed in greater detail in a later section. In general, these heights lie in the outer half of the boundary layer.

As an individual pressure disturbance penetrates the laminar boundary

layer the strength of the shocklets in the wave signature will vary according to equation (4). Whether the nonshock portions of the pressure wave (the lower frequency components) tend to change in strength according to the equation depends upon how closely the geometric acoustic requirement is met that the acoustic wavelength must be small in comparison with the length scale of the nonuniform medium. The latter length may be characterized by the thickness of the laminar boundary layer. The length of the incoming pressure signature can be characterized by the thickness of the nozzle turbulent boundary layer (most of the acoustic energy is contained in wavelengths which range from somewhat less than the signature length to longer than this length). The important ratio is therefore that of the tunnel wall boundary layer thickness to the laminar boundary layer thickness on the model, and as can be imagined, this ratio is certainly not less than one and in fact can be very large near the leading edge of the test model. Thus it appears likely that geometric acoustics will be appropriate only for the shocklets in the pressure wave, and as previously discussed, there may be conditions when it is not even appropriate for these owing to their finite thickness. This of course says nothing about the low-frequency behavior, but it will be assumed that the very low frequencies are not focused. At the caustic the pressure signature might therefore appear as it did in the free-stream with the exception of pressure spikes appearing at the shocklet locations as a result of the focusing. The shocklets would be reflected at the caustic as pressure spikes, and below the caustic the signature would be shock free. Incidently, it is not unusual for sonic boom signatures to show spikes, and these are attributed to small scale nonuniformities in the atmosphere (refs. 92 and 111).

Below the caustic is an extended subsonic region. In this region, based on theoretical and experimental results for the stationary shock case, upstream spreading of the pressure wave would be expected (and downstream as well). In the theoretical analysis of upstream propagation of unsteady disturbances in the supersonic boundary layer, Schneider (ref. 112) has found that low-frequency large-wavelength disturbances with small phase velocities can propagate many boundary layer thicknesses upstream in the subsonic portion of the boundary layer. The damping coefficient was found to decrease with decreasing frequency. For a given frequency, the damping coefficient also diminished with decreasing Reynolds number. Some theoretical work (ref. 77) on the stationary interaction case shows that at a given interaction station the upstream influence is greater for the lower unit Reynolds numbers (and thus for the thicker boundary layers). But a survey, done in connection with Appendix C, of some of the shock-boundary layer interactions experiments in which weak shocks were used shows that the data is not consistent on this point (upstream influence $\simeq$ 10 δ). With the thicker subsonic regions in the downstream moving shock case, it seems reasonable to assume that the upstream influence of the interaction would be greater than for the stationary case. Dore (ref. 113) studied the problem of the interaction of a slowly moving shock with the boundary layer and found that the upstream influence was greater for a downstream moving shock than for a stationary one. The thickness of the subsonic region is a maximum when the relative Mach number just becomes -1 at the surface. This occurs for downstream speeds of 0.5 u_∞ for $M_\infty \geq 4$, and the corresponding thickness is about 0.7 δ for $M_\infty \geq 4$ (the thickness for the stationary case is 0.4 δ for $M_\infty \geq 2.5$).

Below the caustic the wave form is thus considered to be distorted by the absence of shocklets and by the spreading of the wave. Whether the spreading significantly distorts the signal would depend on the extent of the upstream spreading in comparison with the wavelength of the pressure signature.

If the relative Mach number of the flow is supersonic near the wall (where the flow velocity will be reversed as indicated in fig. 14), downstream spreading (i.e., towards the aft end of the model) would cease. There would be a tendency toward wave coalescence into shocklets, but is unlikely that a shocklet could form before the disturbance reached the wall because of the short distance involved. The magnitudes of relative (reversed) supersonic Mach numbers at the wall are low. For example, the fastest moving shocklet in a Mach 16 tunnel has a relative Mach number at the wall of only -2.4.

Whether the relative flow is subsonic or supersonic next to the wall, presumably at the surface there is pressure doubling for the bulk of the signature. As the signal propagates back toward the free-stream after the surface reflection, it would undergo the complicated processes similar to that which occurred on its incoming journey. If and when shocklet coalescence occurs, it would likely be in the free-stream inasmuch as the outer supersonic layer is relatively thin. Disturbances which have spread upstream may also have generated very weak pressure waves which radiate into the free-stream.

Summarizing, if the boundary layer behaves passively, the interaction process might be as follows. The shocklets in an incoming wave are focused at the caustic and the caustic signature is thus a spiked one. These spiked or pressure ridged portions of the signal are reflected at the caustic back into the free-stream. This is illustrated in figure 15, where the length scale of the disturbance has necessarily been greatly compressed. Below the caustic the signature is shockless and undergoes spreading. The spreading pressure field may generate weak signals which also propagate into the free-stream. The main rounded signature (the lower frequency components) reflects from the solid surface, with pressure doubling at the surface, and propagates back into the free-stream with possible additional spreading in the subsonic region. Shocklets may eventually reappear in this portion of the signature due to the nonlinear coalescence process, but this is likely to occur outside the boundary layer. The reflection and outward progression of the low-frequency portion of the signal is not shown in figure 15. The incoming and outgoing signals would occupy much of the same physical space inside the laminar boundary layer and even in regions well outside of the layer. Transducers monitoring the noise field near but outside of the laminar boundary layer, for example, would receive a mean-square signal contribution from the incoming and outgoing signals which, because of the spatial correlation, would not just be the sum of the squares of the two signals.

One other item should be mentioned. The region behind the leading edge shock from a flat plate model is, in the geometric acoustic approximation, shielded from noise sources passing beneath the plate. In reality a diffracted signal field should exist in the so-called shadow zone. The strength of this field may be weak (no one has made calculations), but it would be strongest near the leading edge of the model.

To contrast with the passive boundary layer response viewpoint the results of Mack (refs. 40 and 41) will be considered (the more complete results are in ref. 40). By a slight modification to his numerical compressible boundary layer stability code, (ref.109), Mack was able to calculate the forced response of the laminar boundary layer to an incoming acoustic field. His numerical results should thus reflect the refraction-diffraction aspects of the problem (not the above mentioned leading edge diffraction problem) as well as the reaction of the boundary layer. For this purpose, Mack modeled

the noise field as disturbances coming from a downstream moving sinusoidal wavy wall. The speed of the wall was taken to be slow enough so that the stream flow was supersonic with respect to the wavy wall. In this situation the disturbances propagate away from the wall along the Mach lines in the downstream direction. At any given distance from the wavy wall the pressure pattern is a sinusoidal one, and this signal is taken to represent one Fourier component of the noise field. Mack studied the interaction of this incoming moving pressure field with a parallel flow flat plate laminar boundary layer.

This form of the incoming noise field was quite suited to the modification of the method of solution Mack used in his stability calculations. In the stability problem analytic solutions of the linear stability equations in the free-stream provided initial conditions for the numerical integration from the edge of the boundary layer to the wall. Two of the independent analytic solutions resembled incoming and outgoing sinusoidal acoustic waves, and in the stability calculations, the incoming solution was rejected. For the forced response of the boundary layer it was necessary only to incorporate the incoming acoustic wave solution. The addition of a solution which matched a wavy-wall acoustic boundary condition eliminated the eigenvalue nature of the problem, and what was being calculated for a given wavy-wall wave number and wave speed was the steady state forced response of the laminar boundary layer to the sound field. Mack actually has two computer programs; one for the viscous theory and one for the inviscid theory in which viscosity is neglected while retaining the laminar boundary layer profile (a simpler system of equations to solve). Forced responses were generally computed using both programs, and of course for the viscous program, a Reynolds number condition for the laminar boundary layer needed to be specified.

With regard to the relevancy of the steady-state type calculations to the pulse-shaped randomly arriving waves which have been emphasized in the present report the following comment can be made. As discussed earlier in the report, for randomly arriving wave pulses only the signature for a single pulse need be considered. The Fourier components of a single pulse have infinite time durations (the components cancel each other except where the pulse occurs), and Mack's wavy wall can be considered to represent such a component. Mack presents all of his results in the form of the ratio of the rms value of the computed quantity to that of the input level at the edge of the boundary layer, and by doing so he is essentially mapping out what would be called the transfer function for the boundary layer.

To be particularly applicable to the experimental work of Kendall (refs. 17 and 18), most of Mack's calculations were done for a free-stream Mach number of 4.5 and a wave speed of 0.65 u_∞ (some limited results were obtained at M_∞ = 5.8 and 7.0). The frequencies chosen for investigation were in the range where Kendall found most of the acoustic energy. In terms of the ratio of the wavelength to laminar boundary layer thickness, λ/δ, one finds that these values ranged from about 10 to 350. Relatively speaking, the computations thus illustrate the response of the boundary layer to low-frequency acoustic excitation.

Inasmuch as the hot-wire anemometer in the experiments was sensitive primarily to mass-flow fluctuations, Mack's results, with one exception, are in terms of ratios of this quantity, although results for a large variety of flow variables were computed. For any combination of Reynolds number, wave speed, and frequency, the fluctuation level was found to peak within the

boundary layer. Only one disturbance profile has been published (ref. 114 , also shown in ref. 58) and the fluctuations peaked where the relative Mach number was one (which was indicated to be near 0.8 δ). The significance of this was not clear because at a lower Reynolds number the height of the peak increased by 20 percent.

For all conditions tested the ratio of the peak rms mass-flow fluctuation level to the incoming rms level, m_p/m_i was found to grow starting at the leading edge, and to reach a maximum value whose x distance and magnitude were inversely proportional to the frequency, and then to decrease slowly (fig. 9, ref. 40; also in ref. 58). From the passive boundary layer behavior viewpoint one expects less interesting things to happen as lower frequencies are examined. The trend found by Mack of greater peak fluctuations with decrease in frequency clearly shows that the boundary layer is reacting to the acoustic field. The maxima of the m_p/m_i were in the range of 10 to 17. (Incidentally, there does not appear to be a correlation between the magnitude of m_p/m_i and the nearness of wave number, wave speed, and Reynolds number conditions to an eigencondition of stability theory.) One wonders whether calculations at higher frequencies would show the trend of decreasing m_p/m_i with increase in frequency to reverse itself as geometric acoustic conditions are approached. Similarly, for a given frequency, would the slow decay downstream of the peak change to growth as small λ/δ values were reached?

For a single frequency, some results showing the effect of wave speed were obtained (ref. 40). At lower Reynolds numbers the boundary layer response increased monotonically with increasing wave speed. At higher Re values the maximum response occurred for a wave speed of 0.65 u_∞. Viscous results were not obtained for wave speeds below 0.4 u_∞, but the results appeared to show that the response would continue to decrease for slower speeds.

Some limited results on wave obliqueness (ref. 40) showed that there was little change with obliquity until the wave angle approached the condition where the relative Mach number was one. Near this condition the boundary layer response decreased abruptly.

Ratios of the rms value of the fluctuating pressure at the wall to that of the incident wave at the edge of the boundary layer were obtained for two-dimensional waves traveling at 0.65 u_∞ ($M_\infty = 4.5$). At any Re_x there was a pressure doubling at the wall for the very lowest frequencies, and at the higher frequencies, the surface pressures dropped with increasing frequency. It appears that the surface pressures are less than the free-stream pressures for $\lambda < 10\delta$.

The final results to be mentioned are the ratios of the rms reflected-to-incident amplitude levels at the edge of the boundary layer (two-dimensional, $M_\infty = 4.5$, wave speed = 0.65 u_∞), (ref. 40). For any given Re_x, this ratio approached one as the frequency approached zero. For increasing frequencies, the ratio would drop to some minimum, climb to a value greater than one, and then asymptotically return to the value of one. The inviscid result showed that the reflected to incident energy was greater than one for $0 < \omega < \infty$. The acoustic interaction apparently can set up conditions which allow the boundary layer to locally extract energy from the free-stream. For a given frequency, the Reynolds number condition at which the greatest energy is absorbed does not coincide with the Reynolds number condition for which m_p/m_i is a maximum. Roughly speaking, for a given frequency the maximum value of m_p/m_i occurs at the Reynolds number condition where the boundary

layer just begins to radiate more energy than it receives.

In summary, using sophisticated techniques Mack has illustrated the behavior of the laminar boundary layer to low-frequency acoustic excitation. The results show that the interaction is a complex one and that viscous effects are quite important. Even in the inviscid case the boundary layer may be considered to interact actively in all but the extreme cases at very low and very high frequency acoustic fields. Whether the computations could be extended to the very high frequencies to recover geometric acoustic behavior is not clear, but for now Mack's findings and the present ones concerning the shocklet behavior may be considered complementary. Mack has shown that very large low-frequency fluctuations can occur in the outer region of the boundary layer (and in at least one case at the caustic layer height), but unfortunately little information has been given concerning the heights of the peak fluctuation levels. There is much experimental data available for comparison purposes on the heights of the peak fluctuation levels.

Height of caustic region. - The caustic layer is the region within the boundary layer where the fluid velocity is sonic relative to the incoming noise shocklet. With u_s representing the shocklet downstream source velocity, this relation may be expressed as

$$u - u_s = a \tag{13}$$

where a is the local sound speed. Where this condition occurs obviously depends on the laminar layer profile and the shock velocity. To use the Mach number and velocity profile results obtained from the computer program of Price and Harris (ref. 110), it is more convenient to write equation (13) in terms of u/u_∞ and M. Letting $\eta = u_s/u_\infty$, the equation can be written as

$$\frac{u}{u_\infty} = \frac{\eta M}{M - 1} \tag{14}$$

For a given M_∞ and η, one can use the computed boundary layer profile information and, by trial-and-error, determine the value of y/δ for which equation (14) is satisfied. This has been done for shocklet speeds from 0 to 0.9 u_∞ over a free-stream Mach number range from 2 to 12, and the results are shown in figure 16. For $M_\infty \geq 5$ the caustic layer heights are remarkedly insensitive to M_∞ and they increase nearly linearly with the shock speed ratio u_s/u_∞. Also shown in the figure are some Mach 6 and Mach 8 cooled boundary layer results ($T_w/T_\infty = 4$). The effect of cooling is to depress the caustic heights. This effect is most pronounced near the wall.

The next desirable step would be to indicate at what height the noise field caustic region would likely lie for a given tunnel Mach number. Inasmuch as figure 16 shows that the caustic layer height depends directly on the shock speed ratio, the problematical issue of the convection speeds of the noise field must be faced. While the source of the radiated field is the turbulent boundary layer on the nozzle wall, there have been no experimental efforts to determine what flow structures are providing the radiation. There have been subsonic experiments in which cross-correlation measurements were taken with a wire in the boundary layer and a surface pressure transducer beneath the layer, and there have been correlations obtained with two wires in the boundary layer. The most extensive set of cross-correlation and convection velocity measurements has been of the surface pressure fluctuations.

Broadband subsonic and supersonic surface pressure convection velocity results have been compiled and are shown in figure 17, and the data show, with a couple of exceptions, that the measured convection speed varies with the pressure transducer streamwise separation distance Δx. For the smallest separations ($\Delta x \simeq 0.5\ \delta^*$, where δ^* is the boundary layer displacement thickness) the broadband convection velocities are around 0.55 u_∞ to 0.60 u_∞, and as the separation is increased, the measured convection velocity increases and reaches a value of about 0.8 u_∞ for Δx greater than, say, 10 δ^*. It may be noted that in visual studies of the low speed turbulent boundary layer, transverse eddies have often been observed in the outer region. These large eddies give the boundary layer edge its corrugated appearance, and the speeds of the centers of these eddies are in the 0.8 - 0.9 u_∞ range. The variation in measured convection velocity with transducer separation distance is generally explained in terms of the coherency of the large eddies. At large separation distances only the large eddies retain coherency; hence at these distances the correlation results reflect the faster speeds of these outer eddies. Using a novel optical technique to detect surface pressures, Emmerling and co-workers (ref. 127) have found large pressure patterns (length $\sim \delta$, span $> \delta$) which travel with speeds up to 0.9 u_∞ as well as small but intense patterns (scale $\sim 0.1\ \delta$) with convection velocities down to 0.2 u_∞. The turbulent boundary layer can thus supply a wide range of speeds for potential noise radiation sources. As seen in figure 16, caustic layer heights for speeds of 0.2 u_∞ and greater lie in the outer half of the boundary layer.

The trend of increase in surface pressure convection velocity with increase in transducer separation distance is found in both low and high speed boundary layers. The particular variation pattern, however, may be a little different for the radiated pressures at the higher Mach numbers. At $M_\infty = 4.5$, Kendall (ref. 17) made cross-correlation measurements in the free-stream with two hot-wires at various separation distances. The present author has estimated that the nondimensional separation distance in these measurements, $\Delta x/\delta^*$, varied over the range of 1.5 to 7.7, where δ^* is the estimated displacement thickness of the nozzle boundary layer at the acoustic origin of the signals reaching the wires ($\delta^* = 1.64$ cm, as estimated in Appendix B). Dividing the separation distances by the time delays of the correlation peaks, little variation of u_s/u_∞ with separation distance was found, with $u_s \simeq 0.7\ u_\infty$. Based on the surface pressure data one would expect to find a variation in the measured convection speed for the range of $\Delta x/\delta^*$ values covered. In the same tunnel and at the same Mach number, Laufer (ref. 57) had earlier found a convection velocity of 0.53 u_∞ by applying the distance-time division technique to a wide-band cross-correlation curve. Laufer's wires, however, had a separation distance of about 1/4 that of the smallest value used by Kendall. Thus the trend of decrease in measured convection speed with decreasing transducer separation distance also appears to exist for the radiated pressure field; however, at this Mach number the relative separation distance, $\Delta x/\delta^*$, apparently must be quite small before the decrease occurs. Using the single-wire technique Laufer (ref. 2) had previously measured convection velocities in the range of 0.42 u_∞ to 0.45 u_∞. This result may be viewed as being consistent with the later findings in that a lower limit was found as $\Delta x \to 0$. Even with these apparently consistent results, the question persists as to their meaning or interpretation. The dual-wire technique discriminates against signals which decrease in coherency between the wires. As the wires approach each other the discrimination factor becomes less important because losses in the coherency decrease. For wires which are very close together, it is experimentally difficult to obtain accurate dis-

persion results; in the limit of just one wire this capability is lost altogether. The one-wire result represents some sort of weighted average of what is happening at a point, and the measured convection speed could, for example, reflect the influence of a few strong signals or perhaps the influence of many weak ones.

Intuition is not infallible when trying to associate frequencies with scales and speeds of disturbances. Consider, for example, the case of signals from two similar families of shocklet-radiating flow structures which have the same average arrival rate at any point (i.e., each family has, on the average, the same number of flow structures passing a point per unit of time). If one family travels slightly faster than the other, its power spectrum will be shifted to higher frequencies and the high end of the combined spectrum would be dominated by the faster family. But if the fast family is too fast, contrary to intuition, the slow family can dominate the upper end of the spectrum. This can happen because the average signal level decreases as the speed increases due to the shorter individual pulse time durations. Thus, while the power spectrum shifts to the right by an amount proportional to the time duration of the pulses, the spectrum level also drops by an amount inversely proportional to the pulse duration squared, and if the speed is too great its spectrum level can drop below that of the slow family, even at the high-frequency end. As a second example, consider the case of flow with two families of turbulence structures present, each having the same average arrival rate, with one having long structures and the other short ones (both of the same amplitude). Recall that earlier it was shown that the behavior at the low-frequency end of the spectrum depends upon $\int f(t)dt$, where $f(t)$ is the typical individual eddy signature and the integration is over the length of the signature. If the longer structures have disturbances such that the integral is nearly zero, then the power spectrum approaches zero as the frequency goes to zero. If the $\int f(t)dt$ for the shorter family is nonzero, then this latter family would dominate the spectrum at the low frequencies. Thus the low frequency portion of the spectrum depends on the shapes of eddy structures and not just on their sizes. In these examples, dispersion measurement results could be altered if one family has a much greater average arrival rate than the other or if one family has much greater signal amplitudes.

In the real flow case there seems to be some evidence that the dispersion in the radiated noise field decreases with increase in Mach number. Laufer commented in reference 48 (p. 57) that the weak maximum in the cross-correlation curves at the lower Mach numbers suggested that the convection occurs over a wide range of velocities. It was mentioned earlier that Owen et al. (ref. 7) did not find dispersion in two Mach 7-8 tunnels. This possible trend is somewhat vexing because at the higher Mach numbers there is a greater speed range over which Mach wave radiation can occur. Perhaps the concentration of speeds with increase in Mach number, if this in fact happens, is the result of the very low densities near the wall. Perhaps the inner structures cannot radiate as effectively as the larger and faster outer structures which lie in a much greater density flow. The very high convection speed of 0.95 u_∞ found in a Mach 20 helium tunnel is probably near to the speed of the outer layer structures, but no dispersion measurements were made (the single wire result of ref. 3 was confirmed later with the dual-wire technique (ref. 128)). Incidently, concerning the dispersion in the surface pressure fluctuations beneath a turbulent boundary layer, there do not appear to be consistent findings. In both subsonic and moderate supersonic experiments one can find cases where the convection velocity increases with decreasing

frequency (refs. 124 to 126, 129 to 132) and other cases where this trend is abruptly terminated by a low-frequency region where the speeds rapidly diminish (refs. 133 to 137).

Returning now to the question of what convection velocity ratios should be used to locate the caustic region heights of the tunnel noise field, the answer seems to be that at any given Mach number no single speed is sufficient. It may well be that at the higher Mach numbers a smaller range of speeds would be appropriate, but this remains to be concretely demonstrated. But just to show a possible trend of caustic region height with tunnel Mach number, the speeds corresponding to the bounds of the data shown in figure 2 were selected (a straight line parallelogram-shaped boundary was used) and the result is shown in figure 18. This figure is misleading because the small scatter in the Mach 2 and Mach 8 data makes it appear as though there is greater certainty in the corresponding caustic region heights. This problem is especially noticeable at $M_\infty = 2$ where Laufer indicated that a variety of speeds appeared to be present. To remedy the situation, dashed lines have been added joining the caustic layer heights for $u_s/u_\infty = 0.2$ and $u_s/u_\infty = 1 - 1/M_\infty$ (fastest possible for Mach wave radiation) at $M_\infty = 2$ with the corners of the parallelogram in the figure. The tolerance band at $M_\infty = 4.5$ encompasses the dispersion found by Kendall. If the dispersion does decrease with increasing M_∞ and the primary noise sources become the outer layer eddy structures, then the main feature of the height of the noise field caustic region would be the increase in the height of the lower bound with increasing tunnel Mach number.

Estimate of focusing strengths. - The linear theory predicts that the pressure rise across an incoming shocklet becomes infinite at the caustic. A more realistic estimate of the maximum amount of focusing is obviously desirable. The previously discussed sonic boom experiments showed that focus factors at a caustic produced by refraction in those cases were actually not very great. Results from sonic boom theory and experiment were used in the present effort to estimate typical focus factors for the shocklet-laminar boundary layer interaction and this procedure will be discussed below. But first it is of interest to consider some simple results using oblique shock theory. In all of the work in the present section it is assumed that shocks of essentially zero thickness are entering the shock refraction region. It should be kept in mind that very weak shocks with their finite thickness would not be subject to the same degree of focusing.

The relation between the local Mach number M* and the shock strength for which subsonic flow exists downstream may be derived from oblique shock theory and is

$$M^* = \sqrt{\frac{6P^2 + 18P + 7}{6P + 7}}$$

where, again, $P=\Delta p/p$.

Simultaneous solution of this equation with the shock refraction equation (4), written as

$$\frac{P}{P_\infty} = \frac{M^*}{M_\infty}\left(\frac{M_\infty^2 - 1}{M^{*2} - 1}\right)^{1/4}$$

provides the means of determining the values of P and Mach number where the three-wave model breaks down and the irregular Mach stem refraction begins. This has been done for a number of free-stream Mach numbers and initial wave

strengths, and the results are shown in figure 19. The figure clearly shows that the weaker the initial wave strength $\Delta p_\infty/p_\infty$ and the further the free-stream Mach number is from $\sqrt{2}$, the closer the value of M^* comes to one. The figure also shows the amount of focusing which occurs at the point where the refraction ceases to be regular. The weaker the initial strength and the closer the free-stream Mach number is to $\sqrt{2}$, the greater is the degree of focusing. The greatest amount of focusing shown in the figure is $\Delta p^*/\Delta p_\infty = 2.7$ (for $\Delta p_\infty/p_\infty = 0.001$). Values obtained by this method should be considered as lower bounds, for it is likely that some additional focusing will occur. But if the results from previously discussed shock focusing experiments as well as the results to be given below are a valid guide, then these lower-bound values are within a factor of, say, three of the maximum amount of focusing.

In sonic boom theory, scaling laws have been developed to describe the strength of the boom in the vicinity of a caustic. The scaling law may be written in the form (ref. 82)

$$\frac{C_{p_{max}}}{C_{p_{ref}}} = \text{Constant} \times \left(\frac{d/r}{(\gamma+1)\, C_{p_{ref}}} \right)^{1/5} \tag{15}$$

where C_p is the pressure coefficient and the reference location is some point away from the caustic; d is the distance of the reference location to the caustic line, and r is the radius of curvature of the shock ray path at the caustic. The constant must come from an analytic or numerical solution to the full nonlinear problem or from experiment. From approximate calculations Gill & Seebass (ref. 82) obtained a value of 2.8 for the constant (in later calculations it appears that a greater $C_{p_{max}}/C_{p_{ref}}$ was found, see figure 10 of reference 83, but no estimate of the scaling law constant was given). Other versions of the scaling law exist. Sanai, Toong, and Pierce (ref. 101) used a law of the form

$$\frac{\Delta p_{max}/p}{\Delta p_{ref}/p} = \text{Constant} \times \left(\frac{2\, d/r}{\Delta p_{ref}/p} \right)^{1/5}$$

and from their ballistic range experiments found their constant to be 1.3. They also examined some of the data of the NASA sonic boom tower experiments and estimated the constant to again be 1.3. There is enough information given in the ballistic range experiment to apply equation (15) and evaluate its constant, and when this is done a value of 2.01 is found ($d = 1.29$ cm, $r = 14.14$ cm, $\Delta p_{ref}/p = 4.5 \times 10^{-2}$, $M_{ref} = 1.09$, $M_{\Delta p\ max} = 1.04$). The 2.01 value is about 30 percent less than the 2.8 value of Gill & Seebass. To estimate the focusing strength in the laminar boundary layer the value of the constant was taken as 2.8 and used in equation (15). It should be noted that the scaling laws show that the weaker waves are focused more, that is, they have higher focus factors. This behavior is similar to that of the lower bounds established earlier.

To use equation (15) three tasks had to be completed: the boundary layer profile specified, the value of r determined, and the value of $C_{p_{ref}}$ obtained. The calculations were limited to two tunnel Mach number conditions: $M_\infty = 4$ and 8. These limited results were thought to be sufficient to indicate the

magnitudes of the focus factors which may be expected in the boundary layer. The velocity and temperature profiles were approximated rather crudely. The T/T_∞ temperature profiles shown in Van Driest (ref. 138) were roughly approximated using cubic polynomials. The u/u_∞ velocity profiles were approximated by straight lines in the linear region, and these were tangentially joined by a circular arc which completed the profile to the outer edge. Specific information about these simulated profiles is given in Appendix F (wherein it is revealed that the Mach 8 temperature profile used is a very poor one).

Some of the details of the tasks of determining r and selecting the reference location are given below. The reader primarily interested in the results is invited to examine figure 20 and to skip to the last paragraph of this section. Complete details concerning the determination of the radius of curvature at the caustic are provided in Appendix F.

Letting η be the ratio of shocklet source convection velocity to free-stream velocity, it is shown in Appendix D that the differential equation of the ray path is

$$\frac{dy}{dx} = \frac{\sqrt{\left(\frac{u}{u_\infty} - \eta\right)^2 M_\infty^2 \frac{T_\infty}{T} - 1}}{\left(1 - \frac{u}{u_\infty}\right)\left(\frac{u}{u_\infty} - \eta\right) M_\infty^2 \frac{T_\infty}{T} + 1} \tag{16}$$

Using this equation, the radius of curvature of the shock ray path of the caustic was obtained by two methods. Both methods utilize the well known formula from calculus for the radius of curvature of a plane curve. Inasmuch as the slope of the ray path is zero at the caustic, the radius of curvature formula reduces to simply the reciprocal of d^2y/dx^2 evaluated at the caustic. With $Y = y/\delta$ $X = x/\delta$, the radius at the caustic becomes

$$\frac{r}{\delta} = \frac{1}{\left.\frac{d^2 Y}{d X^2}\right|_c}$$

where the c refers to caustic conditions. Since $dy/dx = dY/dX$, the first method involved differentiating equation (16), evaluating the result at the caustic, and then taking its reciprocal. From equation (16) one finds that the caustic is located where

$$\left(\frac{u}{u_\infty} - \eta\right)^2 M_\infty^2 = \frac{T}{T_\infty}$$

Since T/T_∞ was approximated by a cubic polynomial, the caustic was located by the solution of a cubic polynomial in the region where the velocity profile was linear. In the outer region of the boundary layer the location would be obtained by a solution of a sixth degree polynomial. This solution could be obtained numerically, but motivated by this additional complexity and by the possibility that in many cases only tabulated profile data would be available, another approach to obtaining the radius was followed. In this approach the ray path differential equation (16) was integrated numerically from the edge of the boundary layer to the vicinity of the caustic. (Some plots of ray paths and deviation of the ray path angle from the wave normal angle are shown in Appendix F). The radius of curvature was then found by the following

simple device. A parabola with vertical axis was least-squares fitted through some of the final points (a collocating parabola worked well also), and the vertex of the parabola was deemed the caustic location. The radius of curvature of the parabola at its vertex is simply the reciprocal of twice the coefficient of the squared term. Results from this approximate method were in excellent agreement with those obtained from the first method.

The radius of curvature results are presented in figure 20. The figure illustrates that there is little difference between the two Mach number results and that the slower convection speed sources have the larger radius of curvature at the caustic. Because the maximum focusing strength varies as $r^{-1/5}$, the faster sources would be expected to be focused the greatest. The range of u_s/u_∞ which has been found experimentally (see fig. 2) is indicated on the figure, and it is seen that the corresponding range of r/δ is from 0.4 to 0.7 for $M_\infty = 4$ and 0.25 to 0.3 for $M_\infty = 8$. For the focusing calculations the conditions corresponding to convection velocities of 0.5 u_∞ for $M_\infty = 4$ and 0.7 u_∞ for $M_\infty = 8$ were selected. Incidently, the horizontal traverse of a ray from the point of boundary layer entry to the caustic varied from about 1/4 δ to 1-1/4 δ for the conditions shown in the figure. Some ray trajectories in the Mach 4 boundary layer for various source speeds are shown in figure 21.

The final item needed to estimate the boundary layer focusing is the reference point location and conditions. The most convenient choice for the reference point location would be a point at the edge of the boundary layer; at this height $C_{p_{ref}}$ would be C_{p_∞}, and the ratio of $C_{p_{max}}/C_{p_{ref}}$ would in this case essentially be the focus factor. In general, however, it would be wrong to select this location. In the analysis of the caustic problem, the solution to the nonlinear governing equation approaches the solution to Tricomi's equation for large y, and it is the solution to the Tricomi equation for large y which thus forms the appropriate boundary condition for the caustic problem (refs. 139 and 140). This requires the signal strength to vary as $y^{-1/4}$ at large y. Such a behavior is consistent with geometric acoustic behavior near a caustic. Near the caustic the gradients may be considered as being linear, and in this case the ray path is circular and the ray tube area varies as $y^{1/2}$. Inasmuch as the signal strength varies inversely as the square root of the ray tube area, the strength thus varies as $y^{-1/4}$. It may be noted that equation (4) exhibits this behavior as the caustic is approached. Thus, to apply the scaling laws, the reference point should be taken away from the caustic and yet be close enough so that the $y^{-1/4}$ behavior occurs. For the two Mach number and convection velocity conditions chosen for the calculation, the relative Mach number between the free-stream and wave is greater than $\sqrt{2}$ in both cases. Thus the wave strengths initially decrease upon entering the boundary layer. The reference distance d was conveniently taken as the distance from the caustic to the height where the wave strength recovered its free-stream value. For this reference location the wave strength behavior should be close to the desired $y^{-1/4}$ variation. The choice is convenient because $\Delta p_{ref}/p = \Delta p_\infty/p$. The relative Mach number at the reference height was obtained from

$$M_{ref} = \frac{M_\infty (1-\eta)}{\sqrt{M_\infty^2 (1-\eta)^2 - 1}}$$

as may be determined from equation (4) (in its relative Mach number form) by setting $\Delta p/\Delta p_\infty = 1$. The relative Mach number at the location of the maximum focusing was taken to be 1.0 (appropriate since $\Delta p_\infty/p$ is so small).

The typical free-stream strength of individual pressure waves is not known. Three values of $\Delta p_\infty/p$ were assumed for the calculations; $\Delta p_\infty/p$ = 0.01, 0.001, and 0.0001. It turned out that the focus factors, $\Delta p_{max}/\Delta p_\infty$, for the two Mach number and convection velocity conditions were nearly identical. For the three values of $\Delta p_\infty/p$, the focus factors were, respectively, 2.5, 4.0, and 6.3. If these factors are at all realistic, the focusing within the laminar layer would not appear to be very great.

The search for experimental evidence of a caustic region. - The obvious place to look for existing evidence of caustic layer behavior is in the experimental supersonic stability-transition literature. There have been a number of investigations in which the laminar boundary layer was surveyed with the hot-wire anemometer and disturbance profiles obtained. The profiles typically show a region where the rms level of the fluctuations reach a maximum. As possible evidence of the existence of the caustic region, the heights of these peaks must be compared with the expected caustic region height. This is done in figure 22, where the heights of the data peaks from a number of investigations have been superimposed on the caustic region results from figure 18. Some of the data points are from conical models and the results have been plotted at the local Mach number values. Because the cone shock refracts the noise shocklets there is some question as to whether such data should be used. Limited calculations, as will be mentioned later, show that it might be appropriate to do so for lower stream Mach numbers ($M_\infty \leq 4.5$), but calculations have not been performed for the extreme condition at $M_\infty = 19$. The figure shows that for tunnel Mach numbers greater than about three the data fall within or near the caustic region. At lower Mach numbers there are some cases in which double peaks were found, and in these cases the upper peaks also fall within the caustic region. On the whole, the experimental results do not appear to contradict the caustic region concept. But before the figure can be interpreted as establishing the existence of the caustic region, two issues must be considered. Since the data come from hot-wire (and hot-film) anemometers, one must first assess the likelihood that the noise field caustic region could be detected with this type of instrumentation. Second, other possible causes of the flow fluctuations must be considered. Concerning this latter issue, there are at least three possible candidates for the source of the peaked disturbance profiles. Two of these have been discussed previously: the low-frequency forced response of the laminar boundary layer as computed by Mack, and the high-frequency and shocklet forced response as described by geometric acoustics. The third candidate is the Tollmien-Schlichting instability wave phenomenon from boundary layer stability theory. In fact, until recent years the peaks in the disturbance profiles were usually attributed to boundary layer instability behavior. These issues will now be discussed.

The hot-wire anemometer responds to mass-flux and total-temperature fluctuations. In a tunnel the radiated noise field induces such fluctuations in the free-stream by virtue of the fact that the waves are moving downstream. The sound field is thus detectable with the hot wire, but this fact is obvious since the instrument has been used for years to measure tunnel noise levels. For the detection of shocklet and high frequency focusing near the caustic the transducer must have a good high-frequency response. This can be a problem with the hot-wire anemometer. Estimates of the frequency response of the hot-wire system are not always reported. To examine the behavior of

frequencies whose wavelengths are the order of the thickness of laminar boundary layers a frequency response of into the hundreds of kilohertz would likely be needed. This may be beyond system limitations in many cases.

The hot-wire is sensitive to velocity fluctuations in the mean direction of the flow. Thus, as the caustic is approached the wave fronts refract and become nearly normal to the flow, and the signal would have a tendency to increase regardless of whether or not the wave was being focused. At the caustic the power spectrum should show an increase in the energy at the high-frequency end of the spectrum due to the caustic focusing. But because the energy level will generally be quite low at this end of the spectrum, it is likely that moderate increases would have a very small affect on the overall mean-square value of the signal. Inasmuch as the mean-square signal levels are found to be greatly enhanced at the height where the fluctuation levels peak, it seems likely that this phenomenon may also be attributed to lower frequencies which are not associated with the caustic focusing. This is not to say that caustic layer phenomena may not be present, but rather that low frequency oscillations are likely dominating the mean-square signal level and the mean-square level cannot be used to infer results about the presence or absence of caustic layer behavior. What apparently is needed is disturbance profile information taken with a very high-pass filter, or else an examination of individual pressure disturbances on an oscilloscope for evidence of pressure wave spiking. With one exception it appears that such information has not been obtained. Kendall mentioned (ref. 18) some findings of filtered signals and these will be discussed in connection with the double peak results.

The data peaks represented in figure 22 may be primarily the result of the low frequency forced response of the boundary layer or of Tollmien-Schlichting (TS) instability wave oscillations. Until Mack's forcing theory results became available, the location of the peak fluctuation height was often referred to as the critical layer. The term critical layer is a progeny of boundary layer stability theory. In the early studies of instability, the inviscid incompressible stability equation was first studied. There is a singularity present in this equation when the wave speed matches the local flow speed and an infinite velocity perturbation is predicted. The height within the boundary layer where this matching condition occurs became known as the critical layer. Unstable TS waves at the lower Mach numbers are relatively low-frequency phenomena. From Mack's stability calculations (fig. 12.2 of ref. 109) one may find that the shortest wavelength of an unstable TS wave at $M_\infty = 2.2$ is about 10 δ. At higher Mach numbers (like 10) the wavelength can get down to around δ. Important instability processes would thus appear to encompass a broader spectrum than the forced response of the boundary layer.

The full viscous stability equations do not have the singular behavior, but low-speed theory and experiment show that the maximum velocity fluctuation level occurs where the wave speed matches the flow speed. The supersonic experimentalist did not have solutions to the compressible stability equations available until the early-to-mid 1960's (Mack's 1969 report, ref. 109, contains the most complete results), and it appears that the term critical layer was applied to the height of the peak fluctuations based primarily upon the subsonic experience. But even with the numerical compressible stability theory results available, the experimentalist has been kept in the dark concerning disturbance profile results, for the publication of eigenfunction results has been extremely rare. The present author knows of only two such presentations. (For the low-speed case, theoretical velocity disturbance profiles are almost

always presented and compared with experiment.) For one Reynolds number and frequency condition, Keltner (ref. 150) showed some eigenfunction profiles for a two-dimensional TS wave in Mach 2.2 and 2.4 flows. The velocity fluctuations peaked at $y/\delta \simeq 0.35$, and it appears that this is close to the height where the wave speed matches the flow speed. Mack (ref. 114) (also shown in ref. 58) showed an eigensolution for a 60^{o} oblique TS wave traveling at 0.67 u_{∞} in a Mach 4.5 boundary layer, and the peak height occurred at $y/\delta \simeq 0.8$ when the relative Mach number was one, but the height where the wave speed matched the local speed was at $y/\delta \simeq 0.55$. The wave obliqueness is a complicating factor here. Mack (ref. 109) has shown that at Mach 2.2 and 4.5 the most unstable first mode TS wave occurs with wave obliquity in the 60^{o}-65^{o} angle region. It would seem likely that the eigenfunction for the oblique condition would peak at a higher y/δ than the 0.35 value of Keltner's two-dimensional wave. It is thus quite conceivable that the lower data point at M = 2.2 in figure 22 could be due to TS waves (it was certainly thought to be so at the time by Laufer and Vrebolovich) and the outer peak may be due to the forced response. Until more information is available concerning the stability eigenfunctions and the forced response disturbance profiles, the speculation remains idle. Apparently, at the higher Mach numbers both phenomena peak within the same vicinity.

The double peak findings shown in figure 22 are interesting. Potter and Whitfield (ref. 143) show a Mach 5 disturbance profile which has a small secondary inner peak, but this peak was not mentioned in their discussion and will not be discussed here. Laufer and Vrebalovich (ref. 141) found a relatively small secondary outer peak at Mach 2.2, and reported that it greatly diminished when the wire overheat ratio was reduced (so that the wire responded primarily to total temperature fluctuations). Such a reduction with decrease in overheat is typical of noise field behavior. The authors did state that mode diagrams (signal level vs. wire overheat ratio) were found to be straight lines inside the boundary layer as well as outside. These facts might indicate that the outer peak was an acoustic phenomenon. The secondary peak was discussed in connection with data obtained at a frequency of 30 kHz, and there is no discussion about the existence of the secondary peak at other frequencies. There is another figure in the report which might be for 23 kHz, and the secondary peak is also present. In any event, for these frequencies the wavelengths are probably a few laminar boundary layer thicknesses at the x station of the measurements, so the conditions are not appropriate for the short wavelength caustic behavior. Kendall (ref. 18) found double peaks of equal magnitude at Mach 3, but the frequencies were over a broad range, and therefore the outer peak could not be considered as strictly due to caustic phenomena. Kendall did find that secondary outer peaks (although not necessarily equal) existed at M = 1.6 and 2.2, and only for higher frequencies. The heights of these peaks were not given. However, these peaks only occurred near the onset of transition (private communication) and hence may be the result of the higher harmonic generation process that occurs just prior to transition. If these heights were near the expected caustic region height one might then argue that here at last was a manifestation of an effect due to the acoustic focusing. On the other hand, the lack of a peak in the region near the leading edge might be taken as evidence that a caustic region did not exist, but to establish this possibility more information would be needed about the filtered frequency ranges used in the experiment.

As a final item to report here, some calculations were made to determine how the caustic layer height would change for the case of a plate tilted forward to reduce the local Mach number. The calculations are given in Appendix

G. The case of a plate tilted in a Mach 4 tunnel so that the local Mach number was reduced to 2 was considered. At Mach 4 the caustic layer region and critical layer region are close together. The purpose of the calculation was to see whether the predicted height of the caustic layer region might stay relatively unchanged inasmuch as the local Mach 2 boundary layer would still be subjected to the same noise field convection speeds of the Mach 4 tunnel environment. If the calculated height of the caustic region did remain relatively unchanged, then perhaps the caustic region and the critical layer region might separate since the latter should behave as it naturally would for a Mach 2 flow, and the critical layer heights are lower at Mach 2 than at Mach 4. Using noise field convection speeds for $M_\infty = 4$ from figure 2 (Laufer's dual-wire results, $u_s/u_\infty = 0.49$), the results showed that the caustic layer height for the tilted plate condition did remain in the outer region. However, the caustic height became very close to where it would be for a flat plate in a Mach 2 tunnel. This is a result of the leading edge shock reducing the local value of u_s/u_∞ to 0.38, a value close to that found in a Mach 2 tunnel. Thus it is likely that even the forced response of the boundary layer would be similar to the Mach 2 tunnel case. A possibly important difference between the tilted Mach 2 and the tunnel Mach 2 cases would be that the noise field should be much more intense in the tilted case inasmuch as the radiated noise field is stronger in the Mach 4 tunnel than the Mach 2 tunnel. The outer disturbance peak in the boundary layer, which was a secondary peak in the Mach 2.2 Laufer and Vrebalovich (ref. 141) experiment, could in the tilted case become a primary peak. The Mach 4 to 2 experiment could be an interesting one. Perhaps an even more interesting one would be Mach 4 to, say, 1.5, since Mach 1.5 boundary layers normally do not experience much tunnel radiated noise. Comparison of the tilted Mach 1.5 case with the Mach 1.5 tunnel case could be revealing. A multi-Mach numbered tunnel would be ideal for such an experiment. Kendall (private communication) has actually performed an experiment at $M_\infty = 4.5$ with a plate tilted to reduce the local Mach number to 3. He found the disturbance profile results to be similar to those found for $M_\infty = 3$. The calculations were then repeated for Kendall's new Mach number conditions (wave speed of $0.69\ u_\infty$ used for $M_\infty = 4.5$), and the same conclusion was obtained as with the previous calculation, i.e., the calculated caustic layer height for the tilted plate corresponded to that for the local M rather than M_∞. While this result appears to agree with Kendall's experimental findings, any further resolution of the original question concerning possible differences in the heights of the critical layer, forced response peak layer, and the caustic region has not been reached.

In summary, in an effort to identify the caustic region, the disturbance profiles from a number of hot-wire investigations of the laminar boundary layer were examined. Most of the published profiles were obtained from broad-band signals, and in the present effort were considered to be of little help. The caustic region is characterized by high frequency behavior, and to identify this region the disturbance profiles must be examined after passing the signal through a high-pass filter. More experimental results are needed. The peaks in the broad-band profiles were likely the result of low-frequency sources such as TS waves and/or the forced response of the boundary layer to the acoustic excitation. To help clarify the problem, more information will be needed about the eigenfunction shapes from stability theory and about the disturbance profiles from forcing theory calculations.

Effect on Transition

The problem of the effect of noise on boundary layer transition provided

the motivation for the present study. There was a naive hope that during the course of the study an important transition promoting mechanism would be clearly revealed, but no such revelation has yet occurred. A few thoughts on the subject will be presented here, primarily concerning some possible effects of the shocklets in the boundary layer noise field.

As discussed earlier in the report, shocklets with zero-thickness wave fronts ensure the presence of a spectrum with the slowest high-frequency drop-off rate, and as has been emphasized, shocklets should be associated with high-frequency behavior. Within the context of linear boundary layer stability theory, these frequencies would appear to be too high to affect transition. This statement may not hold, however, for high Mach number flow. Mack (figures 12.2 to 12.7 of reference 109) has published neutral stability curves on wave number-Reynolds number diagrams for Mach numbers in the range of 1.6 to 10.0. At the lower Mach numbers the shortest wavelength for an unstable instability wave is about 10δ. As the Mach number increases higher mode oscillations can exist, and by $M = 10$ the shortest unstable wavelength has decreased to about 0.5δ. This may be considered a relatively high-frequency oscillation, and the presence of shocklets ensures that free-stream disturbances in this frequency range exist.

If a shocklet is focused by the boundary layer, a distortion of the boundary layer profile would occur in the immediate vicinity of the caustic. In the two-dimensional case, near the triple point the profile may be locally wake-like because the flow passing through that point would be retarded slightly more than flow passing either above or below the point (assuming that the shock strength is greatest at the triple point). The vertical scale of this wake-like flow, however, would be very small; typically around 1/2 percent or less of the laminar boundary layer thickness. This region, with its doubly inflected profile, would be unstable, and passing shocklets could provide the high frequency input disturbances to make this flow go locally turbulent. For the three-dimensional interactions associated with the oblique portions of the incoming shocklet, the perturbation may be weaker, but cross flows would be induced and the flow pattern made more complex. The overall picture would seem to be that of very small vertical scale turbulent regions, akin to vortex sheets or wakes, embedded in a relatively thick laminar layer, and it is difficult to see how this aspect of the acoustic phenomenon could significantly affect the overall boundary layer transition pattern. However, the streamwise extent of the small wakes and their local speeds in relation to local TS wave speeds may be of significance in the early nonlinear stages of transition.

Under low-level disturbance environmental conditions, boundary layer instability phenomena are thought to play a major role in the zero pressure gradient transition process. One wonders, perhaps based on the knowledge that water waves are generated most efficiently when the wind speed, and thus the pressure field, matches the wave speed (ref. 151), whether TS waves are induced more efficiently when the convection speed of the noise field matches the speed of the TS waves. If the TS waves happened to be in the unstable wave number-Reynolds number region, one further wonders whether the noise field would then be a more effective promoter of transition. This idea seems plausible but the mechanism remains obscure as to how the free-stream disturbances generate or affect the TS waves. This problem has been termed the receptivity problem (refs. 33 and 36). If the matching of speeds is important, it may be observed that Mack's stability calculations (fig. 13.21 of ref. 109) show that in the Mach number range of about 2 to 4, the

most unstable first-mode TS wave had an x-direction propagation speed which was supersonic with respect to the free-stream. Thus, in this Mach number range the convected speeds of the Mach wave radiation noise disturbances could match the downstream speeds of the TS waves. These TS waves were oblique waves such that the Mach number component normal to the phase fronts were subsonic, and therefore these waves would be too oblique to match the obliqueness angle of noise disturbances. Nonetheless it is interesting to observe that tunnel transition Reynolds numbers are generally the lowest in the Mach 3 to 4 range. For the cases where phase velocities of the TS waves are greater than the downstream convection speed of the radiated noise field, there could be a match between the TS speeds and the velocity of the aforementioned possible vortex-sheet type of disturbance created in the interaction process. Thus vorticity could possibly be feeding into TS waves, but the importance of the match in speed might be offset by the mismatch in the vertical scales of the disturbances.

In the supersonic case some researchers (refs. 18, 41, 58) have talked about the forced disturbances turning into TS waves, and Mack (ref. 41) has expressed the thought that the conversion would most likely occur if the forced disturbance amplitude profile matched the eigenfunction. A close match can apparently occur with first mode eigenfunctions at M = 4.5 (again, see fig. in refs. 114 and 58). However, for higher frequencies associated with the shocklets, the match would likely have to be with higher mode TS waves. Such a matching would appear to be difficult to achieve. (Incidently, it appears that the wall pressures associated with TS waves can sometimes be much greater than the levels at the outer edge of the boundary layer, see Mack's (ref. 114) figures 12.13 and 12.14. This situation never occurs for the forced response of the boundary layer.)

Experimental evidence will be needed to determine with any certainty whether caustic focusing of the noise shocklets affects transition. When the shocklet thickness is assumed small compared to the boundary layer thickness, the caustic layer behavior would not be expected to change much with increase in distance from the leading edge of a model. If measurements at low Re_x values were to show that fluctuations at the caustic layer height increased with downstream distance, then, provided this behavior is not the low-frequency response predicted by Mack, perhaps it could be concluded that there is some credible transition promoting mechanism associated with the focusing. In this regard one can again mention the low Mach number finding of Kendall (ref. 18) that a high frequency outer region peak did show up near the onset of transition.

As a final thought, it should be pointed out that with shocklets present in the noise signatures there could be some interesting shocklet-on-shock interactions with the detached shock at the leading edge of the model. With a flat plate model, for example, there is always a small detached shock region at the leading edge and the intersections due to shocklets moving downstream from all sides of the model would be rippling back and forth along the leading edge. For slow sources (picture, for example, a sidewall source) the intersection region could be subsonic with respect to the subsonic flow immediately behind the models detached shock; for the faster source the region could move supersonically with respect to the stagnation region flow.

Obviously, much more work is required to even detect and measure the presence of caustic behavior, and to determine if and how the phenomenon affects transition would require a super sleuth with unique experimental equipment and unique patience.

Receptivity-Related Observations

The problem of how TS waves are generated by free-stream disturbances is obviously important to the transition process and is at the core of the receptivity issue. In calculations of the forced response of the boundary layer to either low-frequency disturbances or shocklets, the receptivity problem is not addressed. In the previous section the problem was touched upon in connection with the shocklet-boundary layer interaction and the possible matching of convection speeds and disturbance profiles with TS wave speeds and eigenfunction shapes. In the present section the shocklet interaction problem will not be considered further, and instead some observations and comments will be presented concerning two of Kendall's experimental findings. The first item is peripheral to the receptivity problem while the second is more directly concerned with the problem. Both items deal with the response of the boundary layer to the tunnel sound.

In figure 7 of reference 18, Kendall presents cross-correlation curves obtained from two hot-wires in the JPL 20-inch tunnel. One wire was located just upstream of the leading edge of a flat plate and the other was located in the laminar boundary layer 5 cm from the leading edge and at the height where the fluctuations were the greatest. Curves for five different free-stream Mach numbers, ranging from 5.6 to 1.65, are shown for conditions of nearly constant unit Reynolds number. The maximum correlation coefficient was found to diminish with decreasing Mach number. This fact may well be an indication that at the lower Mach numbers tunnel sound may be less effective than other unsteadiness modes in disturbing the boundary layer, but another possibility is offered here for consideration. The decay in the correlation results with decreasing Mach number may simply be reflecting the decay of the coherency of the noise field itself.

The sound field remains substantially correlated only over a limited downstream distance. Kendall (ref. 17) made measurements at $M_\infty = 4.5$ in the free-stream with various wire separation distances, and the results show that the correlation coefficient was down to 0.1 at a wire separation distance which may be estimated to be about six tunnel wall displacement thicknesses (at the location of the acoustic origin of signals reaching the wire; from Appendix B, $\delta^* \approx 1.64$ cm). This behavior may perhaps be typical of other Mach number conditions as well. The displacement thickness on the tunnel walls becomes smaller as the tunnel Mach number is reduced, and therefore, with a constant wire separation distance the relative separation distance, $\Delta x/\delta^*$, increases as the tunnel Mach number is reduced. The present author has estimated (see Appendix B) that for the flat plate measurements (ref. 18) the ratio of wire separation distance to tunnel wall displacement thickness increased from 2.7 to 10 as the tunnel Mach number dropped from 5.6 to 1.65 ($\delta^* \approx 1.85$ to 0.50 cm, respectively). This factor would seem to bias the correlation results in favor of the higher Mach numbers. Thus, even if the Mach 1.65 laminar boundary layer was just as responsive to the sound field as the Mach 5.6 layer, it appears reasonable to expect that the correlation coefficient would be smaller for the lower Mach number cases because of the relative decrease in coherency of the incoming forcing sound field at the larger values of $\Delta x/\delta^*$. As Kendall states, further investigation on this matter is needed.

The second item is also concerned with the free-stream boundary layer correlation data. Kendall presented (ref. 17) Mach 4.5 and 2.2 correlation curves for three different x-locations of the downstream wire (whereas the results

discussed above were for one wire separation distance). These curves are shown in figure 23 of the present report (because of space limitations the portions of the curves for time delays greater than 400 μsec have been omitted). The most unusual and interesting feature of the curves is the growth of the negative peak with increasing downstream distance. This negative-peak growth is not present in the free-stream cross-correlation curves (at least at $M_\infty = 4.5$, which is the only case shown in reference 17), and in turbulence work in general the peaks in space-time correlation curves, both positive and negative, decrease as the transducer separation distance is increased. The growth in the negative peaks shown in figure 23 thus seems unusual enough to warrant attention. The following simple observation can be made concerning the peaks.

If the separation distances are divided by the time delays of the peaks to determine convection speeds, albeit a very questionable procedure when dispersion is present, one obtains the following results for the $M_\infty = 4.5$ case. The speed associated with the positive peaks is about $0.65\ u_\infty$ and that with the negative peaks is about $0.87\ u_\infty$ (the curve for $x = 2.54$ cm has been ignored since the negative peak has not substantially developed). These speeds are rather close, respectively, to the convection speed of the focusing sound field (and again, it is questionable to talk about a single speed) and speeds of unstable TS waves (from fig. 13.21 of ref. 109, at $Re_x = 2.25 \times 10^6$ the phase and group speeds of the most unstable first-mode TS disturbance, which is a 60° oblique wave, are, respectively, approximately $0.82\ u_\infty$ and $0.92\ u_\infty$). Thus, the positive peaks appear to be associated with the forced response of the boundary layer to the sound field while the negative peaks may be associated with TS wave behavior. The negative peaks grow because the unstable TS waves move faster than the forced waves and with increasing downstream distance the TS waves move ahead of the forced waves and thus reveal their identity.

As was mentioned earlier in the report, the wave speed as a function of frequency can be obtained from the phase information in the Fourier transform of the correlation curves. Kendall determined this information from each of the three Mach 4.5 curves shown in figure 23 and also from three additional correlation curves (not published) for positions further downstream. The dispersion results show that at all frequencies the measured speeds increase with downstream distance of the boundary layer wire (the six dispersion curves are also shown in the review article by Reshotko, ref. 58). At the greatest Re_x of the downstream wire at 2.2×10^6, the dispersion curve was found to resemble that of a 60° oblique first-mode TS wave. The increase in the measured speed with downstream distance has been described (refs. 17 and 58) as an acceleration of the wave system, and the fact that the speeds farthest downstream are similar to those of unstable TS waves has been taken as evidence of a conversion from the forced waves to the free TS waves. Inasmuch as those flow processes which dominate the correlation curves also have the greatest impact on the dispersion measurements, one can interpret the "acceleration" as reflecting the fact that the greatest correlation shifted from the "slow" positive peak to the "fast" negative one with increase in downstream distance. It seems likely that the negative peak also dominated the correlation results at the maximum downstream distance condition, and hence the fact that the dispersion curve resembled TS wave behavior may be construed as further evidence that the negative peak reflects TS wave processes.

At $M_\infty = 2.2$, the positive and negative peaks for the two most downstream correlation curves in figure 23 corresponds to speeds of, respectively, $0.37\ u_\infty$ and $0.55\ u_\infty$. Again, the positive peak has a speed which corresponds closely to the forcing sound field speed and the negative peak corresponds rather

closely to the speeds of unstable TS waves (the phase and group speeds of the most unstable TS wave at Mach 2.2 are, respectively, approximately 0.49 u_∞ and 0.59 u_∞). Dispersion results have not been published, but it seems likely that the acceleration type pattern would be found. It should be noted that for both Mach number cases the smallest Re_x values for the downstream wire are greater than the calculated critical Reynolds number.

The picture which emerges here is that within the supersonic laminar boundary layer there are two major unsteady flow processes, the forced response of the layer to the tunnel acoustic excitation and the TS wave generation and propagation. Each travels at its own appropriate speed and transducers respond to both types of fluctuations. What is new here and pertains directly to the receptivity issue is the idea that the measurements could be showing that the forced response and the TS waves are negatively correlated with respect to each other. An incoming acoustic disturbance which has a positive change in mass flux, for example, induces a forced response also with a positive change in mass flux and a TS wave with a negative change in mass flux at a given location. Why the forced and TS waves should be anticorrelated remains to be explained. (Could it have something to do with the maintenance of a zero initial condition for induced responses at the leading edge stagnation region?)

The question arises as to whether the negative correlation result could be due to the particular y/δ value of the downstream wire. The answer would appear to be no because most of the disturbances are low-frequency first-mode oscillations. If the $M_\infty = 4.5$ mass-flux oblique wave eigenfunction published by Mack (ref. 114; also in ref. 58) is typical of first-mode behavior, then there is no phase reversal of the oscillations across the boundary layer (in contrast to the incompressible case and the $M_\infty = 2.2$ two-dimensional case (ref. 150) where a 180° phase reversal occurs in the outer region of the boundary layer). With no phase reversal, the sign of the correlation would not depend on the vertical location of the wire within the boundary layer.

A consequence of negative correlation would be that forced and TS waves destructively interfere near the leading edge. Perhaps the cancellation process partly accounts for the fact that the measured amplitude of the fluctuations fall below the theoretical forcing theory values. Inasmuch as the higher frequency TS waves travel faster than the lower ones, cancellation effects would change in a complicated fashion with increase in x. More experimental work, wind tunnel or numerical, would of course be helpful.

Use of Pressure Transducers for Noise Measurements

The free-stream data which have been presented and discussed in the present report come primarily from published hot-wire anemometer measurements. The majority of published tunnel noise measurements, however, have been made with pressure transducers. Often these measurements have been made in connection with transition experiments and often only to obtain a relative measure of the change in the noise level with change in the tunnel pressure (i.e., change in Reynolds number). Convection velocity measurements of the free-stream noise have not been attempted with pressure transducers. The transducers have been employed by two different means. In most cases the transducer has been flush mounted on a flat plate, wedge, or cone model, with the transducer near enough to the leading edge so that it is under the mounting model's laminar boundary. More recently the transducers have also been used in a pitot

tube to measure the fluctuating pitot pressure. The pressure transducer approach is generally chosen because it ostensibly does not require a long development program, but the pressure transducer method is open to serious question.

Although researchers are a little more cautious now, the implicit assumption in the flat plate-pressure transducer technique has been that the laminar boundary layer is transparent to the tunnel noise. Based on the previous refraction considerations, it would appear that this assumption is not very good. Even without a boundary layer present there would be a considerable problem due to the fact that the ratio of surface pressure rise to incident pressure rise across a shocklet varies with the angle of incidence of the shock. But the boundary layer changes all of this. As belabored in the present report, the shocklets are refracted away from the surface at the caustic, and thus the boundary layer acts as a low-pass filter to the surface. According to Mack's calculations (ref. 40), the boundary layer reacts to low frequency long wavelength acoustic disturbances. The results were Reynolds number dependent, but generally there was a diminution of surface pressure levels with increase in frequency of the incoming noise field. There appear to be enough questions concerning the pressure transducer technique to put its real efficacy into serious doubt. However, comparisons of hot-wire measurements with pressure transducer measurements (ref. 72) show that at times there can be fair agreement.

With the fluctuating pitot pressure method the concern is over the normal shock standing in front of the diaphragm. Depending on the convection velocity of the source, the shocklet-normal shock interaction region can move along the normal shock at speeds which are subsonic, sonic (termed a resonance condition), and supersonic with respect to the flow immediately behind the shock. This factor can significantly affect the strength of the wave transmitted across the normal shock. For the case of a shock source where the interaction is of the subsonic type, the disturbance transmitted through the normal shock is no longer a shocklet but instead becomes a pressure wave whose strength decreases with distance from the normal shock (ref. 152). In this case the normal shock standoff distance becomes important and this distance depends on the stream Mach number and the diameter of the pressure probe. The distortion of the incoming waves could be quite significant when the diameter of the probe is about the same as or larger than the thickness of the radiating boundary layer. Both this method and the flat plate method suffer from partial pressure cancellations across the face of the diaphragm if the diameter of the diaphragm is not significantly less than the thickness of the radiating boundary layer. Finally, it is well known that vorticity and temperature spots create sound pulses upon passage through a shock and this could be troublesome in some cases. Again, comparisons of hot-wire and fluctuating pitot pressure data sometimes show reasonable agreement (refs. 4 and 62).

The measurement of fluctuating quantities is never an easy task. Perhaps some of the problem is due to the difficulties mentioned above.

4. CONCLUDING REMARKS

Motivated by the noise-boundary layer transition problem in supersonic tunnels, a study of the noise field and the noise-laminar boundary layer interaction was made. The noise field is dominated by the sound radiating from the tunnel nozzle turbulent boundary layers, and in the present study a simple model of this noise field was adopted. The noise field has been modeled as a Mach wave radiation field consisting of discrete waves emanating from coherent turbulent entities moving downstream within the supersonic turbulent nozzle wall boundary layer. The individual disturbances are likened to miniature sonic booms and these strafe any object in the test section as the sources move downstream. The weak shock wave feature of the noise model is in agreement with existing optical evidence concerning the radiated noise from turbulent boundary layers. While this unsophisticated model would be considered a retrograde step from a turbulence modeling viewpoint, none the less, the statistical equations describing the noise field point out in a limited qualitative fashion the importance of number, size, shape, and speed of the acoustic sources on the statistical properties of the noise field. The mean, autocorrelation, and power spectral density of the field are expressed in terms of the wave shapes and their average arrival rate. The modeled rms amplitude distribution across the wind tunnel test section and the shape of the power spectral density curve agree quite well with experiment. With considerable empirical input it could be used for quantitative predictive purposes, but this is beyond the scope of the present study.

The emphasis in the analysis of the interaction of the wave field with the laminar boundary layer was on the weak shock behavior. When weak shocks interact with the laminar boundary layer they are refracted, and equations show that focusing of the wave fronts will occur. The refraction equations for the two-dimensional interaction, which are known, were rederived using two linear methods, a conventional fluid dynamics approach (a repeat of an existing derivation) and the method of geometric acoustics for a nonuniform moving medium (a new derivation). In the latter approach the shock strength variation is described in terms of the shock ray paths, and the differential equation describing the ray path was determined. Some typical ray trajectories through a Mach 4 laminar boundary layer for waves with different source speeds were computed and shown. In this approach the focusing is considered to ultimately be due to convergence of the ray paths and complete convergence occurs at the height within the boundary layer where the flow velocity is sonic with respect to the wave. This classic focusing condition is called a caustic; the linear theories predict an infinite pressure rise across the shock at the caustic. For oblique three-dimensional interactions complete collapse of the ray tubes does not occur.

The height at which the weak shocks undergo this focusing, termed the caustic layer height, depends upon the boundary layer profile and the downstream convection velocity of the source of the wave. The caustic layer height within the laminar boundary layer was computed for a range of free-stream Mach numbers and source-to-free-stream convection velocity ratios. The heights were found to lie in the outer half of the boundary layer for all but the very slowest sources (even stationary waves are focused at a height of four-tenths of the boundary layer thickness). Cooling the boundary layer lowers the height of the caustic layer. More knowledge about the source speeds of the noise field as a function of tunnel Mach number will be needed to more precisely locate probable caustic layer regions. Detection of the caustic layer is not

a clear-cut matter because in supersonic flow the fluctuations associated with Tollmien-Schlichting instability waves also reaches maximum intensity in the outer half of the boundary layer near their critical layer heights, and it appears that steady state forced response of the boundary layer to the sound field also peaks in the outer region.

The phenomenon of the focusing of weak shocks has been studied rather extensively by sonic boom researchers, and some results of shock focusing experiments are cited. A scaling law from sonic boom theory was used to estimate the maximum amount of focusing near the caustic. The scaling law requires the value of the radius of curvature of the shock ray path at the caustic. To estimate this radius for the boundary layer case some rather simple approximations of Mach 4 and 8 laminar boundary layer profiles were used and the radii were determined using the ray path differential equation. This exercise indicated that the maximum amount of focusing may not be too intense. Wave strength increases were a factor of two to six for incoming shock strengths of 1 to 0.01 percent of the free-stream pressure.

Another element which has been considered is the thickness of the very weak shock waves associated with the noise radiation process. For weak shock waves the equations show that the thickness is inversely proportional to the shock strength and the free-stream unit Reynolds number. Shock thicknesses in the radiated pressure field could occupy significant portions of the disturbance pressure signatures from individual sources in small tunnels (which have small scale disturbances) operating at low unit Reynolds numbers. Such smoothed shock fronts reduce the high-frequency content of the noise spectrum. The shock thickness factor could thus be an important element in some noise modeling problems. An expression is given which shows the ratio of the shock thickness to laminar boundary layer thickness as a function of the length Reynolds number and Mach number. For a length Reynolds number of 10^6, the thickness ratio could be close to one for the weak noise field shocks; for lower Reynolds numbers the ratio progressively increases. Thus, because the shock refraction equations are for shocks or high-frequency Fourier components of the wave field (wavelength small compared to laminar boundary layer thickness), the computed focus factors should perhaps be regarded as upper bounds rather than predicted values. The peak in the mean-square signal level from a hot-wire anemometer that is commonly found in the outer portion of the laminar boundary layer in a supersonic tunnel is likely due to Tollmien-Schlichting waves or the low-frequency forced response of the boundary layer as a result of the acoustic forcing field.

Concerning the all-important noise-transition problem, little substance is offered here. From a boundary layer stability standpoint the high frequencies associated with the shocklets are probably too high to be important except possibly at very high Mach numbers where wavelengths less than the boundary layer thickness can be unstable. The shocklets may have importance in some nonlinear aspect of the "receptivity" problem, particularly since they move downstream at the same velocities as portions of the boundary layer.

Some observations concerning hot-wire anemometer cross-correlation measurements are presented. Finally, considering that high-frequency components of the noise field are possibly refracted back into the freestream by the boundary layer in the outer region, and that the low-frequency components are possibly exaggerated by the forced response of the boundary layer, the use of microphones under laminar boundary layers to measure the noise field is considered a rather questionable technique.

Appendix A

Noise Field Intensity Distribution Across Test Section

The approach to be taken is as follows. One can think of the test section walls as being divided into a number of longitudinal alleyways, each of width Δs, along which the wall bodies travel with a random spacing. The signal contribution from an alley to the mean-square value of a free-stream probe will be proportional to Δs because, as shown later, the signal contribution is proportional to the average arrival rate of wall body wave signatures, and the wider the alley the greater the number of bodies passing along it. If $f(t)$ is the signal shape variation with time from a typical wall body, then the signal contribution from the alley will also depend on $f^2(t)dt$, where the integral is evaluated over the duration of the typical individual $f(t)$ signature. From sonic boom work it is known that the strength of the shock wave system decreases with distance from the body, and it will be shown next that an approximation to the preceding integral is proportional to b^{-m}, where b is the distance from the body path and m is a positive constant. Thus, if a probe is at a distance b from a wall alley, the contribution from the alley to the mean-square value of the probe's signal will be proportional to $b^{-m}\,\Delta s$. Inasmuch as the signals from the various alleys may be considered statistically independent, the total mean-square signal level will be proportional to $\Sigma_i\, b_i^{-m}\,\Delta s_i$, where the summation is over all of the alleys. (Actually this summation would be proportional to the variance of the signal since the mean is assumed subtracted from the mean-square level in accordance with the experimentalist's practice of removing the dc signal content.) For the purpose of evaluating the sum it is convenient to let the Δs_i approach zero, in which case the sum becomes the line integral $\oint b^{-m}(s)ds$, where the path of integration is around the test section perimeter.

Close to a body, in the so-called near field, the sonic boom wave system can be rather complex if the shape of the body is complicated. However, far from the body, in the far field, the wave system coalesces into a simple shape, the well known N wave. This coalescence is a nonlinear effect, and the stronger the wave (or, for a given body shape, the higher the Mach number) the sooner the N wave developes. In the far field the strength of the pressure wave decays as $b^{-3/4}$, where b is the distance from the flight path. As discussed above, it is not just the amplitude that is important but the value of $\int \Delta p^2(t)dt$, where $\Delta p(t)$ is the time signature of the pressure change and the integration is over one signature wavelength. If λ is the spatial signature wavelength, then according to reference 153, the area under the pressure signature curve is independent of distance from the path if the signature is plotted in the form of $(\Delta p/p_\infty)\,(b/\lambda)^{3/4}$ vs. $(x/\lambda)\,(b/\lambda)^{-1/4}$, where x is a coordinate parallel to the flight path. Hence

$$\int_0^1 \frac{\Delta p(x/\lambda)}{p}\left(\frac{b}{\lambda}\right)^{3/4} d\left(\frac{x/\lambda}{(b/\lambda)^{1/4}}\right) = \text{const.}_1$$

or

$$\int_0^1 \frac{\Delta p(x/\lambda)}{p}\, d(x/\lambda) = (b/\lambda)^{-1/2}\ \text{const.}_1$$

In the far field the signature shape in the above format does not change with b, and one then finds that

$$\int_0^1 \left[\frac{\Delta p(x/\lambda)}{p} \left(\frac{b}{\lambda} \right)^{3/4} \right]^2 d\left(\frac{x/\lambda}{(b/\lambda)^{1/4}} \right) = \text{const.}_2$$

or

$$\int_0^1 \frac{\Delta p(x/\lambda)}{p} \, d(x/\lambda) = (b/\lambda)^{-5/4} \, \text{const.}_2$$

Therefore, in the far field the integral of the pressure fluctuation squared is proportional to $(b/\lambda)^{-5/4}$. In the near field, even though $\Delta p(t)dt$ is still proportional to $b^{-1/2}$, the signature shape in the above format does change and hence $\int \Delta p^2(t)dt$ would probably not follow the $b^{-5/4}$ behavior. This is unfortunate because the wall bodies are considered to have such weak shocks that their wave systems are likely to remain as near field signatures as the wave propagates across the test section. In an effort to retain the -5/4 decay law it is argued here (rather unconvincingly) that because of the rather limited range of b/λ involved, where λ is, say, about the size of the thickness of the wall boundary layer, the spatial format signature shapes do not change very much and the -5/4 decay law can be used. Under these circumstances, the line integral to be evaluated becomes $\oint b^{-5/4}(s)ds$, where s is the circumferential distance around the test section from some reference point to a body path line.

The preceding integral was numerically evaluated around a circular-and a square-shaped test section geometry for various probe locations across the test section. To simulate the rms signal level the square root of the integral values was taken. The results are displayed in figure 24 along with hot-wire data of Laufer (ref. 154) taken in the JPL 20-inch tunnel. To the scale of the figure there was no difference between the estimated distributions for a circular or square test section. The figure shows that for a circular or square test section the estimated intensity distribution is quite uniform across most of the test section and, except in the vicinity of the boundary layer, the result is in agreement with the data.

The scatter shown for the data is a result of the difficulty in trying to replot Laufer's data in the form of the present plot. Laufer presented results for three different free-stream Mach numbers of the variation with distance from the wall of the rms velocity fluctuation level nondimensionalized by the level at the centerline. The distances were nondimensionalized by the wall boundary layer thicknesses, and neither the values of δ nor the tunnel flow conditions were given. To extract the actual distances for use in figure 24, values of δ had to be estimated, and the cross-hatched region reflects the uncertainty in the estimated δ values. The values of δ were obtained using reference 155, wherein Laufer presented test section noise levels in the JPL 20-inch tunnel versus δ for various Mach numbers and tunnel pressures. The Mach numbers were 2.2, 3.0, 3.5, 4.0, 4.5, and 5.0. The tunnel conditions were again not specified, but it is likely that they encompassed the typical conditions used in Laufer's experiments. From his figure the following range of δ values were estimated and used in figure 24; M = 2.0, δ = 2.5 - 3.8 cm; M = 3.5, δ = 3.9 - 4.6 cm; and M = 4.5,

δ = 5.0 - 5.8 cm.

The estimated boundary layer edge locations are shown in figure 24, where the distance from centerline to wall was taken as 25.4 cm. Laufer's data (ref. 154) show that with increasing Mach number there is a decrease in the extent of the nonuniform region outside of the boundary layer. The height above the boundary layer at which the signal departed from the centerline value fall from approximately 3.2δ at M = 2 to 2.2δ and 1.1δ for Mach numbers of 3.5 and 4.5, respectively. Thus in figure 24, the Mach 2 data lie in the left-hand portion of the cross-hatched region and the Mach 4.5 data make up the right-hand portion of the region. The present model is therefore more in agreement with the high Mach number data than the low Mach number data. It is of interest to note that at Mach 2.0 most of the noise-producing eddies travel downstream within the boundary layer at a subsonic Mach number with respect to the free-stream. Mach wave radiation would not be possible but velocity fluctuations would still be induced in the free-stream. Phillips (ref. 156), in his theoretical study of the irrotational motion outside of subsonic turbulent flows, predicted that the motion of the interface between turbulent and nonturbulent flow at the edge of the boundary layer induced velocity fluctuations in the free-stream irrotational flow which are inversely proportional to the fourth power of the distance from the source. Phillip's prediction has been verified by Bradbury (ref. 157), for the case of a two-dimensional jet in a slow moving stream, and by Bradshaw (ref. 158), Kibens and Kovasznay (ref. 159), and Kovasznay, Kibens, and Blackwelder (ref. 160) for the subsonic boundary layer. Thus, near the wall at the lower Mach numbers the subsonically induced free-stream fluctuations could be significantly contributing to the total fluctuation level. Because the subsonically and supersonically induced fluctuations follow different distance decay laws, it could be expected that at the lower Mach numbers the intensity distribution of the free-stream disturbances would be Mach number dependent near the edge of the boundary layer. The present model does not take into account the subsonic disturbances and is thus more appropriate for the higher Mach number flows. The comparison with Laufer's data at the higher Mach numbers is indeed more satisfactory.

Appendix B

Estimates of the Boundary Layer Thickness and Displacement Thickness Along the Nozzle of the JPL 20-Inch Tunnel

In the present report, knowledge of the boundary layer thickness and displacement thickness along the nozzle of the JPL 20-inch tunnel was needed for an analysis of some of Kendall's hot-wire anemometer measurements taken in the JPL tunnel (refs. 17, 18, 68). Inasmuch as the boundary layer data was not available in the literature, estimates of the thicknesses had to be made for a variety of Mach number and stream unit Reynolds number conditions. The method of obtaining these estimates along with the calculated results are presented herein.

The estimates of the nozzle boundary layer displacement thickness for $M_\infty \leq 5$ were obtained using a very simple formula given in the report of Maxwell & Jacocks (ref. 161). This formula is

$$\delta^* = \overline{\delta^*}\, kx^{6/7}$$

where,

$$k = 0.0131 \left(\frac{\mu_o}{\rho_o a_o}\right)$$

with,

δ^* = displacement thickness, ft

x = longitudinal distance from throat, ft

a_o = speed of sound at stagnation conditions, ft/sec

μ_o = coefficient of viscosity at stagnation conditions, $lb_f\text{-sec}/ft^2$

ρ_o = density at stagnation conditions, $lb_f\text{-sec}^2/ft^4$

$\overline{\delta^*}$ is a dimensionless boundary layer parameter which depends on M_∞. A curve of $\overline{\delta^*}$ vs. M_∞ is given in the Maxwell & Jacock report, and the present author found that the following equation fitted the curve rather well in the Mach number range of 1 to 6.7:

$$\overline{\delta^*} = 20.0 - 18.0 \sin A$$

where A is a quantity in radians given by

$$A = [0.275\ (6.7 - M_\infty)]^{0.94}$$

ρ_o is calculated from $p_o/g_c RT_o$, where $g_c = 32.2\ lb_m\text{-ft}/lb_f\text{-sec}^2$. The adequacy of the above formula for the present case was determined by comparing calculated δ^* values with those measured in the test section of the JPL 20-inch tunnel. Test section boundary layer measurements of the curved wall boundary

layer were taken by Dayman (ref. 107). The x in the formula is for the longitudinal distance from the throat to the end of the nozzle, but the x values in the Dayman report are for the distance along the curved wall to the test section measurement station. Dayman's x values were used in the formula for simplicity. The following table presents the tunnel parameters, the measured and calculated displacement thicknesses, and the percent error. Values of viscosity were obtained using Sutherland's law, $\mu[(lb_f\text{-sec})/ft^2] = (2.2 \times 10^{-8} \sqrt{T})/(1 + 198.6/T)$.

M_∞	p_o(psia)	T_o(^oR)	x(in)	δ^* (cm) measured	δ^* (cm) calculated	% error
1.4	21.27	570	66	0.434	0.382	-11.93
1.64	22.24	573	79	0.511	0.482	- 5.62
2	6.58	540	92	0.767	0.759	- 1.10
2	26.11	580	92	0.632	0.631	- 0.15
3	10.83	538	112	1.392	1.405	0.90
3	29.01	579	112	1.209	1.236	2.27
4	17.41	558	119	2.243	2.268	1.12
4	49.32	580	119	1.943	1.968	1.30
5	63.82	605	118	2.885	2.861	-0.82

It is seen that except for the M = 1.4 calculation, very good agreement exists between the results from the simple formula and the measured values.

Estimates were next made of the displacement thickness at the acoustic origin of the signals reaching a hot-wire anemometer in the center of the test section. Kendall made such measurements, although the x location of his wire was not given. It was assumed here that the x locations given above corresponded to the wire locations. Disturbances on the Mach wave front from a moving source travel along a path which nearly traces the Mach angle, θ, for the free-stream. As may be seen in the sketch shown in figure 25, an "average" source path lies somewhere off the centerline of the walls. This distance was taken as 12.7 cm from the centerline (half the distance to the wall). For the calculations of δ^*, the x distance used was the x distance in the previous table minus the value of D as calculated by the expression given in the sketch. For the conditions of interest in Kendall's work, neither the stagnation temperatures nor pressures were given. The unit Reynolds numbers, however, were specified. The values of T_o were guessed, based on the previous table information. With M_∞ and ^oT_o known, the values of unit Reynolds number per unit of stagnation pressure can be computed. The parameters and results are shown in the table below.

M_∞	$Re/cm \times 10^{-4}$	T_o (^oR)	P_o (psia)	x(in)	δ^* (cm)	δ/δ^*	δ (cm)
1.65	4.2	540	7.37	64	0.50	4.77	2.38
2.2	3.4	540	4.42	73	0.73		
2.4	3.9	540	5.60	76	0.81	3.74	3.03
3	4.2	540	8.22	80	1.10		
3.25	4.0	540	8.91	79	1.22	2.9	3.58
4.5	3.7	560	15.90	70	1.81	2.23	4.04
4.5	3.9	560	16.77	70	1.80	2.23	4.01
4.5	5.7	560	24.51	70	1.70	2.23	3.79
4.5	7.2	580	32.79	70	1.64	2.23	3.66
5.6	3.3	580	23.50	57	1.93	1.87	3.60
5.6	4.3	580	30.62	57	1.85		

For Mach numbers greater than five, Pate (ref. 8) noted that the existing values of $\overline{\delta^*}$ result in δ^* values which are too large. Based on Pate's figure B-7, the present author chose to represent $\overline{\delta^*}$ for $5 \leq M_\infty \leq 9.5$ by

$$\overline{\delta^*} = 1.882\ (M-1) + 4$$

This equation was used in the computation of the M = 5.6 results above. Some values of δ are also given in the Table. These values were obtained from the δ^* values using the δ/δ^* ratios given in the Table. In the textbook of Shapiro (ref. 108, p. 1093) a table is given from which this ratio may be determined for flat plate turbulent boundary layers at various Mach numbers (0 to 10 in 0.2 increments). A formula which the present author devised which fitted these ratios to within 3.5% for $M \geq 1.6$ is

$$\delta^*/\delta = 0.1 + 0.1574\ e^{-0.8M} + 0.63\ \sin \frac{(M-1)\pi}{16}$$

where the argument is in radians. This formula was used to provide the needed δ/δ^* ratios.

Appendix C

Linearized Analysis of Weak Shock Wave-Supersonic Shear Layer Interaction

PART I - Incoming Wave

As in the main text, the problem considered here is that of the refraction through the boundary layer of a weak plane shock. The boundary layer in the interaction zone can be considered as a medium in which the fluid properties vary only in the vertical direction. In wave propagation problems, a medium in which properties vary in only one direction, whether continuously or discontinuously, is often called a "stratified" or "layered" medium. The present problem is therefore the refraction of a weak plane shock through a horizontally stratified medium. The stratified medium presents a much simpler problem than the general nonuniform medium case, but the stratified problem is still a difficult one and one must often be satisfied with approximate solutions.

One solution technique that is used to solve the stratified problem is to approximate the continuously varying medium properties using a layered model. Here it is assumed that the medium properties in each layer are constant and that discontinuities exist in the properties at the layer boundaries. The propagation problem is then solved by examining the series of reflections and transmissions that occur as the wave reaches each of the interfaces between the layers. The greater the accuracy demanded, the greater the number of subdivisions used. If it is desired, one can let the thickness of the layers approach zero, and in the limit obtain a differential equation describing some aspect of the problem. As mentioned in the main text, this was the approach taken by a number of fluid dynamicists around 1950 to examine the weak shock boundary layer interaction. It is the details of this approach that are given in the present appendix.

In another solution technique the layered approximation is not used and the properties of the medium are allowed to vary continuously. But in this case, restrictions are imposed on the nature of the wave and property variations. The geometric acoustic method exemplifies this approach, and this method is discussed in a Appendix D. The present appendix can be considered as a fluid dynamicist's approach to the boundary layer interaction problem; the geometric acoustic approach would likely be that of the acoustician. In Part I of this appendix an analysis of the behavior of the strength of an incoming weak shock will be presented; Part II will be concerned with the reflected wave system. Part II also contains a discussion of an attempt to find in the published literature evidence of the reflected wave system.

The following is based largely on Barry's method of solution (ref. 74). The incoming shock wave is assumed to be weak. The shear layer is considered to be composed of a number of inviscid fluid layers which are separated by slip planes across which some of the fluid properties may vary discontinuously. Within each layer the fluid properties are considered to be constant. The situation is depicted in figure 26. The static pressure is assumed to be constant across the shear layer. The refraction of an incident wave at a slip plane as well as the nomenclature used in the analysis are shown in figure 27.

At a slip plane the incident wave splits into a reflected wave and a

transmitted wave. The reflected wave is shown here as an expansion wave and this fact is denoted by the dashed line (of course, the flow deflection angle also shows that the wave is an expansion wave). The change in Mach number across the weak incident wave is neglected. The heart of the analysis lies in the weak-wave assumption and the requirement that the static pressure and the flow deflection angle remain constant across a slip plane.

If the incident wave is weak, linearized theory can be used. In this case, provided the flow is not transonic, the pressure change across the wave may be written as

$$\frac{p_d - p_u}{p_u} = \pm \frac{\gamma M^2}{\sqrt{M^2 - 1}} |\theta| \tag{C1}$$

where the subscripts u and d refer, respectively, to conditions upstream and downstream of the wave, θ is the flow deflection angle, and the plus or minus sign is used when the incident wave is compressive or expansive, respectively. For the present, only incoming waves such as shown in figure 27 will be considered. If θ is taken as positive in the clockwise direction, equation (C1) can be taken without the absolute value or plus or minus operators. Defining the pressure rise coefficient, P, as

$$P = \frac{p_d - p_u}{p_u} = \frac{\Delta p}{p_u}$$

equation (C1) Becomes

$$P = f(M)\theta \tag{C2}$$

where

$$f(M) = \frac{\gamma M^2}{\sqrt{M^2 - 1}}$$

Because the static pressure must remain constant across a slip plane, $p_1 = p_2$ and $p_4 = p_3$, and hence,

$$p_3 - p_2 = p_4 - p_1 \tag{C3}$$

or

$$p_3 - p_2 = p_5 - p_1 + p_4 - p_5$$

With a few manipulations eq. (C3) may be written in terms of the pressure rise coefficient $P = \Delta p/p$ as

$$P_t = P_i + P_r (P_i + 1) \tag{C4}$$

where the subscripts i, t, and r refer to, respectively, the incident, transmitted, and reflected waves. For a weak incident wave $P_i \ll 1$, and equation (C4) reduces to

$$P_t = P_i + P_r \tag{C5}$$

Since P is a function of M and θ, the total differential dP is

$$dP = \frac{\partial P}{\partial M} dM + \frac{\partial P}{\partial \theta} d\theta \tag{C6}$$

The partial derivatives may be obtained from equation (C2) as

$$\frac{\partial P}{\partial \theta} = f(M)$$

$$\frac{\partial P}{\partial M} = \theta \frac{df}{dM}$$

Substituting these equations into equation (C6) gives

$$dP = \theta df + f d\theta \tag{C7}$$

The change in pressure rise coefficient, δP, as the incident wave crosses the slip plane is $P_t - P_i$, and hence, from equation (C5), it is seen that $\delta P = P_r$. As can be seen from figure 27, $\theta_t = \theta_i + \theta_r$, and thus, similarly, $\delta\theta = \theta_r$. Inasmuch as the incident wave is weak and the change in Mach number across the slip plane is small, the reflected wave itself is weak and therefore obeys eq. (C2). Thus $P_r = -f(M)\ \theta_r$ (a negative sign is needed), and hence, using the preceding incremental relations for P_r and θ_r,

$$\delta P = -f\ \delta\theta \tag{C8}$$

In the limit of the change in Mach number across the slip plane approaching zero, eq. (C8) may be substituted into eq. (C7) giving the following differerential equation

$$\frac{d\theta}{\theta} = -\frac{1}{2}\frac{df}{f}$$

This equation may be integrated to give

$$\frac{\theta}{\theta_\infty} = \frac{M_\infty}{M}\left[\frac{M^2 - 1}{M_\infty^2 - 1}\right]^{1/4} \tag{C9}$$

where θ_∞ and M_∞ are the free-stream boundary conditions. Equation (C9) is eq. (3) of the main text. The equation describes the strength of the wave in terms of flow deflection angle as the wave traverses the shear layer.

The wave strength variation in terms of pressure rise is obtained by substituting for θ from equation (C2). The result is

$$\frac{\Delta p}{\Delta p_\infty} = \frac{M}{M_\infty}\left[\frac{M_\infty^2 - 1}{M^2 - 1}\right]^{1/4} \tag{C10}$$

It is easily shown that Δp possesses a minimum at $M = \sqrt{2}$. Thus if $M_\infty > \sqrt{2}$, the wave strength will initially decrease as the wave enters the boundary layer. Later it will be shown that the reflected wave field changes from expansive to compressive as the wave passes into the region where the

Mach number is less than $\sqrt{2}$. The behavior of Δp can therefore be associated with the nature of the reflected wave field.

It is important to realize that in the analysis the flow Mach number has been that relative to the wave. If the wave is stationary in a tunnel, this flow Mach number is also the usual Mach number of the flow relative to the tunnel. If, however, the wave is moving, a situation of prime interest in the present report, then, of course, the value of M in equation (C10) is not the conventional flow Mach number such as would be measured in a tunnel boundary layer. A simple transformation allows the equations to be expressed in terms of the tunnel-fixed coordinates. If u_f is the fluid velocity in the usual tunnel-fixed coordinate system, and u_s is the downstream velocity of the wave source in the fixed system, then M, the quantity which is presently representing the Mach number of the flow relative to the wave, is

$$M = \frac{u_f - u_s}{a} \tag{C11}$$

where a is the local speed of sound. In terms of Mach number, using the fact that $M_s = u_s/a_\infty$, equation (C11) may be expressed as

$$M = M_f - M_s \frac{a_\infty}{a} \tag{C12}$$

The relative free-stream Mach number is

$$M_\infty = M_{f_\infty} - M_s \tag{C13}$$

Substituting equations (C12) and (C13) into (C10) yields the important result

$$\frac{\Delta p}{\Delta p_\infty} = \frac{M_f - M_s \frac{a_\infty}{a}}{M_{f_\infty} - M_s} \left[\frac{(M_{f_\infty} - M_s)^2 - 1}{(M_f - M_s \frac{a_\infty}{a})^2 - 1} \right]^{1/4} \tag{C14}$$

When the shock is stationary, $M_s = 0$, and equation (C14) reduces to a form similar to equation (C10). Equation (C14) is the principal result of the analysis. For the remainder of Part I of the present appendix, the relative Mach number M will continue to be used. Whenever it is desired to apply the equations in terms of the usual tunnel-fixed coordinate system, M and M_∞ can be utilized using equations (C12) and (C13), respectively.

To determine the wave strength in terms of the longitudinal velocity fluctuation, the relation between Δu and Δp from linearized theory can be used, namely,

$$\frac{\Delta u}{u} = -\frac{1}{\gamma M^2} \frac{\Delta p}{p}$$

Substituting this equation into equation (C10) yields

$$\frac{\Delta u}{\Delta u_\infty} = \frac{u}{u_\infty} \frac{M_\infty}{M} \left[\frac{M_\infty^2 - 1}{M^2 - 1} \right]^{1/4}$$

or

$$\frac{\Delta u}{\Delta u_\infty} = \frac{a}{a_\infty}\left[\frac{M_\infty^2 - 1}{M^2 - 1}\right]^{1/4}$$

As illustrated in figure 8, within the boundary layer, provided that $M_\infty > \sqrt{2}$, there are conditions of pressure coefficient and flow deflection angle which match those of the incoming wave at the edge of the boundary layer. These matching conditions occur at the same local Mach number and hence at the same height in the boundary layer. It is only below this location that pressure fluctuation amplitudes can exceed the free-stream strengths. The value of this Mach number, found by setting $\Delta p/\Delta p_\infty = 1$ in equation (C10), is

$$M_{P=P_\infty} = \frac{M_\infty}{\sqrt{M_\infty^2 - 1}} \tag{C15}$$

Some implications of this result are given in the main text.

The linearized approach becomes increasingly inaccurate as the sonic condition is approached. In addition to this problem, the model itself becomes invalid at the condition where the flow behind the incident wave is subsonic and no reflected shock can exist. To find where this condition occurs, oblique shock theory can be used. The relation between the Mach number and shock strength for which subsonic flow exists downstream may be derived from oblique shock equations contained in reference (105, eq. 157) and is

$$M^* = \sqrt{\frac{6P^2+18P+7}{6P+7}}$$

The simultaneous solution of this equation with the refraction shock strength equation (C10), written as

$$\frac{P}{P_\infty} = \frac{M^*}{M_\infty}\left[\frac{M_\infty^2 - 1}{M^{*2} - 1}\right]^{1/4}$$

provides the means of determining the values of P and M where the three-wave model breaks down. This has been done for a number of relative free-stream Mach numbers, M_∞, and a variety of initial wave strengths, P_∞, and the results were shown in figure 19 of the main text.

Concerning additional use of oblique theory, the deflection angle of an oblique shock is related to the Mach number and pressure ratio coefficient by (ref. 105, eq. 160)

$$\tan^2\theta = \left[\frac{P}{\gamma M^2 - P}\right]^2 \frac{2\gamma M^2 - P(\gamma+1) - 2\gamma}{P(\gamma+1)+2\gamma} \tag{C16}$$

From this equation

$$\frac{\partial \tan^2\theta}{\partial M} = \frac{4\gamma^2 P^2 M(P+2-M^2)}{(\gamma M^2 - P)[P(\gamma+1)+2\gamma]} \tag{C17}$$

The oblique shock theory can be shown to be consistent with linearized theory by noting from (C17) that $d\theta/dM = 0$ at $M = \sqrt{P + 2}$, with θ a minimum, and as $P \to 0$, $M \to \sqrt{2}$, a finding consistent with linearized theory. Barry stated that for an incoming shock, an expansion wave will be reflected for $M > \sqrt{P + 2}$ and a compression wave will be reflected for $M < \sqrt{P + 2}$. The earlier remarks on the nature of reflected waves still apply if the expression $M^2 = P + 2$ is used for the extrema instead of $M^2 = 2$ (a result also shown by Henderson in reference 80).

As in linearized theory, oblique shock theory also indicates that there are two Mach numbers at which the shocks have the same pressure ratio and deflection angle. By using (C16), one can show that

$$M^2_{P=P_\infty} = \frac{M_\infty^2\left(\gamma + \frac{\gamma+1}{2} P_\infty\right) - P_\infty (P_\infty+2)}{\gamma M_\infty^2 - \left(\gamma + \frac{\gamma+1}{2} P_\infty\right)}$$

For $P = 0$, this equation reduces to equation (C15). The variation of with M_∞ for various values of P_∞ was shown in figure 9. Also shown in the figure is a cutoff curve indicating the conditions for which subsonic flow exists behind the incident wave. For very small values of P_∞, this condition is of course quite close to $M = 1$. Expressions suitable for finding the flow deflection angle and shock strength across a shear layer based on the three-wave model using oblique shock theory rather than linearized theory can be found in Moeckel (ref. 76) and Friedman and Chou (ref. 102).

Part II - Reflected Wave System

The emphasis in the preceding section was on the incoming wave, and now a close examination of the reflected wave field will be made. Using equation (C2), equation (C5), may be rewritten as

$$f(M_2)\theta_t = f(M_1)\theta_i - f(M_1)\theta_r$$

Using the fact that $\theta_t = \theta_i + \theta_r$, the above equation may be written as

$$f(M_2)\ (\theta_i + \theta_r) = f(M_1)\ \theta_i - f(M_1)\theta_r$$

or

$$\theta_r = \frac{f(M_1) - f(M_2)}{f(M_1) + f(M_2)}\ \theta_i \tag{C18}$$

For very small changes in Mach number across the slip plane,

$$\frac{f(M_1) - f(M_2)}{f(M_1) + f(M_2)} = -\frac{\Delta f(M)}{2f(M)}$$

and in the limit as the change in Mach number approaches zero,

$$\lim_{\Delta M \to 0} \frac{\Delta f(M)}{2f(M)} = \frac{-\,df(M)}{2f(M)}$$

$$= -\frac{1}{2}\ \frac{1}{f(M)}\ \frac{df(M)}{df}\ dM$$

$$= -\frac{1}{2}\ \frac{d[\ln f(M)]}{dM}\ dM$$

Therefore, for this limiting condition, eq. (C18) becomes

$$d\theta_r = -\frac{1}{2}\ \frac{d}{dM}\ [\ln f(M)]\theta_i dM$$

Substituting for f(M) and performing the differentiation gives

$$d\theta_r = -\frac{1}{2}\ \frac{M^2 - 2}{M(M^2 - 1)}\ \theta_i\ dM \tag{C19}$$

This equation shows that at $M = \sqrt{2}$ no reflected wave exists and that the sign of $d\theta_r$ changes at this value. For a compression wave entering a boundary layer with a free-stream Mach number greater than $\sqrt{2}$, the reflected wave will initially be an expansion wave. At $M = \sqrt{2}$ no reflected wave will exist and at Mach numbers below $\sqrt{2}$ compression waves will be reflected. The situation was depicted in the text figure 7. Whereas θ of the incoming wave depended upon only the value of the local Mach number for given initial conditions, the strength of the reflected wave depends both on the local Mach number and local variation of the Mach number in the shear layer. The reflected wave strength is seen to be a differential quantity.

The above analysis was based on Barry's work (ref. 74). Marble (ref. 75) carried the analysis further by using equation (C19) to determine the flow direction along the edge of the boundary layer due to the integrated effect of the reflected wave field, and this problem will be considered here. The wave of strength $d\theta_r$ propagates back out into the free-stream undergoing a refraction process similar to that of the incoming wave. In fact, the same relationships used to describe the incoming wave with an initial strength θ_∞ can be used to describe the outgoing wave of initial strength $d\theta_r$. This is the approach used below to estimate the flow direction along the outer edge of the boundary layer due to the reflected waves. This would be an important quantity, for it would describe the manner in which the free-stream would be disturbed by the reflected wave field. The analysis is for the two-dimensional case of an incoming weak plane wave, and it is of course a linearized approach in which the Mach number is assumed to be unchanged across the waves.

As previously stated, any of the reflected waves, which will be called primary reflected waves, will go through a refraction process as it propagates back toward the outer edge of the boundary layer. This process itself generates secondary reflected waves which in turn refract and generate additional reflected waves. Ultimately, a diffuse pattern is set up by any of the primary reflected waves. It is thus seen that a primary reflected wave is not isolated in its outward progress. However, any wave which contributes to a primary reflected wave will have undergone at least two additional reflections. Since it has been shown that, except near $M = 1$, any reflected wave is of greatly diminished in strength (see eq. (C19), it is consistent with the present approximation scheme to neglect the effects of the contributor waves. Thus the reflected wave field can be considered to be composed only of the primary reflected waves.

The goal here is to describe the effect on the boundary layer edge streamline of the reflected wave field produced by the refraction process of the incoming weak shock wave. The analysis will ultimately involve an integration of equation (C19). To begin this process, at any location, M_i, θ_i in equation (C19) can be expressed, using eq. (9), in terms of the initial conditions at the edge of the boundary layer of the incoming wave as

$$\theta_i = \frac{M_\infty}{M_i}\left[\frac{M_i^2 - 1}{M_\infty^2 - 1}\right]^{1/4} \theta_\infty$$

Substituting this expression for θ_i into (C19) gives

$$d\theta_r = -\frac{M_i^2 - 2}{2M_i(M_i^2 - 1)} \frac{M_\infty}{M_i}\left[\frac{M_i^2 - 1}{M_\infty^2 - 1}\right]^{1/4} \theta_\infty \, dM_i \qquad \text{(C20)}$$

Again, the subscript i here refers to the condition, i.e., the location, where a primary reflected wave is initiated. Using (C9) again, the value of the reflected wave, $d\theta$, at any location (at any M) as it propagates back out through the shear layer can be expressed in terms of its initial strength at M_i as

$$d\theta = \frac{M_i}{M}\left[\frac{M^2 - 1}{M_i^2 - 1}\right]^{1/4} d\theta_r$$

Substituting for $d\theta_r$ from (C20) gives

$$d\theta = -\frac{M_i^2 - 2}{2M_i(M_i^2 - 1)} \frac{M_\infty}{M} \left[\frac{M^2 - 1}{M_\infty^2 - 1}\right]^{1/4} \theta_\infty \, dM_i \tag{C21}$$

To find the value of flow directions at the edge of the boundary layer, the value of M takes on the value M_∞ in eq. (C21). The result is

$$d\theta_{R\delta} = -\frac{M_i^2 - 2}{2M_i(M_i^2 - 1)} \theta_\infty \, dM_i \tag{C22}$$

where the subscript $R\delta$ has been used to indicate the value of the flow deflection angle of the reflected wave field at the edge of the boundary layer. Equation (C22) is seen to be of the same form as the starting equation (C19), except that in place of the variable θ_i the constant θ_∞ is present. Equation (C22) can be directly integrated in order to describe the behavior of $\theta_{R\delta}$ as a function of the Mach number within the boundary layer. The result is

$$\frac{\theta_{R\delta}}{\theta_\infty} = \ln \frac{M_\infty}{M} \left[\frac{M^2 - 1}{M_\infty^2 - 1}\right]^{1/4}$$

Actually, the total flow direction at the outer edge of the boundary layer is the sum of that due to the incoming wave at the edge of the boundary layer, θ_∞, plus the effects of the reflected wave field. Thus,

$$\theta_\delta = \theta_\infty + \theta_{R\delta}$$

and hence,

$$\frac{\theta_\delta}{\theta_\infty} = 1 + \ln \frac{M_\infty}{M} \left[\frac{M^2 - 1}{M_\infty^2 - 1}\right]^{1/4} \tag{C23}$$

Equation (C23) gives a relationship between the local value of Mach number M and the flow direction at the edge of the boundary layer which is produced as a result of the cumulative effects of the reflected wave field originating within the region between M_∞ and M. Values of $\theta_\delta/\theta_\infty$ vs. M are shown in figure 28 for three values of M_∞. As M decreases from its free-stream value, θ_δ initially increases ($M_\infty > \sqrt{2}$ for the examples), meaning that the flow is turned toward the wall. The maximum turn toward the wall occurs in the region of the reflected wave field originating from the $M = \sqrt{2}$ vicinity. This is expected because the nature of the reflected waves changes at $M = \sqrt{2}$. As the Mach number is further decreased the turning to the wall is lessened due to the compressive nature of the reflected waves. Eventually the flow is turned away from the wall, and ultimately the results show unrealistic values due to the linear analysis.

Equation (C23) does not enable a boundary layer edge streamline to be constructed. To do so requires a relationship between θ_δ and x, the down-

stream distance. The problem is illustrated in figure 29 where an incoming wave and a typical theoretical outer edge streamline (greatly exaggerated) are shown. As has been stated, the maximum flow angle towards the wall occurs at the location where a reflected wave originating from the $M = \sqrt{2}$ region would strike the edge of the boundary layer. To find this location, or the location of any wave striking the edge of the boundary layer, the equations describing the location of the incoming and each reflected waves are needed. Because the waves have been assumed to be very weak, all the waves can be assumed to propagate along the characteristics. Thus, the equation describing the characteristics

$$\frac{dy}{dx} = \pm \frac{1}{\sqrt{M^2-1}}$$

can be used. Because it is assumed that there is no Mach number change across any of the waves, the Mach number is a function of y only and this greatly simplifies the problem. The nomenclature for the problem is also illustrated in the figure, where the value of x is used to locate a coordinate on the incoming wave, and X is used to describe the location of the intersection of a reflected wave originating at x, y with the edge of the boundary layer. It can be seen that because of the very small deflections of the outer edge of the boundary layer, the symmetry of the problem allows the simplification of $X = 2x$ to be made. This problem will be solved for example cases of an incoming wave from a stationary source interacting with a "laminar" boundary layer and a "turbulent" boundary layer in Mach 2 and 4 tunnels. Quotation marks have been used here because the boundary layer Mach number profiles are approximated in a very crude fashion.

The equation of the incoming characteristic can be written as

$$-d\left(\frac{x}{\delta}\right) = \sqrt{M^2 - 1} \quad d(y/\delta) \tag{C24}$$

To solve the problem, the Mach number profile is needed in order to express M as a function of y. The simplest profile would be a linear one, and in fact, for laminar boundary layers the Mach number profile is approximately linear for stream Mach numbers up to about 4. Therefore, a profile of the form

$$\frac{y}{\delta} = \frac{M}{M_\infty} \tag{C25}$$

was used for the laminar interaction study. Substituting equation (C25) into (C24) gives the differential equation

$$-d\left(\frac{x}{\delta}\right) = \frac{1}{M_\infty} \sqrt{M^2 - 1} \quad dM$$

Integrating and using the fact that $X = 2x$ yields

$$\frac{X}{\delta} = \sqrt{M^2 - 1}\left(1 - \frac{M}{M_\infty}\right) + \frac{1}{M_\infty} \ln \frac{\sqrt{M^2 - 1} + M}{\sqrt{M_\infty^2 - 1} + M_\infty} \tag{C26}$$

Using equations (C23) and (C26), results in the form of $-\theta_\delta/\theta_\infty$ vs X/δ for $M_\infty = 2$ and $M_\infty = 4$ are shown in figure 30 and will be discussed as soon as the turbulent results are presented. The negative of the deflection angle ratio is plotted so that the sense of the directions shown on the figure corresponds to the actual physical situation for a boundary layer interaction such as depicted in figure 29.

For comparison with the laminar boundary layer interaction, an approximate "turbulent" Mach number profile was used. For this case, the following profile was assumed:

$$\frac{M}{M_\infty} = \left(\frac{Y}{\delta}\right)^{1/7}$$

Substituting this relation into equation (C24) gives the following differential equation:

$$d\left(\frac{X}{\delta}\right) = -\frac{14}{M_\infty^7} M^6 \sqrt{M^2 - 1} \quad dM$$

or

$$\frac{X}{\delta} = -\frac{14}{M_\infty^7} \int_{M_\infty}^{M} M^6 \sqrt{M^2 - 1} \quad dM$$

This equation was integrated numerically, and the plotted results for $M_\infty = 2$ and $M_\infty = 4$ are shown in figure 30 along with the laminar results.

Inasmuch as M_∞ is greater than $\sqrt{2}$ in the cases shown in the figure, the reflected wave field is initially an expansive one. The outer flow thus initially undergoes a turning toward the wall which is in addition to that produced by passage through the incoming shock itself. Ultimately the outer flow is seen to turn sharply away from the wall as a result of the strong reflected compression field which originates below $M = \sqrt{2}$ near the sonic line. The fullness of the turbulent profile results in interactions occurring over a considerable longitudinal distance and the terminal compression region is more abrupt than in the laminar case. The laminar curves are not horizontal at the beginning of the interaction because of the assumed straight-line Mach number profile (the assumed turbulent profiles are better in this regard). The figure shows that the greater the free-stream Mach number the greater the turning toward the wall. The very rapid turn away from the wall for all conditions must be considered unrealistic inasmuch as this is due to the reflected compression field originating near the sonic line, and the theory is inappropriate for this transonic region.

In an effort to determine whether some of the features predicted by the linearized analysis of the weak shock wave interaction process actually occur, a study of published schlieren photographs of shock wave-boundary layer interactions was undertaken. Schlieren photographs of such interactions are usually presented for the case of the horizontal knife-edge and therefore density gradients in the direction normal to the wall are revealed.

It is, of course, well known that a reflected compression wave has always

been observed in shock wave-boundary layer interactions. Many texts begin the study of the interaction by presenting the inviscid (no boundary layer) case for which the reflected wave is shown to be necessary in order to turn the flow back parallel to the solid wall. From the present linearized interaction study, this wave could be considered to be the result of the merging of the compression waves generated by the refractions process near the sonic line. However, the theory is least appropriate for this region and therefore the reflected compression wave would not be the best feature to identify in trying to relate actual flow phenomena to that predicted by the theory. In the inviscid case, the reflected wave is a compression wave only, and thus the predicted possible expansion wave field would have to be considered a unique phenomenon directly associated with the outer boundary layer interaction refraction process. The predicted expansion region would be greatest at the higher Mach numbers (M_∞ must be greater than $\sqrt{2}$) and for thin boundary layers, the greatest expansion region would also be located very close to the expected merging compression waves. This could present a practical problem in identification, for then the expansion region would be optically obscurred by the reflected compression waves if the shock generator was not strictly parallel to the schlieren beam or perhaps be obscurred by shock-side wall boundary layer interference. Figure 30 shows that the laminar rather than the turbulent layer would provide the greater opportunity to observe the expansion field just downstream of the incoming wave without optical interference from the reflected compression waves. Unfortunately, the laminar boundary layer is generally known to separate upstream of the interaction "point". This results in the boundary layer first turning away from the wall, generating upstream compression waves, and then turning toward the wall around the separation region before finally turning again to become parallel to the wall. The latter two flow turning conditions generate expansion and compression waves, respectively. Thus, expansion waves can be present, but they can be the result of both the flow separation process and the refraction generation process. The identification of the features directly corresponding to those predicted from the theory is thus expected to be difficult.

Schlieren photographs in references 162 to 169 were examined. The shocks were generated by wedges in the free-stream, and the boundary layers were, in all but one case, those created by sharp flat plates also mounted in the free-stream. The Mach number range was 1.4 to 8. The shock strengths were stronger than the acoustic strength case for which the above theory was appropriate. It could be expected, however, that even for stronger waves a continuous reflected wave field would exist.

As expected, the previously mentioned complications did present problems in trying to identify a reflected wave field generated in the outer regions of the boundary layer. Except for Pickney (ref. 166), all of the authors presented schematic drawings of the features seen in the original schlieren photographs. Except for Barry, Shapiro, and Newman (ref. 162 - the same Barry of the incremental Mach number analysis), none of the authors presented sketches showing a reflected wave field illustrating the refraction generated reflection feature. The authors describe the interactions as the aforementioned compression-expansion-recompression feature interaction. In fact, in the discussion by Barry, et al., the generation of the expansion region is primarily attributed to the thickened subsonic layer near the wall which tends to present a constant pressure boundary condition and thus a reflected expansion wave. In this reference, Mach 2 schlieren photographs are presented for wedge flow deflection angles of 1° to 6°. An expansion region appears to be present even for the weakest interaction. The photographs are quite small, however,

and essentially reliance must be placed on the author's description. In reference 163, photos (figures 12 and 16) are shown for Mach 1.4 with 3° to 4 1/2° shock generator interactions with laminar and turbulent boundary layers. For the laminar case, a distinct expansion fan is shown emanating from the interaction, but because most of the boundary layer is at Mach numbers less than $\sqrt{2}$, the interaction should produce only compression reflections according to the theory. The expansion wave is thus the result of the thickened and probably separated subsonic region.

In reference 169 Kaufman and Johnson present results from a shock wave laminar boundary layer interaction investigation where weak incident shocks were used. For $M_\infty = 8$, flat plate boundary layer interactions were studied for incident shock deflection angles of 1°, 3°, and 5°. The boundary layer at the interaction point was relatively thick ($\delta \approx 0.6$ cm for the lowest tunnel pressure), and schlieren photos were presented. Although clarity is a problem, it appears to the present author that there was always a compression-expansion-compression reflected wave process, even for the 1° case where it was stated that the boundary layer did not separate. This pattern also appears to occur in the interaction of the very weak shock from the flat plate's leading edge with the boundary layer on the flat plate shock generator. The linearized interaction predicts that only an expansion-compression pattern should occur, and the verification of the refraction features is not conclusive.

There does not appear to be a reflected wave field definitely identifiable as being generated by the refraction process in the boundary layer interaction photographs in any of the reports studied. Rose (ref. 170), however, in reviewing the schlieren photographs from one of his previous hypersonic investigations (ref. 167), states that the refraction generated expansion region is evident. This phenomenon was not mentioned or schematically illustrated in the report of the experimental investigation or in a later note (ref. 171). In the later study (refs. 170, 171) a computer program employing the method of characteristics was used for calculating the inviscid interaction in the outer region of the boundary layer, and a refraction generated reflected wave field was predicted. This was perhaps the reason for the re-examination of the schlieren photographs. These photographs as they exist in the published version examined, do not appear to exhibit the described feature.

In the investigation by Green (ref. 168), the interaction with a Mach 2.5 turbulent boundary layer was studied. Unseparated interactions and ones strong enough to cause separation were studied. Green was aware of refraction analysis results and made an effort to observe in the schlieren photographs the predicted expansion waves from the refraction process within the boundary layer. For the unseparated boundary layer, no expansion waves were seen, and in the separated case, effects of the shock refraction were lost in the expansion fan created by the separated layer (the subsonic vicious part of the layer was reported to dominate the outgoing wave behavior). It was concluded that it was uncertain to what degree the refraction phenomena contributed to the overall wave pattern.

The problem with the boundary layer in trying to identify the refraction features is the presence of the subsonic layer. The refraction analysis was for a shear layer which was entirely supersonic. Liepmann, Roshko, and Dhawan (ref. 163) did attempt a supersonic shear layer shock wave interaction experiment in their shock wave boundary layer interaction investigation. The purpose was to check the applicability of the linearization of the incremental Mach number profile refraction analysis (in this case, that of Marble's work, ref. 75). The wake from a very thin flat plate (0.16 cm thick, 3.8 cm long) provided

the shear layer, and the shock source was from a 4.5° wedge located above the wake. Two schlieren photographs are presented showing shock interactions at distances of 3 cm and 5 cm, respectively, behind the plate's trailing edge. The Mach number was stated to be 1.36 for the conditions of the photographs. Some typical Mach number profiles across the wake are also shown. The conditions for the survey were apparently a little different from the photo conditions, for the local free-stream Mach number was about 1.44 for the survey. At the 3 cm location, the wake centerline Mach number was 1.25. If the same centerline M/M_{∞} condition holds for the $M_{\infty} = 1.36$ case, then the centerline Mach number at the 3 cm location would be about 1.18 (and about 1.22 for the 5 cm location). For a 4.5° wedge at $M_{\infty} = 1.36$ the wave strength would be about $p_2/p_1 = 1.25$. A wave of this strength without focusing would produce subsonic flow downstream of the interaction for an incoming Mach number of 1.18. Thus it may have been that subsonic flow existed downstream of the interaction near the wake centerline. The linearized theory would not be adequate for this region.

A diffuse reflected compression wave field is visible in the photographs and it appears to originate from the upper half of the wake. Inasmuch as the free-stream Mach number is less than $\sqrt{P + 2}$, the refraction analysis would predict that a reflected compression wave field would be generated above the wake centerline and an expansion field below the centerline. The fact that the expansion field is not visible may perhaps be due to the ultimate weakening that this field must experience upon traversing the upper half of the shear layer or to a subsonic flow region around the centerline. The photographs thus appear to demonstrate that partial reflection from a continuous Mach number gradient exists and in a manner perhaps in accord with theory. The wake, however, appears to be turbulent (no Reynolds number information is given) and the conditions are therefore not strictly in agreement with a steady laminar shear layer implicitly assumed in the analysis. If the turbulence is taken as presenting an unsteady Mach number gradient, then the present technique could still be applied and the result would be an unsteady reflected wave field. The diffuse reflected wave pattern seen in the photographs does admit an unsteady-field interpretation and thus the basic reflected-field contention is supported.

It should be mentioned that there exists a separate and sizable body of literature concerned with the problem of the interaction between turbulence and shock waves. The research shows that sound waves are generated as a result of the shock-turbulence interaction; and these researchers would quite likely accept the schlieren photographs as evidence supporting their theories.

Shock-turbulence studies (e.g., refs. 152, 172 to 174) show that when vorticity, temperature spots, or sound waves interact with a shock, all three disturbance modes are generated; the shock wave couples all of the modes. While the methods of analysis differ from the refraction methods in the present report, the spirit is comparable. To investigate shock-turbulence theories, some of the researchers have conducted shock-turbulent wake interaction experiments. Some of this work will be briefly reviewed here inasmuch as any generated sound field will be viewed here as evidence supporting the laminar reflected wave field contention. Schlieren photos of shock interactions with laminar wakes would have been the ideal data to examine for evidence of the continuous reflected wave field, but no such photos were found.

Kovasznay (ref. 175) investigated the interaction of a shock from a 10° wedge with the axisymmetric wake from a one-inch rod at a free-stream Mach number of 1.75. The object of the investigation was to compare fluctuations

in the wake before and after passage through the shock and to locate sound waves emanating from the interaction zone. The principal tool was the hot-wire. Unlike the Liepmann et al. investigation (which was published before the major studies of the shock-turbulence interaction were published), no reference was made to any of the linearized incremental Mach number analyses of the shear layer-shock interaction. The shock wave-turbulence interaction was considered likely to produce sound waves that travel outward approximately along the Mach lines, and these were to be detected with the hot-wire. Schlieren photographs were taken, though not presented, to examine the refraction of the shock wave through the wake. A hot-wire traverse parallel to and just outside the wake revealed a rather intense sound field to be present downstream of the interaction region. It was stated that the sound disturbances seemed to originate in a near-sonic region where the wake crossed the shock wave.

At $M = 1.75$ a 10° wdge produces a shock with a wave strength of about $p_2/p_1 = 1.65$. This wave strength is strong enough to be a normal shock at a Mach number of about $M = 1.25$. Kovasznay reported wake centerline Mach number measurements, and at the approximate location where the shock crossed the centerline the Mach number was about 1.19. It could thus perhaps be expected that an irregular refraction process would have to occur near the centerline. Moeckel (ref. 76 - see footnote "a" p. 12) discusses the possibility of separated flow regions in a free shear layer under these conditions with the possibility of a lambda shock existing outside the shear layer. Henderson (refs. 80, 81, 176) discusses the irregular nature of possible shock refractions. Such a situation is not in accord with the conditions for which the theories for the generated noise field were derived.

In the investigation by Radcliffe (ref. 177), similar shock wave-supersonic shear layer interaction experiments were conducted, and again it was deemed an investigation of the radiated pressure fluctuations caused by the interaction of turbulence with shock waves. A wake from a thin plate was used as the turbulence source, and a 10° wedge was used as the shock generator. Two different Mach numbers were primarily used in the investigation; $M_{\infty} = 1.99$ and $M_{\infty} = 3.14$. To sense the fluctuating acoustic pressures, a small microphone (.07 in dia.) was installed near the sharp leading edge of a small flat plate (1x1 inch) movable instrument head. Shadowgraph photographs were also taken, and thus shock waves could be expected to be easily located, but expansion or compression regions would be difficult to identify. No wake Mach number measurements were made. It was reported that for the $M = 1.99$ flow, a reflected wave was visible, but for the $M = 3.14$ flow, no reflected waves were seen (perhaps for the want of schlieren apparatus). For the high Mach number case it is unlikely that an irregular reflection would occur and the lack of a reflected wave in the shadowgraph appears to confirm this. The present author only had a microfilm copy of the report available, and only one flow photograph, for $M = 1.99$, was successfully reproduced so that details could be seen. For the lower Mach number condition, the shock wave appeared to become normal to the flow within the wake, and the reflected wave system had the appearance of the so-called Mach reflection condition. For $M = 1.99$ and a 10° wedge, the shock strength is strong enough to become normal at $M = 1.42$. The centerline Mach number was estimated to be about 1.37 and thus the irregular shock system could be expected. For both Mach number flows, the output from the microphone reached a maximum when the diaphragm was in the vicinity of the location of a Mach line drawn from the edge of the wake. Agreement between the measured fluctuating pressure levels and that estimated from theory was not found to be good. It was also concluded that inspection of the spectra of the microphone responses revealed no clear indication of the source of the fluctuating pressures.

Appendix D

Geometric Acoustic Approach to the Weak Shock Wave Boundary Layer Interaction

As in the main text, the problem considered here is the refraction through the laminar boundary of a weak plane wave. In the interaction the boundary layer can be considered as a medium in which the fluid properties vary only in the vertical direction. Such a medium is called a stratified or layered medium, and owing to the fact that the earth's atmosphere and oceans can often be considered as stratified media, sound wave propagation in stratified media has been extensively studied. As Tolstoy points out in his wave propagation text (ref. 93, p. 87), the subject "propagation in stratified media" has, over the years, almost become a discipline by itself as a subdivision of wave theory. Geometric acoustics is part of this discipline. In sound propagation problems the method of geometric acoustics is frequently used, and it appeared that such an approach could be applied to the laminar boundary layer case and perhaps yield additional insight into the interaction problem. The method is a linear one, and the result should agree with those of the more conventional fluid dynamics approach in Appendix C.

In the field of supersonic aerodynamic research, the method of geometric acoustics has been used most often in the study of the propagation through the atmosphere of the sonic boom (see, for example, refs. 39, 99, 178, 179). In this application the method is essentially used as a means of studying the propagation of weak shock waves through a nonuniform medium. In the present study the boundary layer noise has been likened to very weak shock waves, and thus it appeared that the problem of the interaction of a weak shock wave with the boundary layer (a nonuniform medium) could be suitably examined using the method of geometric acoustics.

In geometric acoustics the signal is considered to propagate along rays. For the steady case the rays are geometric entities, and the concept of rays is probably most familar from studies of elementary optics. Classically, the method of geometric optics represents a specialized solution to the wave equation. This specialized solution is for the limiting case of the wave length of the disturbance approaching zero (or the frequency approaching infinity - see, for example, refs. 84, 180). These restrictions are often stated in the manner that geometrical optics is appropriate for the case in which the changes in the properties of the medium over a wavelength are a small fraction of themselves. Thus, geometric optics solutions are appropriate for many practical situations of high frequency propagation problems (a more thorough statement of the criteria is given by Kerr in ref. 181). The similarities between light and sound propagation have long been recognized, and the criteria for the use of geometric optics are similar to those used for acoustic phenomena. (The descriptive use of ray geometry was applied to sound nearly 100 years ago by Rayleigh (ref. 88), but the term geometric acoustics was coined much more recently; perhaps appearing first in the work of Blokhintsev (at least in the English translations - refs. 38, 182)). For acoustic phenomena, however, there is another factor which imposes a limitation on the use of geometrical methods. This is the requirement that the strength or amplitude of the wave system be small enough to be appropriate for the use of the wave equation.

For the case of the zero wavelength limit in a nonmoving inviscid medium,

the wave equation, $\nabla^2\psi = \frac{1}{a^2}\frac{\partial^2\psi}{\partial t^2}$, can be reduced to the so-called eikonal equation

$$|\vec{\nabla S}|^2 = \mu^2 \ (x,y,z)$$

where $S\ (x,y,z)$ is the phase function of the wave, the eikonal function; and the wave surfaces are defined as surfaces of equal phase; $\mu\ (x,y,z)$ is the index of refraction and is defined to be $\frac{a_o}{a\ (x,y,z)}$, where a_o is some wave velocity adopted as a reference. The eikonal equation is obtained by assuming a solution of the form $\psi\ (x,y,z,t) = A\ (x,y,z)e^{i[k_o S(x,y,z)-\omega t]}$, where $k_o = \omega/a_o = 2\pi/\lambda_o$ is the reference wave number, and substituting it into the wave equation and then neglecting the terms involving $\nabla^2 A$ (e.g., ref. 84). The eikonal equation can be regarded as an infinitesimal formulation of Huygens' principle for wave surface construction. The solution $S\ (x,y,z)$ of the eikonal equation can in principle be found for a given $\mu\ (x,y,z)$ and initial surface S = constant. However, the point of view of geometric acoustics is to deal directly with the ray trajectories rather than finding them by initially solving the eikonal equation each time for the eikonal function $S\ (x,y,z)$. The ray paths for a stationary medium are normal to the wavefronts, and the equations for ray paths are derived by making use of the fact that the gradient of S is a vector perpendicular to S and thus in the direction of the ray. A resulting equation is

$$\frac{d}{ds}(\mu\hat{s}) = \vec{\nabla}\mu \qquad \text{(D1)}$$

where s is the arc length of the ray and $\hat{s}$ is the unit vector in the ray direction. Equation (D1) is a differential equation from which ray trajectories may be obtained. Equation (D1) can also be shown to be equivalent to Fermat's principle of "least time". In many practical situations, such as propagation through the atmosphere or ocean, the index of refraction is often a function of only one coordinate and the three scaler equations (D1) can be integrated readily. A resulting expression in this particular instance is immediately recognized as the ordinary Snell's law, and, in the more general cases, the results are sometimes referred to as generalized Snell's laws. A more thorough discussion of these brief statements can be found in ref. 84. The connection between ray and wave optics is discussed in detail in ref. 85.

In this very brief introduction to geometrical acoustics, the method has been presented as being appropriate for the case of periodic disturbances of very high frequency. This is an oft stated condition arising from the heritage of classical geometrical optics. But geometric acoustics is also quite appropriate for weak shock waves (acoustic discontinuities). Keller (ref. 86) observed that certain shock wave phenomena had often been described in optical terms, and he proceeded to show that weak shocks could be analyzed by the methods of geometric optics and stating, in fact, that the theory of weak shocks could be called geometrical acoustics. Heller (ref. 183) has given a derivation of a generalized eikonal equation for the case of a pressure discontinuity propagating through an inhomogeneous moving medium. Friedlander (ref. 87) also developed the theory of geometric acoustics out of the need for the description of the propagation of sound pulses (acoustic shocks), and in fact, describes his book as an essay on the pulse solutions of the wave equation. Kline and Kay (ref. 85) begin their approach to electromagnetic

theory and geometrical optics by considering the propagation of discontinuities in the electric and magnetic field strength; the latter part of the book presents geometric optics from the high-frequency periodic wave viewpoint. They state that in acoustics, shock waves are the "geometric optics" of the ordinary waves. It is also mentioned that in view of well developed wave theory for acoustics, the introduction of geometrical acoustics might appear to be a step backward, comparable to abandoning Maxwell's equations in favor of geometrical optics. Because of the interest in weak shock waves, it was reasoned, the method of geometric acoustics was warranted. Thus, geometric acoustics is eminently suited for the study of weak shock waves (see also Kline, ref. 184).

In the traditional sense of classical geometric optic studies, the interest has been primarily in the determination of the ray paths and not in the amplitude of the disturbances. The amplitude of the wave disturbances, however, can be found by the use of the theory. It is possible to find the wave amplitudes by an integration along the ray paths (refs. 84, 86 for example), but the method most often used in weak shock studies involves the use of the ray tube and energy considerations. A ray tube is essentially a bundle of adjacent rays. The ray tube is a differential area quantity similar to the stream tube from fluid dynamics (just as the ray is similar to the steady flow streamline). Because the energy propagates along the ray paths, the energy flow along a ray tube is constant. The convergence or divergence of adjacent rays because of gradients in the medium (i.e., refraction effects) cause the ray tube cross sectional area to decrease or increase. This results in an increase or decrease in the intensity of the energy flux and, as will be shown below, a corresponding change in the wave strength.

In order to take advantage of the energy flow invariance along a ray tube, a relationship between the wave strength and energy content of a wave system is needed. For conditions appropriate for the use of geometric acoustics, the curvature of the wave fronts is so slight that locally the wave fronts appear planar. It is thus appropriate to consider the portion of wave front intersecting the differential area ray tube to be a plane wave and the rather simple expression for the energy density of a plane wave can be used. The acoustic energy density for a plane wave is:

$$\frac{\rho(\Delta u)^2}{2} + \frac{(\Delta p)^2}{2\rho a^2}$$

where Δu and Δp are the amplitudes of the particle velocity and pressure change associated with the wave, respectively. The energy density is half kinetic and half potential (see, for example, Chapter 5 of refs. 84 or 185). The total energy is therefore $(\Delta p)^2/\rho a^2$ [or $\rho(\Delta u)^2$]. For the stationary atmosphere, the energy flow is invariant along the ray tube, and this quantity is equal to the energy density $(\Delta p)^2/\rho a^2$, times the volume flow rate aA_n, where A_n is the normal cross sectional area of the ray tube. The invariant quantity is therefore

$$\frac{(\Delta p)^2}{\rho a^2}\ [aA_n] = \frac{(\Delta p)^2}{\rho a}\ A_n = \text{constant}$$

When a nonuniform medium is moving the situation becomes more complex. In a moving medium the ray paths are not normal to the wave fronts and the energy flow is no longer invariant along the ray tubes. The lack of energy flow

invariance occurs because essentially the waves themselves do not constitute a conservative system; they can exchange energy with the mean flow. There is, however, a quantity akin to the expression in the above equation which is invariant, and this was first presented by Blokhintsev. Blokhintsev (refs. 38, 182) made a detailed study of acoustics in a nonhomogeneous moving medium. Using approximations consistent with a geometric acoustic approach, he derived an expression for a generalized eikonal equation which can be written as

$$|\vec{\nabla}s|^2 = \mu^2 \left[1 - \frac{\vec{V}\cdot\nabla s}{c_o}\right]^2 \tag{D2}$$

where $\vec{V}$ is the velocity vector of the moving fluid, and c_o is a reference sound speed. This expression of course reduces to the usual eikonal equation when $\vec{V}$ is zero. Other derivations of the generalized eikonal equation have been presented by Kornhauser (ref. 186) and Heller (ref. 183). By differentiating the equation of a moving phase surface ($k_o s(x,y,z)-wt$ = const) with respect to time and using eq. (D2), Blokhintsev further showed that the phase velocity of the wave equaled the sum of local velocity of sound and the component of the medium velocity in the direction of the normal to the wave front. That is

$$c_n = a + V_n = a + \hat{n} \cdot \vec{V} \tag{D3}$$

where $\hat{n}$ is the unit normal to the wave front (surface of constant phase). The phase velocity has been designated by c_n because it will shortly be shown that this quantity is the projection of the ray velocity, c, in the direction of the normal to the wave front. Blokhintsev was further able to show that the ray velocity, or the velocity of the energy flow (often referred to as the group velocity), is the vector sum of the local sound speed and the medium velocity. That is,

$$\vec{c} = a\,\hat{n} + \vec{V} \tag{D4}$$

It is evident that $c_n = \hat{n}\cdot\vec{c}$, and for a moving medium the ray direction is not in the direction of the wave normal. The relationship between c_n and $\vec{c}$ is illustrated in figure 10.

Historically, equations (D3) and (D4) have been in use since the early part of this century for ray tracing problems concerned with atmospheric sound propagation, but they were the basic assumptions for the studies rather than derived results. For example, Milne (ref. 187) used equation (D4) as a basic principle for the determination of sound rays. A more recent treatment of ray tracing for the propagation of sound in a moving medium have been presented by Groves (ref. 98), Thompson (ref. 188), Engelke (ref. 189), and Uginčius (ref. 190) (and see the references contained in these).

As indicated earlier, the energy invariant along the ray tube for a stationary medium is not appropriate for a moving medium. Blokhintsev derived an acoustic energy transport equation suitable for the geometric acoustic applications as

$$\frac{\partial E}{\partial t} + \vec{\nabla} \cdot (E\vec{c}) = 0 \tag{D5}$$

where E can be written as

$$E = \frac{(\Delta p)^2}{\rho a^3} c_n$$

For the steady case, $\vec{\nabla}\cdot E\vec{c} = 0$ (a continuity equation for $E\vec{c}$), and thus for a ray tube of cross sectional area A_n

$$E|\vec{c}|A_n = \text{constant}$$

or

$$\frac{(\Delta p)^2}{\rho a^3} c_n [\vec{c}\cdot\vec{A}] = \text{constant} \qquad \text{(D6)}$$

where $\vec{A}$ is the area vector of the ray tube area normal to the rays. The expression in equation (D6) is similar to the earlier discussed energy invariant quantity for a stationary medium, and it is an energy density $(\Delta p)^2 c_n/\rho a^3$ times a volume flow rate $\vec{c}\cdot\vec{A}$. Hayes refers to the expression in (D6) as the Blokhintsev invariant. Equation (D5) and expressions equivalent to (D6) have also been derived by Ryshov and Shefter (ref. 191) in a very different manner than that of Blokhintsev (in a manner perhaps more akin to an aerodynamicist's approach). Ribner (ref. 192) expressed concern over the lack of higher-order terms in the energy flow expression, but advocated its use after he applied the Blokhintsev expression to a particular problem for which he had previously worked out the energy flow density and found agreement. A brief outline of some of Blokhintsev's results is presented by Ingard (ref. 193). Blokhintsev's results have been generalized by Bretherton and Garrett (ref. 194) to include the case of wave trains propagating in slowly time varying media. For the steady flow case an equation similar to (D5) was developed with the E replaced by E'/ω', where E' and ω' represent the energy density and frequency relative to a frame of reference in which the mean flow is locally at rest. The E'/ω' ratio was called the wave action. The wave action concept has been discussed by Lighthill (refs. 94, 195). Candel (refs. 196, 197), discusses and uses other forms of acoustic energy in aeroacoustic problems.

The problem considered in the present analysis is the interaction of a plane acoustic-strength shock with the laminar boundary layer. The source of the wave is assumed to be far enough away so that the plane wave assumption is locally valid. To apply the method of geometric acoustics a coordinate system must be established. A convenient and natural way of doing this is to select a system which is fixed with respect to the fluid which moves immediately adjacent to the shock source. In the present noise model this fluid is assumed to be the tunnel free-stream, although in fact, the sources are inside the tunnel nozzle turbulent boundary layer. With this reference system the source appears to move supersonically through a uniform and stationary medium in the direction of the nozzle throat. This situation provides straightforward initial conditions for the wave and rays. In the stationary uniform medium the ray paths are parallel and in the direction of the wave normal, and the initial angles are easily related to the source relative Mach number. In this coordinate system the laminar boundary layer presents steady but nonuniform wind and temperature conditions to the locally plane wave. The situation was depicted earlier in figure 11. The problem is now very much like the sonic boom refraction problem. Hayes, Haefeli, and Kulsrud (ref. 39) have presented a study of the case of the sonic boom propagating through a horizontally stratified atmosphere with wind conditions allowed, and their study is very suitable for the present problem. The present approach was guided by their report. A brief paper presenting the highlights of their analysis may be found in refs. 198 and 199, and an even shorter account is outlined in ref. 200. (In ref. 198 it appears that θ was

inadvertently defined to be the angle from the horizon to the ray, whereas it should have been from the horizon to the normal to the wave front; the ray direction and wave normal direction no longer coincide when wind conditions are present).

The Blokhintsev invariant, quantity (D6), will be used to determine the behavior of the strength of the weak incoming wave as it propagates through the laminar boundary layer. The quantity actually sought is $\Delta p/\Delta p_\infty$, and thus only ratios of various quantities will be needed. Specifically, using the invariant, the pressure rise ratio is easily seen to be

$$\frac{\Delta p}{\Delta p_\infty} = \sqrt{\frac{\rho a^3}{\rho_\infty a_\infty^3} \frac{c_{n_\infty} (\vec{c}_\infty \cdot \vec{A}_\infty)}{c_n (\vec{c} \cdot \vec{A})}} \tag{D7}$$

This equation may be simplified immediately by using the fact that $a^2 = \gamma RT$. The first fraction under the radical sign may thus be written as

$$\frac{\rho a^3}{\rho_\infty a_\infty^3} = \frac{\rho RTa}{\rho_\infty RT_\infty a_\infty} \tag{D8}$$

where R is the gas constant. But, by the ideal gas law, $p = \rho RT$, and since the static pressure is constant, equation (D8) becomes simply

$$\frac{\rho a^3}{\rho_\infty a_\infty^3} = \frac{a}{a_\infty}$$

Thus, equation (D7) reduces to

$$\frac{\Delta p}{\Delta p_\infty} = \sqrt{\frac{a\, c_{n_\infty} (\vec{c}_\infty \cdot \vec{A}_\infty)}{a_\infty\, c_n (\vec{c} \cdot \vec{A})}} \tag{D9}$$

The quantities a, c_n, and $\vec{c} \cdot \vec{A}$ must be evaluated at points along the ray path.

The quantity c_{n_∞}/c_n in equation (D9) may be expressed in terms of the wave angles by the use of Snell's law for a moving medium. For a local stream velocity, V, this law may be written as

$$\text{const} = a \sec \phi + V = \frac{a + \hat{n} \cdot \vec{V}}{\cos \phi} = \frac{c_n}{\cos \phi} \tag{D10}$$

where it is assumed that the horizontal component of the wave velocity and the flow velocity are in the same direction (i.e., sound is traveling with the wind). Thus,

$$\frac{c_{n_\infty}}{c_n} = \frac{\cos \phi_\infty}{\cos \phi}$$

and equation (D9) becomes

$$\frac{\Delta p}{\Delta p_\infty} = \sqrt{\frac{a \cos \phi_\infty (\vec{c}_\infty \cdot \vec{A}_\infty)}{a_\infty \cos \phi (\vec{c} \cdot \vec{A})}} \tag{D11}$$

The $\vec{c}\cdot\vec{A}$ terms in equation (D11) can easily be expressed in terms of the fluid variables and the wave angle. $\vec{A}$ and $\vec{c}$ are collinear and therefore,

$$\vec{c}\cdot\vec{A} = |\vec{c}|\ |\vec{A}| = c\ A$$

where A is the magnitude of the cross sectional area of the ray tube. Referring to figure 10 of the text again, by the use of the law of cosines, c may be expressed as

$$c = \sqrt{a^2 + V^2 + 2aV \cos \phi}$$

or

$$c = a \sqrt{1 + M^2 + 2M \cos \phi}$$

Outside the boundary layer, $c = a_\infty$, and equation (D11) may finally be written as

$$\frac{\Delta p}{\Delta p_\infty} = \sqrt{\frac{\cos \phi_\infty}{\cos \phi} \frac{A_\infty}{A} \frac{1}{\sqrt{1+M^2+2M \cos \phi}}} \tag{D12}$$

Equation (D12) will now be applied specifically to the problem at hand. To do this, additional details and nomenclature of the coordinate system must be established.

As previously stated, the coordinate system is fixed relative to the free-stream. The situation is depicted in figure 11 of the main text where it is seen that the noise source is moving in the negative direction with speed $|u_{sr}|$. The subscript s refers to the wave source, and the subscript r indicates quantities referenced to the coordinate system attached to the free-stream (the relative system). An absence of the r subscript denotes velocities as determined in the usual tunnel stationary coordinate system. The boundary layer is also moving in the negative direction with speed $|u_\infty|$ at the wall. The velocity of the fluid in the present coordinate system is determined from

$$u_r(y) = u(y) - u_\infty \tag{D13}$$

and the wave source has a velocity given by

$$u_{sr} = u_s - u_\infty \tag{D14}$$

With the coordinate system and nomenclature now established, each of the three ratios in equation (D12) will next be evaluated individually. The quantity $\cos \phi_\infty / \cos \phi$ will be attacked first.

In the new notation, Snell's law becomes

$$\frac{a}{\cos \phi} - u_r = \text{const} \tag{D15}$$

where, since the wave velocity (actually, the horizontal component of it) and the flow velocity are in the same direction, a negative sign is needed because

u_r, as seen from equation (D7), is a negative quantity. The value of the constant is easily established using the free-stream conditions. In the free-stream, $u_r = 0$, and equation (D15) becomes

$$\text{constant} = \frac{a_\infty}{\cos \phi_\infty} \tag{D16}$$

In the free-stream the wave angle is just the Mach angle, and hence, with μ representing the wave angle,

$$\sin \mu_\infty = \frac{1}{-M_{sr}} \tag{D17}$$

Again, the negative sign is needed because M_{sr} is a negative quantity. Therefore, since $\phi_\infty = 90^o - \mu_\infty$, in terms of ϕ_∞, equation (D17) becomes,

$$\cos \phi_\infty = \frac{1}{-M_{sr}} \tag{D18}$$

and substituting into eq. (D16) gives

$$\text{constant} = -a_\infty M_{sr}$$

$$= -u_{sr}$$

Snell's law may then be written as:

$$\frac{a}{\cos \phi} - u_r = -u_{sr}$$

Solving for $\cos \phi$ gives

$$\cos \phi = \frac{a}{u_r - u_{sr}}$$

$$= \frac{1}{M_r - M_{sr} \frac{a_\infty}{a}} \tag{D19}$$

The quantity $M_r - M_{sr} \frac{a_\infty}{a}$ will show up frequently in the remaining work, and it is important to understand the meaning of this term. Dividing equations (D13) and (D14) by a and a_∞, respectively, yields

$$M_r = M - M_\infty \frac{a_\infty}{a} \tag{D20}$$

and

$$M_{sr} = M_s - M_\infty \tag{D21}$$

Consequently,

$$M_r - M_{sr} \frac{a_\infty}{a} = M - M_s \frac{a_\infty}{a} \tag{D22}$$

or

$$M_r - M_{sr} \frac{a_\infty}{a} = \frac{u - u_s}{a}$$

This result shows that $M_r - M_{sr}\, a_\infty/a$ is just the local Mach number of the fluid relative to the wave. In view of this fact, equation (D19) shows that the wave is inclined at the angle which is just the Mach angle corresponding to the local relative Mach number condition. This is what one would expect, and thus Snell's law conforms with one's understanding of basic facts from elementary gas dynamics texts. Note that if the source is not moving, equations (D22) and (D19) reduce to the familiar result that the Mach angle μ is given by $\sin \mu = \cos \phi = 1/M$. The desired ratio $\cos \phi_\infty / \cos \phi$, may finally be expressed as, using equations (D18) and (D19),

$$\frac{\cos \phi_\infty}{\cos \phi} = \frac{M_r - M_{sr} \dfrac{a_\infty}{a}}{- M_{sr}} \tag{D23}$$

Because the quantity $M_r - M_{sr} \dfrac{a_\infty}{a}$ will show up so frequently, it is convenient in the algebraic manipulations to represent it by a single symbol, say B. Equation (23) then becomes

$$\frac{\cos \phi_\infty}{\cos \phi} = \frac{B}{- M_{sr}} \tag{D24}$$

The third ratio in equation (D12) will next be evaluated (temporarily skipping the second one, A_∞/A). With respect to the relative coordinate system, the ratio is

$$\frac{1}{\sqrt{1 + M^2 + 2\, M \cos \phi}} = \frac{1}{\sqrt{1 + M_r^{\,2} - 2\, M_r \cos \phi}}$$

Substituting for the $\cos \phi$ from (D24) and (D18) gives

$$\frac{1}{\sqrt{1 + M_r^{\,2} - 2\, M_r \cos \phi}} = \sqrt{\frac{B}{B\, M_r^{\,2} - 2\, M_r + B}} \tag{D25}$$

The final ratio to be evaluated in equation (D12) is A_∞/A. This quantity is evaluated with the aid of figure 31. In the two dimensional interactions considered, the horizontal distance between two rays will remain constant due to uniform free-stream flow and the assumption of a parallel flow in the boundary layer. Thus if two rays have an initial separation distance of dx, as seen in the figure, the cross sectional mean ratio is simply

$$\frac{A_\infty}{A} = \frac{\sin \gamma_\infty}{\sin \gamma}$$

where γ is the angle of the ray from the horizontal. Inasmuch as $\gamma_\infty = \phi_\infty$, the only unknown quantity is $\sin \gamma$. The $\sin \gamma$ may actually be determined in terms of a, c, u_r, and θ by using trigonometric identities and relationships involved in the triangle of figure 10. However, in figure 31 it is also seen that $\tan \gamma = dy/dx$, and hence

$$\sin \gamma = \frac{dy}{\sqrt{(dx)^2 + (dy)^2}}$$

or,

$$\sin \gamma = \frac{dy/dx}{\sqrt{1 + \left(\dfrac{dy}{dx}\right)^2}}$$

The area ratio may therefore be written as

$$\frac{A_\infty}{A} = \frac{\left.\frac{dy}{dx}\right|_\infty}{\frac{dy}{dx}} \sqrt{\frac{1 + \left(\frac{dy}{dx}\right)^2}{1 + \left(\frac{dy}{dx}\right)_\infty^2}} \tag{D26}$$

The area ratio has now been given in terms of the slope of the ray path, dy/dx. If an expression for dy/dx can be obtained, then one also has the first-order differential equation for the ray path! This is strong inducement, indeed, to evaluate the area ratio by the use of equation (D26). Inasmuch as the differential equation can be derived rather quickly and will actually be used later (in Appendix G), this will be done now. Once the differential equation is available, the evaluation of equation (D26) will be quite simple.

To derive the differential equation an incremental velocity profile as shown in figure 32 is used. The ray path and coordinate system are also shown in the figure. Inside each Δy interval the fluid properties are assumed constant and the ray path will thus be straight. The problem is to calculate the (x_i/y_i) coordinates of the path at the boundaries of each of the zones. The details of the path through a zone are shown in figure 33. The geometry shown is appropriate for Snell's law for a moving medium, and the figure is similar to figure 10. The $\Delta x_i/\delta$ is the specific quantity desired, where δ is the boundary layer thickness, and this is determined as follows. From the geometry, assuming constant thickness Δy intervals,

$$\tan \gamma_i = \frac{\Delta y/\delta}{\Delta x_i/\delta} \tag{D27}$$

Also from the geometry

$$\tan \gamma_i = \frac{a_i \sin \phi_i}{-u_{ri} + a_i \cos \phi_i} \tag{D28}$$

where a_i and u_{ri} are, respectively, the sound speed and relative velocity in the ith zone. A negative sign is again needed in front of u_{ri}, for in the configuration shown, u_{ri} is a negative quantity. Substituting equation (D27) into (D28) and dropping the i's and simplifying, gives

$$\frac{\Delta x}{\delta} = \frac{\Delta y}{\delta} \quad \frac{-u_r + a \cos\phi}{a \sin\phi}$$

or

$$\frac{\Delta x}{\Delta y} = \frac{-B M_r + 1}{\sqrt{B^2 + 1}}$$

Taking the limit as the Δy increments approach zero gives the desired ray path differential equation

$$\frac{dy}{dx} = \frac{\sqrt{B^2 - 1}}{-B M_r + 1} \tag{D29}$$

Kornhauser (ref. 186) derived the ray path differential equation (his eq. 36) in a form which can be shown to reduce to equation (D29).

Returning to the evaluation of A_∞/A via equation (D26), the value of $\left.\frac{dy}{dx}\right|_\infty$ is still needed. Outside the boundary layer $M_r = 0$ and $B = -M_{sr}$. Hence,

$$\left.\frac{dy}{dx}\right|_\infty = \sqrt{M_{sr}^2 - 1} \tag{D30}$$

Substituting equations (D29) and (D30) into (D26) yields, after simplification,

$$\frac{A_\infty}{A} = \frac{\sqrt{M_{sr}^2 - 1}}{-M_{sr}} \sqrt{\frac{B\,(B\,M_r^2 - 2\,M_r + B)}{B^2 - 1}} \tag{D31}$$

The three ratios needed to evaluate $\Delta p/\Delta p_\infty$ in equation (D12) have now been formulated. Substituting equations (D23), (D25) and (D31) into equation (D12) results in

$$\frac{\Delta p}{\Delta p_\infty} = \frac{B}{-M_{sr}} \left[\frac{M_{sr}^2 - 1}{B^2 - 1}\right]^{1/4}$$

or, replacing B,

$$\frac{\Delta p}{\Delta p_\infty} = \frac{M_r - M_{sr}\frac{a_\infty}{a}}{-M_{sr}} \left[\frac{M_{sr}^2 - 1}{(M_r - M_{sr}\,a_\infty/a)^2 - 1}\right]^{1/4} \tag{D32}$$

In terms of the usual fixed coordinate system, equation (D32) may be written, with the use of equations (D20) and (D21), as

$$\frac{\Delta p}{\Delta p_\infty} = \frac{M - M_s\frac{a_\infty}{a}}{M_\infty - M_s} \left[\frac{(M_\infty - M_s)^2 - 1}{(M - M_s\,a_\infty/a)^2 - 1}\right]^{1/4} \tag{D33}$$

The final result, equation (D33), agrees precisely with the result from the linearized fluid dynamics approach, Appendix C equation (C14). The two methods of approach utilize very different models of the interaction process, but while giving the same equation describing the strength of the wave, each seems to have a different phenomenon which it "explains" better. The caustic is nicely explained in the geometric acoustic approach as the convergence of the ray tube and consequent increase in strength of the wave amplitude. The phenomenon of the decrease and subsequent increase in wave strength as it propagates through a region where the magnitude of the relative Mach number decreases from greater than to less than the $\sqrt{2}$ is nicely explained in the fluid dynamic approach by the fact that the continuously reflected wave field changes its nature from an expansion to a compression field. The geometric acoustic approach is silent on the matter of continuous partial reflections.

Appendix E

Thickness of Shocks

The problem of the flow through a normal shock is one of the few cases where the full compressible Navier-Stokes equations can be solved in a direct fashion. With some special assumptions concerning the properties of the gas, the solution for the velocity distribution through the shock is obtained in the form of a simple integral which can be evaluated numerically. For a weak shock the solution can even be expressed in the form of an algebraic formula. These results will be derived herein. G. I. Taylor (ref. 201) gave a solution for weak shocks in 1910, and the problem is discussed in various degrees in a number of textbooks. The approach followed here resembles that of Morduchow & Libby (ref. 202) and White (ref. 203).

It is assumed in the analysis that the problem is a one-dimensional one and hence all variables are a function of x only. It is further assumed that the flow is adiabatic and that there are no body forces. In this case the continuity, momentum, and energy equations are, respectively,

$$\frac{d}{dx}(\rho u) = 0 \tag{E1}$$

$$\rho u \frac{du}{dx} = -\frac{dp}{dx} + \frac{d}{dx}\left[(2\mu + \lambda)\frac{du}{dx}\right] \tag{E2}$$

$$\rho u \frac{dh}{dx} = u\frac{dp}{dx} + \frac{d}{dx}\left(k\frac{dT}{dx}\right) + (2\mu + \lambda)\left(\frac{du}{dx}\right)^2$$

where λ is the second coefficient of viscosity. The inviscid theory holds far upstream and downstream, and the normal shock equations may thus be used to relate these two uniform boundary regions.

The shock problem is seen to be one in which the second coefficient of viscosity is present. Inasmuch as λ is not present in the boundary layer equations and does not occur in incompressible flow problems, this aspect of the problem is rather unusual in viscous flow problems. In the present analysis Stokes' hypothesis will be invoked and λ given the value of $-2/3\mu$. This is equivalent to assuming that the coefficient of bulk viscosity, $\lambda + 2/3\mu$, is zero. This condition is assumed to occur in the kinetic theory of gases for monatomic gases and may not be appropriate for air, but most authors have implicitly made the assumption in the shock problem. In view of the present purpose, Stokes' hypothesis is considered acceptable, especially since little is known about how λ behaves as a function of pressure and temperature.

Integrating the continuity equation gives

$$\rho u = \text{const.} = \rho_i u_i = \rho_f u_f \tag{E3}$$

where the subscripts i and f refer to the initial and final conditions, respectively. Substituting this result into the momentum equation and using this equation to eliminate dp/dx from the energy equation gives

$$\rho_i u_i \frac{dh}{dx} = \frac{4}{3}\left[u\frac{d}{dx}\left(\mu\frac{du}{dx}\right) + \mu\left(\frac{du}{dx}\right)^2\right] - \rho_i u_i u\frac{du}{dx} + \frac{d}{dx}\left(k\frac{dT}{dx}\right)$$

$$= \frac{4}{3}\frac{d}{dx}\left(u\mu\frac{du}{dx}\right) - \rho_i u_i u\frac{du}{dx} + \frac{d}{dx}\left(k\frac{dT}{dx}\right)$$

Integrating yields

$$h + \frac{u^2}{2} - \frac{1}{\rho_i u_i}\left(k\frac{dT}{dx} - \frac{4}{3}u\mu\frac{du}{dx}\right) = \text{const} \tag{E4}$$

Further, assuming the gas to be ideal allows the use of the relation $dh = c_p dT$, where h is the enthalpy and c_p the specific heat at constant pressure, and from the definition of the Prandtl number, $Pr = \mu c_p/k$, equation (E4) may be written as

$$h + \frac{u^2}{2} - \frac{4}{3}\frac{\mu}{\rho_i u_i}\frac{d}{dx}\left(\frac{3}{4}\frac{h}{Pr} + \frac{u^2}{2}\right) = \text{const}$$

Dictated by the 3/4 factor in the equation, the Prandtl number of the gas is assumed to be 3/4, which also happens to be a reasonable value for air, and the equation becomes

$$h + \frac{u^2}{2} - \frac{4}{3}\frac{\mu}{\rho_i u_i}\frac{d}{dx}\left(h + \frac{u^2}{2}\right) = \text{const}$$

This equation may be separated and integrated, and the solution which does not diverge at infinity is

$$h + \frac{u^2}{2} = \text{const}$$

or

$$c_p T + \frac{u^2}{2} = \text{const} = c_p T_i + \frac{u_i^2}{2} \tag{E5}$$

Using the fact that for an ideal gas $c_p = \gamma R/(\gamma - 1)$. Equation (E5) may be expressed as

$$RT = \frac{\gamma-1}{\gamma}\left(\frac{\gamma R}{\gamma-1}T_i + \frac{u_i^2}{2} - \frac{u^2}{2}\right) \tag{E6}$$

The momentum equation may be directly integrated to give

$$\rho_i u_i u + p - \frac{4}{3}\mu\frac{du}{dx} = \rho_i u_i A = p_i + \rho_i u_i^2 \tag{E7}$$

where A is an integration constant. Using the continuity equation (E3), the ideal gas law may be written in the form

$$p = \frac{\rho_i u_i}{u} RT$$

and equation (E7) may then be written as

$$u^2 + RT = \frac{4}{3}\frac{\mu u}{\rho_i u_i}\frac{du}{dx} + \frac{u}{u_i}(RT_i + u_i^2) \tag{E8}$$

Substituting equation (E6) into (E8) gives, after some manipulation and letting $V = u/u_i$,

$$\frac{4}{3}\frac{\mu}{\rho_i u_i} V\frac{dv}{dx} = \frac{\gamma-1}{2\gamma} + \frac{\gamma+1}{2\gamma}V^2 - V - \frac{RT_i}{u_i^2}(V - 1) \tag{E9}$$

But

$$\frac{RT_i}{u_i^2} = \frac{p_i}{\rho_i u_i^2} = \frac{1}{\gamma M_i^2}$$

and equation (E9) may be written in the form

$$\frac{4}{3}\frac{\mu}{\rho_i u_i} V \frac{dV}{dx} = \frac{\gamma+1}{2\gamma}\left[\frac{\gamma-1}{\gamma+1} + V^2 - \frac{2\gamma}{\gamma+1} V - \frac{2(V-1)}{(\gamma+1)M_i^2}\right] \tag{E10}$$

Using the normal shock relation

$$\frac{u_f}{u_i} = V_f = \frac{\gamma-1}{\gamma+1} + \frac{2}{(\gamma+1)M_i^2} \tag{E11}$$

equation (E1) may be written as

$$\frac{4}{3}\frac{\mu}{\rho_i u_i} V \frac{dV}{dx} = \frac{\gamma+1}{2\gamma}\left[(V-1)(V-V_f)\right]$$

or

$$\rho_i u_i dx = \frac{-8\gamma}{3(\gamma+1)} \frac{\mu V dV}{(1-V)(V-V_f)}$$

Dividing through by μ_i and integrating gives

$$Re_x = \frac{-8\gamma}{3(\gamma+1)} \int \frac{\mu/\mu_i \, V dV}{(1-V)(V-V_f)} + \text{const} \tag{E12}$$

Using a power law for viscosity, $\mu/\mu_i = (T/T_i)^n$, and the fact that

$$\frac{T}{T_i} = 1 + \frac{\gamma-1}{2} M_i^2 (1-V^2) \tag{E13}$$

equation (E12) may finally be written as

$$Re_x = \frac{-8\gamma}{3(\gamma+1)} \int \frac{\left[1 + \frac{\gamma-1}{2} M_i^2 (1-V^2)\right]^n V}{(1-V)(V-V_f)} dV + \text{const} \tag{E14}$$

Equation (E14) is the desired result and expresses the velocity variation through the shock as a function of the distance Reynolds number evaluated using upstream gas properties. Morduchow & Libbey (ref. 202) have used $n = 0.768$ for air, and White (ref. 203) has used the value of 2/3. Again, equation (E14) is appropriate for an ideal gas with $Pr = 3/4$ and zero bulk viscosity.

Once the velocity distribution is known the temperature distribution may be obtained from equation (E13). Other quantities may be obtained from the relations below.

$$\frac{\rho}{\rho_i} = \frac{u_i}{u} = \frac{1}{V}$$

$$\frac{p}{p_i} = \frac{\rho}{\rho_i}\frac{T}{T_i} = \frac{1}{V}\left[1 + \frac{\gamma+1}{2} M_i^2 (1-V^2)\right]$$

$$\frac{M}{M_i} = \frac{u}{u_i}\left(\frac{a_i}{a}\right) = V\left(\frac{T}{T_i}\right)^{-1/2}$$

$$= V\left[1 + \frac{\gamma-1}{2} M_i^2 (1-V^2)\right]^{-1/2}$$

$$\frac{s-s_i}{c_v} = \text{Ln}\left\{\left[1 + \frac{\gamma-1}{2} M_i^2 (1-V^2)\right] V^{\gamma-1}\right\}$$

where s is the entropy and c_v the constant volume specific heat.

The primary interest in the present case is in weak shocks. For weak shocks the temperature would not vary much through the shock and hence the viscosity may be assumed to be constant. With $\mu = \mu_i$ in equation (E12), or $n = 0$ in equation (E14), the integral may be evaluated analytically to give the result

$$\text{Re}_x = \frac{8\gamma}{3(\gamma+1)(1-V_f)} \text{Ln} \frac{1-V}{(V-V_f)V_f} + \text{const} \qquad \text{(E15)}$$

Equation (E15) expresses the velocity distribution through the shock in terms of a relatively simple algebraic formula.

In 1910 Taylor (ref. 201) obtained a weak-shock solution which differs slightly from equation (E15). He presented additional details of his solution technique in a later article (ref. 104), and this solution is presented in greater detail in the textbook of Curle & Davies (ref. 2[illegible]). Taylor's solution will be derived here because the solution is a good one.

Taylor's solution can be obtained as follows. The continuity and momentum equations, equations (E1) and (E2), may be directly integrated, and this has been done in equations (E3) and (E7). The energy equation may also be directly integrated if it is written in the form

$$\rho u \frac{d}{dx}\left(h + \frac{u^2}{2}\right) = \frac{d}{dx}\left(k \frac{dT}{dx}\right) + \frac{4}{3} \frac{d}{dx}\left(\mu u \frac{du}{dx}\right)$$

Integrating and using the integrated continuity equation yields

$$\rho_i u_i \left(h + \frac{u^2}{2}\right) - \frac{4}{3} \mu u \frac{du}{dx} - k \frac{dT}{dx} = \rho_i u_i B$$

where B is a constant of integration. Using the ideal gas law and relation for c_p, h may be replaced by $\gamma pu/(\rho_i u_i(\gamma-1))$, and the energy equation may be expressed as

$$\frac{\gamma}{\gamma-1} pu + \rho_i u_i \frac{u^2}{2} - \frac{4}{3} \mu u \frac{du}{dx} - \frac{k}{R\rho_i u_i} \frac{d(pu)}{dx} = \rho_i u_i B \tag{E16}$$

A differential equation for u may now be obtained by eliminating p from equations (E7) and (E16). The result is

$$\frac{-k}{R\rho_i u_i} \frac{d}{dx} \left(\frac{4}{3} \mu u \frac{du}{dx}\right) + \left(\frac{4}{3} \frac{\mu u}{\gamma-1} + \frac{2ku}{R} - \frac{KA}{R}\right) \frac{du}{dx}$$

$$= \rho_i u_i \left[\frac{1}{2} \left(\frac{\gamma+1}{\gamma-1}\right) u^2 - \frac{\gamma}{\gamma-1} Au + B\right] \tag{E17}$$

At $x = \pm \infty$ the gradients du/dx vanish. Thus, u_i and u_f must be the roots of

$$\frac{1}{2} \left(\frac{\gamma+1}{\gamma-1}\right) u^2 - \frac{\gamma}{\gamma-1} Au + B = 0$$

Therefore, there is a constant, C, such that

$$\frac{1}{2} \left(\frac{\gamma+1}{\gamma-1}\right) u^2 - \frac{\gamma}{\gamma-1} Au + B = C(u-u_i)(u-u_f)$$

Hence

$$C = \frac{1}{2} \left(\frac{\gamma+1}{\gamma-1}\right)$$

and equation (E17) may now be written as

$$-\frac{k}{R\rho_i u_i} \frac{d}{dx} \left(\frac{4}{3} \mu u \frac{du}{dx}\right) + \left(\frac{4}{3} \frac{\mu u}{\gamma-1} + \frac{2ku}{R} - \frac{kA}{R}\right) \frac{du}{dx}$$

$$= \frac{\rho_i u_i}{2} \left(\frac{\gamma+1}{\gamma-1}\right) (u-u_i)(u-u_f) \tag{E18}$$

The solution obtained by Taylor is based on neglecting the first term and assuming the coefficient of du/dx is constant. The justification for neglecting the first term was based on order of magnitude arguments. Thompson (ref. 205), using some results from the kinetic theory of gases, shows that the ratio of the first two terms in equation (E18) is of the order of the ratio of the molecular mean free path to the shock thickness, a quantity which is small for weak shocks. Dividing equation by u_i^2 and neglecting the first term yields

$$\left(\frac{4}{3} \frac{\mu V}{\gamma-1} + \frac{2kV}{R} - \frac{k}{R} \frac{A}{u_i}\right) \frac{dV}{dx} = \frac{\rho_i u_i}{2} \left(\frac{\gamma+1}{\gamma-1}\right) (V-1)(V-V_f) \tag{E19}$$

Treating the coefficient of dV/dx as a constant by taking $V=1$, equation (E19) becomes

$$\left(\frac{4}{3} \frac{\mu_i}{\gamma-1} + \frac{k}{R} \frac{\gamma-1}{\gamma}\right) \frac{dV}{dx} = -\frac{\rho_i u_i}{2} \left(\frac{\gamma+1}{\gamma-1}\right) (1-V)(V-V_f)$$

Dividing through by μ_i, integrating, and simplifying gives

$$Re_x = \frac{2}{\gamma+1}\left(\frac{4}{3} + \frac{\gamma-1}{Pr}\right)\frac{1}{1-V_f}\ln\left(\frac{1-V}{V-V_f}\right)$$

With a Prandtl number of 3/4, the result simplifies to

$$Re_x = \frac{8\gamma}{3(\gamma+1)(1-V_f)}\ln\left(\frac{1-V}{V-V_f}\right) \qquad \text{(E20)}$$

With this formula $Re_x = 0$ when the velocity is the mean of the upstream and downstream velocities (and hence x=0 corresponds to the average velocity location).

Comparing equation (E20) with the result given by equation (E15) shows that Taylor's solution is similar but slightly simpler, and that Taylor's solution approaches (E15) as $V_f \to 1$. In view of the assumptions involved it might appear that Taylor's result would be the poorer of the two, but such is not the case. This is illustrated in figure 34, where, for $M_i = 1.70$, the computed shock velocity distributions from the two approximation formulas, (E15) and (E20), and the numerical integration of (E14) with $n = 0.76$ are compared. For $M_i = 1.70$, $V_f = 0.455$ and $1 - V_f$ is certainly not $\ll 1$. This shock Mach number would appear to be a case where the shock is far too strong for the weak-shock assumptions in the Taylor solution. But the figure shows that the Taylor solution is closer to the "exact" numerical result than formula (E15), and, in fact, that the Taylor solution gives a surprisingly good approximation to the correct solution. For lower shock Mach numbers the approximation formulas of course become more accurate. The conclusion here is that Taylor's solution, which is the most attractive because of its simplicity, is quite appropriate for use in the present work because of the weak shocks which are considered.

The problem of the shock thickness can now be addressed. As in the case of the thickness of the boundary layer, the thickness of the shock involves an arbitrary definition of the "edge" of the nonuniform region. When considering the thickness based on velocity, the thickness of the shock is taken as the distance over which the velocity change is some fraction of the total change in velocity through the shock. In this report, the upstream and downstream edges of the shock will be taken such that they are at equal velocity increments from the mean of the initial and final velocity states. Using these "symmetrical" edge conditions (the velocity profile itself has no symmetry property) and the Taylor weak-shock velocity solution, the expression for the shock thickness Reynolds number will be derived. The derivation given below will be kept general enough so that any fraction of the total velocity change may be used to define the shock thickness.

The shock profile and thickness-defining conditions are illustrated in figure 35. $\Delta V = 1 - V_f$ is the total change in velocity across the nonuniform region and $r\Delta V$ is the fraction of this change used to define the shock thickness (e.g., $r = 0.99$). $\Delta = x_2 - x_1$ is the shock thickness, and V_1 and V_2 are, respectively, the upstream and downstream velocity conditions at the defined edge of the shock region. Using equation (E20), the Reynolds number based on the shock thickness is

$$Re_\Delta = Re_{x_2} - Re_{x_1} = \frac{8\gamma}{3(\gamma+1)(1-V_f)}\left[\ln\left(\frac{1-V_2}{V_2-V_f}\right) - \ln\left(\frac{1-V_1}{V_1-V_f}\right)\right]$$

Since V_{ave} equals $(1 + V_f)/2$ as well as $(V_1 + V_2)/2$, we have that $1 - V_1 = V_2 - V_f$. Hence, equation (E20) may be written as

$$Re_\Delta = \frac{8\gamma}{3(\gamma+1)(1-V_f)} \ln\left(\frac{1-V_2}{1-V_1}\right)^2 \tag{E21}$$

It is easy to show that $(1-V_2)/(1-V_1) = (1+r)/(1-r)$, and therefore equation (E21) simplifies to

$$Re_\Delta = \frac{8\gamma}{3(\gamma+1)} \frac{2}{1-V_f} \ln\left(\frac{1+r}{1-r}\right) \tag{E22}$$

Furthermore, using equation (E15) to express V_f as a function of incoming Mach number, equation (E22) may be written entirely in terms of initial conditions as

$$Re_\Delta = \frac{8\gamma}{3} \frac{M_i^2}{M_i^2 - 1} \ln\left(\frac{1+r}{1-r}\right) \tag{E23}$$

Equation (E23) is the principal result of this appendix and is used in the main text of the report. For $r = 0.995$ and $\gamma = 1.4$, the result is

$$Re_\Delta = 22.36 \frac{M_i^2}{M_i^2 - 1}$$

It may be noted that if the $n = 0$ solution, expression (E15), is used to determine the shock thickness, it will be found that

$$\frac{Re_{\Delta\ Taylor}}{Re_{\Delta\ n=0}} = \frac{2}{1+V_f} = \frac{\gamma + 1}{\gamma + 1/M_i^2}$$

As a final result, the shock thickness Reynolds number will be expressed in terms of the shock pressures. Using

$$\frac{p_f}{p_i} = \frac{2\gamma M_i^2 - (\gamma-1)}{\gamma + 1}$$

and $\Delta p = p_f - p_i$, one finds that

$$Re_\Delta = \frac{8\gamma}{3} \frac{\frac{p_f}{p_i} + \frac{\gamma-1}{\gamma+1}}{\frac{p_f}{p_i} - 1} \ln\left(\frac{1+r}{1-r}\right)$$

and

$$Re_{\Delta} = \frac{8\gamma}{3}\left[1 + \frac{2\gamma}{(\gamma+1)\frac{\Delta p}{p_i}}\right] \ln\left(\frac{1+r}{1-r}\right)$$

Appendix F

Estimates of Radius of Curvature at the Caustic of Incoming Boundary Layer Noise Ray Paths

For the two-dimensional noise-laminar layer interaction case, a caustic occurs. Formulas obtained from sonic boom work indicate that the maximum amount of focusing of a weak shock at a caustic depends on the radius of curvature of the shock rays near the caustic. Therefore, to estimate the amount of focusing in the noise-laminar layer interactions by the use of these formulas, the radius of curvature of the ray paths at the caustic inside the boundary layer must be known. In the present appendix, two procedures for obtaining this radius are developed, and the procedures are applied to the interactions occurring in Mach 4 and Mach 8 tunnels. In these example cases the laminar velocity and temperature profiles are crudely approximated piecewise by polynomials, and the calculations cover a range of source convection velocity ratios, $\eta = u_s/u_\infty$.

In the first procedure, the radius of curvature at the caustic is found directly by use of the formula from calculus for the radius of curvature of a plane curve. This procedure essentially involves determining d^2y/dx^2 of the ray path and evaluating this quantity at the caustic. Inasmuch as an expression for dy/dx is available from Appendix D, only a single differentiation is required. The necessary differentiation is straightforward in the case of a linear velocity profile, but becomes more tedius for the outer region of the boundary layer where the profile is curved. For this situation a second procedure is developed (actually, plain curiosity provided the real motivation here). In the second procedure, the ray path differential equation is integrated numerically to provide the coordinates of the ray path. The radius of curvature at the caustic is then determined by least-squares fitting a parabola through some of the points near the caustic and then applying the radius of curvature formula to the parabola at its vertex. The vertex is assumed to be the location of the caustic. Specific details and results are given below.

In Appendix D, equation (D29), the differential equation of the ray path was given as a

$$\frac{dy}{dx} = \frac{\sqrt{(M_r - M_{sr} a_\infty/a)^2 - 1}}{-M_r(M_r - M_{sr} a_\infty/a) + 1} \tag{F1}$$

where the subscript r indicates that the quantities are relative to a coordinate system which is attached to the tunnel free-stream with positive x in the direction of the tunnel exit. The magnitude of M_{sr} is the relative Mach number of the shock source. a_∞/a is the ratio of the speed of sound outside the boundary layer to the local value. Equation (F1) is more useful if expressed in terms which are referred to the usual tunnel fixed coordinate system, and this is easily done using equations (D20) and (D22) of Appendix D, namely,

$$M_r = M - M_\infty\, a_\infty/a$$

$$M_r - M_{sr}\, a_\infty/a = M - M_s\, a_\infty/a \tag{F2}$$

With these substitutions, equation (F1) becomes

$$\frac{dy}{dx} = \frac{\sqrt{(M-M_s a_\infty/a)^2 - 1}}{(M_\infty a_\infty/a - M)(M-M_s a_\infty/a) + 1} \qquad \text{(F3)}$$

Furthermore, because laminar velocity and temperature profile information will ultimately be used, equation (F3) is even more useful if expressed in terms of velocity ratios. With η defined by

$$\eta = \frac{u_s}{u_\infty} = \frac{M_s}{M_\infty}$$

equation (F3) may be expressed as

$$\frac{dy}{dx} = \frac{\sqrt{(u/u_\infty-\eta)^2 M_\infty^2 (a_\infty/a)^2 - 1}}{(1-u/u_\infty)(u/u_\infty-\eta) M_\infty^2 (a_\infty/a)^2 + 1} \qquad \text{(F4)}$$

Using the fact that

$$(a_\infty/a)^2 = T_\infty/T$$

the final result is

$$\frac{dy}{dx} = \frac{\sqrt{(u/u_\infty-\eta)^2 M_\infty^2 T_\infty/T - 1}}{(1-u/u_\infty)(u/u_\infty-\eta) M_\infty^2 T_\infty/T + 1} \qquad \text{(F5)}$$

Equation (F5) is a first-order differential equation describing the ray path through a boundary layer in terms of the tunnel Mach number, the source convection velocity ratio, and the velocity and temperature profile parameters u/u_s and T_∞/T. It can be integrated to provide the ray path coordinates, or as will be shown next, it can be differentiated to provide the radius of curvature information.

It is known from calculus that the radius of curvature of a plane curve is given by the formula

$$r = \frac{[1+(dy/dx)^2]^{3/2}}{|d^2y/dx^2|}$$

At the caustic the ray path is horizontal, so $dy/dx = 0$, and hence,

$$r_c = \frac{1}{|d^2y/dx^2|_c}$$

where the subscript c indicates that a quantity is evaluated at the caustic. Now

$$\frac{d^n y}{dx^n} = \frac{1}{\delta^{n-1}} \frac{d^n(y/\delta)}{d(x/\delta)^n}$$

and thus,

$$\frac{r_c}{\delta} = \frac{1}{\left|d^2Y/dX^2\right|_c} \tag{F6}$$

where

$$Y = y/\delta$$

$$X = x/\delta$$

Inasmuch as the ray path is smoothly concave upwards, the second derivative is positive and thus the absolute value symbol is not necessary here.

The location of the caustic is determined from the condition that the ray path is horizontal there. This implies, from equation (F4), that at the caustic

$$(u/u_\infty - \eta)^2 M_\infty^2 T_\infty/T - 1 = 0 \tag{F7}$$

With u/u_∞ and T_∞/T expressed as a function of Y, equation (F7) may be solved for Y_c. It may be noted that equation (F7) is consistent with the fact that the horizontal speed of the wave relative to the fluid is sonic at the caustic. This is so because equation (F7), which stems from equation (F1), expresses the fact that at the caustic $M_r - M_{sr} a_\infty/a = 1$. From equation (F2) $M_r - M_{sr} a_\infty/a = (u-u_s)/a$, and hence at the caustic $u-u_s = a$ as asserted.

To determine the radius of curvature at the caustic, equation (F6) indicates that the problem is reduced to that of differentiating equation (F5) with respect to X, inasmuch as $dy/dx = dY/dX$. Equation (F5) is of the form of a fraction $dY/dX = N/D$, where N and D are the numerator and denominator respectively. Thus,

$$\frac{d^2Y}{dX^2} = \frac{DN' - ND'}{D^2}$$

At the caustic $N = 0$, and therefore

$$\frac{d^2Y}{dX^2} = \frac{N'_c}{D_c}$$

hence,

$$\frac{r_c}{\delta} = \frac{D_c}{N'_c} \tag{F8}$$

The problem is thus seen to involve only differentiation of the numerator of equation (F5).

With

$$P = \frac{T}{T_\infty}, \quad U = \frac{u}{u_\infty}$$

and S and Q defined as the functional coefficients of Y' in, respectively,

$$U' = SY'$$
$$P' = QY'$$

N' may be written as

$$N' = \frac{M_\infty^2 [2P(U - \eta)S - (U - \eta)^2 Q]Y'}{2P^2 N}$$

At the caustic N' is seen to be of the form 0/0 and L'Hospital's rule must be used. This gives

$$N_c' = \lim_{y \to y_c} \frac{M_\infty^2 Y'(\ldots) + M_\infty^2 [2P(U - \eta)S - (U - \eta)^2 Q]Y''}{2P^2 N' + 4\,QPNY'}$$

which reduces to

$$N_c' = \frac{M_\infty^2 [2P_c(U_c - \eta)S_c - (U_c - \eta)^2 Q_c]Y_c''}{2P_c^2 N_c} \qquad \text{(F9)}$$

Again, since $Y' = N/D$, at the caustic $Y_c'' = N_c'/D_c$, and therefore, equation (F9) becomes

$$N_c' = \frac{M_\infty^2 [2P_c(U_c - \eta)S_c - (U_c - \eta)^2 Q_c]}{2P_c^2 D_c}$$

Substituting back into equation (F8), the radius of curvature at the caustic is therefore

$$\frac{r_c}{\delta} = \frac{2P_c^2 D_c^2}{M_\infty^2 [2P_c(U_c - \eta)S_c - (U_c - \eta)^2 Q_c]}$$

At the caustic, $U_c - \alpha$ is just $\sqrt{P_c}/M_\infty$, as may be seen from equation (F7), and D_c is

$$D_c = \frac{M_\infty}{\sqrt{P_c}} (1 - \eta)$$

The final result is thus

$$\frac{r_c}{\delta} = \frac{2M_\infty^2 (1 - \eta)^2}{2M_\infty S_c \sqrt{T_c/T_\infty} - Q_c} \qquad \text{(F10)}$$

The laminar profile information is considered next.

Typical supersonic laminar boundary layer velocity and temperature profiles for air are illustrated in figure 36. These were obtained using the computer program of Price and Harris (ref. 110). Velocity profiles have a large region in which the velocity increases linearly with distance from the wall. Above the linear region the profile curves to asymptotically approach the free-stream velocity. The temperature profiles show the temperature to be near the free-stream

value at the outer edge of the boundary layer and to increase to the so-called recovery temperature (a value somewhat below the stagnation temperature) at the insulated wall. For present computational purposes these profiles are approximated in the manner shown in figure 37. The inner region of the velocity profile is approximated appropriately by a straight line. The outer region is approximated by a circular arc which is tangent to the linear portion at the point of joining and has a horizontal slope at the edge of the boundary layer. For this type of approximation, the only quantities which distinguish profiles for different free-stream Mach numbers are the coordinates of the end of the linear region. Based on the Van Driest profiles shown in reference 138, the following values appeared reasonable for the coordinates of this point:

	u/u_∞	y/δ
$M_\infty = 4$	0.95	0.89
$M_\infty = 8$	0.90	0.79

These values give the following velocity profile equations:

	Linear Range	Curved Range	
$M_\infty = 4$	$u/u_\infty = 1.067\ y/\delta$	$u/u_\infty = 0.84695 + \sqrt{(0.15305)^2 - (y/\delta - 1)^2}$	(F11)
$M_\infty = 8$	$u/u_\infty = 1.139\ y/\delta$	$u/u_\infty = 0.715667 + \sqrt{(0.284333)^2 - (y/\delta - 1)^2}$	

These values do not jibe well with the profiles shown in figure 36. The computer runs with the Price and Harris code were made well after the task in this appendix had been completed. The Mach 8 approximate profile agrees well with the Van Driest profile, but that profile closely matches the Price and Harris Mach 4 profile. The Mach 4 approximate profile is the poorer of the two; to better match the Van Driest profile the linear-circular joining point should have at $u/u_\infty = 0.8$, $y/\delta = 0.6$ (determined from an enlargement of the Van Driest report figure). As it is, this profile closely matches the Price and Harris Mach 8 profile.

The temperature profiles are approximated by a cubic equation as indicated in figure 37. Inasmuch as a cubic has four coefficients, four pieces of information about the curve can be specified to define the curve. The four items of information to be used are indicated in the figure. The curve has to go through the outer edge point (1,1), and it is to have a zero slope at this point. It is also to go through a specified value at the wall which depends on M_∞. An intermediate point is selected which makes the curve have a shape appropriate to the M_∞ conditions. This results in a nonzero slope at the wall; a more sensible curve would have zero slope at the wall and a slightly negative dT/dy at the outer edge. The particular constraints selected and the resulting equations are given below.

	$(y/\delta,\ T/T_\infty)$ coordinates	
$M_\infty = 4$	(0,4.2), (0.35, 4.1), (1,1)	
$M_\infty = 8$	(0,12.4), (0.33, 10.0), (1,1)	
$M_\infty = 4$	$T/T_\infty = 9.2444(y/\delta)^3 - 15.2889(y/\delta)^2 + 2.8444\ y/\delta) + 4.2$	(F12)
$M_\infty = 8$	$T/T_\infty = 26.55(y/\delta)^3 - 41.7(y/\delta)^2 + 3.75\ y/\delta + 12.4$	

The Mach 4 approximate temperature profile is adequate. The Mach 8 profile, as might be expected from the terrible zero-slope choice for the outer boundary condition, poorly represents the theoretical profile in the outer region. The Mach 8 ray path results should therefore be considered with some suspicion.

Equation (F10) will now be used to calculate the nondimensional radius of curvature at the caustic for the two Mach number conditions and a range of convection velocity ratios. For a reason to be given shortly, only the linear velocity profiles will be used in this exercise. For this case the velocity and temperature profiles respectively, may be represented by, respectively,

$$U = AY$$

and

$$P = aY^3 + bY^2 + cY + d$$

Differentiating yields

$$U' = AY'$$

$$P' = (3aY^2 + 2bY + c)Y'$$

and hence

$$S = A$$

$$Q = 3aY^2 + 2bY + c$$

The radius of the curvature at the caustic is thus

$$\frac{r_c}{\delta} = \frac{2M_\infty^2 (1 - \eta)^2}{2M_\infty A \sqrt{aY_c^3 + bY_c^2 + cY_c + d - (3aY_c^2 + 2bY_c + C)}}$$

The remaining problem is to determine Y_c. From equation (F7), the caustic height, Y_c, may be found from the solution of the polynomial equation

$$(AY_c - \eta)^2 = \frac{aY_c^3 + bY_c^2 + cY_c + d}{M_\infty^2} \qquad \text{(F13)}$$

The reason for restricting the application to the linear velocity profile region lies in this step of the problem. Equation (F13) is a cubic equation and one may find its solution directly. For the outer nonlinear velocity profile, equation (F13) would be a sixth degree polynomial. The roots of such a polynomial are easily found by numerical procedures, but this was not pursued here. Continuing with the solution of equation (F13), the equation may be expressed in the form

$$Y_c^3 + \beta_1 Y_c^2 + \beta_2 Y_c + \beta_3 = 0$$

where

$$\beta_1 = \frac{b - M_\infty^2 A^2}{a}, \quad \beta_2 = \frac{c + 2A\alpha M_\infty^2}{a}, \quad \beta_3 = \frac{d - M_\infty^2 \alpha^2}{a}$$

Using the formula for the solution of a cubic equation, the desired root is

$$Y_c = 2\sqrt{-G}\ \cos(\alpha/3 + 240^\circ) - \beta_1/3$$

where

$$G = \frac{3\beta_2 - \beta_1^2}{9}$$

$$\alpha = \cos^{-1} \frac{H}{\sqrt{-G^3}}$$

$$H = \frac{9\beta_1\beta_2 - 27\beta_3 - 2\beta_1^3}{54}$$

The preceding results provide an algebraic means for determining Y_c and r_c/δ for the assumed case of a linear velocity profile. Taking the values of A, a, b, and c from the profile equations (F11) and (F12), values of Y_c and r_c/δ were computed and the results are included in Table F1. These results will be discussed later. Also included in the table are results for the non-linear portion of the velocity profile as well as results concerning the length of the horizontal traverse of the ray from entry point to the caustic. These additional results are from the second method of approach, and this method will be discussed next.

The trajectory of the ray path can be obtained by numerical integration of the ray path differential equation, equation (F5). This procedure does not yield a radius of curvature, however, and an additional approximate technique must be used. A very simple and attractive method is to approximate the trajectory near the caustic by a concave upward parabola and to take the radius of curvature of the parabola at its vertex to be the radius of curvature of the ray path at the caustic. Inasmuch as the slope of the parabola is zero at the vertex, the radius of curvature is again obtained from equation (F6). For a parabola of the form

$$Y = \gamma_1 X^2 + \gamma_2 X + \gamma_3$$

the result is simply

$$\frac{r_c}{\delta} = \frac{1}{2\gamma_1}$$

The location of the caustic is the vertex location, and this is given by

$$X_c = -\frac{\gamma_2}{2\gamma_1}, \quad Y_c = -\frac{\gamma_2^2}{4\gamma_1} + \gamma_3$$

The method is seen to be quite straightforward, and the specific details are discussed next.

The integration problem is an initial-value one, and specifying that $X = Y = 1.0$, equation (F5) was integrated using the standard Runge-Kutta fourth-order method (which is equivalent in the present case, to applying Simpson's integration rule to the problem). A numerical step size of $\Delta Y = -0.01$ was used until $Y - Y_c \simeq 0.03$, and then the step size was reduced to $\Delta Y = -0.001$. The integration was automatically terminated very near the caustic; in all cases the Y of the last computed point was within .001 of the caustic.

The parabolic curve was fit in a least squares manner to the trajectory

points. Since the computed path is generally not a quadratic one, the computed radius of curvature depends on which points are selected for the curve fit. To determine the effect of the number of points on the radius of curvature, Y_c/δ was computed for the cases of fits through the last 3, 5, 10, and 20 points. Generally the 3-point and 5-point results agreed within 0.001. It was found that for $M = 4$ and $\eta \leq 0.5$, the percent change in r_c/δ in going from 5 points to 20 points was less than 3% (the greatest change occurred for $\eta = 0.7$ and was 9%). For $M_\infty = 8$ and $\eta \leq 0.6$, the percent change in r_c/δ in going from 5 to 20 points was less than 2% (the maximum change occurred for $\eta = 0.8$ and 13%). Since method 1 provided the correct values of r_c/δ in the linear profile range, the accuracy of the numerical procedure could be assessed. For the r_c/δ values obtained using the 3 or 5 point procedures, the greatest percent error was -3.2% (occurred for $\eta = 0.7$, $M_\infty = 8$). Thus method 2 appears quite sufficient, and the results for the nonlinear profile range can be accepted with some confidence.

The final results are presented in table F1. The radius results were presented in figure 20. The figure illustrates that there is little difference between the two Mach number results, and that the slower the convection speed of the source, the larger the radius of curvature at the caustic. The range of u_s/u_∞ which has been found from free-stream hot-wire measurements is indicated on the figure, and it is seen that corresponding values of r_c/δ fall between 0.3δ and 0.7δ for $M_\infty = 4$ and between 0.25δ and 0.3δ for $M_\infty = 8$.

Table F1 also shows that the horizontal traverse of a ray from point boundary layer entry to the caustic varies from about $\frac{1}{4}\delta$ to $1\frac{1}{4}\delta$. Some ray trajectories through the $M_\infty = 4$ laminar boundary are shown in figure 21.

As a final item of information, the difference in direction between the wave normal and the ray path will be considered. In Appendix D it was shown that the wave angle from the horizontal is just the local relative Mach angle, an expected result. Thus the angle of the wave normal from the horizontal is

$$\theta = \cos^{-1} \frac{1}{M - M_s \frac{a_\infty}{a}}$$

For the ray path, since dy/dx is the tangent of the angle from the horizontal of the path, equation (F5) provides the needed result. The ray path angle is thus

$$\gamma = \tan^{-1} \frac{\sqrt{(\frac{u}{u_\infty} - \eta)^2 M_\infty^2 \frac{T_\infty}{T} - 1}}{(\frac{u}{u_\infty} - \eta)(1 - \frac{u}{u_\infty}) M_\infty^2 \frac{T_\infty}{T} + 1}$$

To illustrate the magnitude of the difference between the two angles, these angles have been computed for a Mach 4 boundary layer and a stationary shock ($\eta = 0$). The results are shown in figure 38, where the respective angles are plotted against y/δ. The ray angle decreases more rapidly than the wave normal angle in the outer portion of the boundary layer. From y/δ of about 0.8 to 0.5 (M from 2.9 to 1.3), both angles decrease at nearly the same rate, with the angles differences remaining in the $20^\circ - 26^\circ$ range. The maximum difference of 26.4° occurs at $y/\delta = 0.67$ ($M = 2.01$).

TABLE F1. - CAUSTIC LOCATION AND RAY PATH TRAITS IN LAMINAR BOUNDARY LAYER[a]

Acoustic source convection speed ratio, u_s/u_∞	Radius of curvature at caustic	Coordinates of caustic[b]	Total horizontal traverse from entry to caustic
		$M_\infty = 4$	
0.7	0.309	0.745, 0.901	0.255
0.6	0.388	0.691, 0.831	0.309
0.5	0.531	0.591, 0.763	0.409
0.4	0.689	0.480, 0.697	0.520
0.3	0.864	0.359, 0.631	0.641
0.2	1.060	0.226, 0.565	0.774
0.1	1.282	0.0798, 0.497	0.420
0	1.541	-0.0820, 0.428	1.082
		$M_\infty = 8$	
0.8	0.237	0.762, 0.858	0.238
0.7	0.280	0.739, 0.787	0.261
0.6	0.427	0.639, 0.726	0.361
0.5	0.592	0.529, 0.665	0.471
0.4	0.774	0.405, 0.604	0.595
0.3	0.976	0.267, 0.541	0.733
0.2	1.203	0.115, 0.478	0.885
0.1	1.761	-0.0524, 0.412	1.052
0	1.761	-0.273, 0.344	1.237

[a] All lengths nondimensionalized by boundary layer thickness.

[b] Ray enters boundary layer at 1.0, 1.0.

Appendix G

Caustic Layer Height for Plate at an Angle of Attack

In this section, the height of the caustic layer will be determined for a case of a flat plate pitched forward to reduce the local Mach number. Once the necessary relations have been derived, calculations will be made for the example cases of: (1) a plate pitched forward in a Mach 4 tunnel so that the local Mach number is 2, and (2) a plate pitched in a Mach 4.5 tunnel so that the local Mach number is 3. For the examples the laminar boundary layer, Mach number and velocity profiles were obtained using the computer code of Price and Harris (ref. 110); tabulated profile information may also be found in the report of Mack, ref. 206, for $M \leq 5$).

The height of the caustic layer is the height where the flow velocity relative to the downstream velocity of the shock is sonic. At this height, then,

$$u - u_s = a$$

where u_s is the shock source convection velocity and a is the local speed of sound. For the ultimate purpose of using laminar boundary layer profile information, this equation can more conveniently be expressed in the form

$$\frac{u}{u_\infty} = \frac{u_s}{u_\infty} \frac{M}{M-1} \tag{G1}$$

At the caustic this relation holds locally for the region above the plate. If the region upstream and downstream of the plate's leading edge shock are denoted with subscripts 1 and 2, respectively, equation (G1) may be written as

$$\frac{u_2}{u_{\infty 2}} = \frac{u_{s2}}{u_{\infty 2}} \frac{M_2}{M_2 - 1} \tag{G2}$$

The quantities M_2 and $u_2/u_{\infty 2}$ are to be obtained from the laminar boundary layer profile information for the given free-stream Mach number $M_{\infty 2}$. The quantity $M_{\infty 2}$ can be obtained from a given $M_{\infty 1}$ by the use of oblique shock relations. There is, however, no such simple means of obtaining u_{s2} for a given u_{s1}. The task in this appendix is essentially to determine u_{s2}, given the upstream flow conditions, the plate angle, and $u_{s1}/u_{\infty 1}$.

The geometry and nomenclature for the pitched plate problem are shown in figure 39. From the figure, u_{s2} may be seen to equal dx/dt, where x is the distance along the plate from the leading edge to the location of the incoming acoustic shock. Thus the problem is to find $\dot{x}$, where the dot refers to time differentiation. From the figure, it is seen that one can write, using the law of sines,

$$\frac{x}{\sin \rho} = \frac{g}{\sin(180^\circ - (\rho+\eta))} \tag{G3}$$

and hence,

$$\frac{\dot{x}}{\sin \rho} = \frac{\dot{g}}{\sin(\rho+\eta)}$$

As seen in the figure, $\dot{g}$ is the velocity along the leading edge shock of the shock intersection point, Q, and hence $\dot{g} = \dot{f}$. Therefore, from equation (G3),

$$\dot{x} = \dot{f} \frac{\sin \rho}{\sin(\rho+\eta)}$$

The problem is thus reduced to that of finding $\dot{f}$ and ρ. $\dot{f}$ will be found first.

By using the law of sines and differentiating, one finds that

$$\dot{f} = \dot{e} \frac{\sin \alpha}{\sin \gamma}$$

But $\dot{e}$ is just u_{s1}, and this may be regarded as a known quantity, given the value of $u_{s1}/u_{\infty 1}$. Let $u_{s1}/u_{\infty 1} = J$. Continuing,

$$\dot{f} = u_{s1} \frac{\sin \alpha}{\sin \gamma}$$

or,

$$\dot{f} = u_{s1} \frac{\sin \alpha}{\sin(\alpha+\theta_s)}$$

Now α is the Mach angle of the moving source, and therefore,

$$\sin \alpha = \frac{1}{M_{\infty 1} - M_{s1}} \tag{G4}$$

Since $M_{s1}/M_{\infty 1} = u_{s1}/u_{\infty 1} = J$, equation (G4) may be written as

$$\sin \alpha = \frac{1}{M_{\infty 1}(1 - J)} \tag{G5}$$

and hence α can be considered know. $\dot{f}$ thus becomes

$$\dot{f} = \frac{J}{1 - J} \frac{a_{\infty 1}}{\sin(\alpha+\theta_s)} \tag{G6}$$

Inasmuch as θ_s comes from oblique shock relations, equations (G5) and (G6) provide the means for determining $\dot{f}$. The angle ρ is next determined.

To find ρ, the angle between the acoustic shock and leading edge shock, a closer examination of the intersection between the two shocks is needed. The intersection region and additional nomenclature are shown in figure 40. The intersection point Q can be considered as a new source of sound emanating into the region behind the leading shock as the intersection point moves up the shock line. A vorticity wave also originates at this point and travels with the flow (see Moore, ref. 152), but this will not be shown in the diagram or discussed further. The acoustic source wave is shown at two instances of time, t_i and t_j. At time t_i a cylindrical pulse wave is considered emitted from point Q_i, and the center of this pulse moves downstream at the local flow velocity. At time t_j the intersection point has moved to Q_j, and the original pulse is now centered around the point R and has a radius of $a_{\infty 2}\Delta t$, where $\Delta t = t_j - t_i$. The point R has moved a distance $n = M_{\infty 2} a_{\infty 2} \Delta t$. If the radius of the cylindrical sound pulse is less than the distance from the center of the pulse to the point Q_j (i.e., if $p < s$), then an envelope

is formed which is identified as the refracted wave. If the radius is greater than the distance to point Q_j (i.e., if $p > s$), then no envelope is formed and, as discussed by Moore, the refracted disturbance is described as an attenuating pressure wave.

In the figure, the line segments involved in the pertinent triangles have been darkened. From the geometry

$$\rho = 180^{\circ} - (\eta + \pi) \tag{G7}$$

$$\pi = 90^{\circ} - \xi \tag{G8}$$

$$\xi = \omega - \varepsilon \tag{G9}$$

Substituting equations (G8) and (G9) into (G7) yields

$$\rho = 90^{\circ} - \eta + \omega - \varepsilon \tag{G10}$$

As seen from the figure,

$$\omega = \cos^{-1} \frac{p}{s} \tag{G11}$$

Application of the law of sines gives

$$\varepsilon = \sin^{-1} \left(\frac{m}{s} \sin \eta \right) \tag{G12}$$

Furthermore,

$$p = a_{\infty 2} \Delta t$$

$$m = \dot{f} \Delta t$$

and

$$s^2 = m^2 + n^2 - 2mn \cos \eta$$

with

$$n = M_{\infty 2} a_{\infty 2} \Delta t$$

Thus

$$s = \Delta t \sqrt{\dot{f}^2 + (M_{\infty 2} a_{\infty 2})^2 - 2\dot{f} M_{\infty 2} a_{\infty 2} \cos \eta}$$

All of the terms on the right-hand side of equation (G10) may now be evaluated, and hence ρ can be determined. The angle η can be obtained from oblique shock relations; expressions for m, p, and s are available and thus ω and ε may be determined from equations (G11) and (G12).

All of the relations and quantities necessary for the determination of $\dot{x}$ have now been developed or discussed. All that remains are the example calculations. For the first example, the tunnel Mach number is chosen to be 4.0, and the tunnel stagnation temperature is assumed to be 322 K (580° R). From the oblique shock chart 4 of reference 105, the plate angle, θ_p, is seen to be about 28° for the local Mach number of 2. The shock angle, θ_s, is 42.3°, as determined from chart 2. From interpolation of Laufer's free-stream convection

velocity measurements (ref. 57) the ratio $J = u_{s1}/u_{\infty 1}$ is about 0.49. The calculations and results are as follows.

$$\eta = \theta_s - \theta_p = 42.3 - 28^o = 14.3^o$$

$$a_{\infty 1} = \sqrt{\gamma R T_{o1} \frac{T_{\infty 1}}{T_{o1}}} = 175.6 \text{ m/sec}$$

where

$$T_{\infty 1}/T_{o1} = [1 + (\gamma-1)M^2]^{-1} = 0.2381$$

$$\alpha = \sin^{-1} \frac{1}{M_{\infty 1}(1 - J)} = 29.4^o$$

$$\dot{f} = \frac{J}{1-J} \frac{a_{\infty 1}}{\sin(\alpha + \theta_s)} = 177.7 \text{ m/sec}$$

$$a_{\infty 2} = a_{\infty 1} \sqrt{T_{\infty 2}/T_{\infty 1}}$$

$$= a_{\infty 1} \sqrt{\frac{(7M_{\infty 1}^2 \sin^2\theta_s - 1)(M_{\infty 1}^2 \sin^2\theta_s + 5)}{36 M_{\infty 1}^2 \sin^2\theta_1}}$$

$$= 268.2 \text{ m/sec}$$

(formula from ref. 106)

$$s = \Delta t \sqrt{\dot{f} + (M_{\infty 2} a_{\infty 2})^2 - 2\dot{f} M_{\infty 2} a_{\infty 2} \cos \eta}$$

$$= 366.9 \, \Delta t \text{ m}$$

$$p = a_{\infty 2} \Delta t = 268.2 \, \Delta t \text{ m}$$

$$\omega = \cos^{-1} \frac{p}{s} = 43.0^o$$

$$\varepsilon = \sin^{-1} \left(\frac{\dot{f} \Delta t}{s} \sin \eta\right) \doteq 6.9^o$$

$$\rho = 90^o - \eta + \omega - \varepsilon = 111.8^o$$

It may be noted that the angle below the horizontal of the refracted acoustic shock is $180^o - (\rho + \theta_s)$, and in the present case this value is 25.9^o. Thus, the acoustic shock is bent upward by 3.4^o upon passage through the leading edge shock.

$$u_{s2} = \dot{x} = \dot{f} \frac{\sin \rho}{\sin(\rho + \eta)} = 204.2 \text{ m/sec}$$

$$u_{\infty 2} = M_{\infty 2} a_{\infty 2} = 536.4 \text{ m/sec}$$

Hence, the caustic, which is located when equation (G2) is satisfied, occurs where

$$\frac{u_2}{u_{\infty 2}} = \frac{0.38 M_2}{M_2 - 1} \qquad \text{(G13)}$$

Using Mach 2 velocity and Mach number boundary layer profiles, equation (G13) was found, by trial-and-error, to be satisfied at $y/\delta \approx 0.73$.

In the second example, the free-stream Mach number is 4.5 and the stagnation temperature is 311 K (560 R). From reference 105 the value of the plate angle to reduce the local Mach number to 3.0 is 17.7^{o} and the corresponding shock angle is 28.9^{o}. The result comparable to equation (G13) is

$$\frac{u_2}{u_{\infty 2}} = \frac{0.536\ M_2}{M_2 - 1}$$

Using Mach 3 profile information, this equation was found to be satisfied at $y/\delta \approx 0.75$.

Acknowledgements: This work was also supported by NASA Grant No. NSG 1505 and Research Contract NASI-15877.

5. REFERENCES

1. Schopper, M. R.: A Model for the Noise Radiated by Turbulent Boundary Layers and its Interaction With Laminar Layers in Supersonic Flow. AIAA Paper No. 79-1523, July 1979.

2. Laufer, J.: Aerodynamic Noise in Supersonic Wind Tunnels. Journal of Aerospace Sciences, vol. 28, Sept. 1961, pp. 685-692.

3. Wagner, R. D., Jr.; Maddalon, D. V.; and Weinstein, L. M.: Influence of Measured Free-stream Disturbances on Hypersonic Boundary Layer Transition. AIAA J., vol. 8, no. 9, Sept. 1970, pp. 1664-1670.

4. Anders, J. B.; Stainback, P. C.; Keefe, L. R.; and Beckwith, I. E.: Fluctuating Disturbances in a Mach 5 Wind Tunnel. AIAA J., vol. 15, Aug. 1977, pp. 1123-1129.

5. Donaldson, J. C.; and Wallace, J. P.: Flow Fluctuation Measurements at Mach Number 4 in the Test Section of the 12-inch Supersonic Tunnel (D). AEDC-TR-71-143, Aug. 1971.

6. Pate, S. R.; and Schueler, C. J.: Radiated Aerodynamic Noise Effects on Boundary Layer Transition in Supersonic and Hypersonic Wind Tunnels. AIAA J., vol. 7, no. 3, Mar. 1969, pp. 450-457.

7. Owen, F. K.; Horstman, C. C.; Stainback, P. C.; and Wagner, R. D.: Comparison of Wind Tunnel Transition and Free-stream Disturbance Measurements. AIAA J., vol. 13, no. 3, Mar. 1975, pp. 266-269.

8. Pate, S. R.: Dominance of Radiated Aerodynamic Noise on Boundary-Layer Transition in Supersonic-Hypersonic Wind Tunnels - Theory and Application. AEDC-TR-77-107, Mar. 1978.

9. Pate, S. R.: Effects of Wind Tunnel Disturbances on Boundary Layer Transition with Emphasis on Radiated Noise: A Review. AIAA Paper No. 80-0431, Mar. 1980.

10. Beckwith, I.E.: Development of a High Reynolds Number Quiet Tunnel for Transition Research. AIAA J., vol. 13, no. 3, Mar. 1975, pp. 300-306.

11. Fischer, M. C.; and Wagner, R. D.: Transition and Hot-Wire Measurements in Hypersonic Helium Flow. AIAA J., vol. 10, no. 10, Oct. 1972, pp. 1326-1332.

12. Stainback, P. C.: Hypersonic Boundary-Layer Transition in the Presence of Wind-Tunnel Noise. AIAA J., vol. 9, no. 12, Dec. 1971, pp. 2475-2476.

13. Pate, S. R.: Measurements and Correlations of Transition Reynolds Numbers on Sharp Slender Cones at High Speeds. AIAA J., vol. 9, no. 6, June 1971, pp. 1082-1090.

14. Pate, S. R.: Comparison of NASA Helium Tunnel Transition Data with Noise-Transition Correlation. AIAA J., vol. 12, no. 11, Nov. 1974, p. 1615.

15. Dougherty, N. S., Jr.: Correlation of Transition Reynolds Number with Aerodynamic Noise Levels in a Wind Tunnel at Mach Numbers 2.0-3.0. AIAA J., vol. 13, no. 12, Dec. 1975, pp. 1670-1671.

16. Whitfield, Jack D.; and Dougherty, N. Sam, Jr.: A Survey of Transition Research at AEDC. Laminar-Turbulent Transition, AGARD-CP-224, 1977, pp. 25-1 to 25-17.

17. Kendall, James M., Jr.: J.P.L. Experimental Investigations. Proceedings of the Boundary Layer Transition Workshop Held 3-5 November 1971. Vol. IV, Prepared by W. D. McCauley, Report No. TOR-0172(S2816-16)-5, The Aerospace Corp., San Bernardino, Calif., Dec. 20, 1971, pp. 2-1 to 2-16.

18. Kendall, J. M.: Wind Tunnel Experiments Relating to Supersonic and Hypersonic Boundary Layer Transition. AIAA J., vol. 13, no. 3, Mar. 1975, pp. 290-299.

19. Beckwith, I. E.; Creel, T. R., Jr.; Chen, F. J.; and Kendall, J. M.: Free Stream Noise and Transition Measurements in a Mach 3.5 Pilot Quiet Tunnel. AIAA-83-0042, January 1983.

20. Ross, Albert O.: Determination of Boundary Layer Transition Reynolds Number by Surface Temperature Measurements of a 10° Cone in Various NACA Supersonic Wind Tunnels. NACA TN 3020, October 1953.

21. Browning, A. C.; Crane, J. F. W.; and Monagham, R. J.: Measurements of the Effect of Surface Cooling on Boundary Layer Transition on a 15° Cone, Part 1, Tests at M = 2 and 3 in an 8-inch by 9-inch Wind Tunnel at R.A.E. Bedford, R.A.E. Technical Note No. Aero 2527, 1958.

22. Rogers, Ruth H.: The Effect of Tip Bluntness on Boundary Layer Transition on a 15° included Angle Cone at M = 3.12 and 3.81. Ministry of Aviation, Aero. Res. Council, C. P. No. 598, 1962.

23. Czarnecki, K. R.; and Jackson, Mary W.: Effects of Cone Angle, Mach Number, and Nose Blunting on Transition at Supersonic Speeds. NASA TN D-634, Jan. 1961.

24. Krogmann, P.: An Experimental Study of Boundary Layer Transition on a Slender Cone at Mach 5. Laminar-Turbulent Transition, AGARD-CP-224, 1977, pp. 26-1 to 26-12.

25. Potter, J. Leith: Observations on the Influence of Ambient Pressure on Boundary-Layer Transition. AIAA J., vol. 6, no. 10, Oct. 1968, pp. 1909-1911.

26. Potter, J. Leigh: Boundary-Layer Transition on Supersonic Cones in an Aeroballistic Range. AIAA J., vol. 13, no. 3, Mar. 1974, pp. 270-277.

27. Reda, D. C.: Boundary Layer Transition Experiments on Sharp Slender Cones in Supersonic Freeflight. AIAA Paper No. 78-1129, July 1978.

28. Demetriades, Anthony: Hypersonic Viscous Flow over a Slender Cone, Part III: Laminar Instability and Transition. AIAA Paper No. 74-535, June 1974.

29. Ross, R.: Boundary Layer Transition on the Same Model in Two Supersonic Wind Tunnels. AIAA J., vol. 12, no. 7, July 1974, pp. 992-993.

30. Laufer, John; and Marte, Jack E.: Results and a Critical Discussion of Transition-Reynolds-Number Measurements on Insulated Cones and Flat Plates in Supersonic Wind Tunnels. JPL Report No. 20-96, Nov. 1955.

31. Owen, F. K.; and Horstman, C. C.: Hypersonic Transitional Boundary Layers. AIAA J., vol. 10, no. 6, June 1974, pp. 769-775.

32. Morkovin, M. V.: Transition from Laminar to Turbulent Shear Flow-A Review of Some Recent Advances in its Understanding. Trans. ASME, vol. 80, May 1958, pp. 1121-1128.

33. Morkovin, Mark V.: Critical Evaluation of Transition from Laminar to Turbulent Shear Layers with Emphasis on Hypersonically Traveling Bodies. AFFDL-TR-68-149, Mar. 1969.

34. Morkovin, Mark V.: On the Many Faces of Transition. Viscous Drag Reduction, ed. by C. Sinclair Wells, Plenum Press, 1969, pp. 1-31.

35. Morkovin, M. V.: Technical Evaluation Report of the Fluid Dynamics Panel Symposium on Laminar-Turbulent Transition. AGARD Advisory Report No. 122, June 1978.

36. Morkovin, M. V.: Instability, Transition to Turbulence and Predictability. AGARDograph No. 236, July 1978.

37. Obremski, H. J.; Morkovin, M. V.; Landahl, M.: A Portfolio of Stability Characteristics of Incompressible Boundary Layers. AGARDograph 134, 1969.

38. Blokhintsev, D.: The Propagation of Sound in an Inhomogeneous and Moving Medium I. J. Acoust. Soc. Am., vol. 18, Oct. 1946, pp. 322-328.

39. Hayes, Wallace D.; Haefeli; Rudolf C.; and Kulsrud, H. E.: Sonic-Boom Propagation in a Stratified Atmosphere with Computer Program. NASA CR-1299, April 1969.

40. Mack, L. M.: Progress in Compressible Boundary Layer Stability Computations, Proceedings of Boundary Layer Transition Workshop, Held 3-5 November 1971, Vol. IV, Prepared by W. D. McCauley, Rept. No. TOR-0172 (S 2816-16)-5, The Aerospace Cor., San Bernardino, California, December 20, 1971, pp. 1-1 to 1-36.

41. Mack, L. M.: Linear Stability Theory and the Problem of Supersonic Boundary Layer Transition. AIAA J., vol. 13, no. 3, Mar. 1975, pp. 278-289.

42. Davies, P.O.A.L. and Yule, A. J.: Coherent Structure of Turbulence. J. Fluid Mech., vol. 69, pt. 3, 1975, pp. 513-537.

43. Laufer, J.: New Trends in Experimental Turbulence Research. Annual Review of Fluid Mechanics, edited by Van Dyke, M., Vincenti, W. G., and Wehausen, J. V., Annual Reviews, Inc., Vol. 7, 1975, pp. 307-327.

44. Willmarth, W. W.: Structure of Turbulence in Boundary Layers. Advances in Applied Mechanics, ed. by Yih, C., Academic Press, vol. 15, 1975, pp. 159-254.

45. Roshko, A.: Structure of Turbulent Shear Flows: A New Look. AIAA J., vol. 14, no. 10, Oct. 1976, pp. 1349-1357.

46. Workshop on Coherent Structure of Turbulent Boundary Layers. Edited by C. R. Smith, and D. E. Abbott, Sponsored by Air Force Office of Scientific Research, published by Department of Mechanical Engineering and Mechanics, Lehigh University, Bethlehem, PA, Nov. 1978.

47. Phillips, O. M.: On the Generation of Sound by Supersonic Turbulent Shear Layers. J. Fluid. Mech., vol. 4, pt. 1, 1960, pp. 1-28.

48. Laufer, J.; Ffowcs Williams, J. E.; and Childress, S.: Mechanism of Noise Generation in the Turbulent Boundary Layer. AGARDograph 90, Nov. 1964, p. 40.

49. Carlson, H. W.: Correlation of Sonic-Boom Theory with Wind Tunnel and Flight Measurements. NASA TR R-213, Dec. 1964.

50. Middleton, W. D.; and Carlson, H. W.: A Numerical Method for Calculating Near-Field Sonic-Boom Pressure Signatures. NASA TN D-3082, Nov. 1965.

51. James, C. S.: Observations of Turbulent-Burst Geometry and Growth in Supersonic Flow. NACA TN 4235, 1958.

52. Jedlicka, J. R.; Wilkins, M. E.; Seiff, A.: Experimental Determination of Boundary-Layer Transition on a Body of Revolution at M = 3.5. NACA TN 3342, 1954.

53. Lyons, W. C.; and Sheetz, N. W.: Free-Flight Experimental Investigation of the Effect of Boundary-Layer Cooling on Transition. NOL TR 61-83, Ballistics Research Report 46, Sept. 1961.

54. Heller, H. H.; and Clemente, A. R.: Fluctuating Surface-Pressure Characteristics on Slender Cones in Subsonic, Supersonic, and Hypersonic Mach-Number Flow. NASA CR-2449, Oct. 1974.

55. Lowson, M. V.; and Ollerhead, J. B.: Visualization of Noise from Cold Supersonic Jets. J. Acoust. Soc. Am., vol. 44, Aug. 1968, pp. 624-630.

56. Laufer, J.; Schlinker, R.; and Kaplan, R. E.: Experiments on Supersonic Jet Noise. AIAA Paper No. 75-478, Mar. 1975.

57. Laufer, J.: Some Statistical Properties of the Pressure Field Radiated by a Turbulent Boundary Layer. Physics of Fluids, vol. 7, Aug. 1964, pp. 1191-1197.

58. Reshotko, E.: Boundary-Layer Stability and Transition. Annual Review of Fluid Mechanics, ed. by Van Dyke, M., Vincenti, W. G., and Wehausen, J. V.; Annual Reviews, Inc., vol. 8, 1976, pp. 311-349.

59. Carlson, H. W.; and Morris, O. A.: Wind-Tunnel Sonic Boom Testing Techniques. J. Aircraft, vol. 4, May-June 1967, pp. 245-249.

60. Morris, O. A.; and Miller, D. S.: Sonic-Boom Wind-Tunnel Testing Techniques at High Mach Numbers. J. of Aircraft, vol. 9, Sept. 1972, pp. 664-667.

61. Werner, F. D.: The Corona Anemometer and its Application to Study of the Effect of Stilling Chamber Turbulence on Test Section Turbulence in a Wind-Tunnel at Mach Number Three. Ph.D Thesis, University of Minnesota, 1955.

62. Anders, J. B.; Stainback, P. C.; and Beckwith, I. E.: A New Technique for Reducing Test Section Noise in Supersonic Wind Tunnels. AIAA Paper No. 78-817, April, 1978.

63. Campbell, M. A.: The Study of Discontinuous Phenomena. Proc. Camb. Phil. Soc., vol. 15, 1909, pp. 117-136.

64. Rice, S. O.: Mathematical Analysis of Random Noise. Selected Papers on Noise and Stochastic Processes, ed. by Nelson Wax, Dover Pub. Inc., 1954, pp. 133-294, (papers originally published in 1944, 1945).

65. Lee, Y. W.: Statistical Theory of Communication. John Wiley & Sons, Inc., 1960.

66. Hogg, R. V.; and Craig, A. T.: Introduction to Mathematical Statistics, 3rd Ed., The Macmillan Co., 1970, pp. 94-96.

67. Korn, G. A.: Random-Process Simulation and Measurement. McGraw-Hill Book Co., 1966.

68. Kendall, J. M.: Supersonic Boundary Layer Transition Studies. JPL Space Programs Summary 37-62, Vol. III, April 1970, pp. 43-47.

69. Bracewell, R.: The Fourier Transform and Its Applications. McGraw-Hill Book Co., 1965.

70. Henderson, H. R.; and Hilton, D. A.: Sonic-Boom Measurements in the Focus Region During the Ascent of Apollo 17. NASA TN D-7806, Dec. 1974.

71. Laderman, A. J.: Review of Wind-Tunnel Free-stream Pressure Fluctuations. AIAA J., vol. 15, no. 4, April 1977, pp. 605-608.

72. Stainback, P. C.; and Rainey, R. A.: Correlation of Free-stream Pressure Disturbances in Supersonic Wind Tunnels. AIAA J., vol. 14, no. 2, Feb. 1976, pp. 286-288.

73. Bergstrom, E. R.; and Raghunathan, S.: Aerodynamic Noise and Boundary-Layer Transition Measurements in Supersonic Test Facilities. AIAA J., vol. 10, no. 11, Nov. 1972, pp. 1531-1532.

74. Barry, F. W.: Refraction and Reflection of a Wave in a Mach Number Gradient. D1C6393, Project Report No. 7, April 1950, in Barry, Shapiro, and Neuman, Gas Turbine Laboratory Report no. 7, M.I.T., April 1950.

75. Marble, F.: The Reflection of a Weak Wave From a Supersonic Shear Layer. Section III From Problems in Shock Reflection, Final Report on Contract No. W33-038 ac-1717 (11592), submitted to the U. S. Army Air Force by the Transonic Research Group, Guggenheim Aeronautical Laboratory, Cal. Inst. of Tech., July 1948.

76. Moeckel, W. E.: Interaction of Oblique Shock Waves with Regions of Variable Pressure, Entropy, and Energy. NACA TN 2725, June 1952.

77. Lighthill, M. J.: Reflection at a Laminar Boundary Layer of a Weak Steady Disturbance to a Supersonic Stream, Neglecting Viscosity and Heat Conduction. The Quarterly J. of Mech. and App. Math, vol. 3, Sept. 1950, pp. 305-325.

78. Whitham, G. B.: On the Propagation of Shock Waves Through Regions of Nonuniform Area or Flow. J. Fluid Mech., vol. 4, Aug. 1958, pp. 337-360.

79. Weinbaum, S.; and Goldburg, A.: The Nonlinear Refraction of Shock Waves by Upstream Disturbances in Steady Supersonic Flow. J. Fluid Mech., vol. 43, pt. 1, 1970, pp. 1-33.

80. Henderson, L. F.: The Reflection of a Shock Wave at a Rigid Wall in the Presence of a Boundary Layer. J. Fluid Mech., vol. 30, pt. 4, 1967, pp. 699-722.

81. Henderson, L. F.: On Shock Impedance. J. Fluid Mech., vol. 40, pt. 4, 1970, pp. 719-735.

82. Gill, P. M.; and Seebass, A. R.: Nonlinear Acoustic Behavior at a Caustic, An Approximate Analytical Solution. Aeroacoustics: Fan, STOL, and Boundary Layer Noise; Sonic Boom; Aeroacoustic Instrumentation, ed. by H. T. Nagamatsu, Vol. 38 of the Progress in Astronautics and Aeronautics, 1975, pp. 353-386.

83. Lung, J. L.; Tiegerman, B.; Yu, N. J.; and Seebass, A. R.: Advances in Sonic Boom Theory. Aerodynamic Analyses Requiring Advanced Computers Part II. NASA SP-347, 1975, pp. 1033-1047.

84. Elmore, W. C.; and Heald, M. A.: Physics of Waves. McGraw-Hill Book Co., 1969.

85. Kline, M.; and Kay, I. W.: Electromagnetic Theory and Geometric Optics. Interscience Publishers, 1965.

86. Keller, J. B.: Geometric Acoustics, I. The Theory of Weak Shock Waves. J. App. Phys., vol. 25, Aug. 1954, pp. 938-947.

87. Friedlander, F. G.: Sound Pulses, Cambridge University Press, 1958.

88. Rayleigh, Lord (John William Strutt): The Theory of Sound, Vol. II, Dover Publications, 1945 (a reprint of the 1929 reprint of the second (1896) edition).

89. Pridmore-Brown, D. C.; and Ingard, U.: Sound Propagation into the Shadow Zone in a Temperature-Stratified Atmosphere Above a Plane Boundary. J. Acoust. Soc. Am., vol. 27, Jan. 1955, pp. 36-42.

90. Haglund, G. T.; and Kane, E. J.: Analysis of Sonic Boom Measurements Near Shock Wave Extremities for Flight Near Mach 1.0 and for Airplane Accelerations. NASA CR-358, Dec. 1965.

91. Onyeowu, R. O.: Diffraction of Sonic Boom Past the Nominal Edge of the Corridor. J. Acoust. Soc. Am., vol. 58, Aug. 1975, pp. 326-330.

92. Pierce, A. D.: Spikes on Sonic-Boom Pressure Waveforms. J. Acoust. Soc. Am., vol. 44, Oct. 1968, pp. 1052-1061.

93. Tolstoy, I.: Wave Propagation. McGraw-Hill Book Co., 1973.

94. Lighthill, J.: Waves in Fluids. Cambridge Univ. Press, 1978.

95. Tolstoy, I.; and Clay, C. S.: Ocean Acoustics. McGraw-Hill Book Co., 1966, Sections 2.9 and 2.10.

96. Barger, R. L.: Some Effects of Flight Path and Atmospheric Variations on the Boom Propagated from a Supersonic Aircraft. NASA TR R-191, Feb. 1964.

97. Haglund, G. T.; and Kane, E. J.: Flight Test Measurements and Analysis of Sonic Boom Phenomena Near the Shock Wave Extremity. NASA CR-2167, Feb. 1973.

98. Groves, G. V.: Geometrical Theory of Sound Propagation in the Atmosphere. J. of Atmospheric and Terrestrial Physics, vol. 7, 1955, pp. 113-127.

99. Carlson, H. W.: Laboratory Sonic-Boom Research and Prediction Techniques. Second Conference on Sonic-Boom Research, ed. by I. R. Schwartz, NASA SP-180, 1968, pp. 29-36.

100. Wanner, J. L.; Vallee, J.; Vivier, C.; and Thery, C.: Theoretical and Experimental Studies of the Focus of Sonic Booms. J. Acoust. Soc. Am., vol. 52, no. 1, pt. 1, 1972, pp. 13-32.

101. Sanai, M.; Toong, T.-Y.; and Pierce, A. D.: Ballistic Range Experiments on Superbooms Generated by Refraction. J. Acoust. Soc. Am., vol. 59, Mar. 1976, pp. 513-519.

102. Friedman, M. P.; and Chou, D. C.: Behavior of the Sonic Boom Shock Wave Near the Sonic Cutoff Altitude. NASA CR-358, Dec. 1965.

103. Myers, M. K.; and Friedman, M. B.: Linear Theory of Superbooms Generated by Refraction. J. of Aircraft, Nov.-Dec. 1967, pp. 486-493.

104. Taylor, G. I.; and Maccoll, J. W.: The Mechanics of Compressible Fluids. In Aerodynamic Theory, vol. 3, ed. by William Frederick Durand, Dover Publications, Inc., 1963, pp. 218-222.

105. Ames Research Staff: Equations, Tables, and Charts for Compressible Flow. NACA Rept. 1135, 1953.

106. Schaefer, William T., Jr.: Characteristics of Major Active Wind Tunnels at the Langley Research Center. NASA TM X-1130, 1965.

107. Dayman, Bain, Jr.: Comparison of Calculated with Measured Boundary-Layer Thicknesses on the Curved Walls of the JPL 20-inch Supersonic Wind Tunnel Two-Dimensional Nozzle. JPL Tech. Rept. No. 32-349, 1963.

108. Shapiro, Ascher H.: The Dynamics and Thermodynamics of Compressible Fluid Flow, Vol. 2. The Ronald Press Co., 1954.

109. Mack, L. M.: Boundary Layer Stability Theory, Jet Propulsion Laboratory Report No. 900-277 (Rev. A), Nov. 1969.

110. Price, J. M.; and Harris, J. E.: Computer Program for Solving Compressible Nonsimilar-Boundary-Layer Equations for Laminar, Transitional, or Turbulent Flows of a Perfect Gas. NASA TM X-2458, April 1972.

111. George, A. R.: The Effects of Atmospheric Inhomogeneities on Sonic Boom. Third Conference on Sonic Boom Research, ed. by I. R. Schwartz, NASA SP-255, 1971.

112. Schneider, W.: Upstream Propagation of Unsteady Disturbances in Supersonic Boundary Layers. J. Fluid Mech., vol. 63, pt. 3, 1974, pp. 465-485.

113. Dore, B. D.: The Upstream Influence Ahead of a Weak, Uniformly Moving Shock or Expansion Wave. Quarterly J. of Mech. and App. Math., vol. 20, Aug. 1967, pp. 333-345.

114. Mack, L. M.: Response of Supersonic Laminar Boundary Layer to a Moving External Pressure Field. JPL Space Programs Summary 37-66, Dec. 31, 1970, pp. 13-16.

115. Speaker, M. V.; and Ailman, C. M.: Spectra and Space-Time Correlations of the Fluctuating Pressures of a Wall Beneath a Supersonic Turbulent Boundary Layer Perturbed by Steps and Shockwaves. NASA CR-456, May 1965.

116. Serafini, John S.: Wall-Pressure Fluctuations and Pressure-Velocity Correlations in a Turbulent Boundary Layer. NASA TR-165, 1963.

117. Kistler, A. L.; and Chen, W. S.: A Fluctuating Pressure Field in a Supersonic Turbulent Boundary Layer. J. Fluid Mech., vol. 16, pt. 1, 1963, pp. 41-64.

118. Willmarth, W. W.; and Wooldridge, C. E.: Measurements of the Fluctuating Pressure at the Wall Beneath a Thick Turbulent Boundary Layer. J. of Fluid Mech., vol. 14, pt. 2, Oct. 1962, pp. 187-210.

119. Willmarth, W. W.: Space-Time Correlations and Spectra of Wall Pressure in a Turbulent Boundary Layer. NASA Memo 3-17-59W, 1959.

120. Maestrello, L.; Monteith, J. H.; Manning, J. C.; and Smith, D. L.: Measured Response of a Complex Structure to Supersonic Turbulent Boundary Layers. AIAA Paper No. 76-83, Jan. 1976.

121. Thomas, A. S. W.: Conditionally Sampled Measurements of the Fluctuating Pressure at the Wall Beneath a Turbulent Boundary Layer. AIAA Paper No. 78-1157, July 1978.

122. Zakkay, V.; Barra, V.; and Wang, C. K.: The Nature of Boundary-Layer Turbulence at a High Subsonic Speed. AIAA J., vol. 17, no. 4, April 1979, pp. 356-364.

123. Raman, K. R.: Surface Pressure Fluctuations in Hypersonic Turbulent Boundary Layers. NASA CR-2386, 1974.

124. Bull, M. K.: Wall-Pressure Fluctuations Associated with Subsonic Turbulent Boundary Layer Flow. J. Fluid Mech., vol. 28, pt. 4, 1967, pp. 719-754.

125. Chyu, Wei J.; and Hanly, Richard D.: Power-and Cross-Spectra and Space-Time Correlations of Surface Fluctuating Pressures at Mach Numbers Between 1.6 and 2.5. NASA TN D-5440, 1969.

126. Maestrello, L.: Radiation from and Panel Response to a Supersonic Turbulent Boundary Layer. J. Sound Vib., vol. 10, no. 2, 1969, pp. 261-295.

127. Dinkelacker, A.; Hessel, M.; Meier, G. E. A.; and Schewe, G.: Investigation of Pressure Fluctuations Beneath a Turbulent Boundary Layer by Means of an Optical Method. The Physics of Fluids, vol. 20, no. 10, Part II, Oct. 1977, pp. 5216-5224.

128. Fischer, M. C.; Maddalon, D. V.; Weinstein, L. M.; and Wagner, R. D.: Boundary-Layer Surveys on a Nozzle Wall at M $\approx$ 20 Including Hot-Wire Fluctuation Measurements. AIAA Paper No. 70-746, June 1970.

129. Schloemer, Howard H.: Effects of Pressure Gradients on Turbulent-Boundary-Layer Wall-Pressure Fluctuations. J. Acoust. Soc. Am., vol. 42, no. 1, 1967, pp. 93-113.

130. Bakewell, Henry P., Jr.: Turbulent Wall-Pressure Fluctuations on a Body of Revolution. J. Acoust. Soc. Am., vol. 43, no. 6, 1968, pp. 1358-1363.

131. Willmarth, W. W.; and Yang, C. S.: Wall-Pressure Fluctuations Beneath Turbulent Boundary Layers on a Flat Plate and a Cylinder. J. Fluid Mech., vol. 41, pt. 1, 1970, pp. 47-80.

132. Hanly, Richard D.: Effects of Transducer Flushness on Fluctuating Surface Pressure Measurements. AIAA Paper No. 75-534, Mar. 1975.

133. Coe, F. F.; Chyu, W. J.; and Dods, J. B., Jr.: Pressure Fluctuations Underlying Attached and Separated Supersonic Turbulent Boundary Layers and Shock Waves. In Aeroacoustics, vol. 38 of the Progress in Astronautics and Aeronautics Series, ed. by H. T. Nagamatsu, 1975, pp. 243-264.

134. Wills, J. A. B.: Measurements of the Wave-Number/Phase Velocity Spectrum of Wall Pressure Beneath a Turbulent Boundary Layer. J. Fluid Mech., vol. 45, pt. 1, 1970, pp. 65-90.

135. Blake, William K.: Turbulent Boundary-Layer Well-Pressure Fluctuations on Smooth and Rough Walls. J. Fluid Mech., vol. 14, pt. 4, 1970, pp. 637-660.

136. Brackenridge, J. B.; Geib, F. E., Jr.; Maidanik, G.; and Remmers, G.: Convection Velocities of Pressure Fields on Plane Boundaries. J. Acoust. Soc. Am., vol. 54, no. 5, 1973, pp. 1189-1200.

137. Lewis, Thomas L.; Dods, Jules B., Jr.; and Hanly, Richard D.: Measurements of Surface-Pressure Fluctuations on the XB-70 Airplane at Local Mach Numbers up to 2.45. NASA TN D-7226, 1973.

138. Van Driest, E. R.: Investigation of Laminar Boundary Layer in Compressible Fluids Using the Crocco Method. NACA TN 2597, 1952.

139. Hayes, W. D.: Similarity Rules for Nonlinear Acoustic Propagation Through a Caustics. Second Conference on Sonic Boom Research, ed. by I. R. Schwartz, NASA SP-180, 1968, pp. 165-171.

140. Seebass, R.: Nonlinear Acoustic Behavior of a Caustic. Third Conference on Sonic Boom Research, ed. by I. R. Schwartz, NASA SP-255, 1971, pp. 87-120.

141. Laufer, J.; and Vrebalovich, T.: Stability and Transition of a Supersonic Laminar Boundary Layer on an Insulated Flat Plate. J. Fluid Mech., vol. 9, Oct. 1960, pp. 257-299.

142. Owen, F. K.: Fluctuation and Transition Measurements in Compressible Boundary Layers. AIAA Paper No. 70-745, June 1970.

143. Potter, J. L.; and Whitfield, J. D.: Effect of Slight Nose Bluntness and Roughness on Boundary-Layer Transition in Supersonic Flow. J. Fluid Mech., vol. 12, pt. 4, 1962, pp. 501-535.

144. Demetriades, A.: An Experiment on the Stability of Hypersonic Boundary Layers. J. Fluid Mech., vol. 7, Mar. 1960, pp. 385-396.

145. Staylor, W. F.; and Morrisette, E. L.: Use of Moderate-Length Hot-Wires to Survey a Hypersonic Boundary Layer. AIAA J., vol. 5, no. 9, Sept. 1967, pp. 1698-1700.

146. LaGraff, J. E.: Observations of Boundary-Layer Transition in a Mach 7 Gun Tunnel with a Hot-Wire Anemometer. AIAA Paper No. 71-199, Jan. 1971.

147. Maddalon, D. V.; and Henderson, A., Jr.: Boundary-Layer Transition on Sharp Cones at Hypersonic Mach Numbers. AIAA J., vol. 6, no. 3, Mar. 1968, pp. 424-431.

148. Nagamatsu, H.; Graber, B. C.; and Sheer, R. E. Jr.: Critical Layer Concept Relative to Hypersonic Boundary Layer Stability. BSD-TR-66-18, Ballistic Systems Division, Deputy for Ballistic Missile Re-entry Systems, Air Force Systems Command, Norton Air Force Base, Calif., Feb. 1966.

149. Demetriades, A.: Hydrodynamic Stability and Transition to Turbulence in the Hypersonic Boundary Layer over a Sharp Cone. AFOSR-TR-75-1435, July 1975.

150. Keltner, G. L.: Spatial Stability and Transition in Compressible Flat Plate Flows. Ph.D Dissertation in Engineering, University of California, Los Angeles, 1973.

151. Stewart, R. W.; and Manton, M. J.: Generation of Waves by Advected Pressure Fluctuations. Geophysical Fluid Dynamics, vol. 2, June 1971, pp. 263-272.

152. Moore, F. K.: Unsteady Oblique Interaction of a Shock Wave with a Plane Disturbance. NACA Report 1165, 1954.

153. Carlson, H. W.; McLean, F. E.; and Shrout, B. L.: A Wind-Tunnel Study of Sonic-Boom Characteristics for Basic and Modified Models of a Supersonic Transport Configuration. NASA TM X-1236, May 1966.

154. Laufer, John: Sound Radiated From a Turbulent Boundary Layer. JPL Tech. Rept. No. 32-119, 1961.

155. Laufer, John: Aerodynamic Noise of Supersonic Boundary Layer. JPL Research Summary No. 36-6, Oct. 1, 1960 to Dec. 1, 1960, pp. 13-14.

156. Phillips, O. M.: The Irrotational Motion Outside a Free Turbulent Boundary. Proc. Camb. Phil. Soc., vol. 51, 1955, pp. 220-

157. Bradbury, L. J. S.: The Structure of a Self-Preserving Turbulent Plane Jet. J. of Fluid Mech., vol. 23, pt. 1, 1965, pp. 31-64.

158. Bradshaw, P.: Irrotational Fluctuations Near a Turbulent Boundary Layer. J. of Fluid Mech., vol. 27, pt. 2, 1967, pp. 209-230.

159. Kibens, Valdis; and Kovasznay, Leslie, S. G.: The Intermittent Region of a Turbulent Boundary Layer. Dept. of Mechanics, The Johns Hopkins University, DA-31-124-ARO-D-313, Jan. 1969.

160. Kovasznay, Leslie S. G.; Kibens, Valdis; and Blackwelder, Ron F.: Large-Scale Motion in the Intermittent Region of a Turbulent Boundary Layer. J. of Fluid Mech., vol. 41, pt. 2, 1970, pp. 283-325.

161. Maxwell, H.; and Jacocks, J. L.: Nondimensional Calculation of Turbulent Boundary-Layer Development in Two-Dimensional Nozzles of Supersonic Wind Tunnels. AEDC-TN-61-153, U.S. Air Force, 1962.

162. Barry, F. W.; Shapiro, A. H.; and Neumann, E. P.: The Interaction of Shock Waves with Boundary Layers on a Flat Surface. J. of the Aeronautical Sciences, vol. 18, no. 4, April 1951, pp. 229-238.

163. Liepmann, H. W.; Roshko, A.; and Dhawan, S.: On Reflection of Shock Waves From Boundary Layers. NACA Report 1100, 1952.

164. Gadd, G. E.; Holder, D. W.; and Regan, J. D.: An Experimental Investigation of the Interaction Between Shock Waves and Boundary Layers. Proc. Roy. Soc. (A), vol. 226, 1954, pp. 227-253.

165. Hakkinen, R. J.; and Trilling, L.: On the Interaction of an Oblique Shock Wave With a Laminar Boundary Layer. IX Congrès International de Méchanique Appliquée, Actes, Vol. IV, Université de Bruxelles, 1957, pp. 5-15. (Note: The wind tunnel is the same as that used in ref. 60).

166. Pinckney, S. Z.: Data on Effects of Incident-Reflecting Shocks on the Turbulent Boundary Layer. NASA TM X-1221, Mar. 1966.

167. Watson, E. C.; Murphy, J. D.; and Rose, W. C.: Shock-Wave Boundary Layer Interactions in Hypersonic Inlets. NASA SP-148, Conference on Hypersonic Aircraft Technology, 1967.

168. Green, J. E.: Reflections of an Oblique Shock Wave by a Turbulent Boundary Layer. J. of Fluid Mech., vol. 40, pt. 1, 1970, pp. 81-95.

169. Kaufman, Louis G. II; and Johnson, Charles B.: Weak Incident Shock Interactions with Mach 8 Laminar Boundary Layers. NASA TN D-7835, 1974.

170. Rose, William C.: A Method for Analyzing the Interaction of an Oblique Shock Wave and a Boundary Layer. Analytic Methods in Aircraft Aerodynamics, NASA SP-228, Symposium held at Ames Research Center, Oct. 28-30, 1969, pp. 541-567.

171. Rose, William C.; Murphy, John D.; and Watson, Earl C.: Interaction of an Oblique Shock Wave with a Turbulent Boundary Layer. AIAA J. vol. 6, no. 9, Sept. 1968, pp. 1792-1793.

172. McKenzie, J. F.; and Westphal, K. O.: Interaction of Linear Waves with Oblique Shock Waves. Physics of Fluids, vol. 11, no. 11, Nov. 1968, pp. 2350-2362.

173. Morkovin, M. V.: Note on the Assessment of Flow Disturbances at a Blunt Body Traveling at Supersonic Speeds Owing to Flow Disturbances in Freestream. J. of App. Mech., June 1960, pp. 223-229.

174. Ribner, H. S.: Acoustic Energy Flux From Shock-Turbulence Interaction. J. Fluid Mech., vol. 35, pt. 2, 1969, pp. 299-310.

175. Kovasznay, Leslie S. G.: Interaction of a Shock Wave and Turbulence. Heat Transfer and Fluid Mechanics Institute, 1955, pp. I-1 to I-12.

176. Henderson, L. F.; and MacPherson, A. K.: On the Irregular Refraction of a Plane Shock Wave at a Mach Number Interface. J. of Fluid Mech., vol. 32, pt. 1, 1968, pp. 185-202.

177. Radcliffe, S. W.: An Experimental Investigation of Pressure Fluctuations Caused by the Interaction of Turbulence With Shock and Expansion Waves. NASA CR-98391, 1969.

178. Pan, Y. S.: Propagation of an N-Wave Across a Nonuniform Medium. AIAA J., vol. 7, no. 4, April 1969, pp. 788-790.

179. Friedman, Manfred P.; Kane, Edward J.; and Sigalla, Armand: Effects of Atmospheric and Aircraft Motion on the Location and Intensity of a Sonic Boom. AIAA J., vol. 1, no. 6, June 1963, pp. 1327-1335.

180. Lanczos, Cornelius: The Variational Principles of Mechanics. Third ed., University of Toronto Press, 1966, Chapter 8, Sections 7 and 8.

181. Kerr, Donald E.: Propagation of Short Radio Waves. McGraw-Hill Book Co., Inc., 1951, Chapter 2.

182. Blokhintsev, D. I.: Acoustics of a Nonhomogeneous Moving Medium. NACA TM 1399, Feb. 1956. Gostekizdat, 1946.

183. Heller, G. S.: Propagation of Acoustic Discontinuities in an Inhomogeneous Moving Liquid Medium. J. Acoust. Soc. Am., vol. 25, no. 5, Sept. 1953, pp. 950-951.

184. Kline, Morris: Electromagnetic Theory and Geometric Optics. In Electromagnetic Waves, ed. by Rudolph E. Langer, The Univ. of Wisconsin Press, 1962, pp. 3-31.

185. Kinsler, Lawrence E.; and Frey, Austin R.: Fundamentals of Acoustics. John Wiley and Sons, 1962.

186. Kornhauser, E. T.: Ray Theory for Moving Fluids. J. Acoust. Soc. Am., vol. 25, no. 5, Sept. 1953, pp. 945-949.

187. Milne, E. A.: Sound waves in the Atmosphere. Philosophical Magazine, vol. 42, July 1921, pp. 96-114.

188. Thompson, Robert J.: Ray Theory for an Inhomogeneous Moving Medium. J. Acoust. Soc. Am., vol. 51, no. 5, 1972, pp. 1675-1682.

189. Engelke, Ray: Ray Trace Acoustics in Unsteady Inhomogeneous Flow. J. Acoust. Soc. Am., vol. 56, no. 4, 1974, pp. 1291-1292.

190. Uginĉius, Peter: Ray Acoustics and Fermat's Principle in a Moving Inhomogeneous Medium. J. Acoust. Soc. Am., vol. 51, no. 5, 1972, pp. 1759-1763.

191. Ryzhov, O. S.; and Shefter, G. M.: On the Energy of Acoustic Waves Propagating in Moving Media. Appl. Math. Mech. (PMM), vol. 26, no. 5, 1962, pp. 1293-1309.

192. Ribner, H. S.: Note on Acoustic Energy Flow in a Moving Medium. UTIA Technical Note No. 21, (AFOSR TN-58-360, AD154 265), April 1958.

193. Ingard, Uno: Acoustics. Presented in Handbook of Physics, ed. by E. U. Condon and Hugh Odishaw, McGraw-Hill Book Co., Inc., 1958, Chapter 8, pp. 3-112 to 3-133.

194. Bretherton, F. P.; and Garrett, C. J. R.: Wavetrains in Inhomogeneous Moving Media. Proc. Roy. Soc., vol. A 302, 1969, pp. 529-554.

195. Lighthill, James: The Fourth Annual Fairey Lecture: The Propagation of Sound Through Moving Fluids. J. Sound and Vib., vol. 24, pt. 4, 1972, pp. 471-492.

196. Candel, Sébastien M.: Numerical Solution of Conservation Equations Arising in Linear Wave Theory: Application to Aeroacoustics. J. Fluid Mech., vol. 83, pt. 3, 1977, pp. 465-493.

197. Candel, S. M.: Acoustic Conservation Principles and an Application to Plane and Modal Propagation in Nozzles and Diffusers. J. Sound and Vib., vol. 41, pt. 2, 1975, pp. 207-232.

198. Hayes, Wallace E.; and Runyan, Harry L., Jr.: Propagation of Sonic Boom Through a Stratified Atmosphere. Analytic Methods in Aircraft Aerodynamics, NASA SP-228, a symposium held at Ames Research Center, Oct. 28-30, 1969, pp. 229-244.

199. Hayes, Wallace D.; and Runyan, Harry L., Jr.: Propagation in Sonic Boom Through a Stratified Atmosphere. J. Acoust. Soc. Am., vol. 51, no. 2, 1972, pp. 695-701.

200. Hayes, Wallace D.: Review of Sonic-Boom Theory. Aerodynamic Noise, Proceedings of AFOSR-UTIAS Symposium held at Toronto, Canada, 20-21 May 1968, University of Toronto Press, 1969, pp. 387-396.

201. Taylor, G. I.: The Conditions Necessary for Discontinuous Motion in Gases. Proc. Roy. Soc., vol. A84, 1910, pp. 371-7; also in the Scientific Papers of Sir Geoffrey Ingram Taylor, vol. 3, ed. by G. K. Batchelor, Cambridge Univ. Press, 1963, pp. 1-6.

202. Morduchow, Morris; and Libby, Paul A.: On a Complete Solution of the One-Dimensional Flow Equations of a Viscous, Heat-Conducting Compressible Gas. J. of Aeronautical Sciences, vol. 16, Nov. 1949, pp. 674-684, 704.

203. White, Frank M.: Viscous Flow. McGraw-Hill Book Co., 1974.

204. Curle, N.; and Davies, H. J.: Modern Fluid Dynamics, vol. 2, Compressible Flow. Van Nostrand Reinhold Co., 1971.

205. Thompson, Philip A.: Compressible-Fluid Dynamics. McGraw-Hill Book Co., 1972.

206. Mack, Leslie M.: Calculation of the Laminar Boundary Layer on an Insulated Flat Plate by the Klunker-McLean Method. JPL Progress Rept. No. 20-352, 1958.

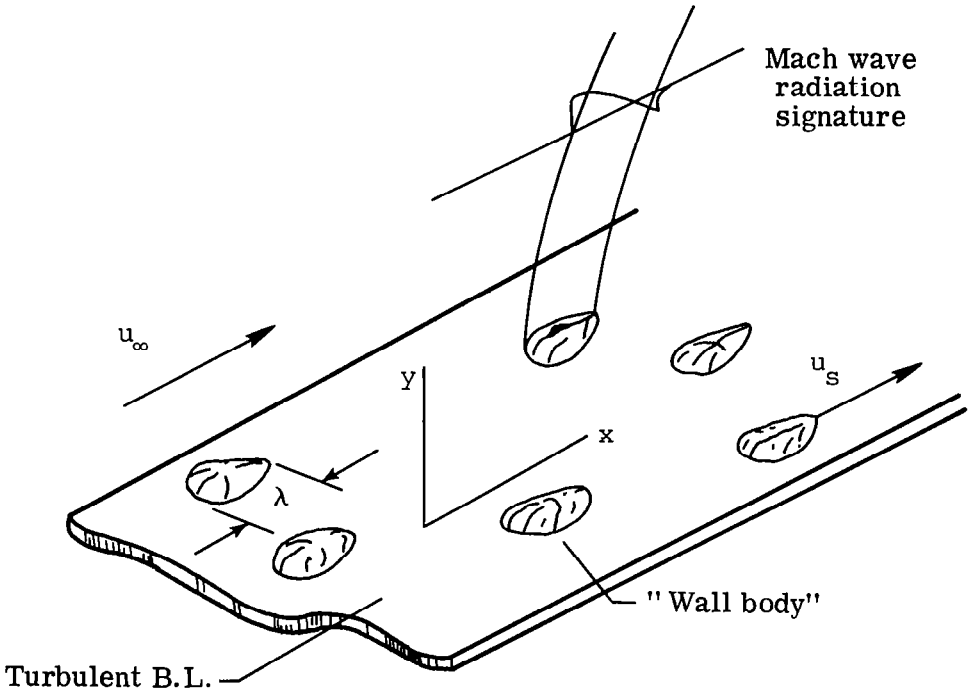

Figure 1.- Noise radiation model.

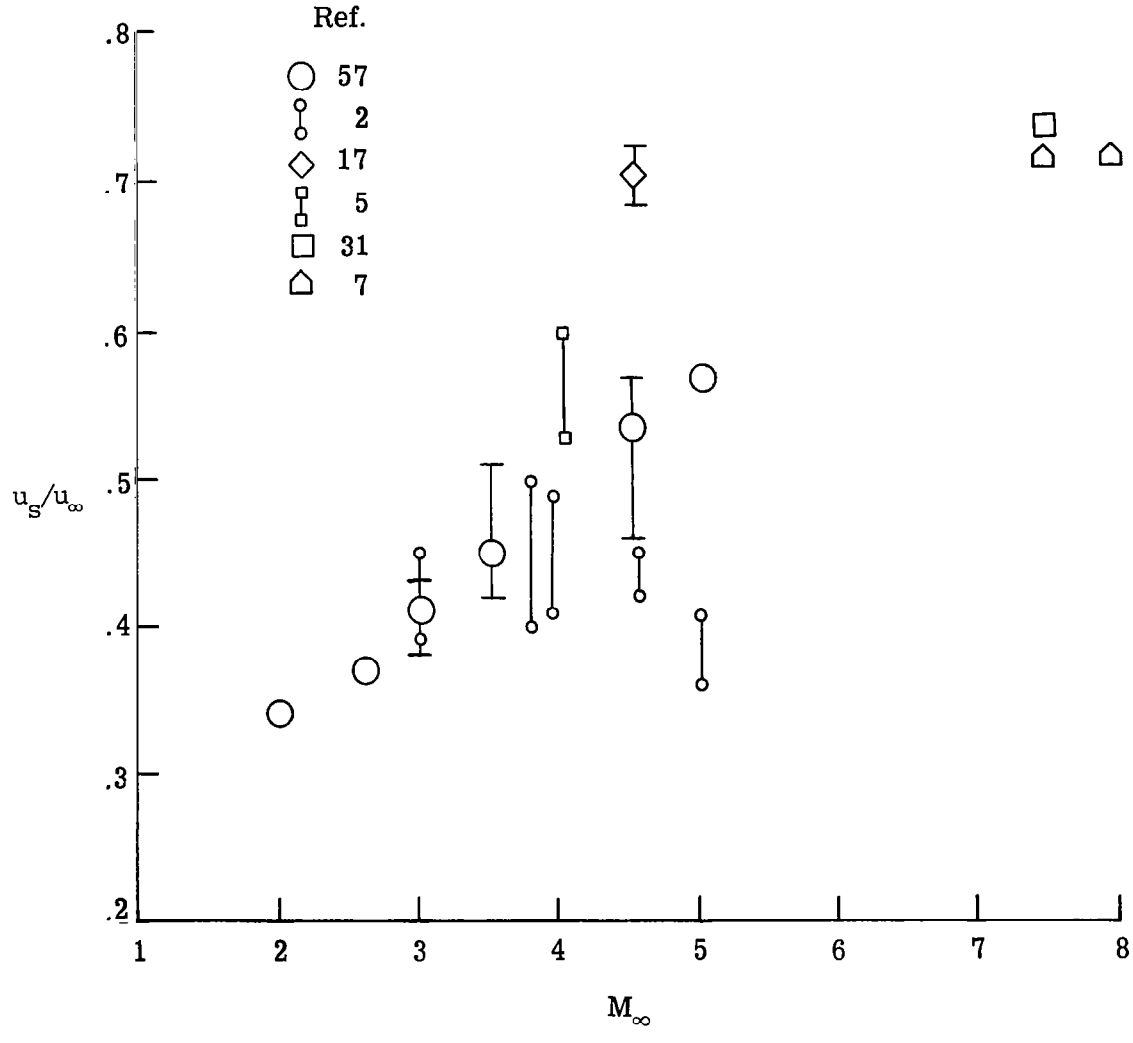

Figure 2.- Noise field convection velocities measured with hot-wire anemometers; large symbols indicate dual-wire results; small symbols indicate single-wire results.

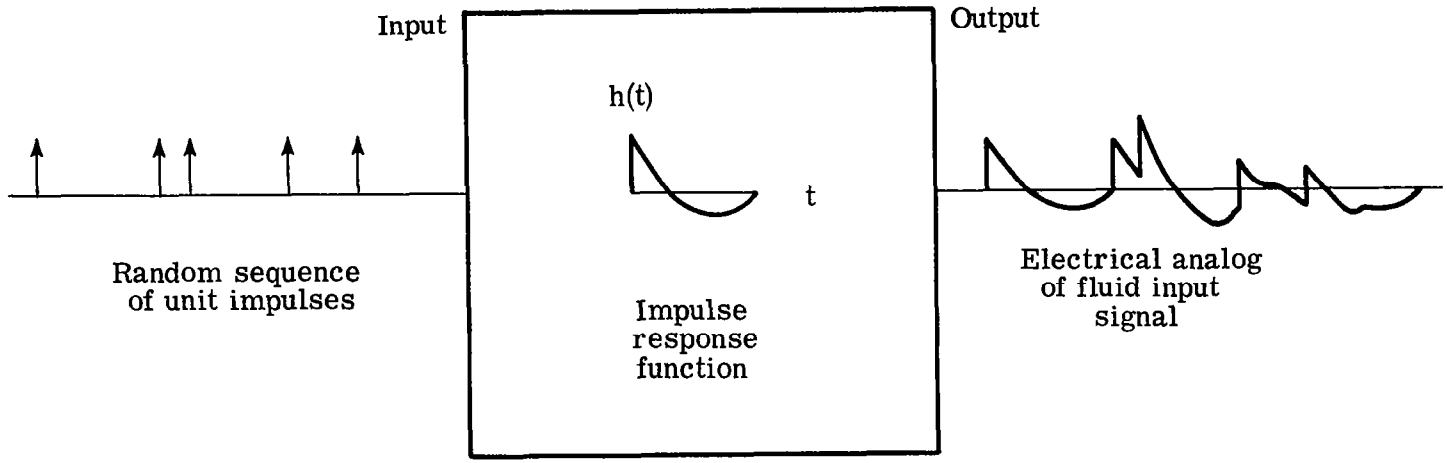

Figure 3.- Linear system scheme to analyze statistical properties of fluid signal.

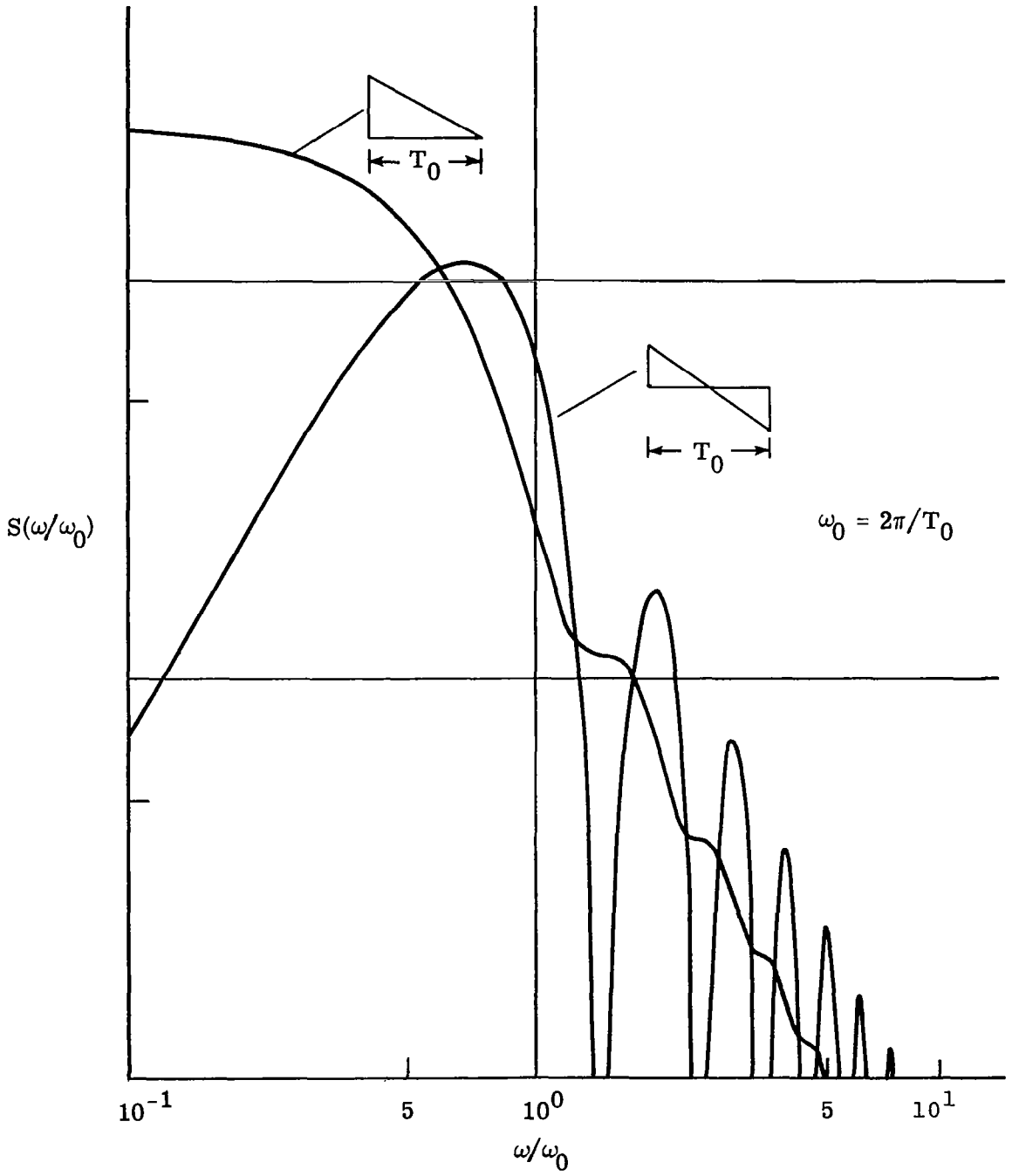

Figure 4.- Comparison of power spectral densities of two example pulse forms. T_0 is the pulse duration. Log-log scales.

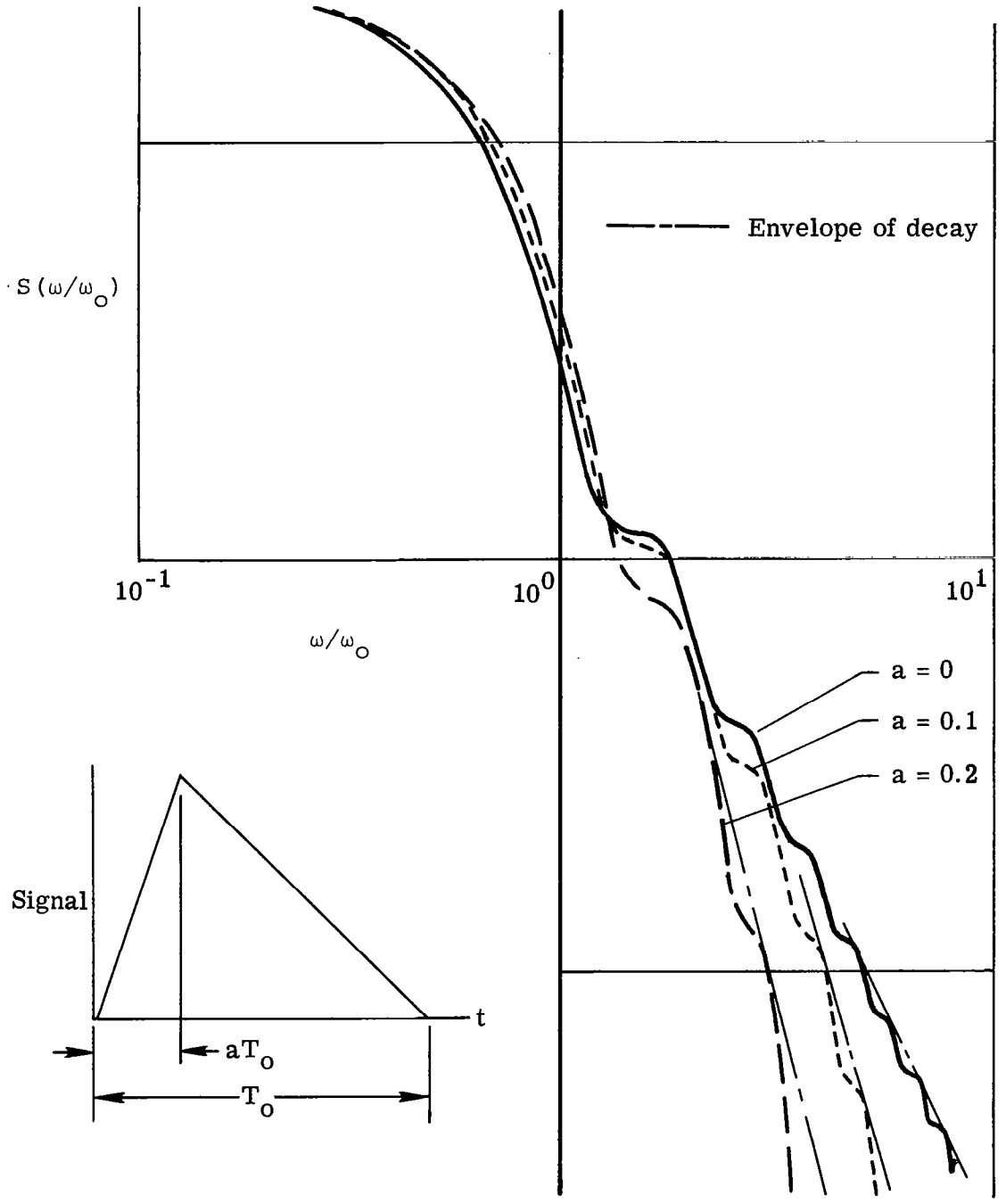

Figure 5.- Effect of rise time on the power spectral density.

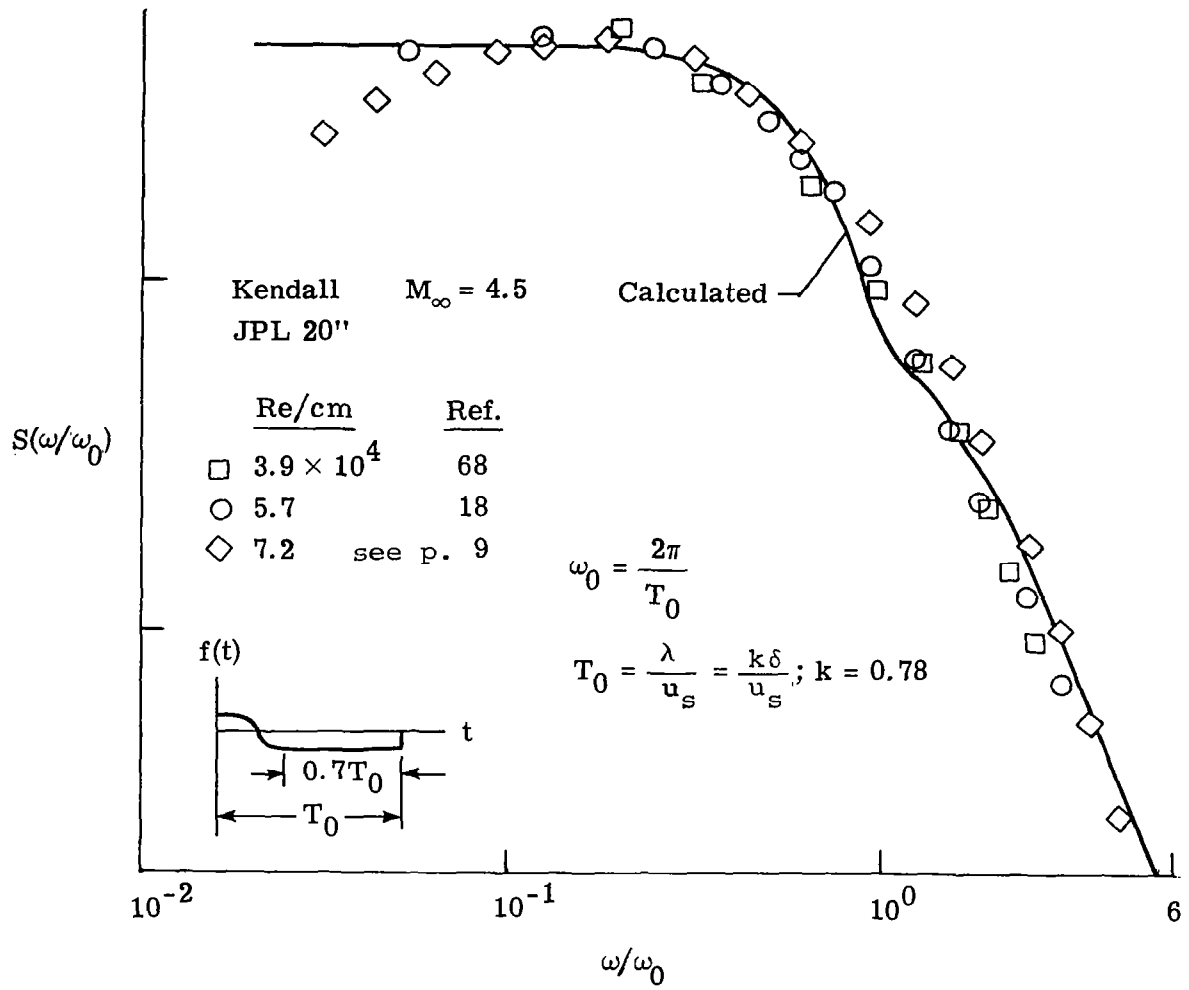

(a) $M_\infty = 4.5$

Figure 6.- Comparison of computed and measured power spectral densities. Log-log scales.

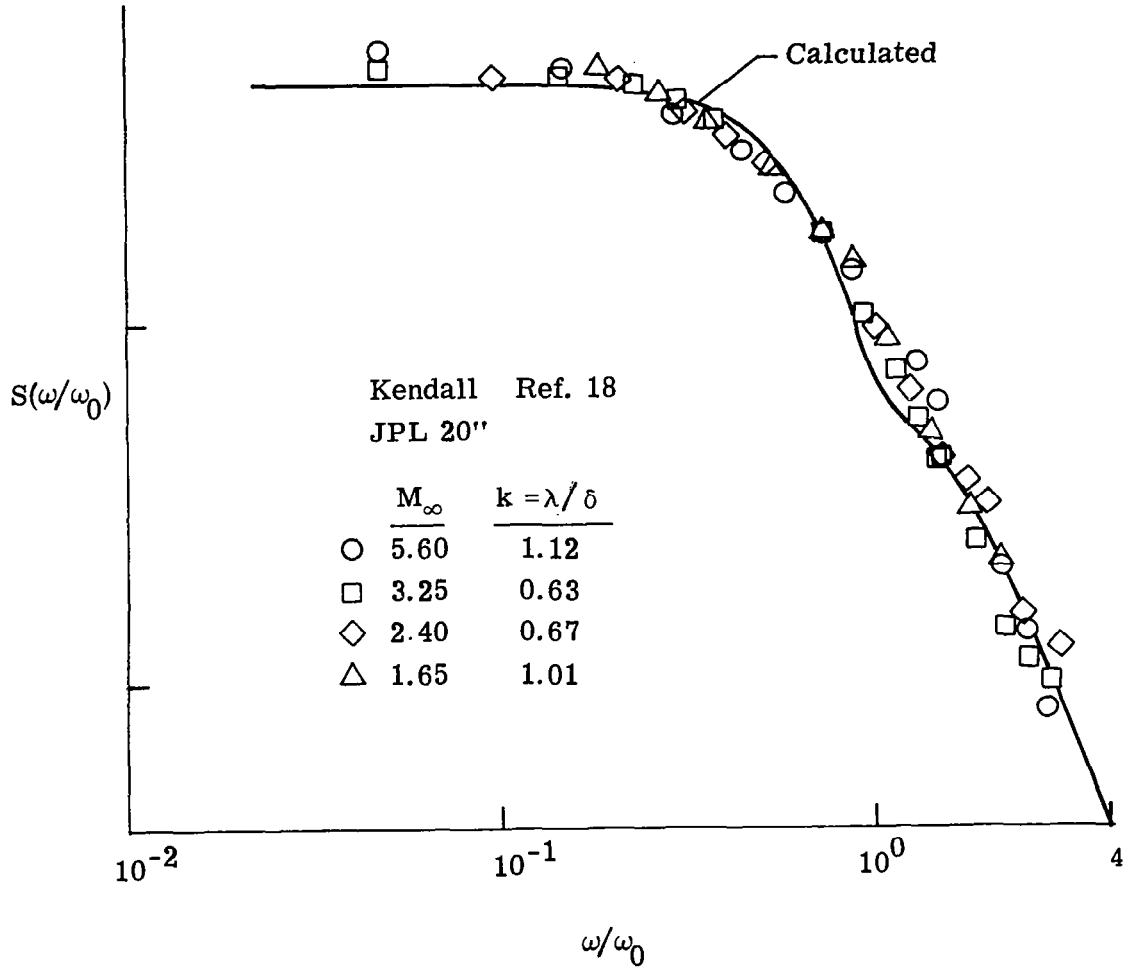

(b) Various Mach numbers

Figure 6.- Concluded.

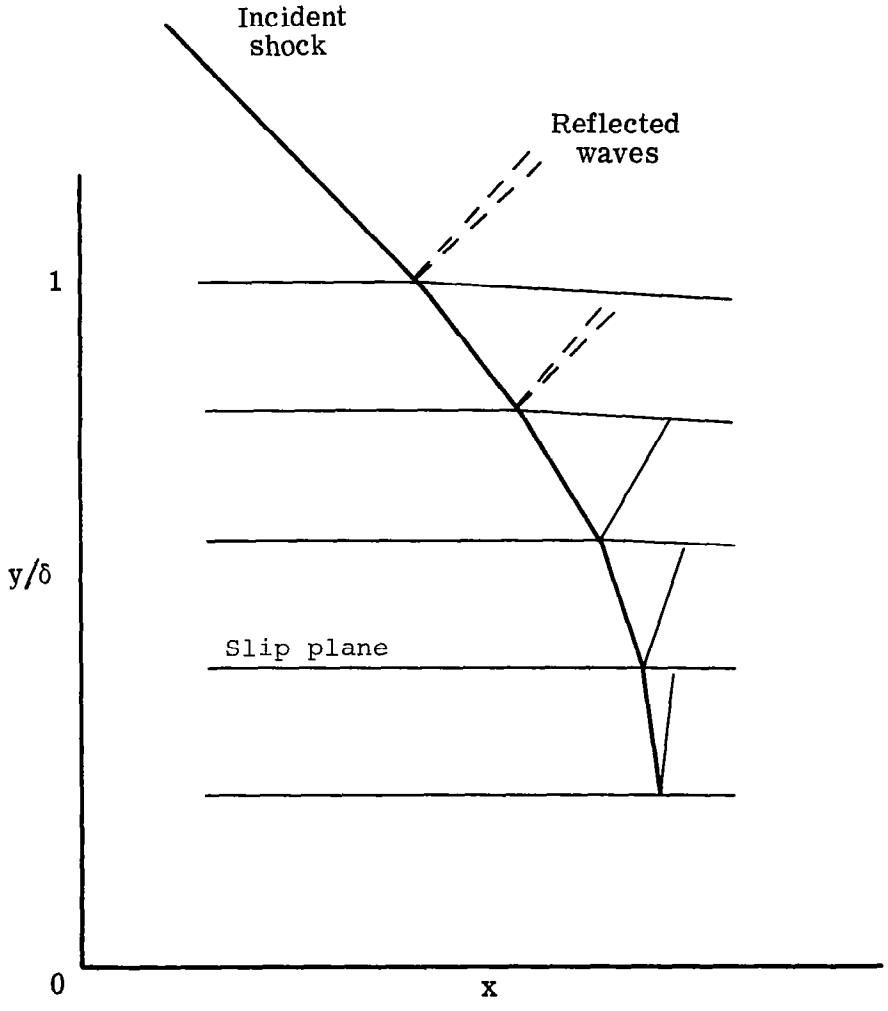

Figure 7.- Layered flow interaction model.

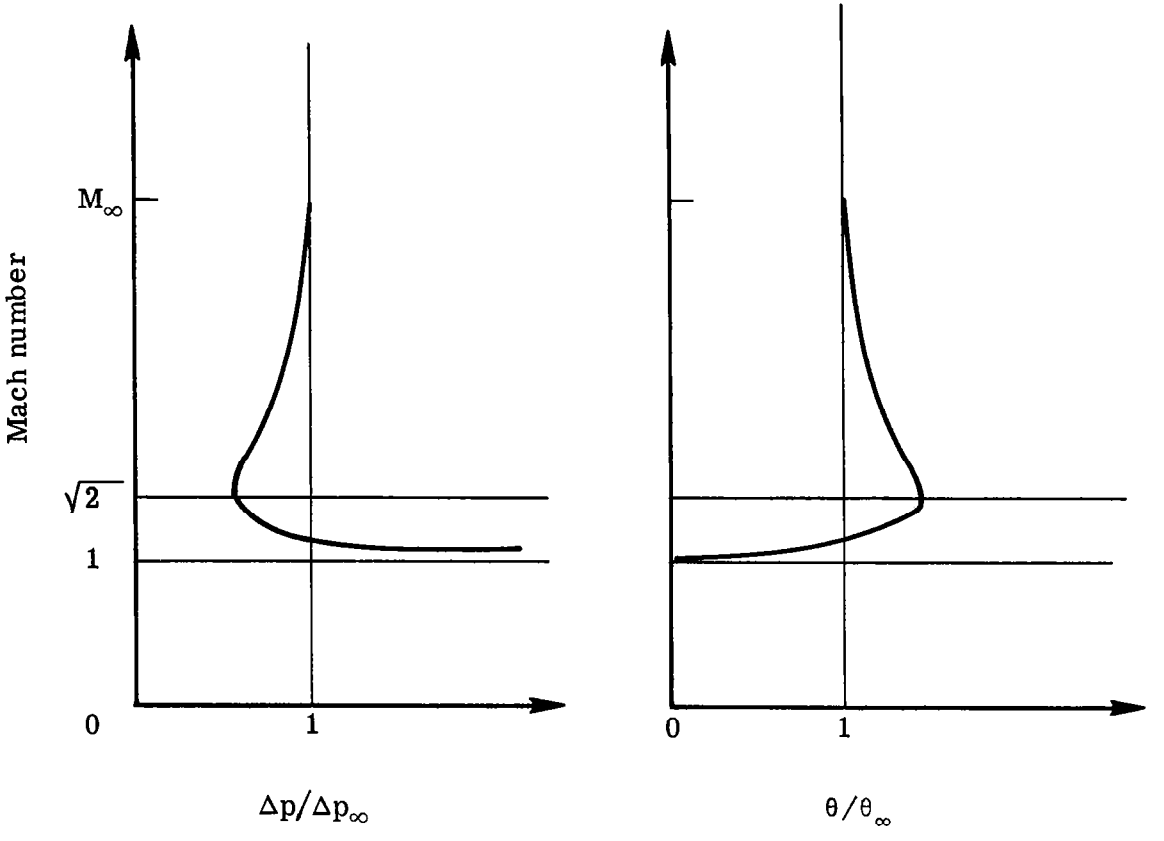

Figure 8.- Variation of pressure rise and flow deflection angle across shock propagating through shear layer.

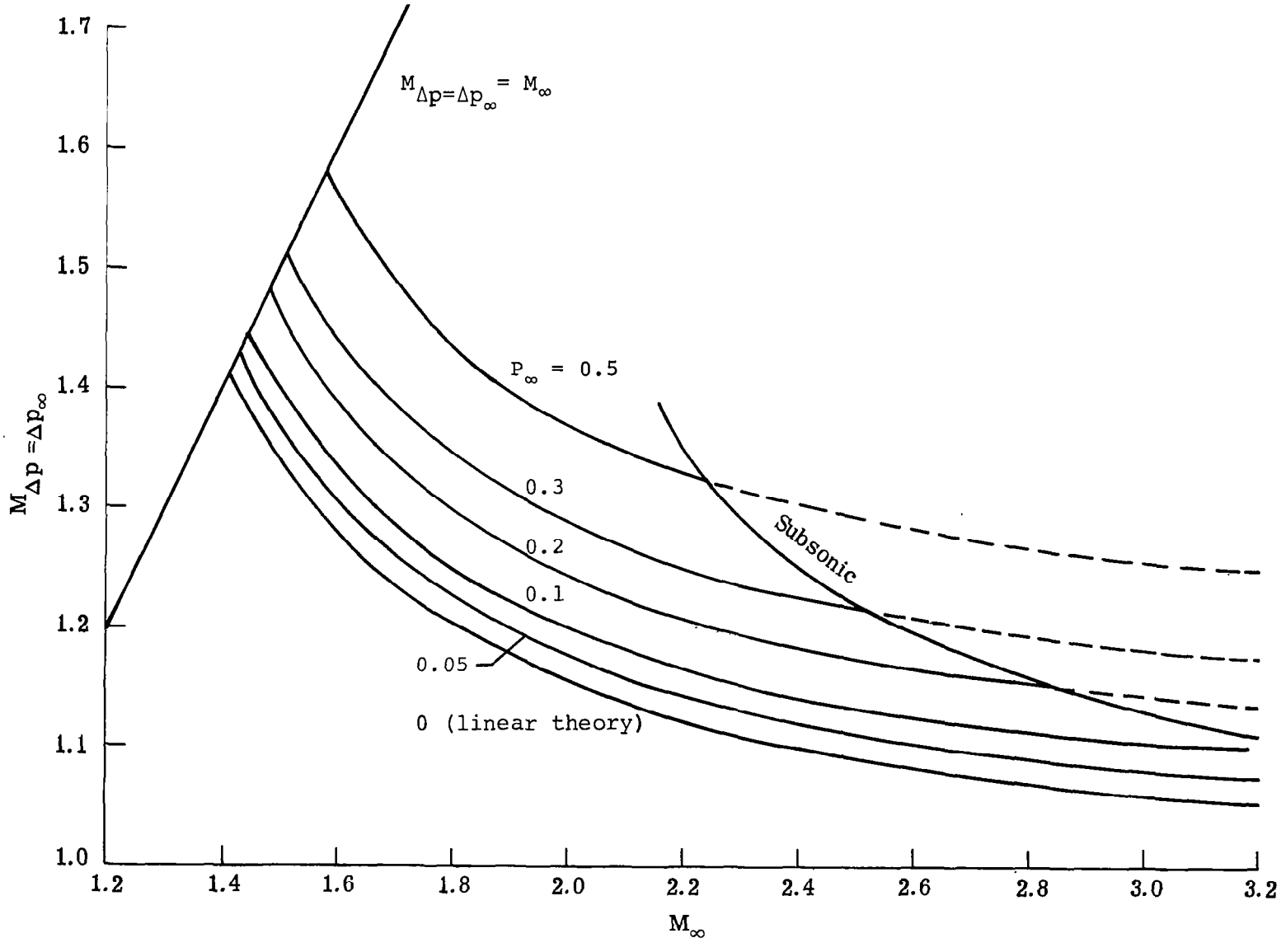

Figure 9.- Variation of Mach number within the boundary layer with freestream Mach number and incoming shock strength for which the change in flow deflection angle and pressure coefficient across the wave match those across the wave at the edge of the boundary layer.

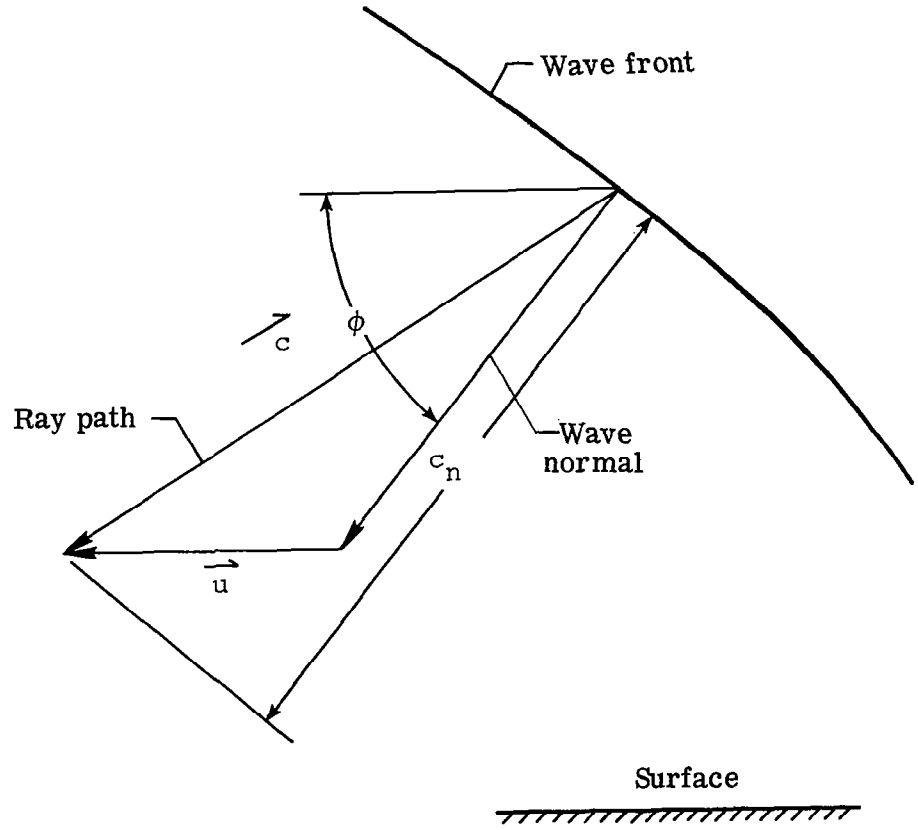

Figure 10.- Wave front - ray path configuration.

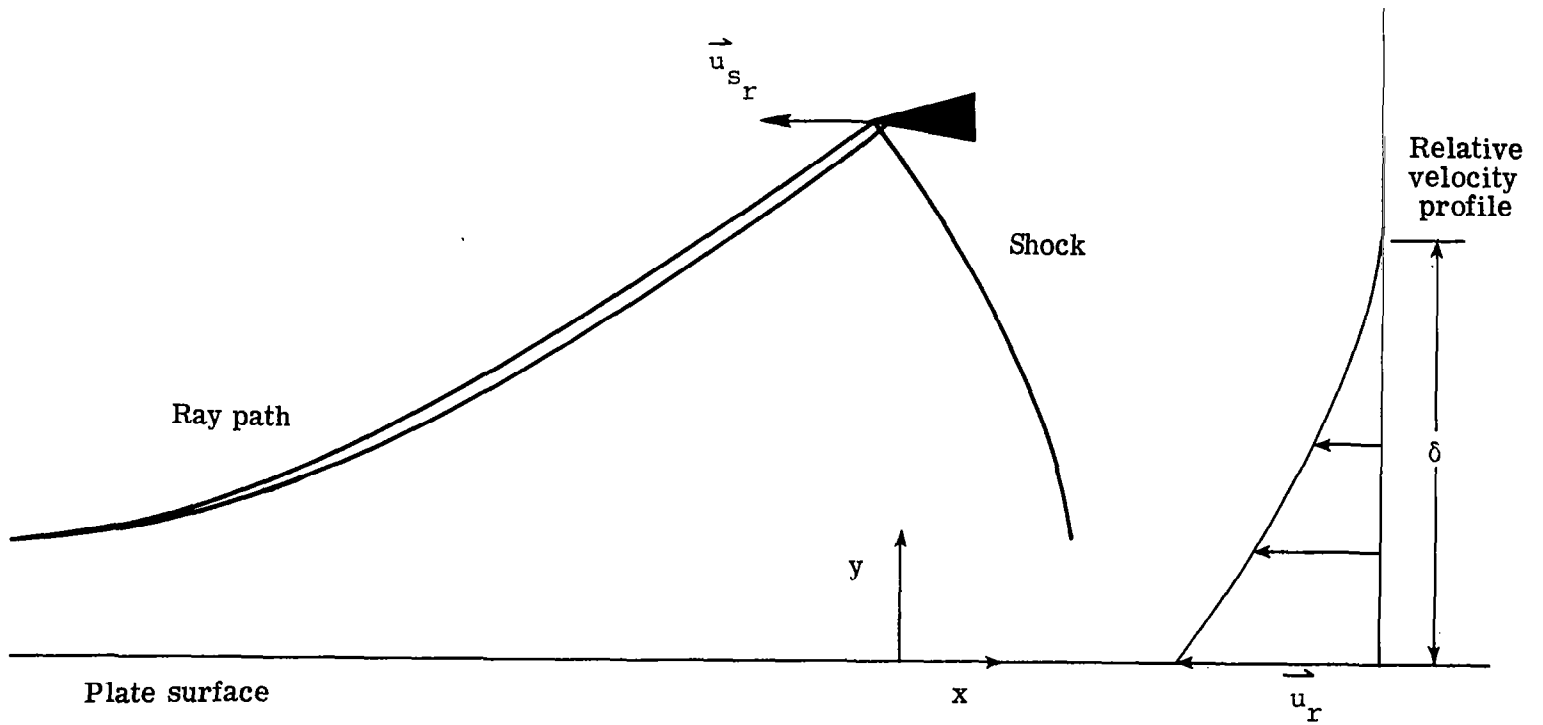

Figure 11.- Geometric acoustic interaction model

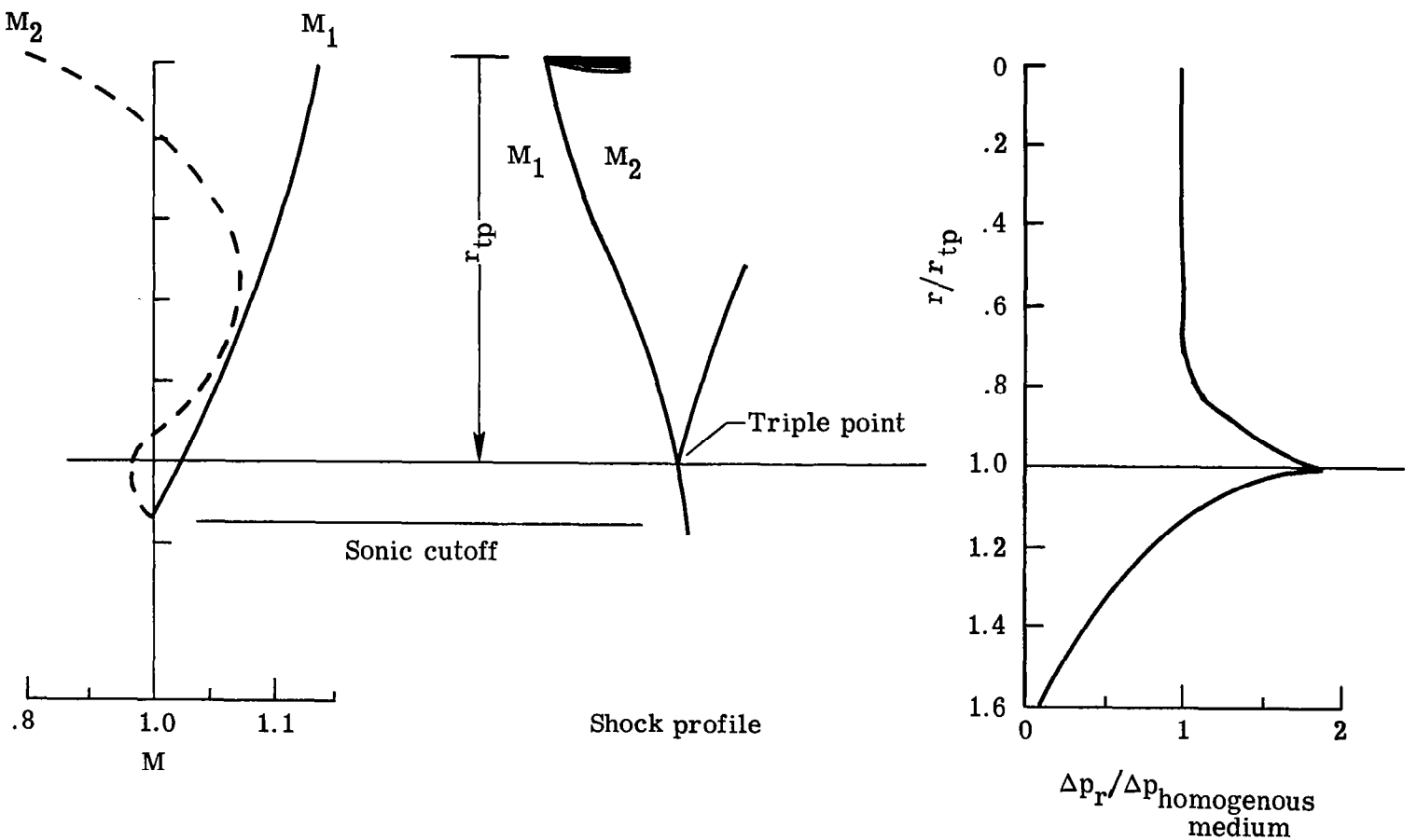

Figure 12.- Sketch of typical results from ballistic range shock refraction experiments of Sanai, Toong, and Pierce, ref. 101.

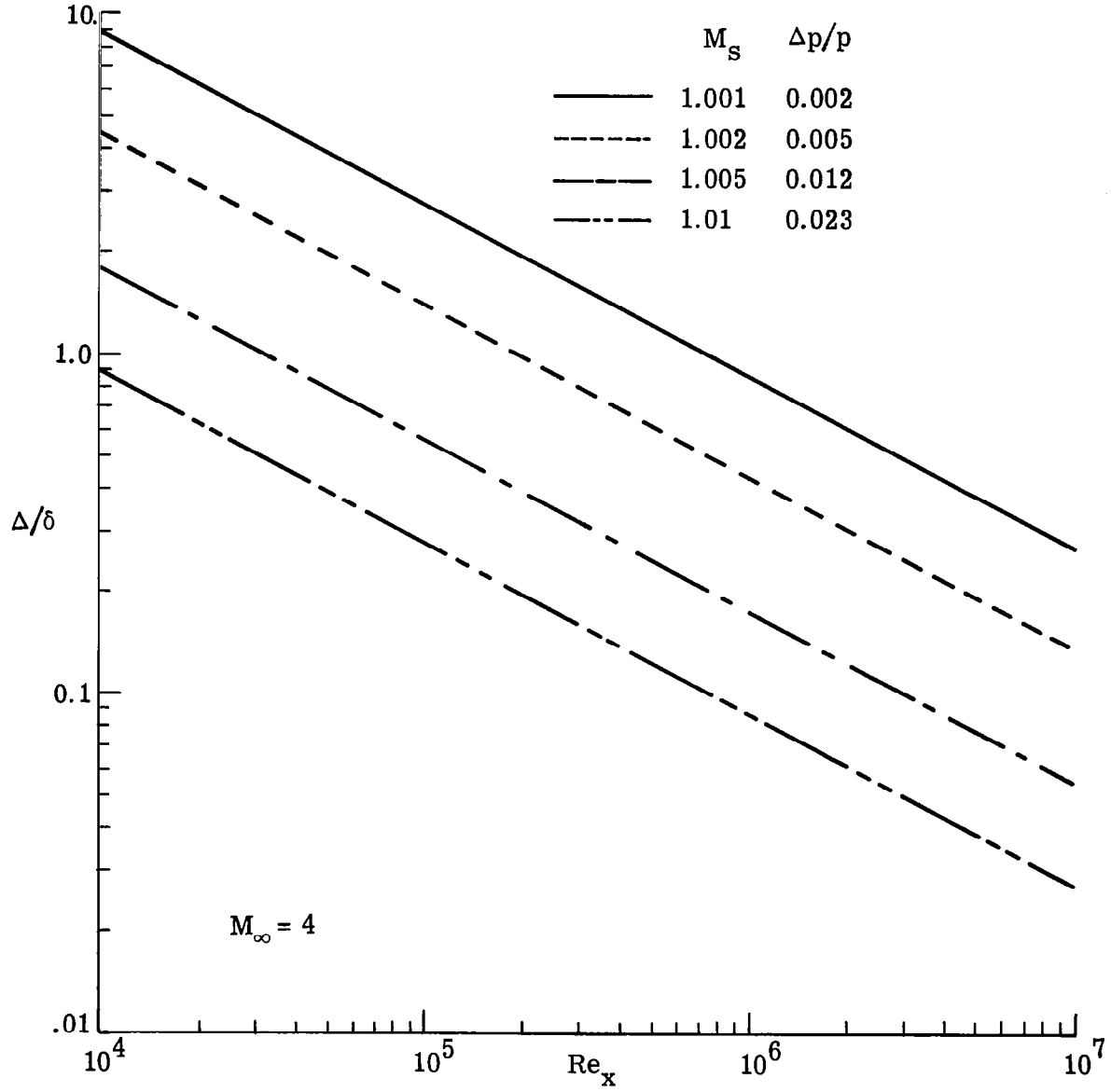

(a) Effect of wave strength or shock Mach number at $M_\infty = 4$

Figure 13.- Variation with Reynolds number of ratio of shock thickness to adiabatic laminar boundary layer thickness at $u = .995u_\infty$.

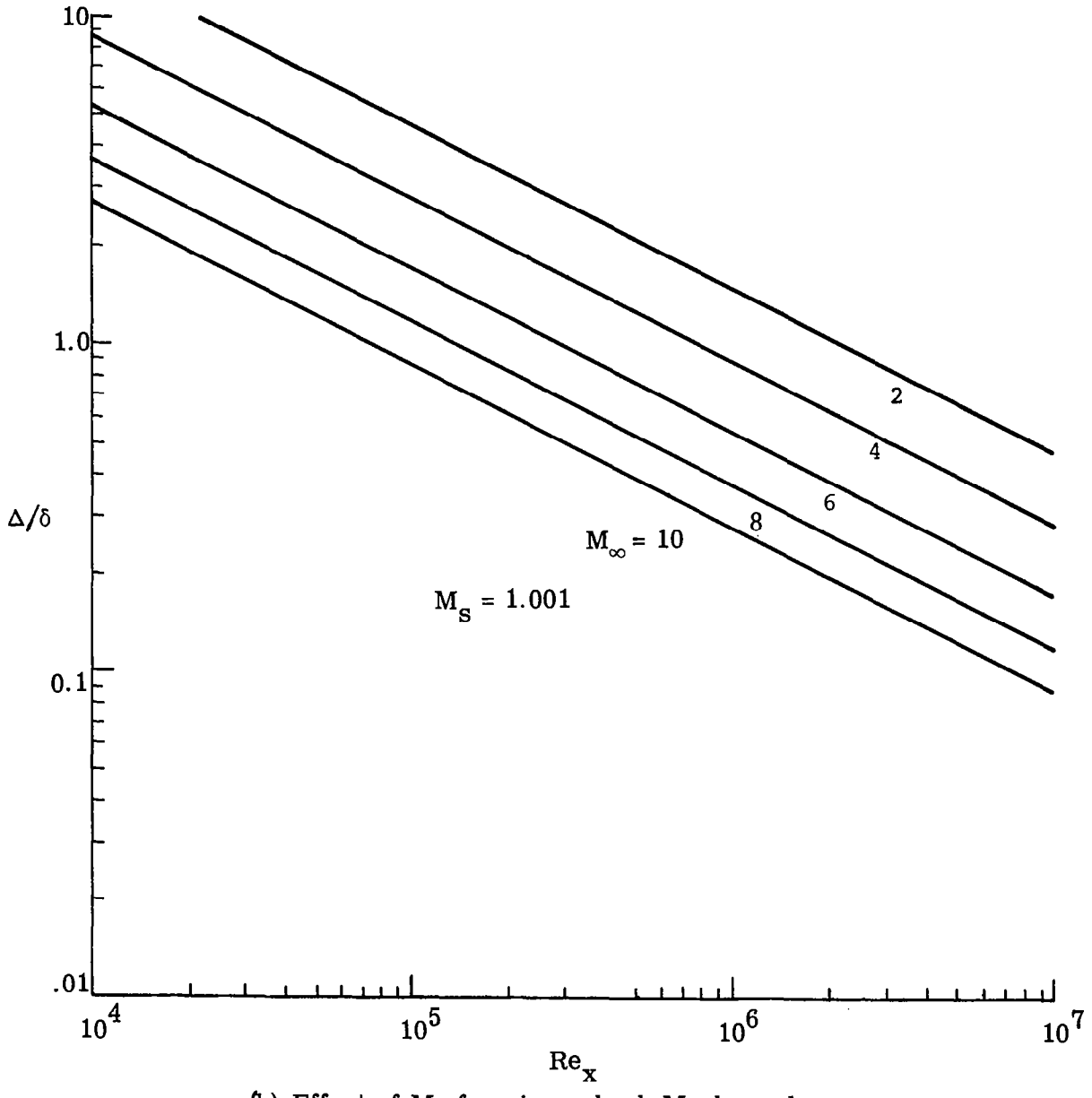

(b) Effect of M_∞ for given shock Mach number.

Figure 13.- Concluded.

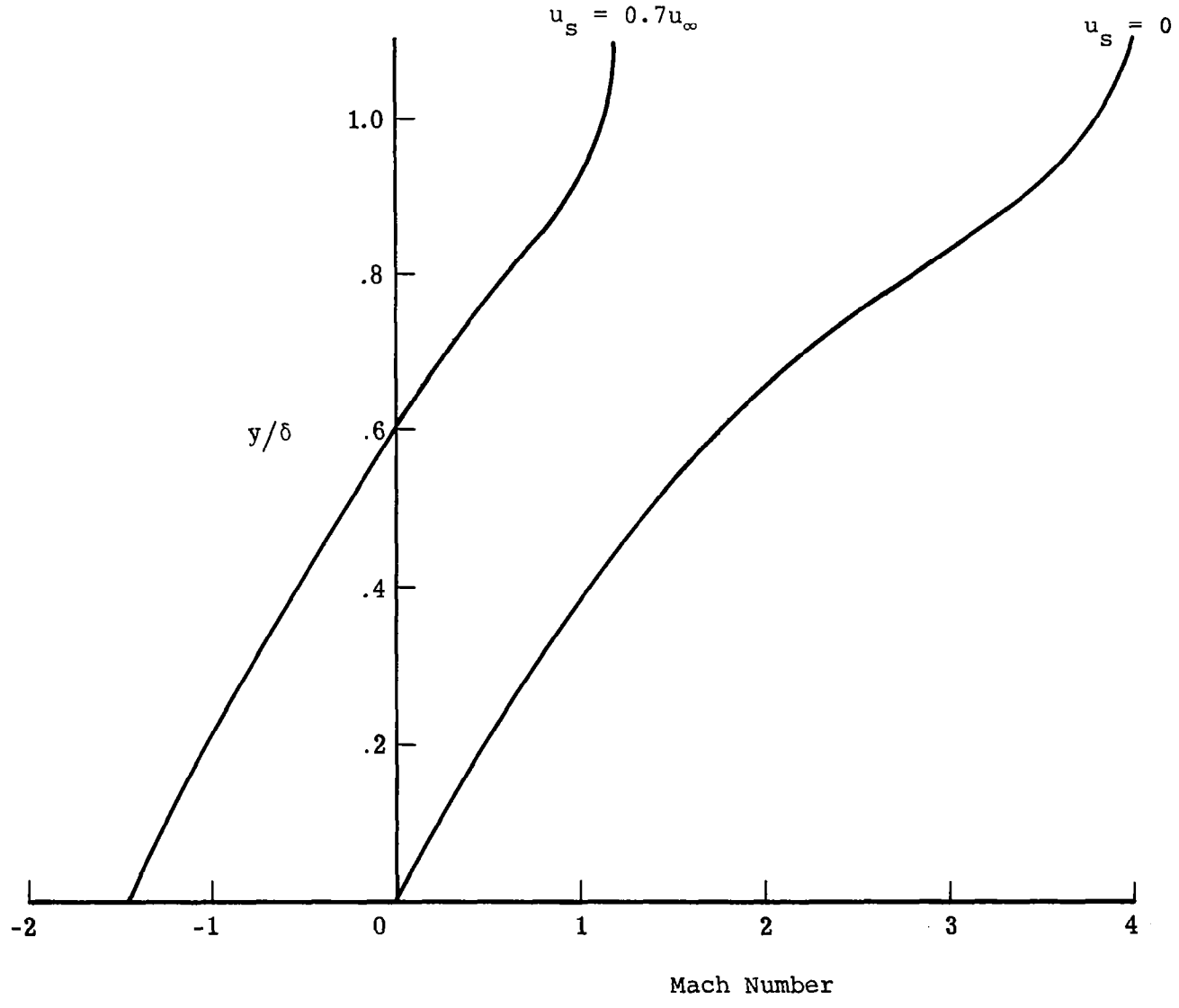

Figure 14.- Laminar boundary layer Mach number profile relative to shock, $M_\infty = 4.0$.

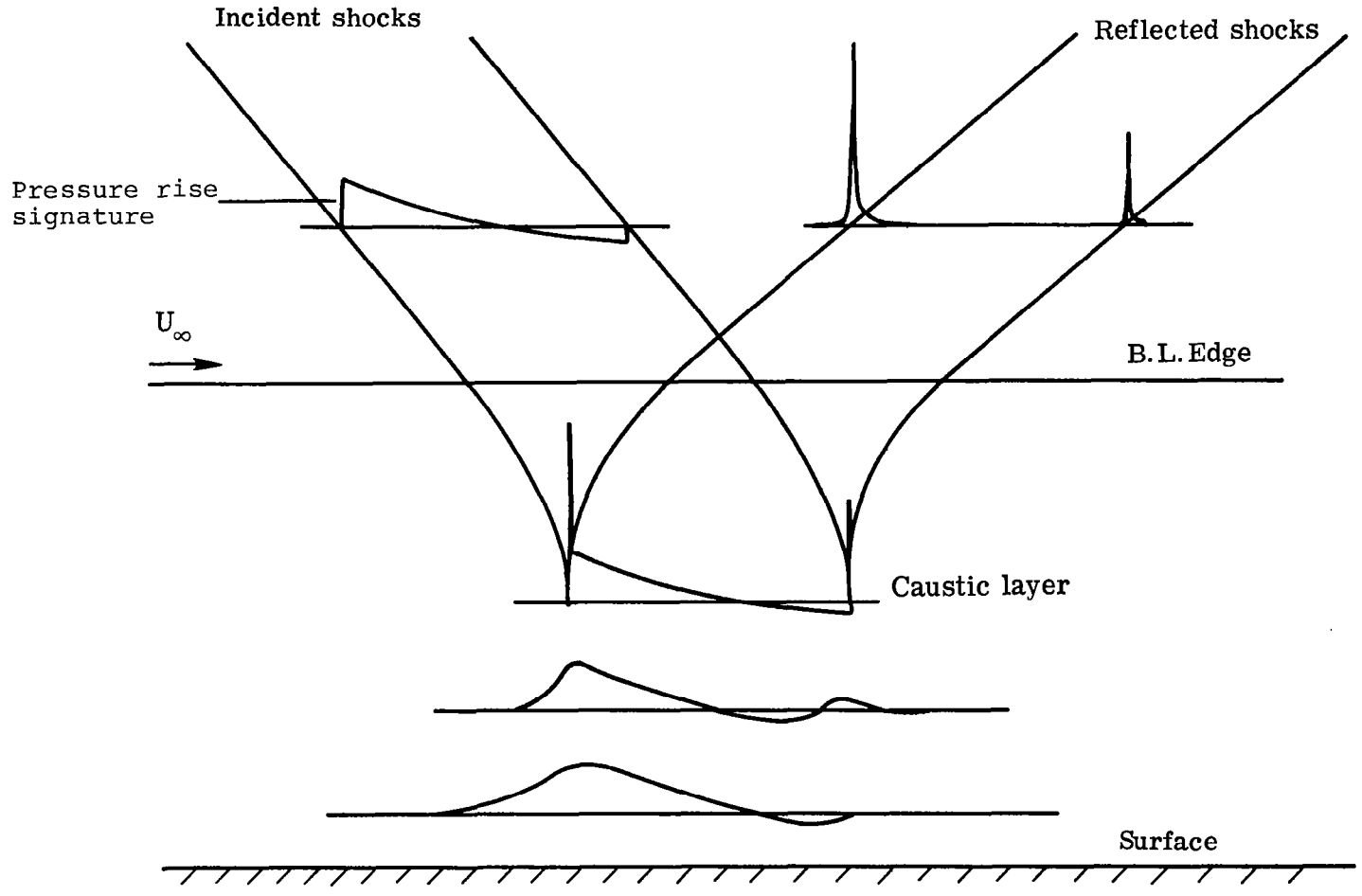

Figure 15.- Sketch of some of the features of noise disturbance-laminar layer interaction; longitudinal scale greatly reduced.

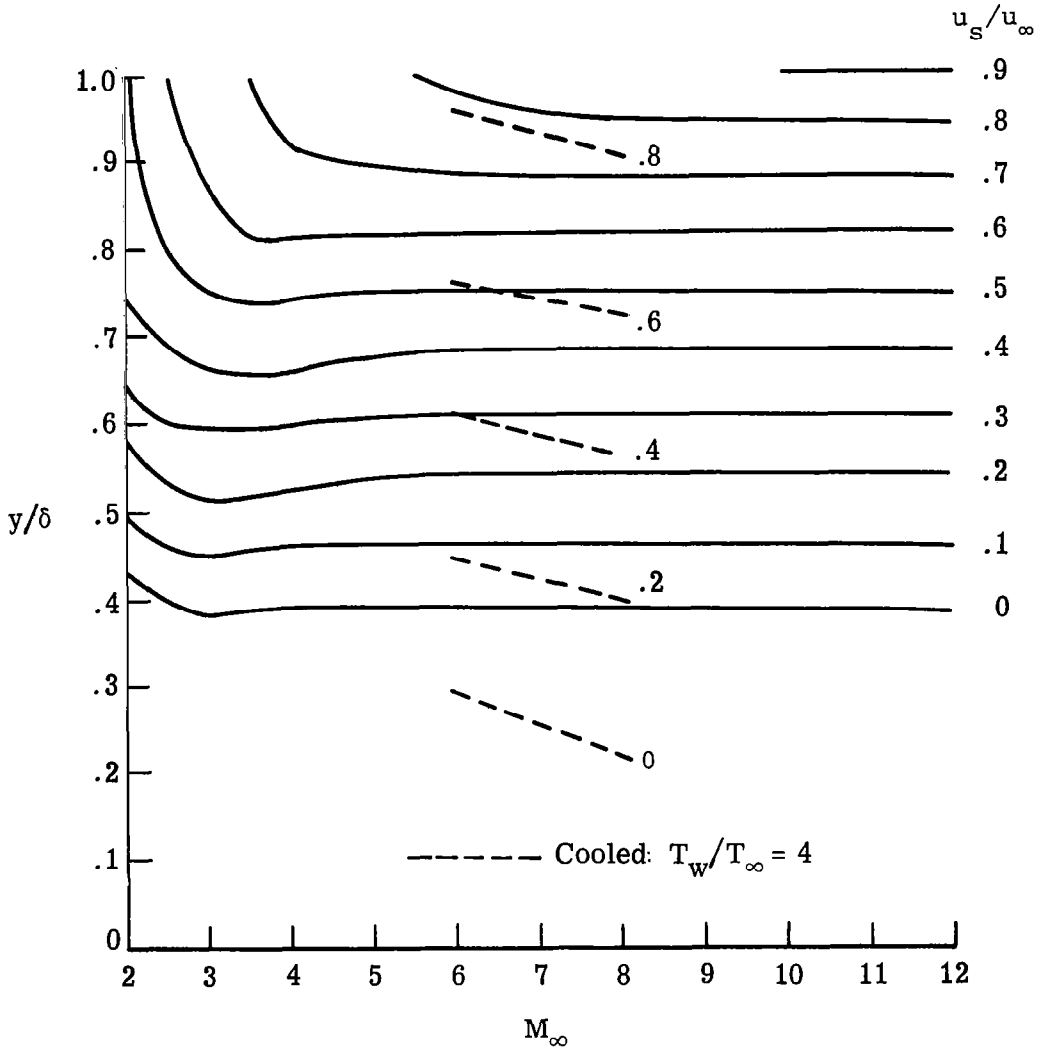

Figure 16.- Range of caustic layer heights.

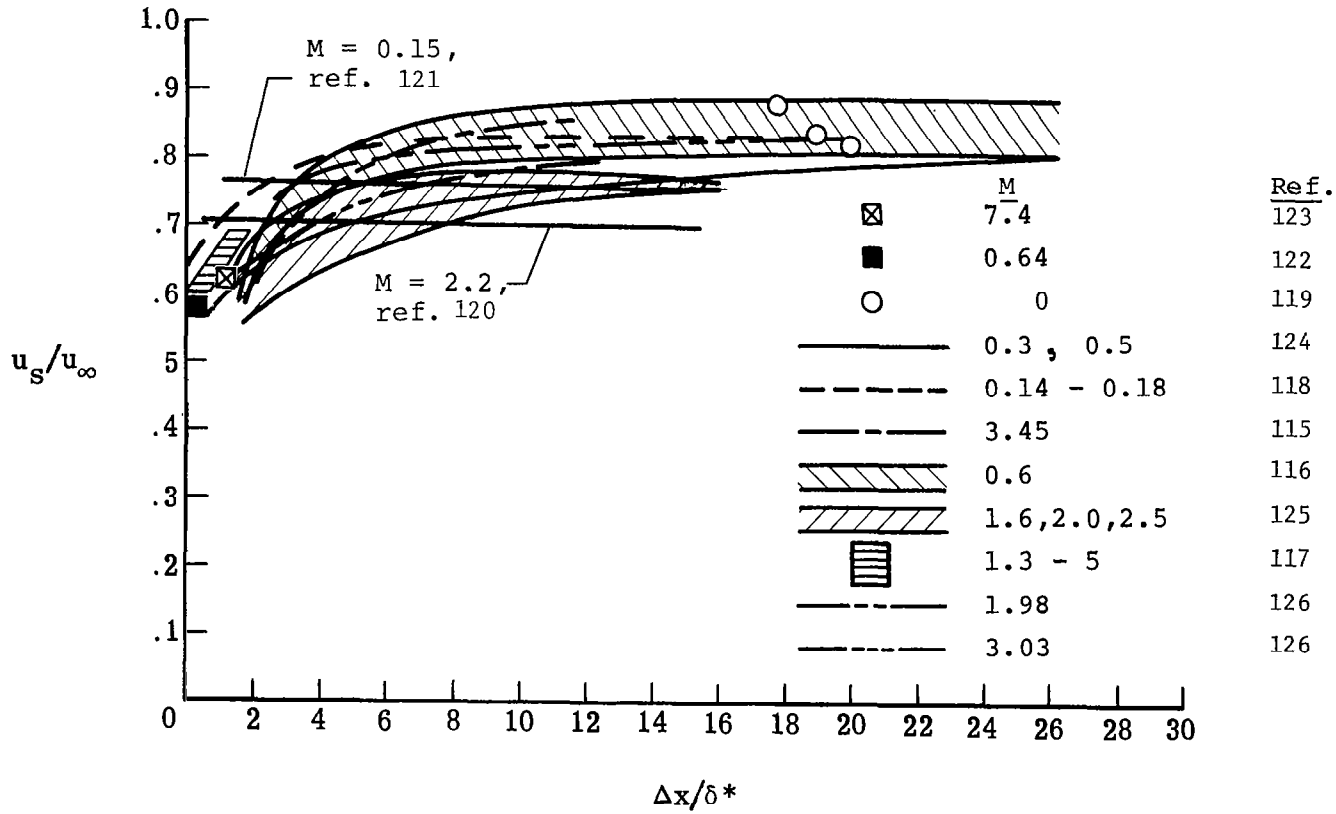

Figure 17.- Variation of measured convection velocities with longitudinal pressure transducer seperation distance under turbulent boundary layers.

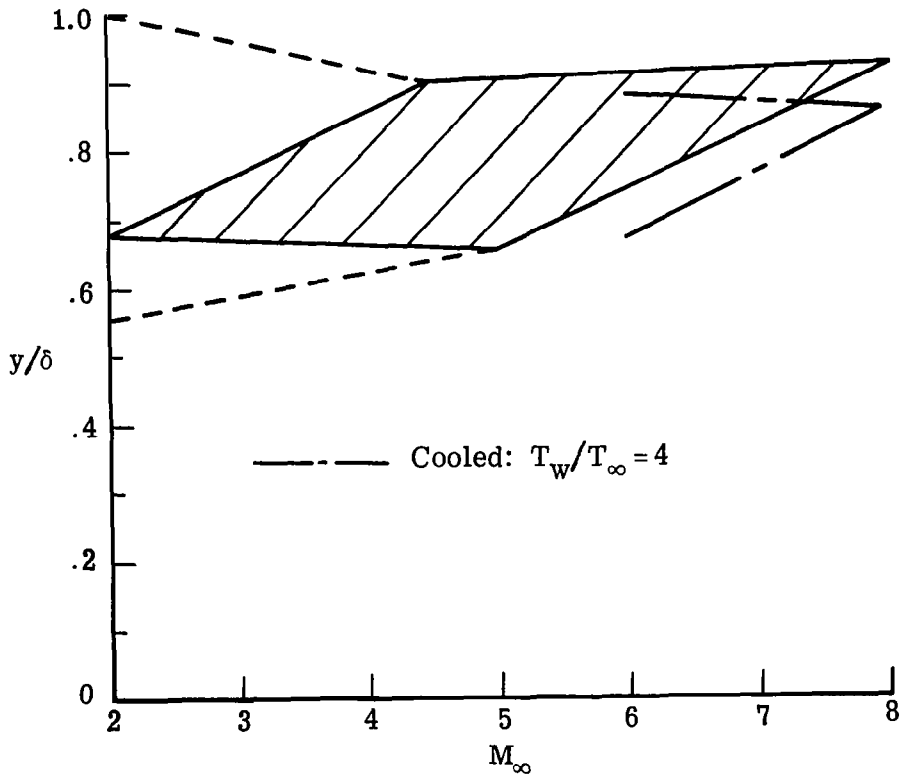

Figure 18. - Caustic region for measured convection speeds.

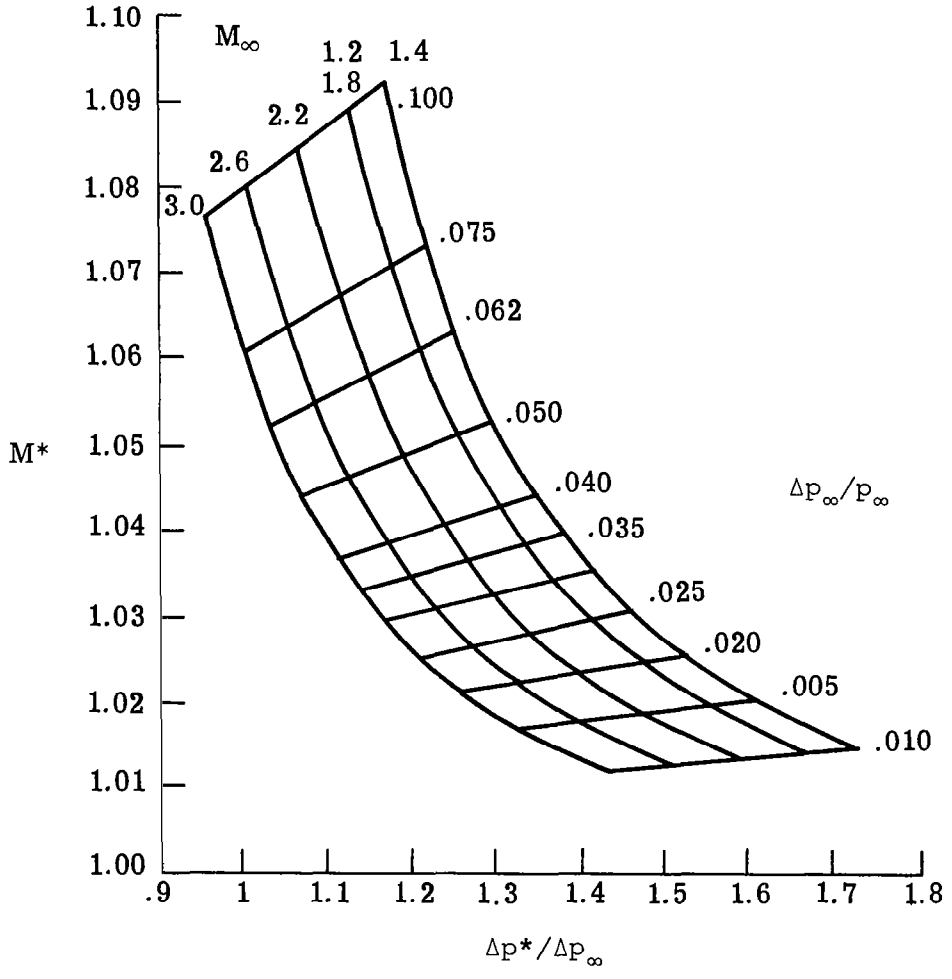

(a) $\Delta p_\infty/p = 0.01 - 0.10$

Figure 19.- Variation with freestream Mach number and initial wave strength of Mach number inside boundary layer M* and focused strength $\Delta p^*/\Delta p_\infty$ at location where flow first becomes subsonic downstream of waves.

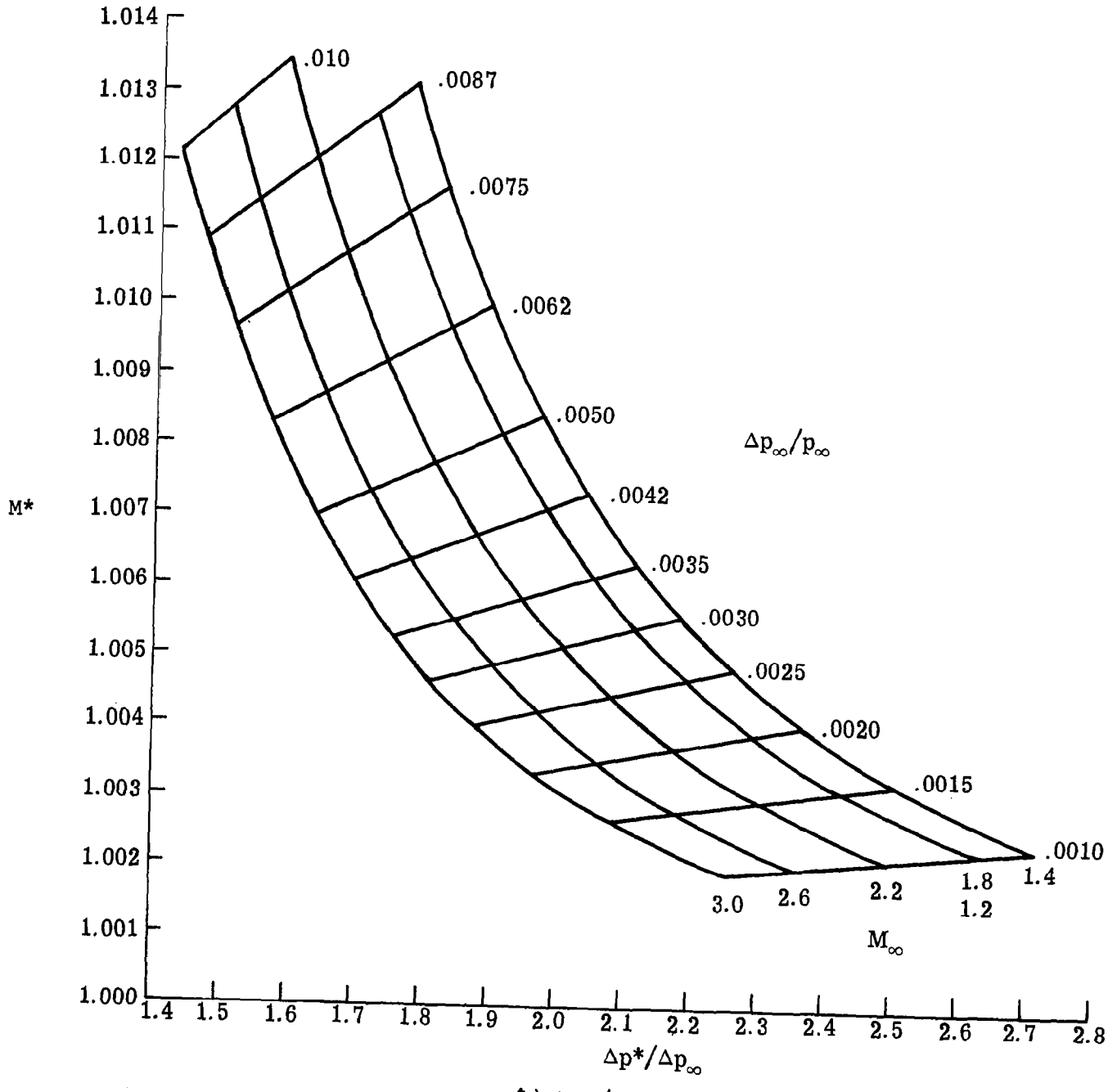

(b) $\Delta p_\infty/p_\infty$ = 0.001 - 0.01

Figure 19.

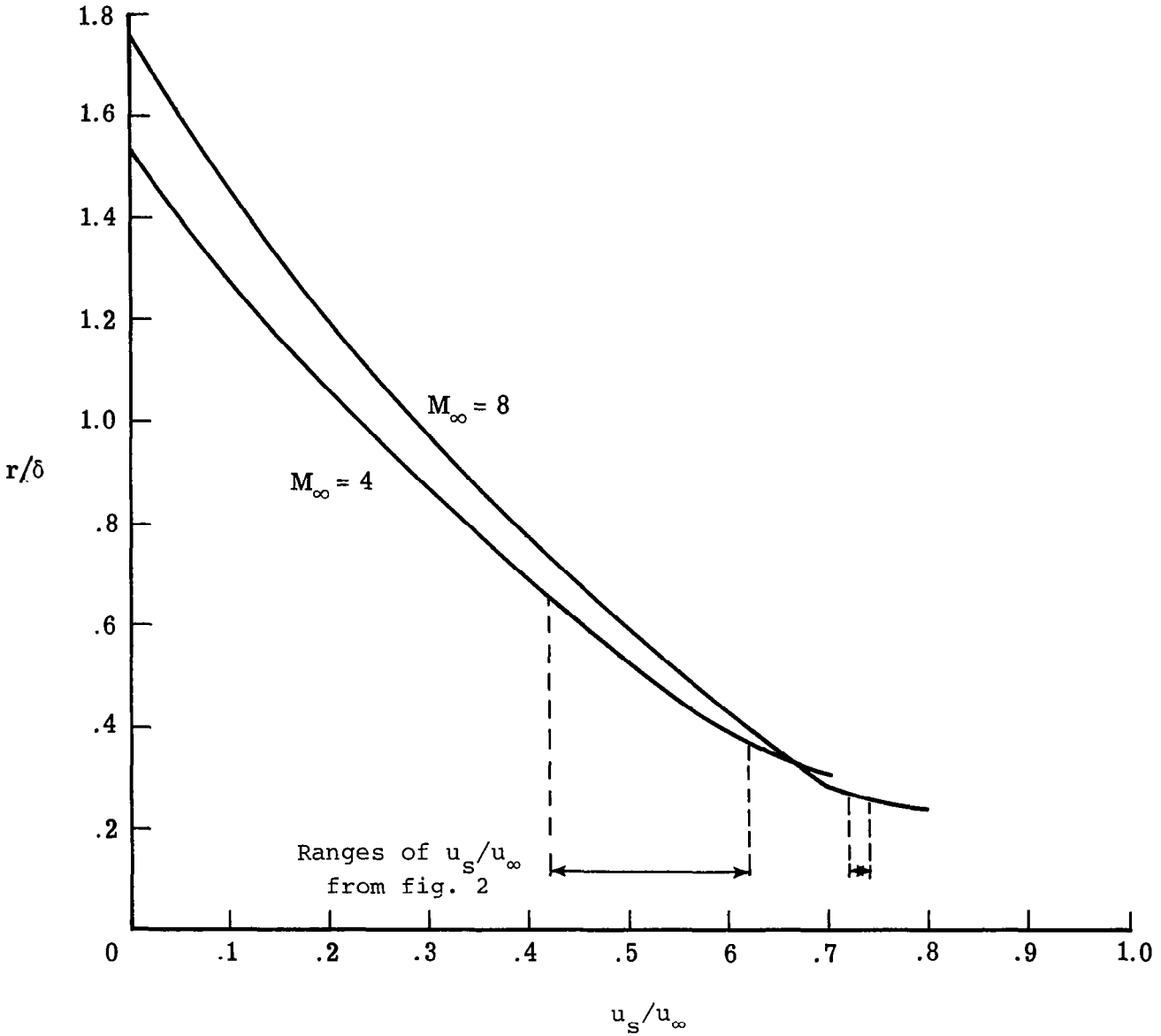

Figure 20.- Variation of ray path radius of curvature at the caustic with flow Mach number and acoustic source convection velocity ratio.

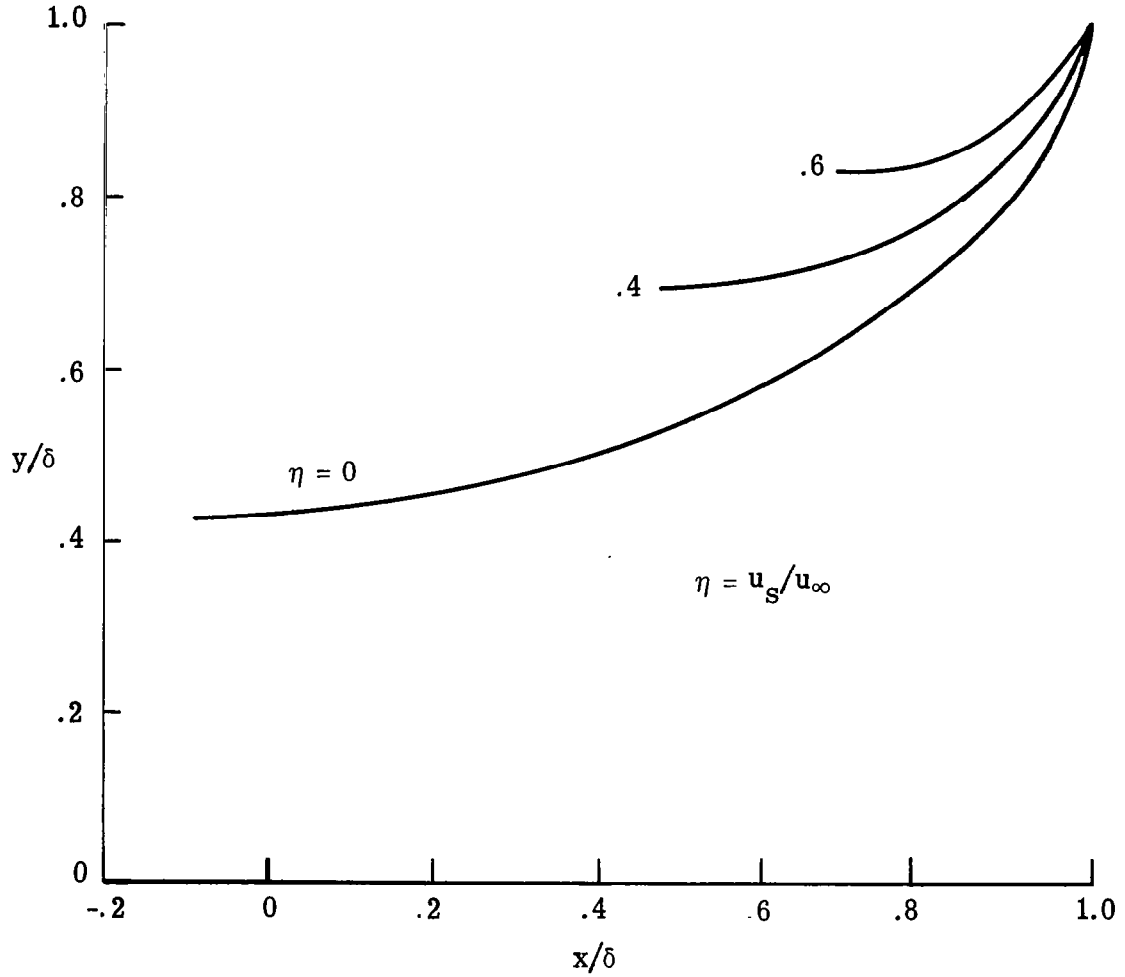

Figure 21.- Shocklet ray paths through Mach 4 laminar boundary layer for various shocklet source convection velocity ratios.

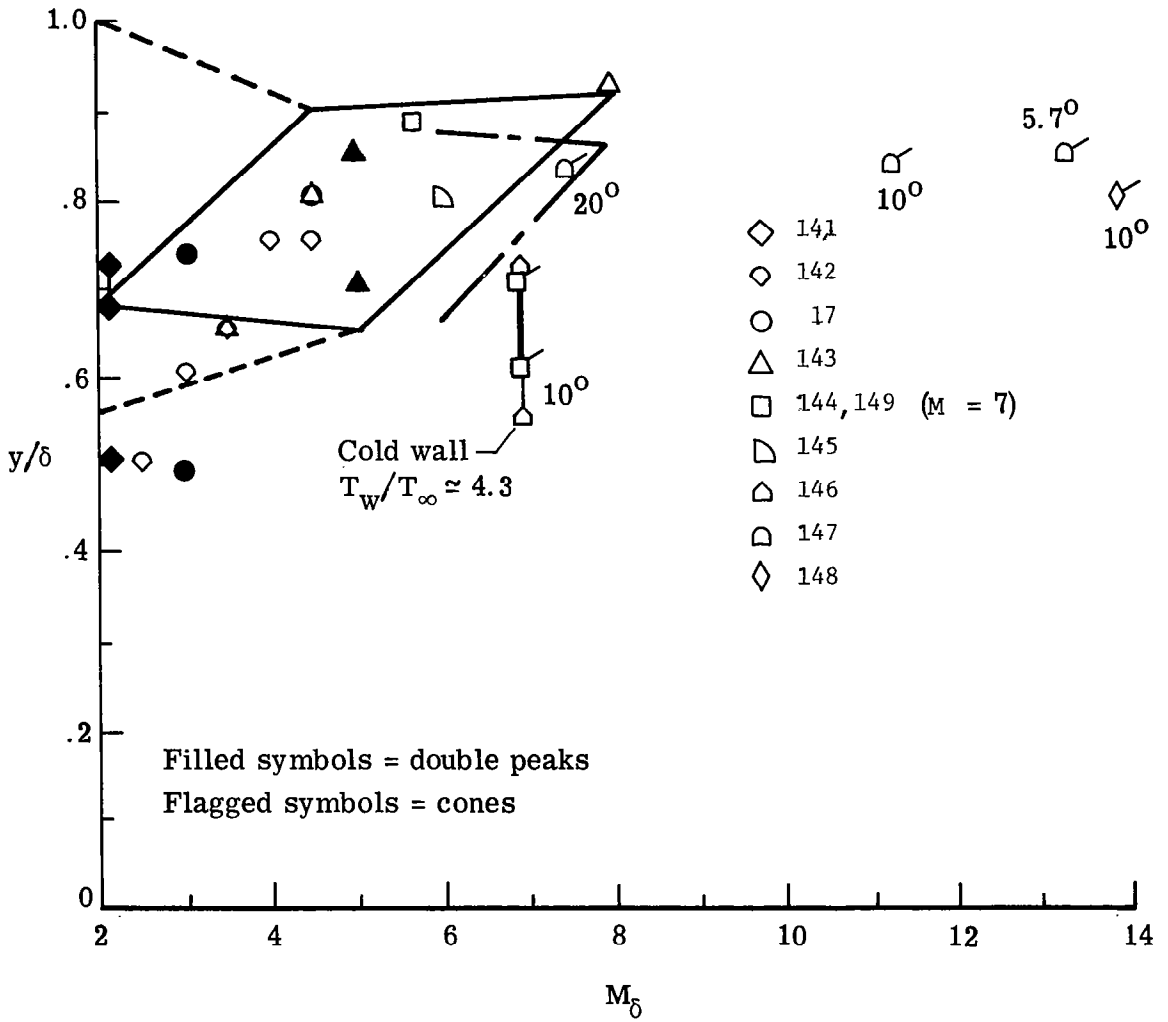

Figure 22.- Heights of caustic region and anemometer signal peaks.

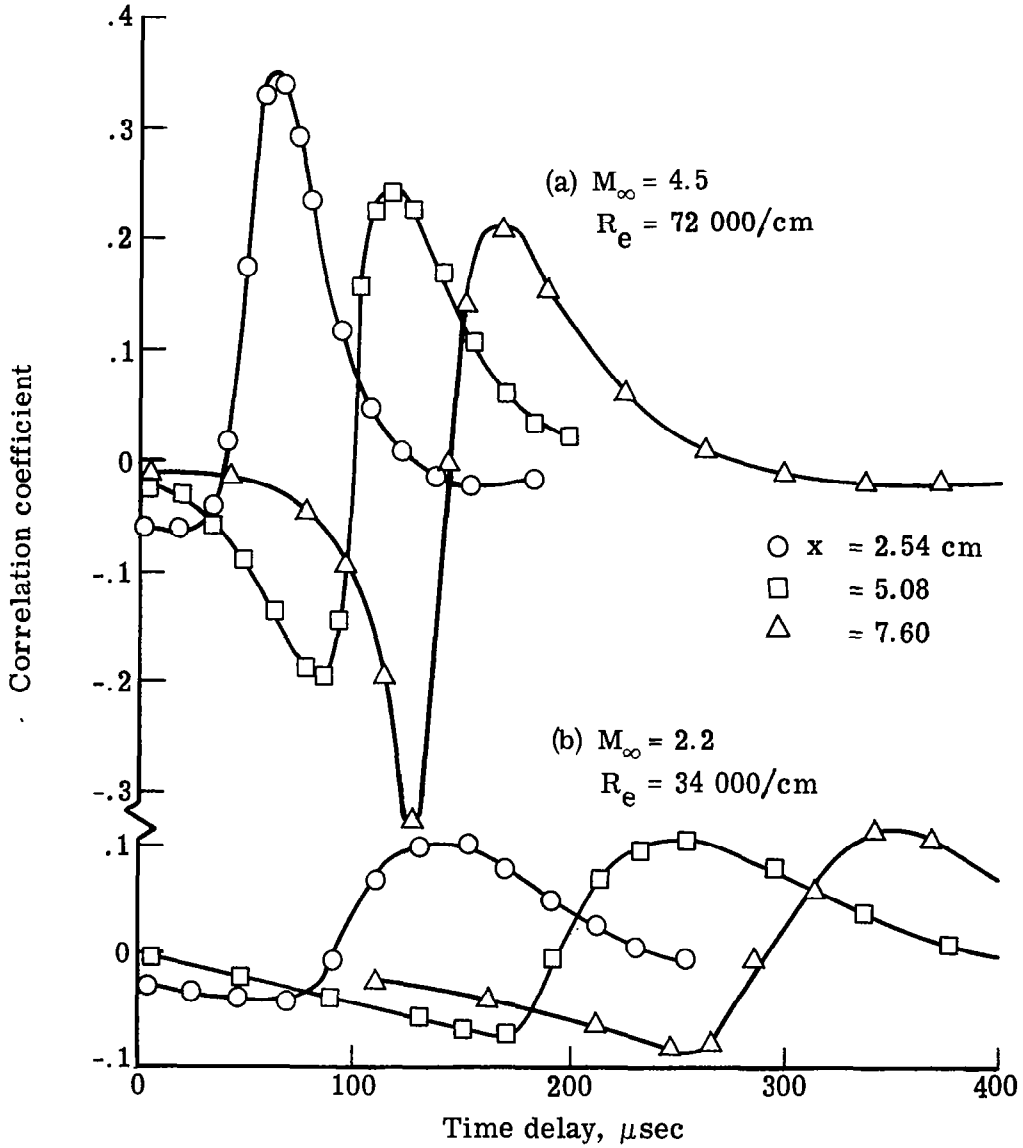

Figure 23.- Cross-correlation of freestream and boundary layer fluctuations (from Kendall, ref. 17).

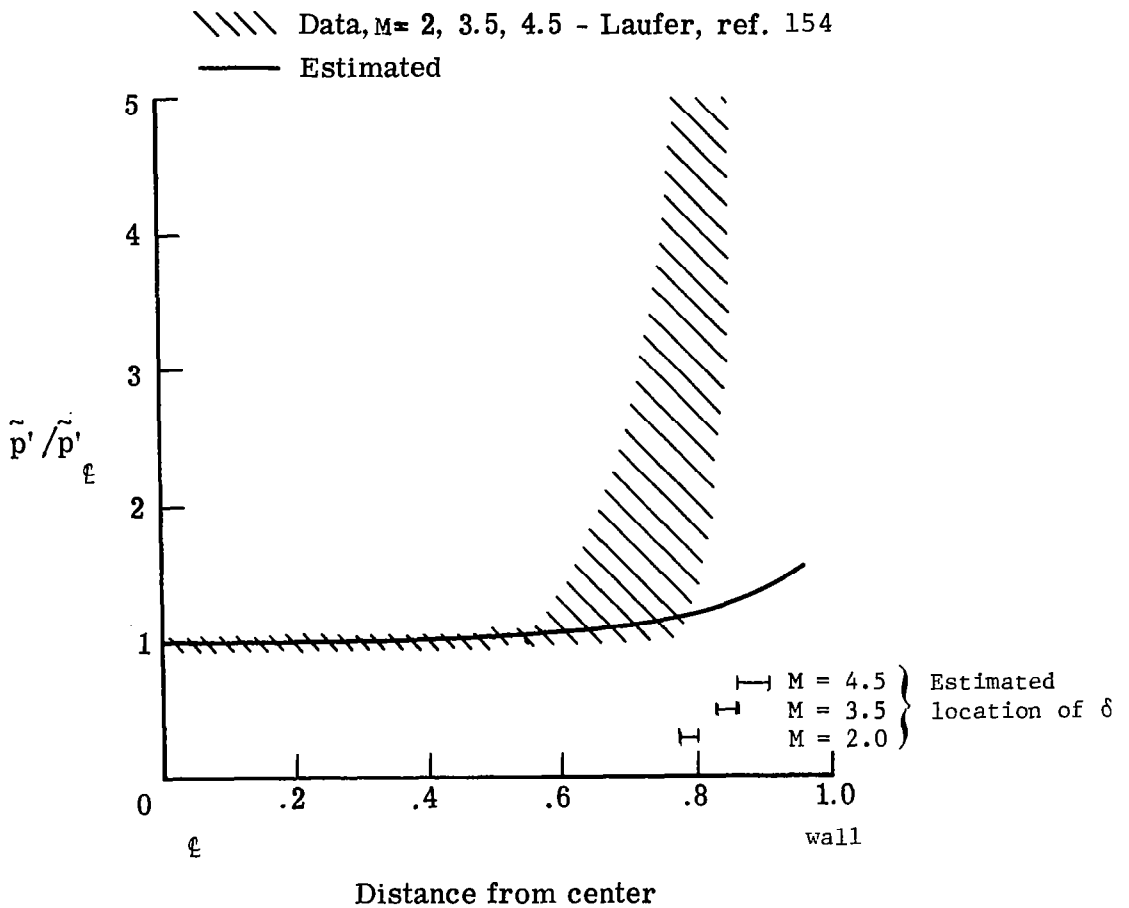

Figure 24.- Comparison of estimated test-section noise field intendity distribution with published experimental data.

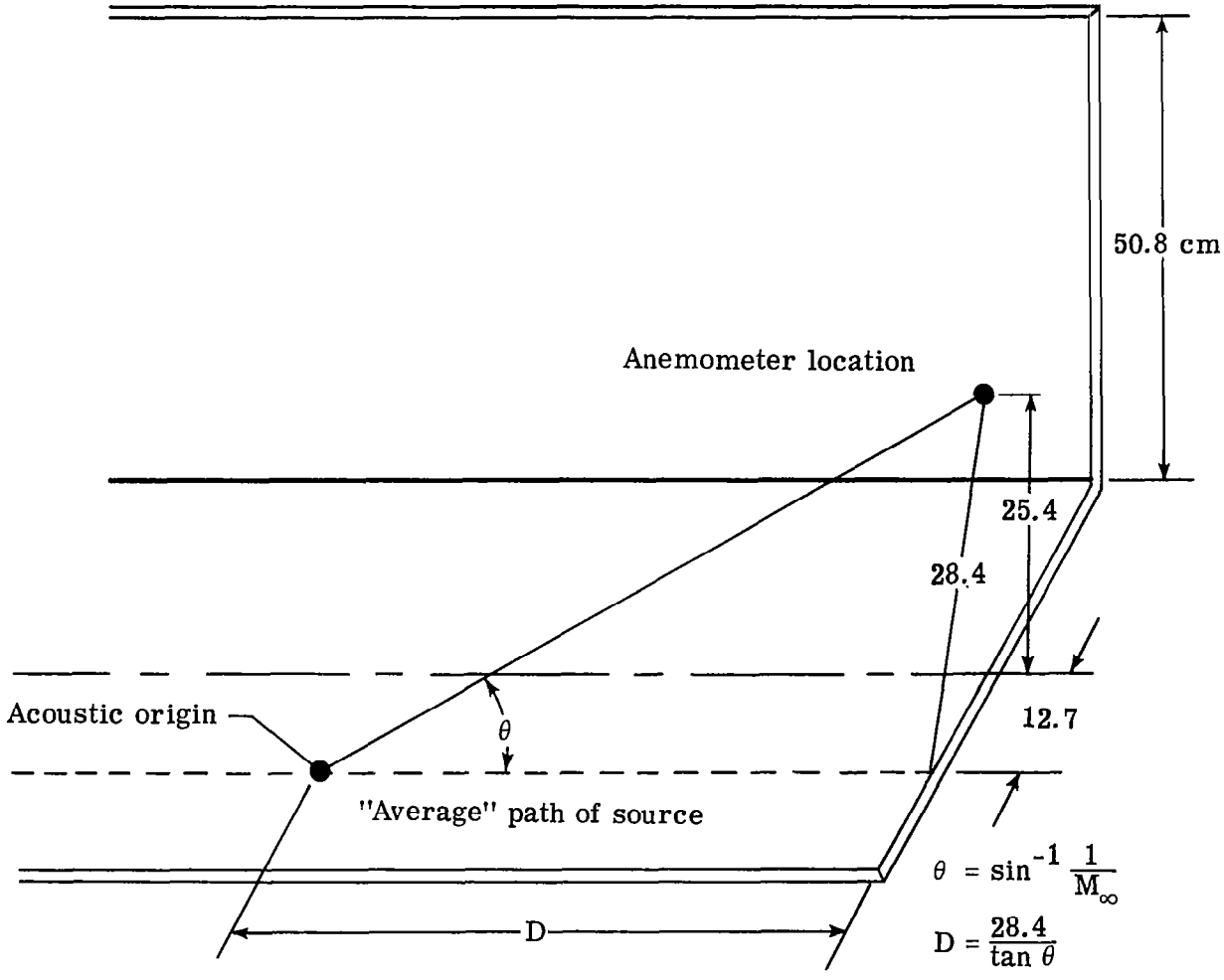

Figure 25.- Illustration of path of "average" disturbance source and of the method of obtaining the distance D.

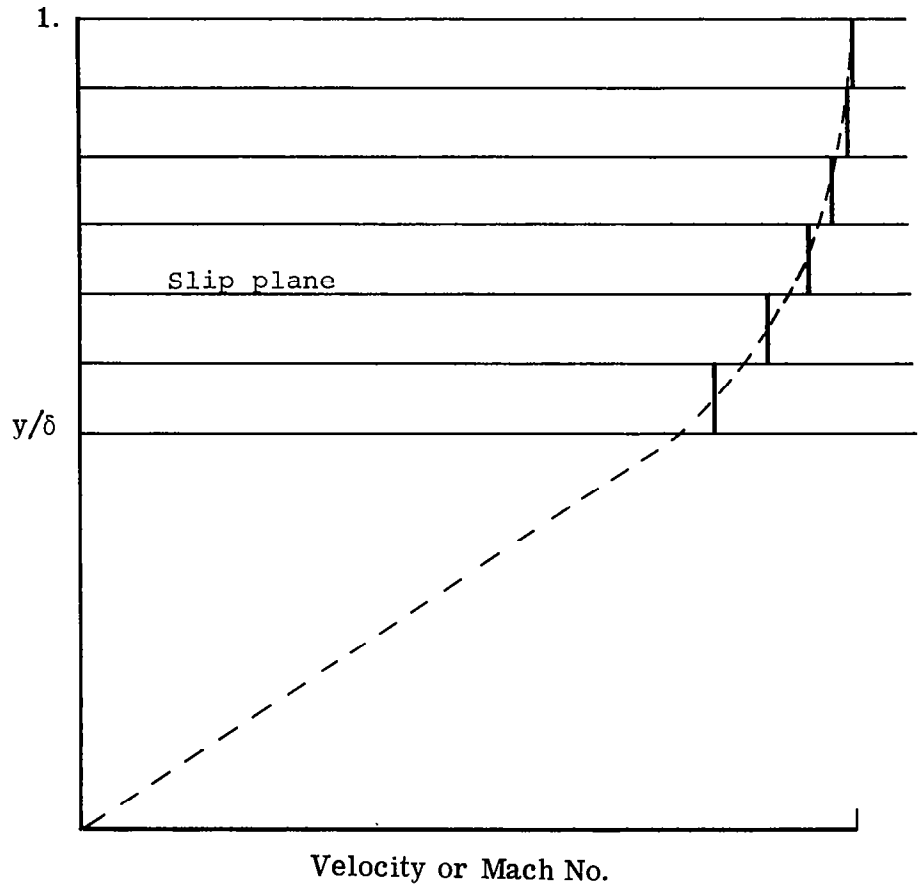

Figure 26.- Boundary layer incremental velocity or Mach number profile approximation.

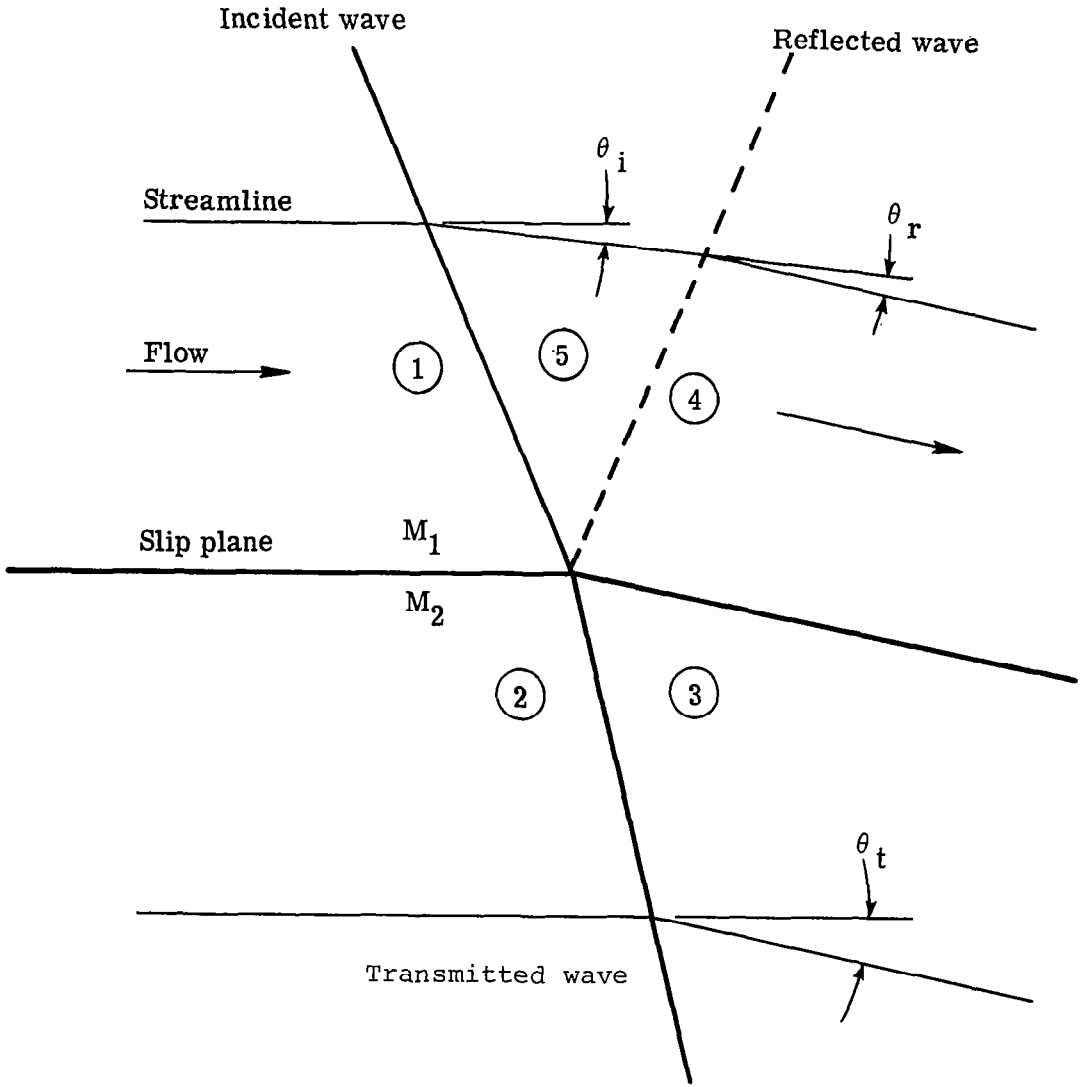

Figure 27.- Three-wave model for refraction analysis.

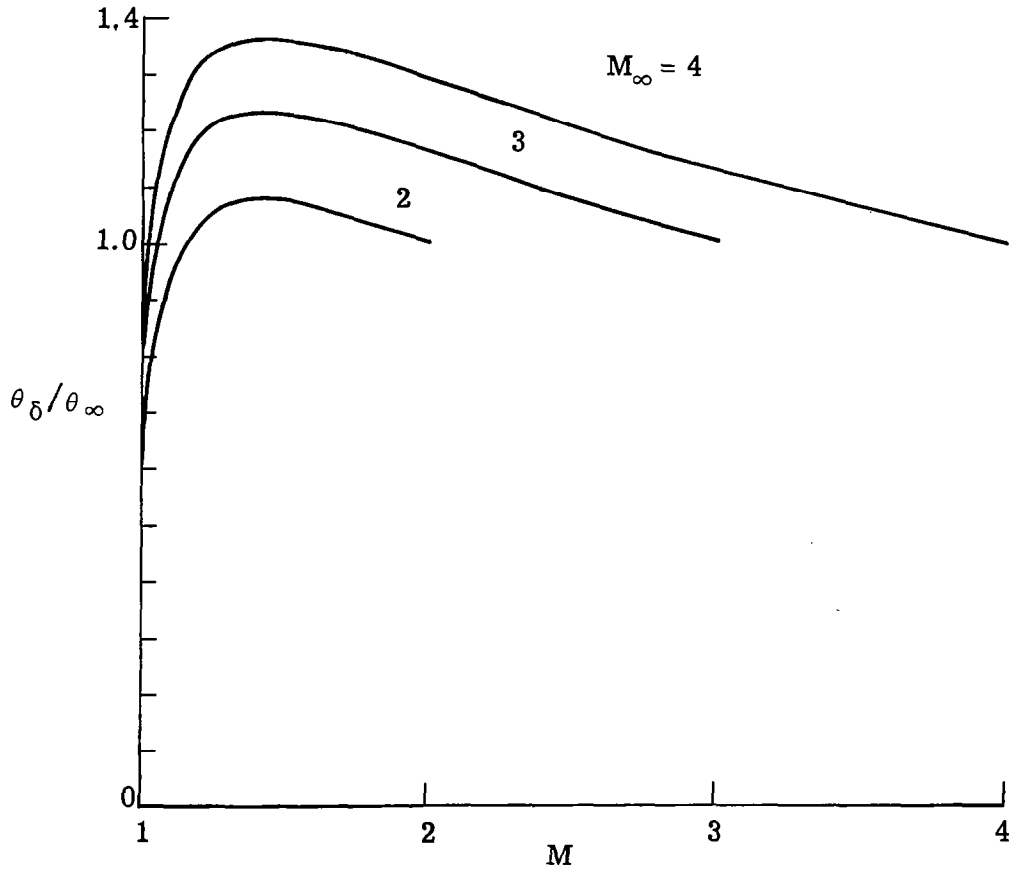

Figure 28.- Variation of flow deflection angle at edge of boundary layer with local Mach number of reflection layer for various freestream Mach numbers.

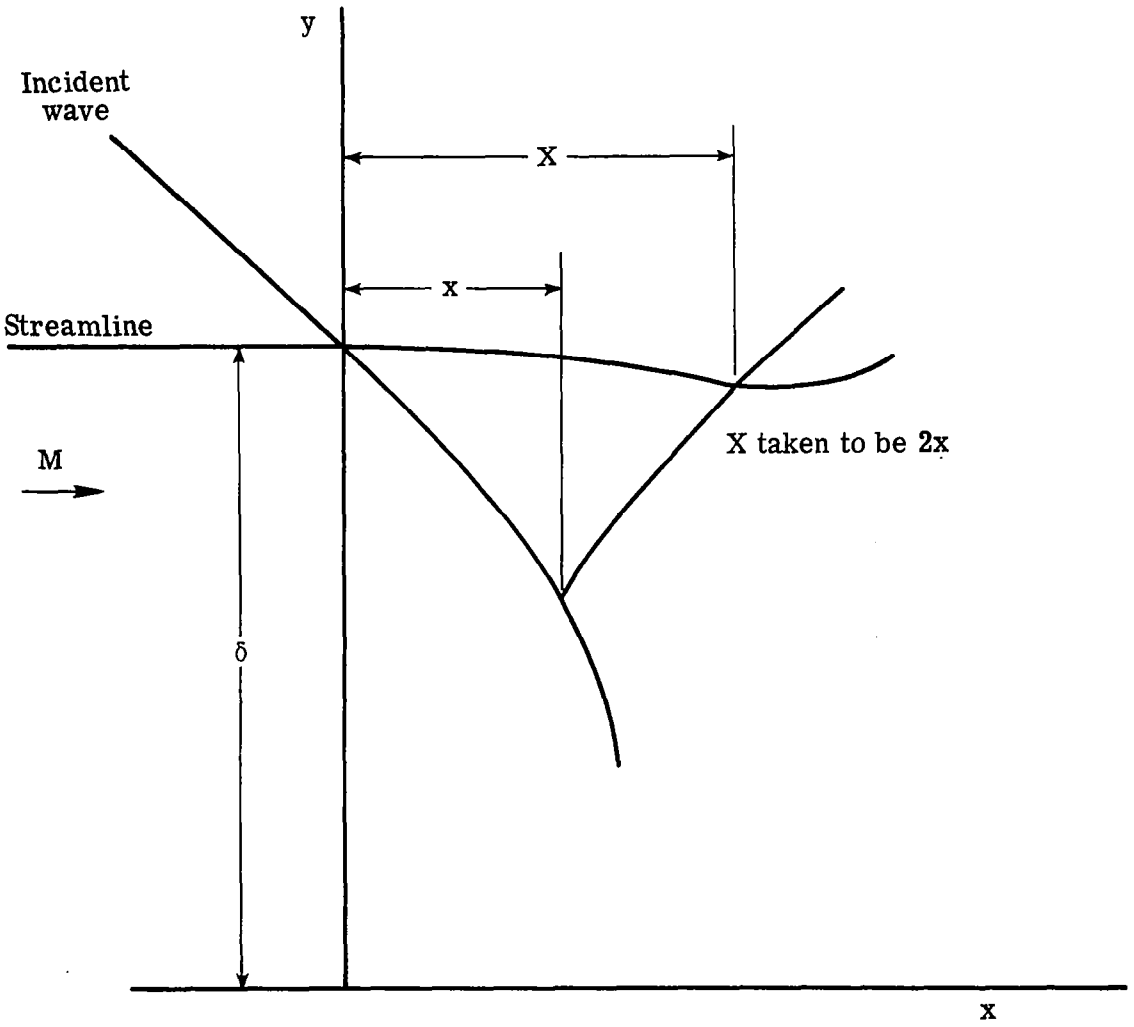

Figure 29.- Wave-boundary layer interaction illustrating flow deflection along edge of boundary layer and definitions of x and X.

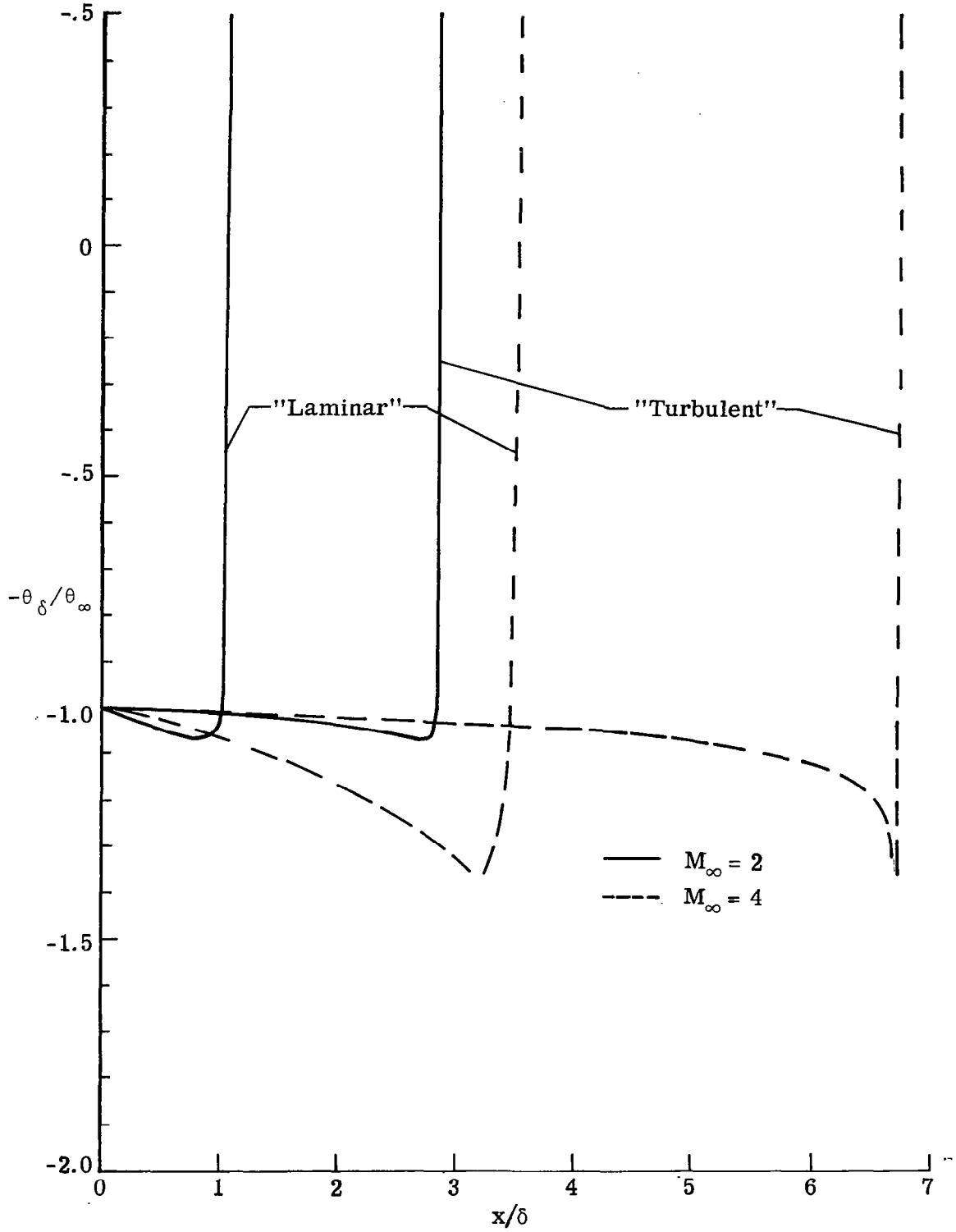

Figure 30.- Flow deflection angle along edge of boundary layer of approximate laminar and turbulent boundary layer profiles.

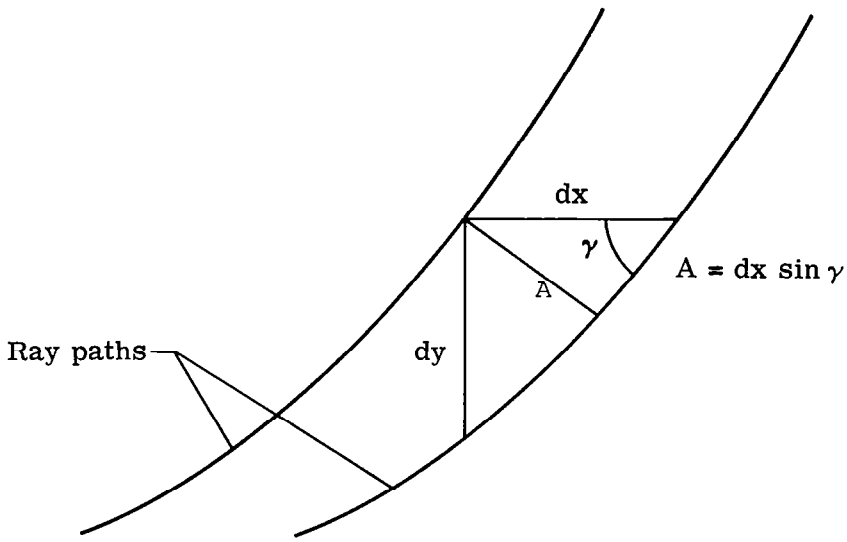

Figure 31.- Geometry for ray tube area determination.

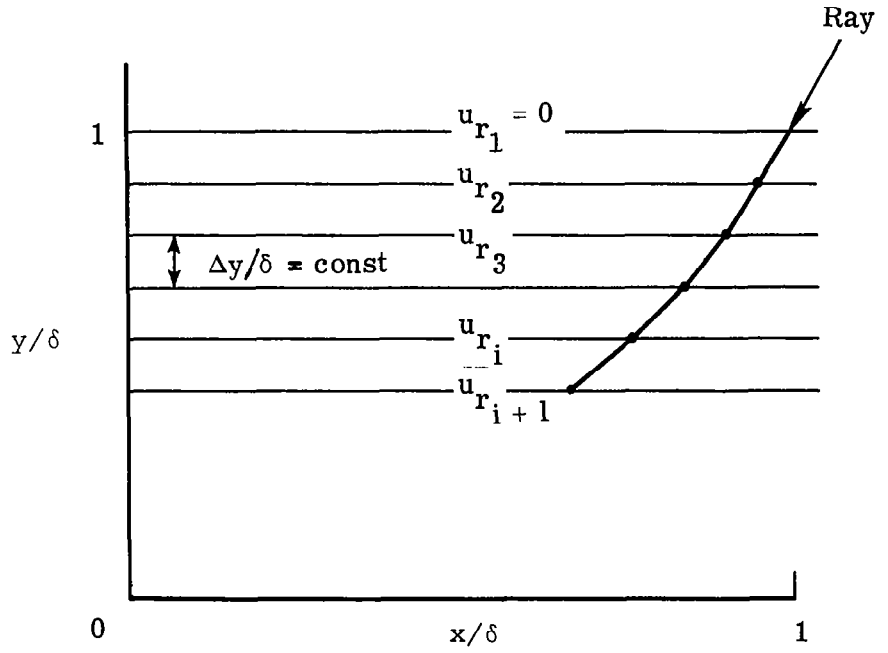

Figure 32.- Ray path geometry and nomenclature used for determining ray path differential equation.

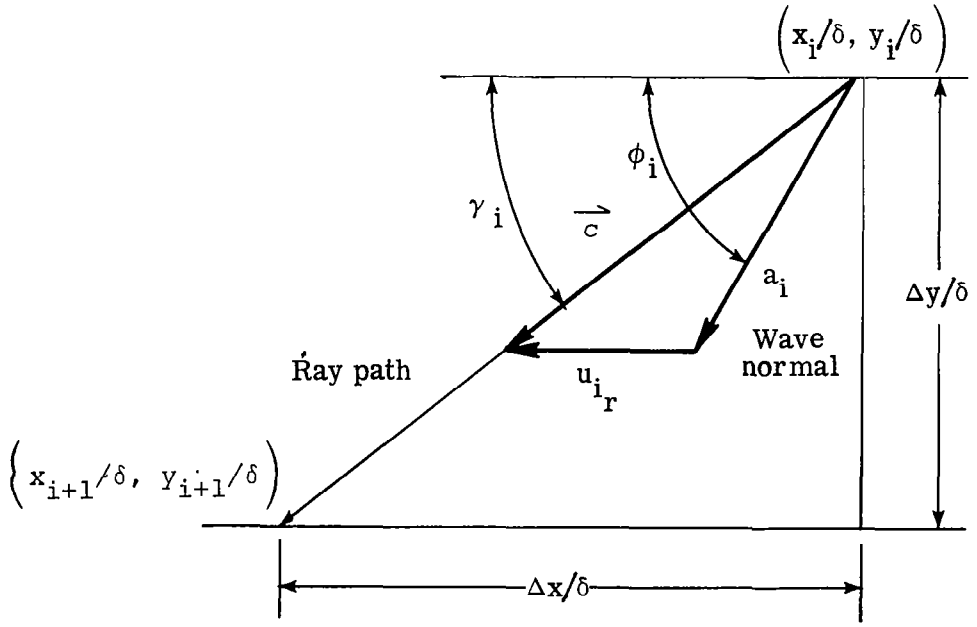

Figure 33.- Details of a single flow layer used in determining ray path differential equation.

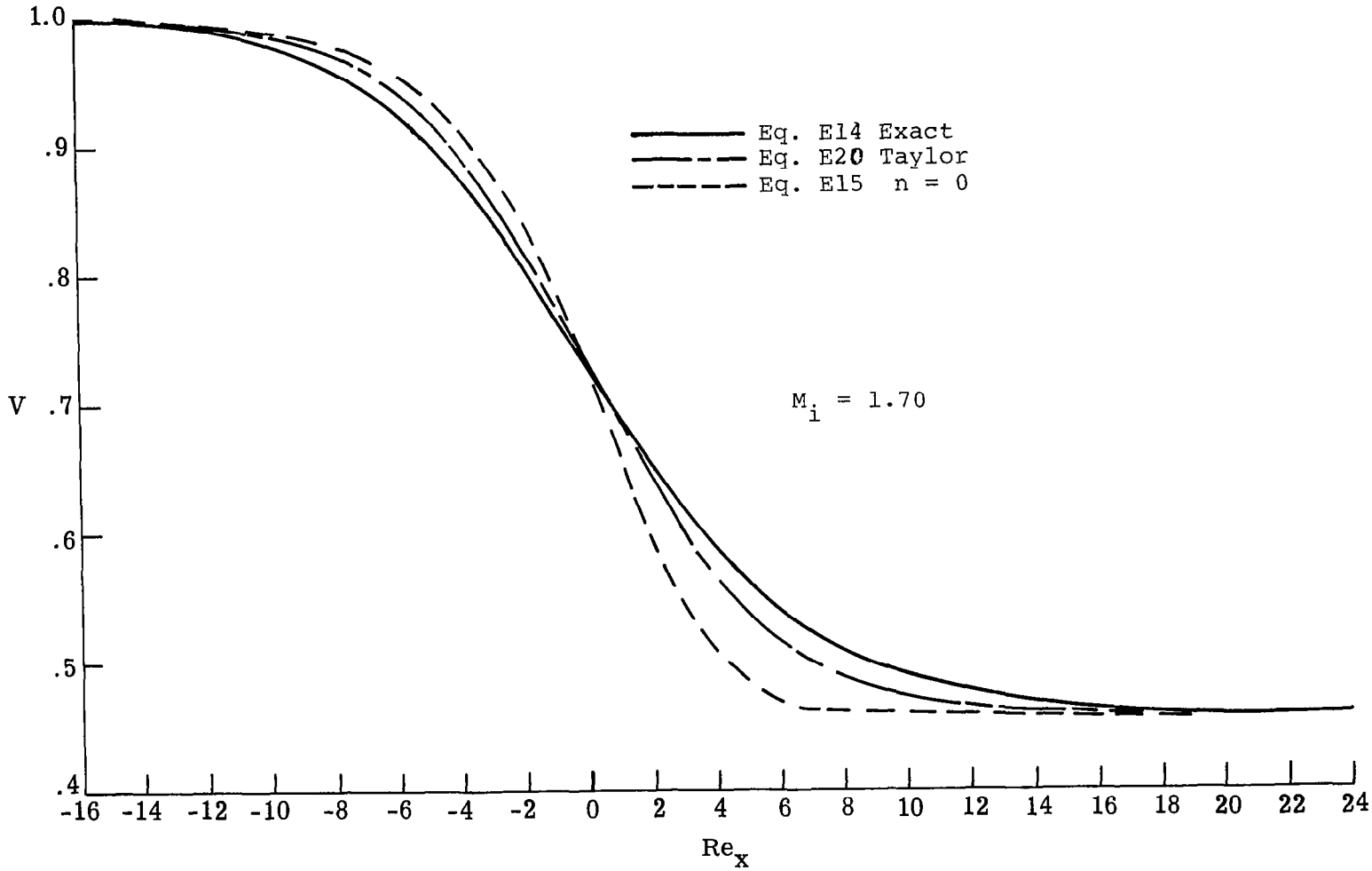

Figure 34.- Comparison of calculated velocity distributions through shock wave. Shock Mach number is 1.70.

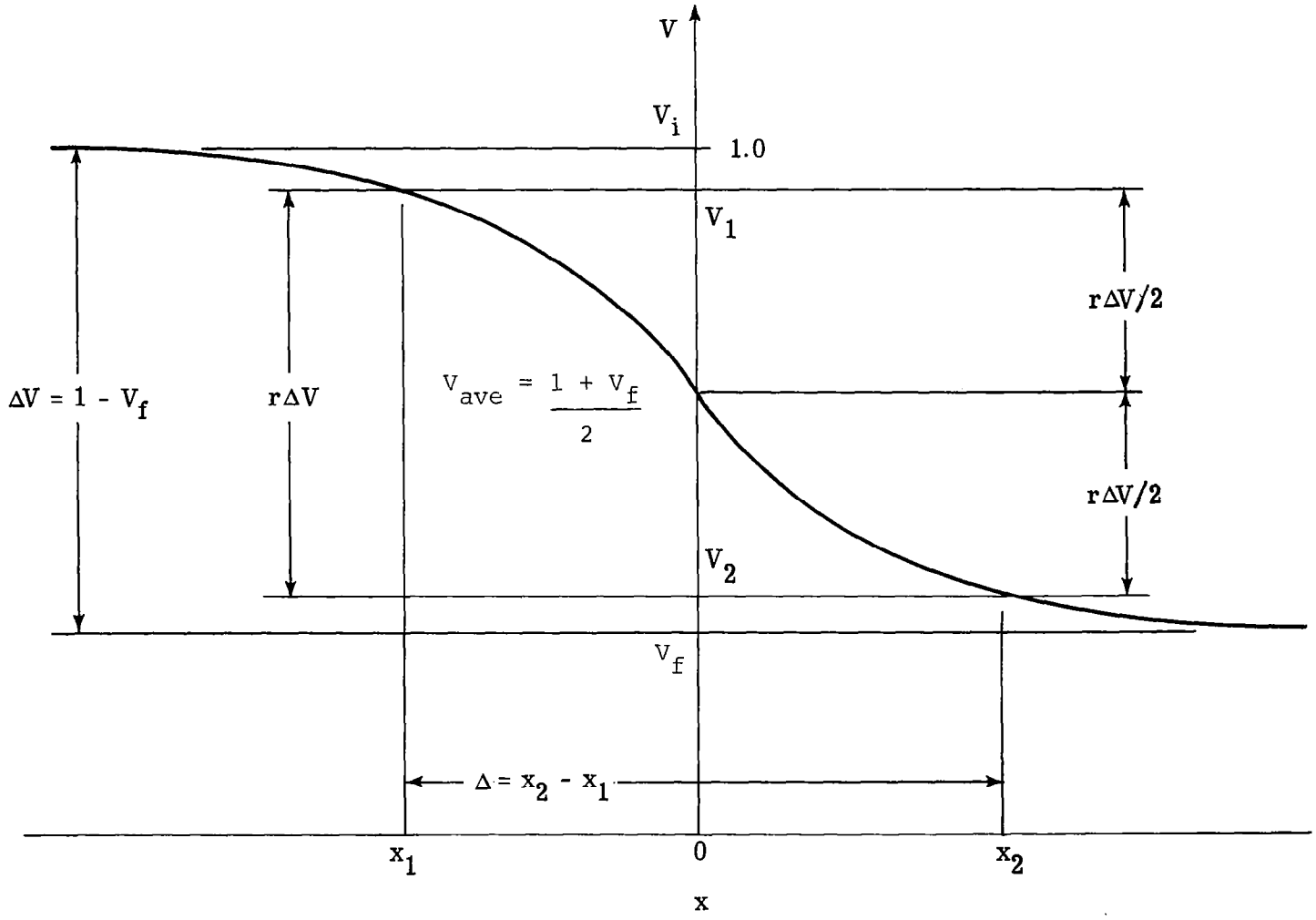

Figure 35.- Illustration of velocity distribution through a shock wave and the nomenclature used to define the shock thickness.

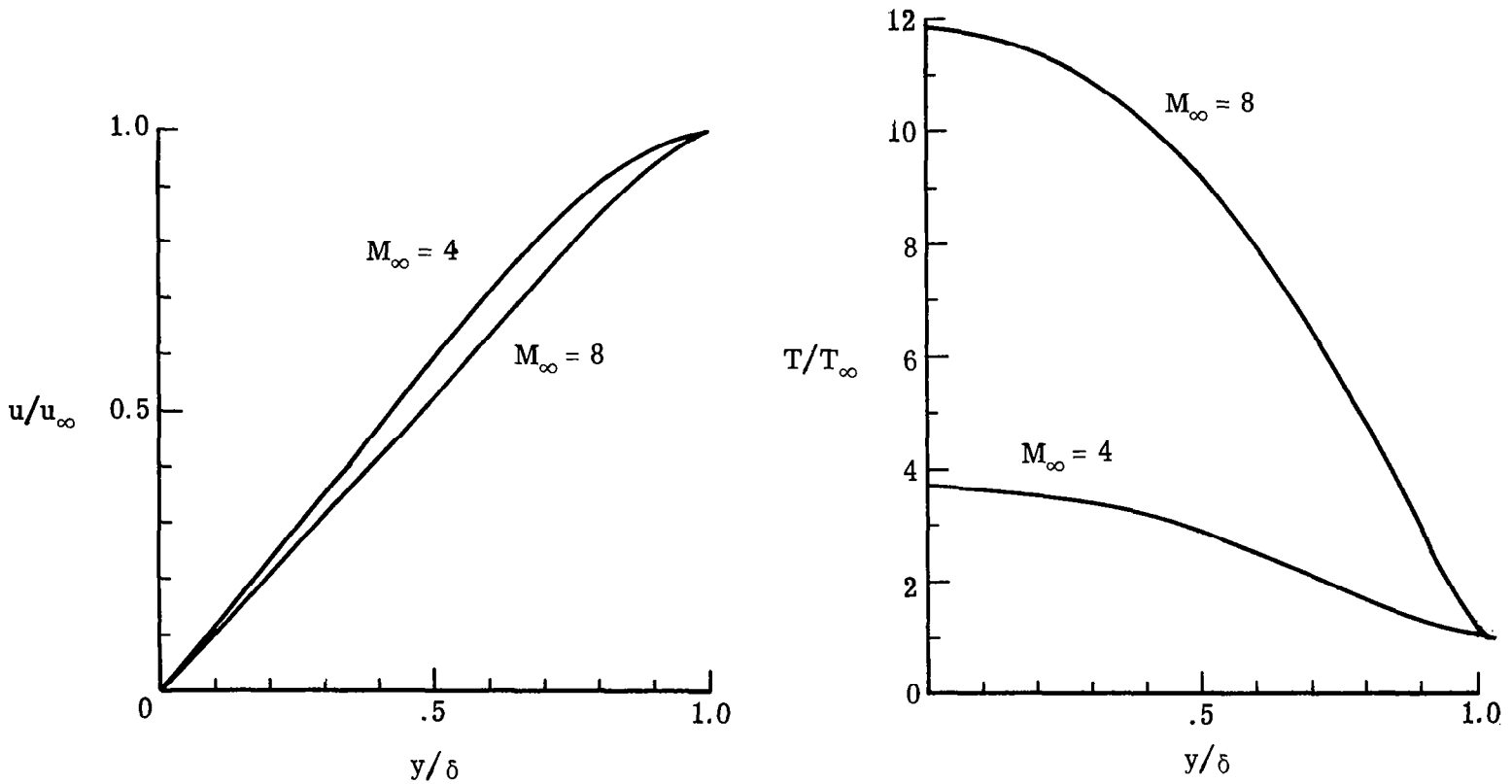

(a) Velocity profiles

(b) Temperature profiles

Figure 36.- Typical supersonic laminar boundary layer velocity and temperature profiles.

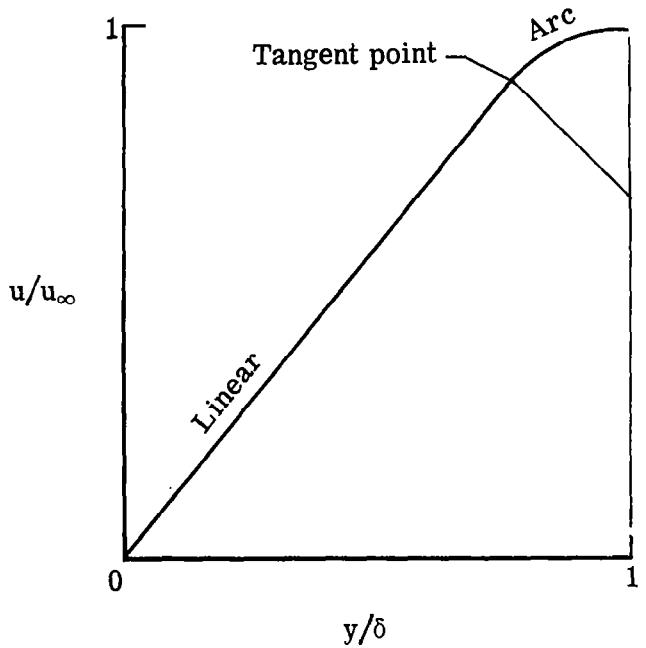

(a) Velocity profiles.

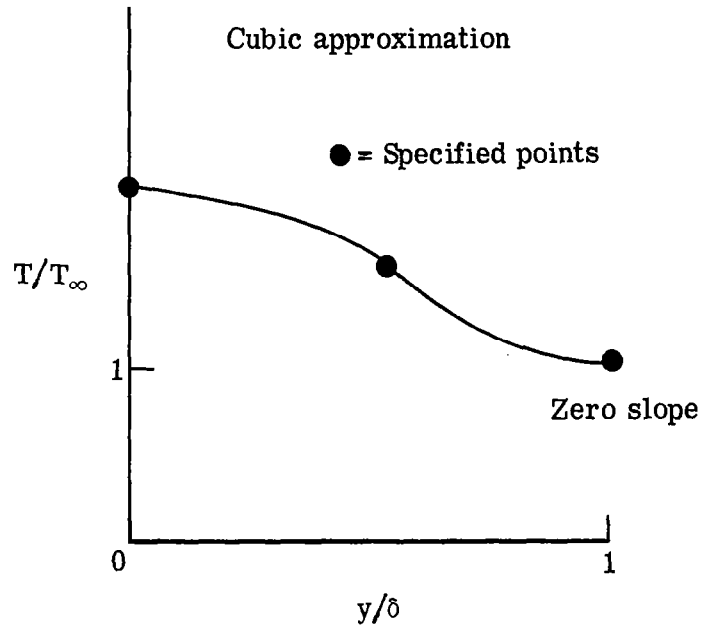

(b) Temperature profiles.

Figure 37.- Form of laminar boundary layer approximate profiles.

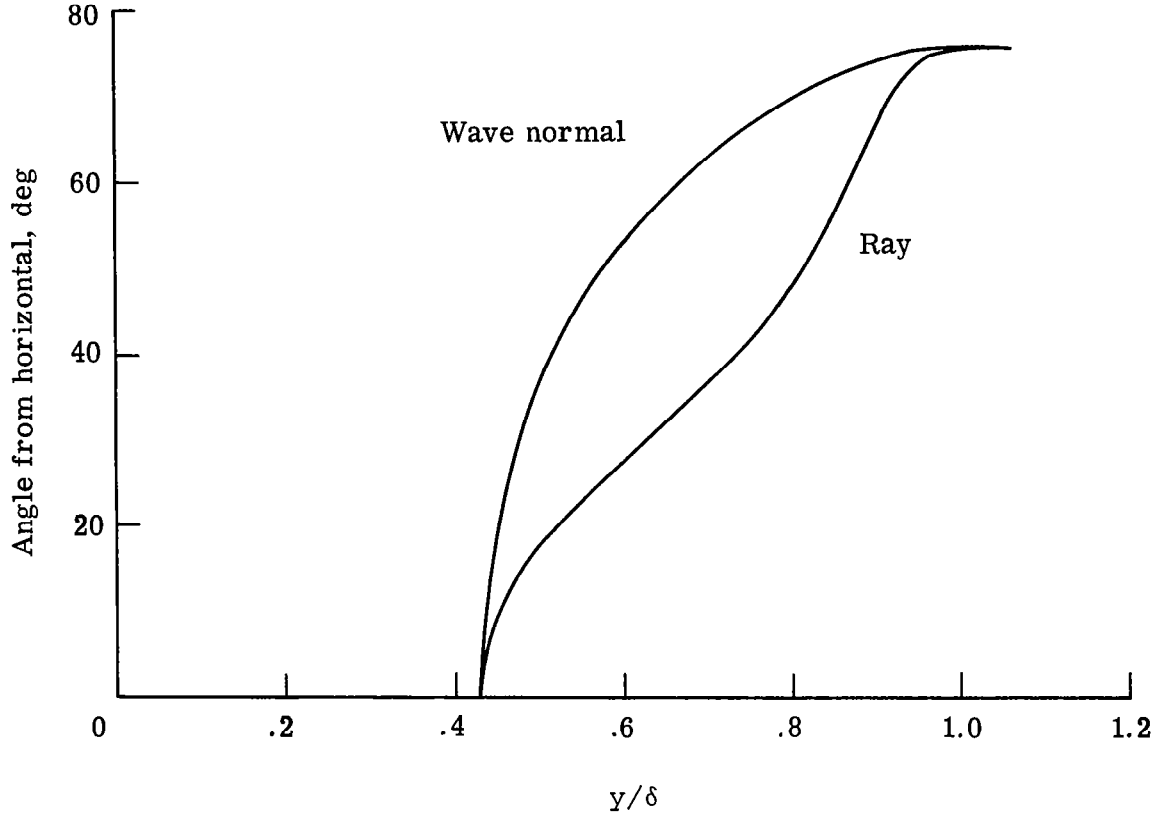

Figure 38.- Comparison of ray path and wave normal angles from the horizontal for the case of a stationary weak shock in a Mach 4 laminar boundary layer.

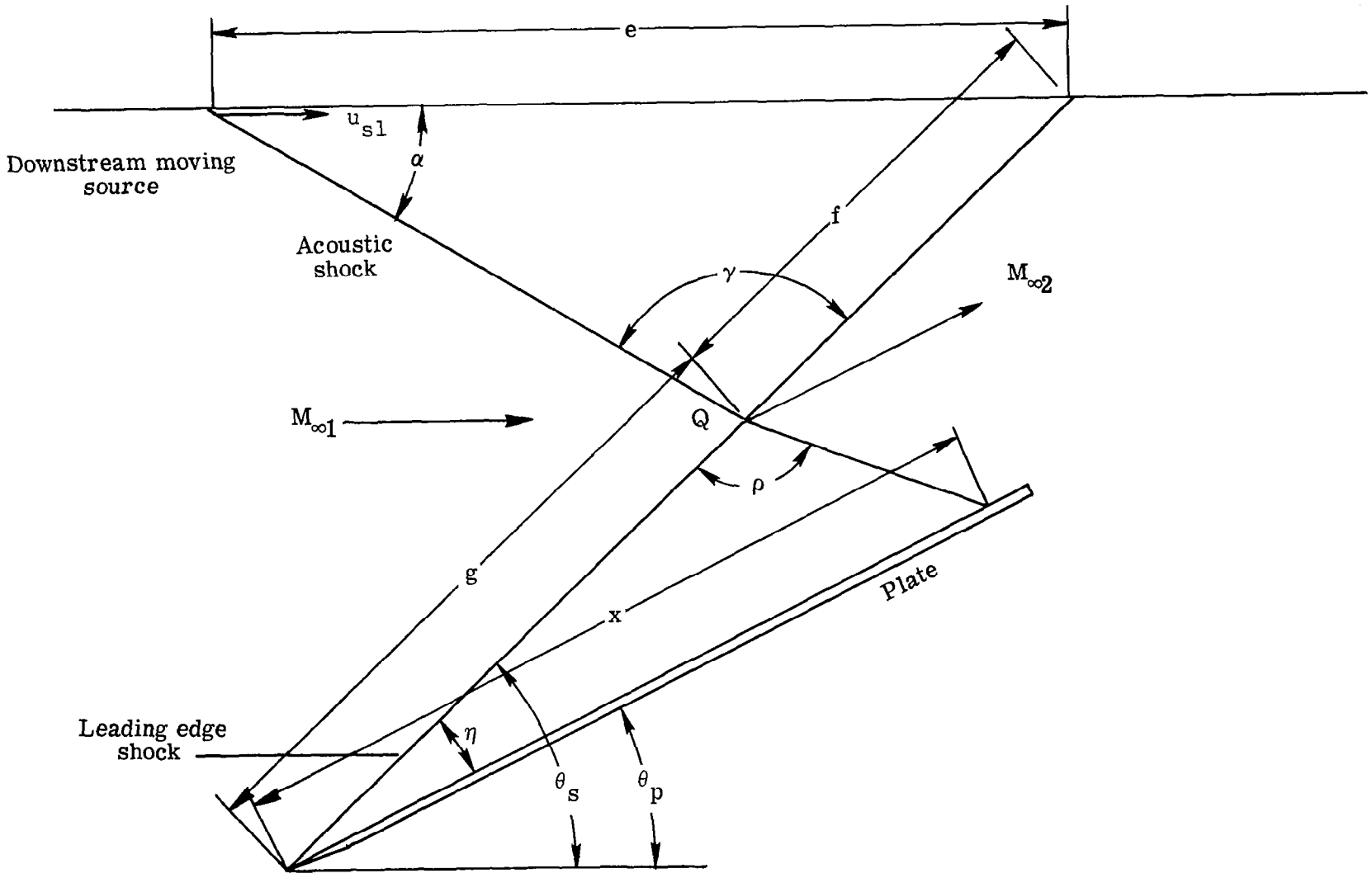

Figure 39.- Illustration of nomenclature used in the analysis.

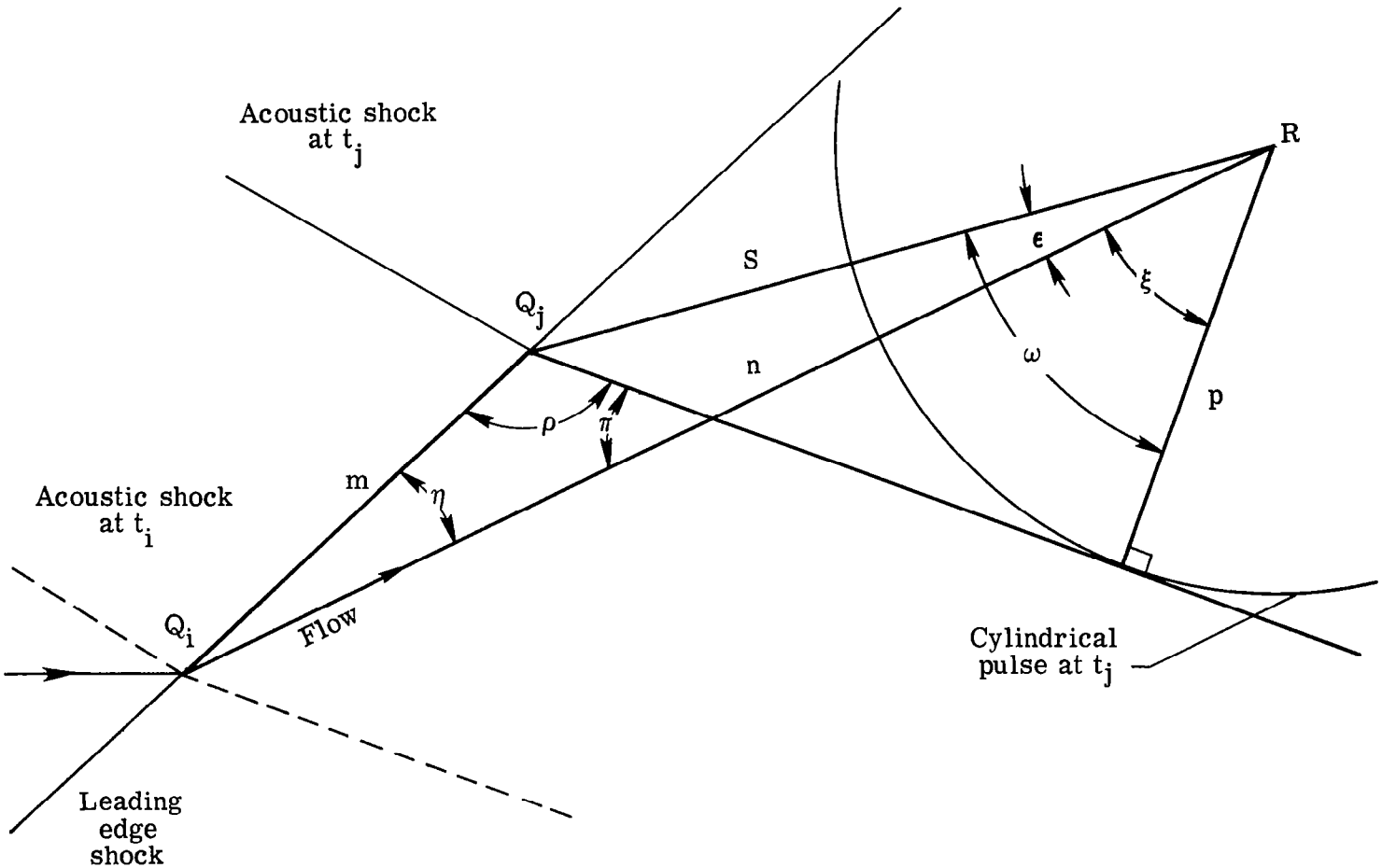

Figure 40.- Details of the intersection region and additional nomenclature

1. Report No.	2. Government Accession No.	3. Recipient's Catalog No.
NASA CR-3621		

4. Title and Subtitle	5. Report Date
INTERACTION OF AERODYNAMIC NOISE WITH LAMINAR BOUNDARY LAYERS IN SUPERSONIC WIND TUNNELS	April 1984
	6. Performing Organization Code
7. Author(s)	8. Performing Organization Report No.
M. R. Schopper	
	10. Work Unit No.
9. Performing Organization Name and Address	11. Contract or Grant No.
Systems and Applied Sciences Corporation 17 Research Drive Hampton, Virginia 23666	NAS1-16572
	13. Type of Report and Period Covered
12. Sponsoring Agency Name and Address	Contractor Report
National Aeronautics and Space Administration Washington, DC 20546	14. Sponsoring Agency Code 505-31-23-03

15. Supplementary Notes

Langley Technical Monitor: Ivan E. Beckwith
Final Report

16. Abstract The interaction between incoming aerodynamic noise and the supersonic laminar boundary layer is studied. The noise field is modeled as a Mach wave radiation field consisting of discrete waves emanating from coherent turbulent entities moving downstream within the supersonic turbulent boundary layer. The individual disturbances are likened to miniature sonic booms and the laminar boundary layer is strafed by the waves as the sources move downstream. The mean, autocorrelation, and power spectral density of the field are expressed in terms of the wave shapes and their average arrival rates. Some consideration is given to the possible appreciable thickness of the weak shock fronts. The emphasis in the interaction analysis is on the behavior of the shocklets in the noise field. The shocklets are shown to be focused by the laminar boundary layer in its outer region. Borrowing wave-propagation terminology, this region is termed the caustic region. Using scaling laws from sonic boom work, focus factors at the caustic are estimated to vary from 2 to 6 for incoming shocklet strengths of 1 to .01 percent of the free-stream pressure level. The situation regarding experimental evidence of the caustic region is reviewed. It is not clear whether the focusing effectively promotes early transition. Additional observations concerning the interaction problem are presented.

17. Key Words (Suggested by Author(s))	18. Distribution Statement
Boundary layer transition Boundary layer noise Wind tunnel noise	Unclassified - Unlimited Subject Category 34

19. Security Classif. (of this report)	20. Security Classif. (of this page)	21. No. of Pages	22. Price
Unclassified	Unclassified	168	A08

For sale by the National Technical Information Service, Springfield, Virginia 22161 NASA-Langley, 1984